ABSTRACT

Title of Document: PLANT-SPECIFIC K^+ TRANSPORTERS WITH DISTINCT PROPERTIES AND THEIR EMERGING ROLES IN ENDOMEMBRANE TRAFFICKING

Salil Chanroj
Doctor of philosophy, 2011

Directed By: Professor Heve Sze
Department of Cell Biology & Molecular Genetics

Plant growth, development and survival are dependent on the dynamic endomembrane system that modulates the delivery of various cargos to their destination or removal of components for degradation in time and in space. Yet the molecular determinants that regulate this dynamic and intricate machinery in plants are poorly understood. The multiplicity of Cation/H^+ eXchangers (CHX) genes in higher plants, but not in metazoans, raises questions about their transport activity and suggests roles characteristic to plant life.

Five CHX proteins from *Arabidopsis thaliana* were implicated in pH homeostasis as each rescued growth of alkaline-sensitive yeast strains, though with distinct properties. Each CHX improved growth of K^+-uptake deficient strain at different pHs. Moreover, CHX17, 18 and 19 conferred hygromycin B resistance when CHX20 could not. Although both CHX17 and CHX20 mediated K^+ uptake when expressed in *Escherichia coli;* their properties suggested differential modes of transport. CHX20, but not CHX17, acidified cytoplasmic pH and alkalinized vacuolar pH in yeast. CHX17 was more effective than CHX20 in reducing secretion of a vacuolar lumen protein in yeast. As

these CHXs were localized to yeast endomembranes, results suggested that CHXs differentially modulate pH and K^+ homeostasis of intracellular compartments which affect protein sorting.

CHX20-tagged with fluorescent protein was localized to ER, whereas CHX16, 17, 18 and 19 localized to prevacuolar compartments (PVC) and to plasma membrane (PM) *in planta*. Brefeldin A diminished PM-associated CHX17, whereas wortmannin caused formation of ring-like structures of CHX17-bound compartments. When full-length CHX17 (820 residues) was truncated, CHX17(1-472) partially restored yeast growth on alkaline medium. However, the truncated protein was localized to Golgi, suggesting a role of the C tail in sorting CHX17 from Golgi to PVC and PM. These results suggest that CHX17 is associated with a subset of endosomes that traffick among PVC, vacuole and PM in cells of whole plants. Together, the results support a model where CHX17 and its homologs modulate localized pH and K^+ environment of distinct endomembrane compartments and so affect membrane trafficking and cargo sorting through the endocytic and/or secretory pathways. CHXs are proposed to facilitate cell wall modifications as plants adapted to dry land.

PLANT-SPECIFIC K^+ TRANSPORTERS WITH DISTINCT PROPERTIES AND THEIR EMERGING ROLES IN ENDOMEMBRANE TRAFFICKING

By

Salil Chanroj

Dissertation submitted to the Faculty of the Graduate School of the
University of Maryland, College Park, in partial fulfillment
of the requirements for the degree of
Doctor of Philosophy
2011

Advisory Committee:
Professor Heven Sze, Chair/Advisor
Professor Rajini Rao
Associate Professor Zhongchi Liu
Associate Professor Shunyuan Xiao
Associate Professor Jose Costa

DEDICATION

To my parents and grandparents.

ACKNOWLEDGEMENTS

It is an honor for me to show my gratitude to my mentor, Dr. Heven Sze. This dissertation would not have been possible without her guidance. I always think that I am fortunate to be her student. It has been six years of precious training to become a Ph.D. graduate. During this time, we have been through lots of argument and joy. Eventually, I deeply admire Dr. Sze as an outstanding teacher who cares for the students, a conservative scientist who is convinced by the strong evidence and a distinguish author who can revise noncompliant pieces into a masterpiece.

I also owe my gratitude to Dr. Scott Angle who accepted me as his graduate student in department of plant sciences and landscape architecture, the University of Maryland, back in 2003 before I transferred to Dr. Sze lab in 2005. During that time, I had a chance to take a plant genomic class taught by Dr. Jose Costa, who introduced me to the Green Revolution and classical genetics. I would like to show my gratitude to Dr. Rajini Rao (Johns Hopkins University School of Medicine) for her time and advice, especially for the manuscript. I am also grateful to Dr. Zhongchi Liu and Dr. Shunyaun Xiao for enlightening my molecular genetics knowledge in classes and for their support and suggestion.

I profoundly feel indebted to my parents, my sister and my girlfriend, Waeowalee Choksawangkarn, for all their love and support. I am also thankful to my colleagues: Senthil Padmanaban, Xiyan Li, Yongxian Lu, Kevin Bock, Emily Chen, Stephanie O-boateng, Christopher Maltbie, Barri Shrager, Daniel Czerny, Robert Su and all friends for their help and advice in and out of the lab. Lastly, this accomplishment is made possible by the Royal Thai Government for the initial fellowship for studying abroad.

TABLE OF CONTENTS

LIST OF TABLES

LIST OF FIGURES

LIST OF FIGURES (continued)

ABBREVIATIONS

ABA	Abscisic acid
ADP	Adenosine diphosphate
Amp	Ampicillin
ARF	ADP-ribosylation factor
ATP	Adenosine triphosphate
BCECF	2',7'-bis-(2-carboxyethyl)-5-(and-6)-carboxyfluorescein
BCECF-AM	2',7'-bis-(2-carboxyethyl)-5-(and-6)-carboxyfluorescein, acetoxymethyl ester
BFA	Brefeldin A
BP	Band pass
BTP	Bis-tris propane
CCCP	Carbonyl cyanide-m-chlorophenylhydrazone
cDNA	Complementary DNA
CHX	Cation/H^+ eXchanger
CPA	Cation Proton Antiporter
CPM	Count per minute
CPY	Carboxypeptidase Y
CYT	Cytosol
DAPI	4',6-diamidino-2-phenylindole

DMSO	Dimethyl sulfoxide
DNA	Deoxyribonucleic acid
EDTA	Ethylenediaminetetraacetic acid
EE	Early endosomes
EIA	Enzyme-immuno assay
ELISA	Enzyme-linked immunosorbent assay
Em	Emission wavelength
EM	Electron microscopy
ER	Endoplasmic reticulum
Ex	Excitation wavelength
ext	External
F1	The first filial generation plants
FM4-64	N-(3-triethylammoniumpropyl)-4-(6-(4-(diethylamino)phenyl)hexatrienyl)pyridinium dibromide
GB	Gibeaut
GEF	Guanine-nucleotide exchange factor
GFP	Green fluorescent protein
Glc	Galactose
Glu	Glucose
HEPES	4-(2-hydroxyethyl)-1-piperazineethanesulfonic acid
HygB	Hygromycin B

IPTG	Isopropyl β-D-1-thiogalactopyranoside
KEA	K^+ Efflux Antiporter
LB	Luria-Bertani
LE	Late endosomes
LP	Long pass
LSM	Laser scanning microscope
MES	2-(N-morpholino)ethanesulfonic acid
MOPS	3-(N-morpholino)propanesulfonic acid
MS	Murashige and Skoog
MVB	Multivesicular body
NHA	Na^+/H^+ Antiporter
NHX	Na^+/H^+ Exchanger
NHX	Na^+/H^+ eXchanger
OE	Over-expressing
PCR	Polymerase chain reaction
PEG	Polyethylene glycol
PI3	Phosphatidylinositol 3-phosphate
PI3K	Phosphoinositide 3-kinase
PM	Plasma membrane
PME	Pectin methylesterase
PVC	Prevacuolar compartment

QTL	Quantitative trait locus
RE	Recycling endosomes
RFP	Red fluorescent protein
RNA	Ribonucleic acid
RT-PCR	Reverse transcription PCR
SD	Standard deviation
SDAP	Synthetic dextrose arginine phosphate
SEM	Standard Error
SGM	Synthetic glycerol mannitol
T-DNA	Transfer DNA
TGN	*Trans*-Golgi network
TM	Transmembrane
vac	Vacuole
Wm	Wortmannin
Wt	Wild-type
YFP	Yellow fluorescent protein
YNB	Yeast nitrogen base
YPAD	Yeast extract peptone adenine dextrose
YTMK	Yeast extract tryptone mannitol potassium

CHAPTER I

WHY DO PLANTS HAVE MULTIPLE CATION/H^+ COTRANSPORTERS?

A. LITERATURE REVIEW

A cell is a fundamental unit of living organisms where biological processes have been confined and maintained inside membranes and compartments. To selectively transport ions and metabolites across membranes, organisms have evolved a large number of membrane transporter proteins. The ultimate goal of these transporters is to maintain cellular homeostasis. One particular system is the regulation of ion and pH homeostasis through monovalent cation proton antiporters (CPA). There are two major CPA families in prokaryotes and eukaryotes which are designated as CPA1 (2.A.36) and CPA2 (2.A.37), respectively (Saier, 2000; Brett et al., 2005).

A.1. Cation Proton Antiporters in Plants

There are 30-60 genes encoding CPAs in higher plants, with 44 genes in *Arabidopsis thaliana*. In the past decade, several studies of these plant transporters had suggested their role in salt tolerance (Apse et al., 1999; Shi et al., 2000; Yokoi et al; 2002). However, recent studies indicated additional roles of CPAs in pH and K^+ homeostasis involved in several physiological processes, including response to K^+ starvation (Venema et al., 2003; Cellier et al., 2004; Zhao et al., 2008), flower coloration (Ohnishi et al., 2005), guard cell movement (Pamanaban et al., 2007), and pollen tube guidance (Lu et al., 2011). Owing to the vast diversity and redundancy of CPAs, the functions of most CPAs have yet to be unveiled in plants.

Fig. I-1. Unrooted phylogenetic tree of CPA1 and CPA2 families in bacteria, fungi and plants.

Analysis was performed using RAxML version 7.2.6 (Stamatakis, 2006) with 100 rapid bootstrap inferences and thereafter a thorough ML search option. The final Maximum Likelihood is -95720.815093. This analysis comprised conserved transmembrane regions of 170 protein sequences obtained from NCBI, JGI and Dr. Charles Dewiche unpublished data which were aligned previously using Muscle version 3.8.31 (Edgar, 2010). Phylogenetic tree was processed further for visualization using Archaeopteryx version 0.957(Han and Zmasek, 2009). Branch color represents selected CPA from corresponding organisms shown on the right. The major dot line separates between family (dark grey) and the minor dot lines separate between clade (light grey).

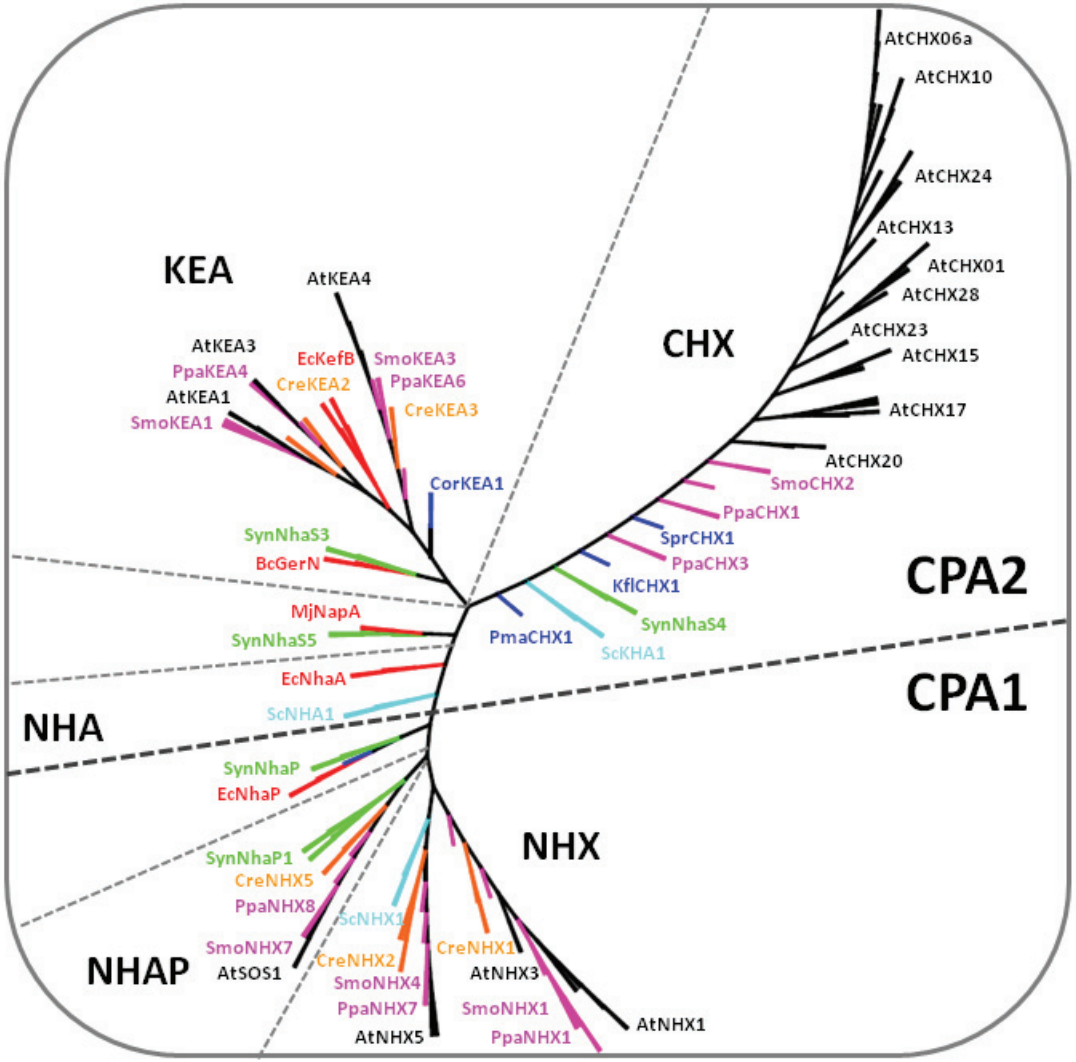

Archaebacteria

Mj: *Methanocaldococcus jannaschii*

Eubacteria

Bc: *Bacillus cereus*

Ec: *Escherichia coli*

Cyanobacteria

Syn: *Synechococcus spp.*

Green algae

Cre: *Chlamydomonas reinhardtii*

Spr: *Spirogyra pratense*
Kfl: *Klebsormidium flaccidum*
Pma: *Penium margaritaceum*
Cor: *Coleochaete orbicularis*

Yeast

Sc: *Saccharomyces cerevisiae*

Land plants

Ppa: *Physcomitrella patens*

Smo: *Selaginalla moellendorffii*

At: *Arabidopsis thaliana*

Table I-1. Summary of characterized CPA1 members (NHXs) in *Arabidopsis*.

Isoform	Expression	Membrane location	Main Functions	References
NHX1	Ubiquitous: epidermal layer in siliques, inflorescence stems, leaves and petals Induced by salt, osmolarity, ABA	Tonoplast (9 TM domains, C-tail in lumen)	$Na^+(K^+)/H^+$ Salt tolerance K^+ compartmentation in vacuole Interact with calmodulin (AtCAM15) regulating Na^+/K^+ selectivity	Apse et al., 1999 Gaxiola et al., 1999 Quintero et al., 2000 Shi et al., 2002 Venema et al., 2002 Yokoi et al., 2002 Apse et al., 2003 Yamaguchi et al., 2003 Yamaguchi et al., 2005 Leidi et al., 2010
NHX2	Ubiquitous Induced by salt, osmolyte, ABA	Tonoplast	Salt tolerance	Yokoi et al., 2002
NHX3	Roots Germinating seeds, flowers and siliques	Tonoplast	K^+/H^+ Low K^+ tolerance	Yokoi et al., 2002 Liu et al., 2010
NHX4	Ubiquitous: stem Induced by high Li^+ or K^+, ABA	Tonoplast	Increase sensitivity to salt	Yokoi et al., 2002 Li et al., 2009
NHX5	Ubiquitous Induced by salt	Golgi/TGN	Vesicular trafficking Salt tolerance	Yokoi et al., 2002 Bassil et al., 2011
NHX6	Ubiquitous	Golgi/TGN	Vesicular trafficking Salt tolerance	Yokoi et al., 2002 Bassil et al., 2011
NHX7 (SOS1)	Root-, stem- and leaf- xylem parenchyma, and epidermal cells of the root tip Induced by NaCl	Plasma membrane	Na^+/H^+ Salt tolerance Control long-distance Na^+ transport from root to shoot Protect K^+ permeability Regulated by protein kinase SOS2 and Ca^{2+} sensor SOS3 through phosphorylation of auto-inhibitory domain at C terminus Interact with RCD1 regulating oxidative stress response	Shi et al., 2000 Qiu et al., 2002 Quintero et al., 2003 Shi et al., 2002 Qi et al., 2004 Katiyar-Agarwal et al., 2006 Quintero et al., 2010
NHX8	Ubiquitous	Plasma membrane	Li^+ tolerance	An et al., 2007

A.1.a. Monovalent cation proton antiporter-1

I conducted phylogenetic analyses confirming that bacterial NhaP was the ancestral gene of the CPA1 family in eukaryotes (Fig. I-1). This family of transporters is predicted to have 10-12 membrane-spanning domains, and appears to mediate electroneutral Na^+/H^+ exchange. Recent study revealed that archaeal NhaP1 had a conformation change between pH 4 and pH 8 where activity was observed at pH 6 but not at pH 8 (Vinothkumar et al., 2005; Goswami et al., 2011). Essentially, CPA1 family is ubiquitously found in all kingdoms, including, bacteria, fungi, plants and animals. There are two major subfamilies within CPA1 in plants, NHX and NHAP.

A.1.a.i. NHX clade

Like its ancestor, NhaP, $\underline{Na}^+/\underline{H}^+$ e<u>x</u>changer (NHX) mediates electroneutral Na^+/H^+ exchange (Darley et al., 2000). NHX is ubiquitous in the plant kingdom as demonstrated by the presence of *NHX* genes in green algae, lower plants and flowering plants (Fig. I-1). Interestingly, there is only one NHX homolog in budding yeast, *Saccharomyces cerevisiae*, ScNHX1. To date, all characterized isoforms of plant and yeast NHXs have been localized to endomembranes including, endosomes and vacuole (Table I-1).

In *Arabidopsis thaliana* (At), there are 6 AtNHX isoforms showing differential tissue expression (Yokoi et al., 2002). Most of them were shown to be associated with salt stress responses (see review by Rodriguez-Rosales et al., 2009; Table I-1). Furthermore, *Ipomea nil*, InNHX1 was shown to play a role in flower color determination caused by alkalinization of vacuolar pH (Ohnishi et al., 2005). This process was al shown to be physiologically associated with NHX1 activity mostly through K^+/H^+ exchange in *Ipomea tricolor* (Yoshida et al., 2009). Besides, it was demonstrated in proteoliposome

reconstitution that AtNHX1 catalyzed Na^+/H^+ and K^+/H^+ exchange with similar affinity (Venema et al., 2002). Moreover, silencing of *Solanum lycopersicon*, LeNHX2 resulted in plants that accumulated less K^+ and was susceptible to salt stress (Rodríguez-Rosales et al., 2008) but over-expression of AtNHX1 in tomato resulted in enhanced K^+ accumulation and resistance to salt (Leidi et al., 2010). Therefore, there is an increasing acceptance that plant NHX has a major role in pH and K^+ homeostasis in plant endomembrane system whereby salt tolerance is conferred by enrichment of intracellular K^+ pool and sequestration of Na^+ in vacuole. Interestingly, endosomal NHXs, for example, LeNHX2, AtNHX5 and AtNHX6 were able to confer salt tolerance (Rodríguez-Rosales et al., 2008; Yokoi et al., 2002; Bassil et al., 2011).

Evidence is emerging that endosomal NHXs play roles in endosomal pH and K^+ homeostasis that regulate protein sorting and membrane trafficking as demonstrated in yeast previously (Bowers et al., 2000; Ali et al., 2004; Brett et al., 2005b; Wagner et al., 2006). In plants, recent study suggested that regulation of endosomal pH and K^+ homeostasis by AtNHX5 and AtNHX6 had a role in protein sorting and cellular stress responses (Bassil et al., 2011).

A.1.a.ii. NHAP clade

Phylogenetic analysis revealed that members of Na$^+$/H$^+$ antiporter (NHAP) clade were derived from bacterial NhaP1 and NhaP2 (Fig. I-1). They are present in bacteria and plants, including green algae. Like NHX clade, NHAP also mediates electroneutral Na^+/H^+ exchange (Qiu et al., 2003). This is why members of the NHAP clade were annotated previously as a part of NHX clade. Later, it was classified as an independent clade in CPA1 (Brett et al., 2005). The major difference between NHX and NHAP is

their membrane localization. NHAP were localized to the plasma membrane (Qiu et al., 2003). Intriguingly, plant NHAP, such as SOS1/NHX7, has a long C-terminal tail compared to plant NHX. Recent studies show that this long C tail interacts with other regulatory proteins (Katiyar-Agarwal et al., 2006; Quintero et al., 2011).

In *Arabidopsis*, there are 2 isoforms, namely AtSOS1 (AtNHX7) and AtNHX8. Most of the studies in plant NHAP have focused on AtSOS1 (Shi et al., 2000; Quintero et al., 2002; Qiu et al., 2003, Zhou et al., 2006; Olias et al., 2009; Fraile-Escanciano et al., 2010). SOS1 was identified in a genetic screen for mutants that were salt-overly sensitive (Wu et al., 1996), and later shown to be associated with salt stress response (Shi et al., 2000) by mediating an extrusion of Na^+ (Qiu et al., 2003; Olias et al., 2009). It was shown that SOS1 had a physiological role in protecting plasma membrane K^+ transporters from Na^+ inhibition (Qi et al., 2004). Furthermore, interaction of AtSOS1 with RCD1 (radical-induced cell death) prevented RCD1, which is important for oxidative stress response, from nuclear localization (Katiyar-Agarwal et al., 2006). This relationship suggested a role of SOS1 in signal transduction. Analysis of *sos1* mutant revealed the consequences of Na^+ accumulation which affected membrane trafficking, vacuolar biogenesis and pH homeostasis in roots (Oh et al., 2010). Curiously, cation specificity for AtSOS1 and AtNHX8 is limited to Na^+ and Li^+ (Qiu et al., 2003; An et al., 2007), suggesting the major role of these transporters in salt stress responses. Therefore, the role of this NHAP clade is restricted to salt stress response but not limited to Na^+ extrusion.

A.1.b. Monovalent cation proton antiporter-2

The CPA2 family is considered to be the largest and the most diverse of all CPAs. Members of CPA2 family are prevalently found in bacteria, fungi and plants; however,

Fig. I-2. Predicted topology of CHXs from CPA2 family.

Protein topology prediction and visualization was performed using SOSUI version 1.11 (http://bp.nuap.nagoya-u.ac.jp/sosui/). A homolog of CHX in *Spirogyra pretense*, SprCHX1, and AtCHX17 are predicted to have 11 TM domains with an amino terminus facing toward luminal side or outside and a long carboxyl terminus in cytoplasm (top and middle). AtCHX20 is predicted to have only 9 TM domains sharing the same orientation with SprCHX1 and AtCHX17. Dark green and light green colored TM domains represent primary and secondary helices, respectively. Black, blue and red colors represent hydrophobic residues, polar residues and acidic residues, respectively.

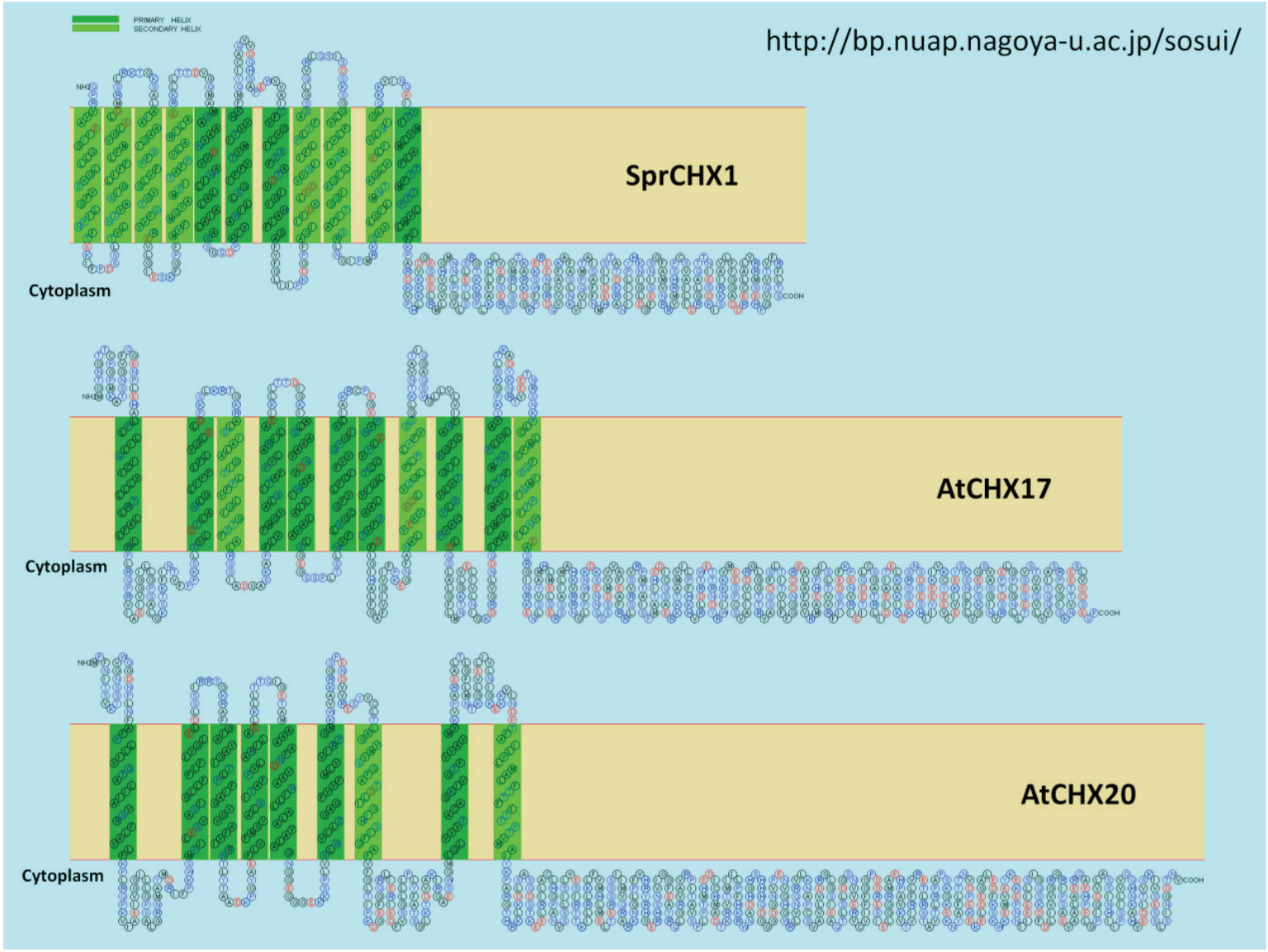
PRIMARY HELIX
SECONDARY HELIX
http://bp.nuap.nagoya-u.ac.jp/sosui/
SprCHX1
Cytoplasm
AtCHX17
Cytoplasm
AtCHX20
Cytoplasm

they are rare in animals (Brett et al., 2005). They are predicted to have 8-14 membrane-spanning domains (Fig. I-2) with a Pfam domain for $Na^+(K^+)$/H+ exchange. Interestingly, substrate and transport mode of CPA2 from bacteria vary among the family members. In general, they catalyze electrogenic transport either through carrier-mediated mode or channel-mediated mode (Saier et al., 2000). CPA2 family is classified into 3 major clades based on phylogenetic analysis and bacterial ancestor, including NHA, KEA and CHX. However, study of CPA2 family has been limited to bacteria and yeast in the past decade.

A.1.b.i. NHA clade

This NHA clade in CPA2 has a close relationship with NHAP clade in CPA1 in terms of phylogenetic data (Fig. I-1) and membrane localization, which is at the plasma membrane (Kinclova et al., 2001). However, two major differences separate NHA from NHAP: i) bacterial ancestor which is NhaA and ii) mode of transport is electrogenic (Ohgaki et al., 2005). Unlike NhaP which is an ancestor of CPA1 family, NhaA is active at pH 8 but inactive at pH 6 (see section A.1; Taglicht et al., 1991). Functionally, two-step activation from pH 6-7 and pH 7-8 was observed where the latter conformation change was induced by substrate ions (Appel et al., 2009). The transport reaction resulted in an exchange of $2H^+$ for $1Na^+$ or $1Li^+$ (see review by Padan 2008). Intriguingly, NHA members are found in bacteria, animals, fungi (Brett et al., 2005), green algae but not found in early land plants or flowering plants (Fig. I-1). Functional analysis in yeast suggested that ScNHA1 mediated both Na^+/H^+ and K^+/H^+ exchange (Banuelos et al., 1998; Sychrova et al., 1999).

A.1.b.ii. KEA clade

The K^+ efflux antiporter (KEA) clade comprises members from bacteria and plants. Based on phylogenetic analysis, KEA is likely descended from bacteria (Bacillus) GerN and cyanobacteria *Synechocystis* NhaS3 (Fig. I-1). GerN is required for germination of Bacillus endospores and proposed to associate with a germination receptor to initiate germination (Thackray et al., 2001). Unlike other ancestral bacteria antiporters mentioned earlier, GerN mediates both $Na^+(Li^+)/H^+$ and $Na^+(Li^+)/H^+$-K^+ antiport though the latter is transported at a higher velocity (Southworth et al., 2001). Interestingly, plant KEA showed high homology to bacterial KefB and KefC (Fig. I-1), indicating that KefB and KefC are KEA orthologs in prokaryotes. These two proteins were associated with bacterial detoxification mechanisms whereby Kef-mediated K^+ efflux was activated by glutathione adducts as a result of oxidative stress (Ferguson et al., 1993). The efflux of K^+ was accompanied by the rapid decrease of intracellular pH (Ferguson et al., 1997). Recent study on KefC demonstrated that KefC together with ancillary protein, KefF, exhibited $K^+(Rb^+)(Na^+)(Li^+)/H^+$ antiport activity and glutathione (GSH) inhibited its activity (Fujisawa et al., 2007). Although, it was suggested that KefC might display channel-like activity without KefF. To date, there is no report on functional studies of plant KEA.

A.1.b.iii. CHX clade

Cation/H+ exchanger (CHX) is the major clade in CPA2 due to the huge number of paralogs in plants. CHX is limited to bacteria, fungi and plants though there is one homolog in budding yeast, ScKHA1. Phylogenetic analysis suggested that eukaryote CHX is likely descended from archaebacteria NapA and cyanobacteria *Synechocystis*

Table I-2. Comparison of characterized CPA2 members (CHXs) in *Arabidopsis.*

Isoform	Tissue expression & membrane localization	Key observation & main function	References
CHX13	Preferentially expressed in pollen Induced in root tip and elongation zone by K^+ starvation Localized to plasma membrane in both yeast and plant cells	Rescue growth in yeast K^+ deficient-mutant at pH 4.5 in plate. Mediate high-affinity K^+ uptake in yeast and plant cells Km = 136.4 μM and 196 μM respectively. *chx13* mutants are sensitive to low K^+ but can be rescued by over-expression of *CHX13* Essential for K^+ acquisition	Zhao et al., 2008 Sze et al., 2004
CHX17	Expressed in pollen and root epidermis and cortex Induced by salt stress, K^+ starvation, acidic pH and ABA Localized to endomembrane in yeast	*chx17* mutants have less K^+ content in roots during salt stress or K^+ starvation. Rescue yeast *kha1* mutant growth at alkaline pH and confer hygromycin B tolerance Involved in K^+ acquisition and homeostasis	Cellier et al., 2004 Sze et al., 2004 Maresova and Sychrova, 2006
CHX20	Preferentially expressed in guard cells and root tip Localized to endomembrane in plant protoplasts	Rescue yeast *kha1* mutant growth at alkaline pH and low K^+. *chx20* mutants show reduction in light-induced stomata opening regardless of the external K^+ Crucial for osmoregulation	Padmanaban et al., 2007
CHX23	Specifically expressed in pollen Localized to endomembrane, possibly ER in pollen tube	*chx21chx23* mutant pollen is infertile due to inability to turn toward the ovule Rescue growth and mediate K^+ uptake in K^+ uptake-deficient *E coli* in pH dependent manner Involved in signaling pathways	Lu et al., 2011

NhaS5 (Fig. I-1). Interestingly, the *Synechocystis* NhaS4, a close homolog of plant CHX (Fig. I-1), showed no Na^+/H^+ antiport activity but exhibited lower K^+ requirement for growth suggesting that NhaS4 was not an Na^+ extrusion system in cyanobacteria (Inaba et al., 2001).

Plant and Fungal CHX

Several studies have suggested that ScKHA1 has a role in K^+ and pH homeostasis in yeast (Ramirez et al., 1998; Maresova and Sychrova, 2005; Maresova and Sychrova, 2010) by homology to KefB, a putative K^+/H^+ antiporter. However, recent study in *Debaryomyces hansenii*, a salt-tolerant yeast, indicated that DhKHA1 is potentially classified as a Na^+/H^+ transporter (Carc´ıa-Salcedo et al., 2007). Both ScKHA1 and DhKHA1 are localized to yeast endomembrane, potentially Golgi (Maresova and Sychrova, 2005; Flis et al., 2005; Carc´ıa-Salcedo et al., 2007).

In plants, a large family of CHX had been annotated recently in both *Arabidopsis* and rice (*Oryza sativa*), corresponding to 28 and 17 genes, respectively (Sze et al., 2004). Intriguingly, 18 *AtCHX* genes are specifically or preferentially expressed in the pollen (Sze et al., 2004). Recent study demonstrated that AtCHX21 and AtCHX23 are essential for pollen tube guidance, possibly through regulation of localized pH and cation balance in endomembrane system of pollen tube (Lu et al., 2011).

Only a few *AtCHX* genes expressed in vegetative tissues have been studied to date (Table I-2). *AtCHX17* is expressed in root epidermal and cortical cells where its expression is induced by environmental stresses, including high salt, potassium starvation, abscisic acid (ABA) and external acidic pH (Cellier et al., 2004). Furthermore, *AtCHX20* is preferentially and highly expressed in guard cells, and was demonstrated to

play a role in light-induced stomata opening, possibly through K^+ and pH homeostasis in the endomembrane system of guard cells (Padmanaban et al., 2007).

Surprisingly, a recent study revealed the role of AtCHX13 in K^+ homeostasis (Zhao et al., 2008). Although the gene is preferentially expressed in pollen, it is expressed in roots during K^+ starvation. Moreover, it was demonstrated that AtCHX13 promoted high-affinity K^+ uptake in both yeast and plant cells (Zhao et al., 2008). Although AtCHX13 is localized at the plasma membrane, it is possible that AtCHX13 might not mediate K^+ uptake directly in plant cells but rather promote other K^+ uptake systems in roots, especially AtAKT1 and AtHAK5 (Rubio et al., 2008; Rubio et.al, 2010; Pyo et al., 2010).

A.2. Evolution of plant-specific cation proton antiporters

Phylogenetic analysis suggests that KEA branch diverged from CHX during evolution. Likewise, NHAP branch also diverged from NHX. Interestingly, KEA and NHAP are found in bacteria, cyanobacteria and plants. In contrast, members of CHX clade are found in cyanobacteria, fungi and plants (Fig. I-1). The similarity is the ancestors of these transporters in plants are also found in cyanobacteria, which is supported by the endosymbiont theory (Weeden et al., 1981). On the other hand, KEA or NHAP are not found in fungi, except for CHX orthologs eg. KHA1 in yeast. Since fungi share similarities with plants, including a protective cell wall and alternation of generations, this information would suggest that only CHX clade has evolved as ancestral organisms evolved into multicellular plants. I think it is most likely that plant NHAP and KEA would retain a primitive function found in bacteria, especially for survival during exposure to toxic metabolites, as demonstrated by KefB and KefC (Ferguson et al., 2000;

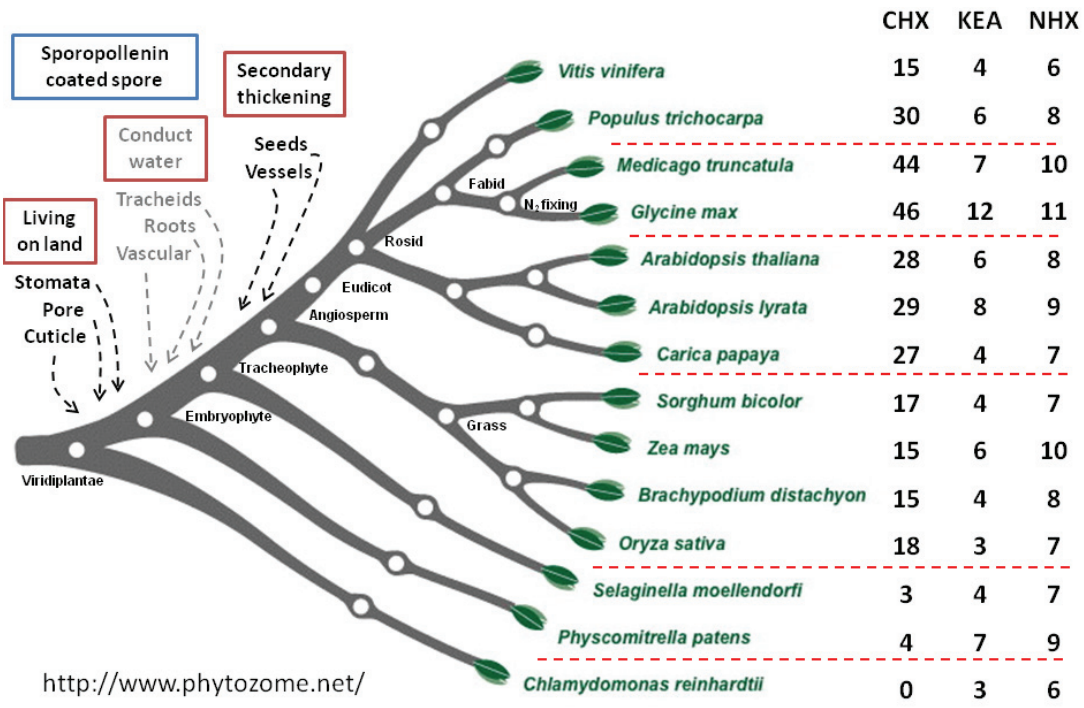

Fig. I-3. Evolution of cation proton transporters from green algae to trees.

Numbers of genes annotated to CHX, KEA and NHX, respectively, in CPA superfamily are shown on the right. NHX represents both NHX and NHAP clades. Results are from www.phytozyme.net. Significant increases in number of genes are observed in CHX clade.

Booth et al., 2003). In contrast, I propose that plant CHX genes might perform unique roles that are specifically required for adaptation of plants to grow, develop, reproduce and survive on dry land.

A.2.a. Origin of CHX in plants

Green plants (*Viridiplantae*) comprise both aquatic and land plant species ranging from algae to flowering plants. Several lines of evidence indicate that charophyte green algae are the ancestors of the land plants (Karol et al 2001; McCourt et al., 2004). Charophyte is one lineage of green algae, Chlorophyte (McCourt, 1995), that shares biochemical, ultrastructural and functional characteristics with land plants (Embryophyte). Recent multigene phylogenetic analysis also supports this hypothesis (Finet et al., 2010; Timme and Delwiche, 2010).

Surprisingly, comparative genomic studies revealed that CHX has evolved from charophyte, but not chlorophyte. This is demonstrated by the presence of at least one CHX homolog in *Spirogyra pratensis*, a species in Zygnematales or conjugated green algae in charophyta whereas none are found in *Chlamydomonas reinhardtii* or *Volvox carteli* which are from the chlorophyte lineage (Fig. I-1, I-3). In contrast, KEA and NHX homologs are ubiquitous in all green plants and also animals (only NHX). Furthermore, the number of CHX orthologs has multiplied as plants evolved into flowering plants (Angiosperm). For instance, early non-vascular land plants, such as moss (*Physcomitrella patens*) and club moss (*Selaginalla moellendorffii*) genomes contains 3-4 CHX members. Interestingly, there are more than 15 CHX paralogs in monocots and up to 46 paralogs in dicots. In particular, legumes, like soybean, *Glycine max* have 46 predicted CHX members raising the possibility for a role in biological nitrogen fixation

(Fig. I-2). In contrast, the number of CHX, KEA and NHX paralogs in early and flowering plants are relatively consistent with 3-8 members.

A.2.b. Evolutionary events during CHX gene duplication

Based on comparative genomic studies, it is possible that there were at least three steps in CHX gene duplication or CHX gene transfer during plant evolution. First, a CHX-like gene was transferred from bacteria to a charophyte. Later, the ancestral gene multiplied by duplication initially in early land plants, and later in vascular and flowering plants.

A.2.b.i. CHX gene transfer to charophyte green algae

Evolution from chlorophyte to charophyte is a major change from marine algae to freshwater algae. This means marine algae had to adapt to hypotonic condition with much lower Na^+ levels compared to the ocean. Interestingly, one trait was lost during this adaptation which is motility. Charophytes became more sessile due to the lack of flagella. Charophytes were multicellular, and developed rhizoids to attach the plant body to the bottom of ponds. Furthermore, they also gained several properties, including dessication-resistant zygospores, cellulose-synthesizing rosettes, plasmodesmata, rhizoidal protonema, sexual reproduction in charophyte (McCourt et al., 2004), pectinized cell walls in *Penium margaritaceum* (Domozych et al., 2007) and auxin signaling in *Spirogyra pratense* (Wodniok et al., 2011). Interestingly, both species are from Zygnematales or conjugated green algae that are being proposed to be a sister of the land plant (Wodniok et al., 2011). It is unknown whether CHX gene was horizontally transferred from a cyanobacterial ancestor, *NhaS4* or bacterial ancestor, *GerN*. NhaS4 is more closely related to plant CHX (Fig. I-1).

A.2.b.ii. CHX gene duplication in lower land plants

To survive on land and avoid desiccation, early land plants developed an extra protection wax layer called the cuticle. However, to facilitate gas exchange through the cuticle barrier, pores and stomata later developed on the surface. Moreover, to support the aerial structures, the cell wall was strengthened with additional components. Spores were also layered with extra tough wall materials to protect against desiccation. It is tempting to speculate that the duplication of *CHX* genes in this step might be related to adaptation to a dry environment of lower non-vascular land plants, though they still strictly required a humid and cool condition for growth.

A.2.b.iii. CHX gene duplication in flowering plants

Development of non-vascular land plant toward flowering plants primarily required the thickening of cell walls to support the larger plants. Vessel walls were also strengthened to support the long-distance transport of water and nutrients. Reproduction and long-term survival in a dry environment required protection of sperms in pollen grains and the development of seeds and fruits. The presence of multiple types of tissues and various growth conditions resulted in the diversity of cell wall components and wax among the flowering plants. The duplication of *CHX* genes might be related to growth and reproductive adaptations of land plants to the environment.

A.2.b.iv. Conserved CHX in flowering plants

Phylogenetic analysis reveals the branching of AtCHXs that are closely related to CHX orthologs in charophyte (SprCHX1) and lower plants (PpaCHXs, SmoCHXs), conserved CHXs, including AtCHX15, 16, 17, 18, 19, 20, 21 and 23 (Fig. I-1). Among

these, CHX15 and CHX23 are specifically expressed in pollen (Sze et al., 2004) and phylogenetically located at the further distance from 'primordial' CHXs when compared to other CHXs in this cluster. It is conceivable that they play roles in pollen tube growth as demonstrated by CHX21 and CHX23 (Lu et al., 2011). Intriguingly, the remaining CHXs apart from this branch (AtCHX15-23) are either preferentially or specifically expressed in the pollen (Sze et al., 2004). This would suggest the evolution of conserved CHXs from CHX15, 21 and 23 toward more evolved CHXs in reproductive systems of the flowering plants.

There are three groups of CHXs in this highly conserved branch, including AtCHX16-19, conserved CHXs and AtCHX20. Interestingly, CHX16-20 are expressed in vegetative tissues whereas CHX18 and 19 are also expressed in the pollen (Sze et al., 2004). CHX17 and CHX20 are suggested to function in K^+ homeostasis (Table I-2) though CHX17 is expressed in root (Cellier et al., 2004) but the latter is preferentially expressed in guard cells and plays a role in light-induced stomata opening (Padmanaban et al., 2007). Thus, it most likely that CHX20 is important for osmoregulation of guard cells through pH and K^+ homeostasis (Padmanaban et al., 2007). Even though the role and function of ancestral CHXs remains unclear, it is predicted to be a unique function required for adaptation of marine algae (chlorophyte) to become freshwater algae (charophyte) mentioned in section A.2.b.i.

What are the biological roles and function of CHXs?

CHX is a novel family of cation-proton antiporters that is unique to plants and fungi in eukaryote. However, scarce information is known about this family. Recent advances in genomics have allowed us to pin-point a common ancestor of the CHX

family, and to select them for in-depth study to answer questions of their biological function and also uncover their roles during the evolution of land plants.

I propose several working ideas:

i) They are most likely crucial for adaptation during the evolution from marine algae to freshwater algae, and then to land plants.

ii) They might have evolved to suit the diverse needs of specific cell-types, so they will show differential expression profile, sub-cellular localization and biochemical properties.

B.1. STATEMENT OF RESEARCH GOALS

To understand the roles of CHXs in plants, I chose to study *CHX* genes from *Arabidopsis thaliana* due to the availability of molecular genetic tools. Many CHXs are specifically or preferentially expressed in pollen, and only a handful are expressed in vegetative tissues, including roots and leaves. I selected 5 CHX genes expressed in vegetative tissues for further study. CHX16-20 in Arabidopsis cluster in one group and share highly conserved homology to charophyte (*Spirogyra pratense*) and lower plants including moss (*Physcomitrella patens*) and club moss (*Selaginalla moellendorffii*). By using multidisciplinary strategies, including bioinformatic, biochemical, molecular, genetic, and cell biology approaches, biochemical properties, subcellular-localization and potential physiological roles and function of these conserved CHXs would be elucidated.

<u>Aim 1.</u> Dissect the properties and function of CHX16-20 in yeast and bacterium

I used a single cell host (*E. coli*, yeast, plant protoplast) as a tool to dissect the activity and biochemical properties of CHX16-20. I demonstrated that this group of CHX from CPA2 has properties distinct from CPA1. Moreover, differential properties were observed among them. I showed direct evidence that CHX17 and/or CHX20 mediated K^+

transport and pH modification. These K^+ transporters were also localized to different endomembranes, including ER and PVC. I propose that the function of CHX17 and/or CHX20 in K^+ and pH homeostasis is linked to their role in mediating protein sorting in yeast (Chapter II).

<u>Aim 2.</u> Determine the biological function of CHX16-19 in plants

To understand the biological roles in plants, I further analyzed the tissue/cell expression of CHX16-19 using promoter::GFP reporter. Furthermore, all these CHX proteins are localized to endosomes, most likely PVC and the PM. Single and higher order T-DNA insertion mutants as well as transgenic plants were obtained. Only less triple or quadruple mutants of *chx17* and *chx18* were recovered than expected. Also, quadruple mutants were smaller than triple mutants or wild-type when grown in hydroponic solution. The underlying mechanism has not been elucidated, yet but these K^+ transporters are unlikely for K^+ nutrition (Chapter III).

<u>Aim 3.</u> Determine the membrane localization of CHX17 and its homologs *in planta*, and the function of the hydrophilic C tail of CHX17

The dual localization of CHX17 to PVC and PM suggested that PVC-associated CHX17-GFP was able to traffic to the plasma membrane, raising questions about the determinants for membrane trafficking and targeting. The carboxylic tail of CHX proteins is long and hydrophilic suggesting this region might serve regulatory functions. I tested the function of truncated CHX17 in yeast, and their membrane localization in plants. These results suggested a role for the CHX17 carboxyl terminus in regulating its own activity and subcellular localization (Chapter III).

CHAPTER II

ARABIDOPSIS CHX16-20 ARE ENDOMEMBRANE CATION TRANSPORTERS WITH DISTINCT ACTIVITIES AND EMERGING ROLE IN PROTEIN SORTING

A. ABSTRACT

The complexity of intracellular compartments in eukaryotic cells evolved to provide distinct environments to regulate processes necessary for cell proliferation and survival. A large family of predicted cation/proton exchangers, represented by 28 *CHX* genes in *Arabidopsis thaliana*, are associated with diverse endomembrane compartments and tissues in plants, although their roles are poorly understood. We expressed a phylogenetically-related cluster of *CHX* genes, encoded by *CHX15*-*CHX20*, in yeast and bacterial cells engineered to lack multiple cation handling mechanisms. Of these, CHX16-CHX20 were implicated in pH homeostasis as their expression rescued alkaline pH-sensitive growth phenotype of the host yeast strain. A smaller subset, CHX17-CHX19, also conferred tolerance to hygromycin B. Further differences were observed in K^+- and low pH-dependent growth phenotypes. Although CHX17 did not alter cytoplasmic or vacuolar pH in yeast, CHX20 elicited acidification and alkalization of the cytosol and vacuole, respectively. Using heterologous expression in *E. coli* strains lacking K^+ uptake systems, we provide evidence for K^+ (^{86}Rb) transport mediated by CHX17 and CHX20. Finally, we showed that CHX17 and CHX20 affected protein sorting as measured by carboxypeptidase Y secretion in yeast mutants grown at alkaline pH. In plant cells, CHX20-RFP co-localized with an ER marker; whereas RFP-tagged CHX17-CHX19 co-localized with prevacuolar compartment and endosome markers. Together, these results suggest that in response to environmental cues, multiple CHX transporters differentially modulate K^+ and pH homeostasis of distinct intracellular compartments which alter membrane trafficking events likely to be critical for adaptation and survival.

B. INTRODUCTION

The dynamic endomembrane system of eukaryotic cells is emerging as a critical and central coordinator in cell development, growth, signaling and adaptation to stress (Jurgens, 2004; Orlowski and Grinstein, 2007). Recent studies have illustrated the increasing complexity of intracellular compartments that sort proteins and membranes in the anterograde or retrograde direction through the biosynthetic and/or the endocytic pathway. Such compartments probably evolved to provide distinct environments in a temporal manner for specific biochemical reactions and protein-protein interactions necessary for cell proliferation and survival (Casey et al., 2010). Yet, the mechanisms that regulate the internal and external environment of these endomembrane compartments in plants are not well understood.

Endomembranes of eukaryotic cells, including those from yeast, mammals and plants, share several transporters in common, indicating that the mechanisms controlling the physico-chemical environment of diverse intracellular compartments are conserved in general. The most prominent is the H^+-pumping vacuolar ATPase which acidifies intracellular compartments, including yeast (Kane, 2006) and plant vacuoles (Sze et al., 1992), *trans*-Golgi network (Schumacher and Krebs, 2010), clathrin coated vesicles, lysosomes, and endosomes of diverse animal cells (Nishi and Forgac, 2002). As the V-ATPase is an electrogenic H^+- pump, acidification of membrane vesicles occurs only if counter ions, such as anions enter to dissipate the electrical potential (Sze, 1985). Several alkali cation/proton exchangers belonging to the Cation-Proton Antiporter 1 (CPA1) family have been found in endomembranes of eukaryotes (Brett et al., 2005; Pardo et al., 2006; Orlowski and Grinstein, 2007). Examples include vacuolar ScNHX1 of yeast, 8

AtNHX genes in Arabidopsis, and NHE6-9 in human. Alkali-cation/proton exchangers provide a leak pathway for H^+ and thus modulate lumenal pH and cation homeostasis within the endomembrane system where they have profound effects on vesicle biogenesis and trafficking in cells (Orlowski and Grinstein, 2007).

In plants, NHX1 represents the best characterized member of the CPA1 family. NHX1 was initially characterized as a vacuolar Na^+/H^+ exchanger, though later findings broadened cation selectivity to include K^+ (Apse et al., 1999; Gaxiola et al., 1999; Venema et al., 2002; Venema et al., 2003; Pardo et al., 2006). In addition to vacuole and prevacuolar endosomes, plant NHX isoforms are found in other endomembranes. Tomato LeNHX2, a homolog of AtNHX5/6, is a K^+-selective H^+ exchanger localized to the Golgi and endosomes (Venema et al., 2003). Recently, AtNHX5 and AtNHX6 were localized to the Golgi or trans-Golgi network (TGN), and shown to play a role in cell expansion as double mutants were dwarfed (Bassil et al., 2011). In addition, NHX7/SOS1, a plasma membrane member is important for conferring salt tolerance probably by controlling long-distance Na^+ transport (Shi et al., 2002). These findings show that members of the plant NHX family modulate Na^+ and K^+ homeostasis at various endomembrane compartments as well as the plasma membrane.

Given the multiplicity of plant NHX genes, it is surprising to discover a family of putative cation/H^+ exchangers (CHX) in a distinct CPA2 superfamily, sharing sequence similarity to bacteria NhaA and KefB (Brett et al., 2005). Intriguingly, most of the eukaryotic genes in CPA2 come from plants and fungi (Sze et al., 2004; Brett et al., 2005). Metazoan genomes each carry only two CPA2 members, NHA1 and NHA2 that appear to have risen by gene duplication (Brett et al., 2005). Human NHA2 shows broad

tissue distribution and confers tolerance to Na^+ and Li^+, but not to K^+, when expressed in yeast (Xiang et al., 2007). In striking contrast, *Arabidopsis thaliana* alone possesses 28 CHX genes and the rice genome has 17 members (Sze et al., 2004). The multiplicity of CHX genes in plants raises questions about their transport activity and their biological functions.

Arabidopsis CHX genes are differentially expressed in plant cell types (Sze et al., 2004; Bock et al., 2006). *AtCHX20* is preferentially expressed in leaf guard cells. Null mutants of *Atchx20* were impaired in light-induced stomatal opening, indicating a role in osmoregulation (Padmanaban et al., 2007). *AtCHX21* and *AtCHX23* play overlapping roles in pollen tube guidance, as double mutants failed to target ovules and exhibited impaired pollen fertility (Lu et al., 2011). *AtCHX17*, expressed in roots, appears to have a role in K^+ homeostasis as mutants had decreased K^+ content (Cellier et al., 2004). *CHX17* and *CHX20* were able to promote growth of alkaline-sensitive yeast strains on medium at pH 7.5 (Maresova and Sychrova, 2006; Padmanaban et al., 2007). However, their transport activity, membrane localization and cellular roles remain unclear.

Here, I have used yeast and *E. coli* as model organisms to distinguish between shared and isoform-specific activities of Arabidopsis *CHX16-20*. These studies provide evidence for dissimilar roles of CPA1 and CPA2 members of cation/proton exchangers and reveal the complexity of multiple plant CHX transporters. I show that CPA2 members transport K^+ and appear to modulate K^+ and pH homeostasis of diverse intracellular organelles in response to external conditions.

C. MATERIALS AND METHODS

C.1. Yeast, bacterium and plant

Saccharomyces cerevisiae strains used here are shown in Table A-II-1. Untransformed strains were grown in YPAD medium. *Escherichia coli* strain LB2003 (*trkAΔ, kup1Δ, kdpABCDEΔ*) (Stumpe and Bakker, 1997; Lu et al., 2011) were grown in YTMK medium at pH 7.3 (Table AII-7B). *Arabidopsis thaliana* (Col-0) plants were grown on Miracle-Gro® potting mix with continuous light at 50 μE m^{-2} s^{-1}, 21°C and 65% humidity.

C.2. cDNA cloning and plasmid preparation

CHX15 to *CHX19* ORF were PCR-amplified (Table A-II-2) from cDNA obtained by reverse-transcription of seedling RNA and cloned into Gateway pDONR221 as described for *CHX20* (Padmanaban et al., 2007). *CHX17* was amplified from a cDNA clone in pSMCHX17. DNA was recombined into entry and destination vectors for expression in yeast (Table A-II-3, A-II-4) using Gateway LR Clonase II Enzyme Mix (Table A-II-5). For empty vector, a 90-bp sequence (Table A-II-3) was inserted into Gateway pENTR/D-TOPO. Plasmid was amplified in *E. coli* strain DH5α (Invitrogen 18265-017) and purified with miniprep kit (Qiagen 27106). For expression in *E. coli*, *CHX17* and *CHX20* were amplified from entry vectors, pECHX17 and pECHX20 (Table A-II-3), using I-proof DNA polymerase (Biorad 172-5331) and suitable primers (Table A-II-6) and subcloned in plasmid pPAB404 (Burrman et al., 1995). Plasmids were amplified in *E. coli* NEB10β (NEB C3019H), and purified as above.

C.3. Yeast transformation and functional assay

Yeasts were transformed with the Li acetate method (Gietz and Schiestl, 2007) and selected on YNB medium containing adenine and required amino acids at pH 5.8. Growth was synchronized in YNB without carbon source unless otherwise indicated. Cells were normalized in water or K^+-free YNB to A_{600} of 0.2. Five µl of each serial dilution was spotted onto YNB or SDAP medium with 2% glucose or 2% galactose (Table A-II-7A), and incubated at 30^{o}C for 3-5 d. Drop-test media had 20 mM MES and pH was adjusted to 7.5 with arginine or to acidic pH's with glutamic acid. K^+ concentration was adjusted with KCl.

C.4. pH_{cyt} and pH_{vac} determination

To monitor cytosolic pH, I used a pH-sensitive GFP variant, superecliptic pHluorin (GB #AY533296) obtained from Dr. Miesenbock (Yale University). A destination vector (pDYpH) harboring *pHluorin* was generated with or without a *CHX* gene by PCR-directed *in vivo* homologous recombination in yeast (Oldenburg et al., 1997) (Fig. A-II-2A) using primers shown in Table A-II-8. To measure cytosolic pH, an aliquot of normalized cells were mixed with YNB media supplemented with 2% glucose at varied pH and K^+ concentration. The plate was immediately placed in a multimode plate reader (BMG FLUOstar Optima model, BMG Labtechnologies) set to 30^{o}C. Emission at 460 nm (F_{460}) and 510 nm (F_{510}) were read using excitation at 400 nm. F_{510}/F_{460} was converted to pH units using a pH calibration curve as described by Brett et al. (Brett et al., 2005b).

To estimate vacuolar pH (Plant et al., 1999), cells were loaded with 50 µM BCECF-AM (2′,7′-Bis(2-carboxyethyl)-5(6)-carboxyfluorescein acetoxymethyl ester;

Sigma B8806). The ratio of fluorescence at 530 nm was determined at F_{ex492}/F_{ex460} and converted to pH units using a pH calibration curve (see appendices section A.1.c).

C.5. Measuring carboxypeptidase Y secretion

Twenty µl normalized cells were added to white opaque ELISA plate (Pierce 15042) containing 180 µl of YNB-Galactose media pH 5.5 supplemented with 4 mM K_2SO_4 or 8 mM KOH (pH 7.3). Plates were incubated at 30^oC to early log phase. Cells were removed and CPY attached to plates were determined using mouse anti-CPY (1:1000, Invitrogen A-6428), followed by anti-mouse IgG conjugated with horseradish peroxidase (Thermo Scientific 31430). Chemiluminescence from 10 cycles were pooled. Relative luminescence units were normalized to cell density at A_{600} (see appendices section A.1.d).

C.6. *E. coli* growth and $^{86}Rb(K^+)$ transport

E. coli strain LB2003 was transformed with pPAB404 or vector with *KAT1* (Uozumi et al., 1998) or a *CHX* by heat shock. Transformants were selected on YTMK or SGM-KN medium (Table A-II-7B) with 50 µg/ml ampicillin (Tsunekawa et al., 2009). Cell growth at A_{600} was tested on medium with 50 µg/ml ampicillin, 0.5 mM IPTG and varied cations or pH (see appendices section A.1.f). ^{86}Rb (K^+) transport was determined by filtration using 0.45 µm nitrocellulose membrane (Whatman Protran BA85). Freshly-transformed cells were K^+-depleted for 2 h and normalized. A typical reaction of 750 µl contained cells at A_{600} 0.4 (~$2.5x10^8$ cells/ml), 0.5 mM IPTG, 0.6 mM RbCl, ^{86}Rb (0.5 µCi/ml) in a 0.25X basal SGM with 80 mM glycerol, 10 mM MES and 10 mM MOPS pH 6.2. Cells and ^{86}Rb were added to start the reaction, and an aliquot was counted to convert dpm to nmole.

C.7. Transfection of plant protoplasts

Cells without cell walls were isolated from 3-week-old leaves, and transfected by the PEG-Ca method (Yoo et al., 2007; Li et al., 2008)**.** Plasmids containing *GFP* or *RFP* fusion constructs are shown in Table A-II-9. Transfected cells were incubated in the dark at 22 ^{o}C for 18-24 h. Efficiency of transformation with a single gene is $\geq$ 50% and with two genes is less due to differential signals and gene expression (see appendices section A.1.g).

C.8. Microscopy

Fluorescent proteins in cells were examined with a Zeiss LSM510 confocal microscope (Carl-Zeiss, Germany) and C-Apochromat 63x/1.2 W corr. lens. Five µl were dropped onto a slide using two 0.5 mm parafilm strips as spacers between slide and cover glass. To enhance cell density, protoplasts were concentrated > 10-fold by centrifugation. Filter sets for excitation (Ex) and emission (Em) were: 488 nm/BP505-530 nm for GFP; 543 nm/BP560-615 nm for RFP; 543 nm/LP650 nm for chlorophyll, and 633 nm for bright field. Signals were captured in multi-channel mode. Images were analyzed and processed in Zeiss LSM image browser (Carl-Zeiss, Germany). Yeast expressing *GFP* were grown overnight in YNB medium, pelleted and incubated in YPAD for 4 h at 30^{o}C. Before microscopy, cells were incubated for 10 min in 10 µM FM4-64 (Invitrogen T-3166), washed with 2% sucrose, and suspended in 0.05% agarose. Filter set for FM4-64 was 488 nm (Ex) /LP650 nm (Em).

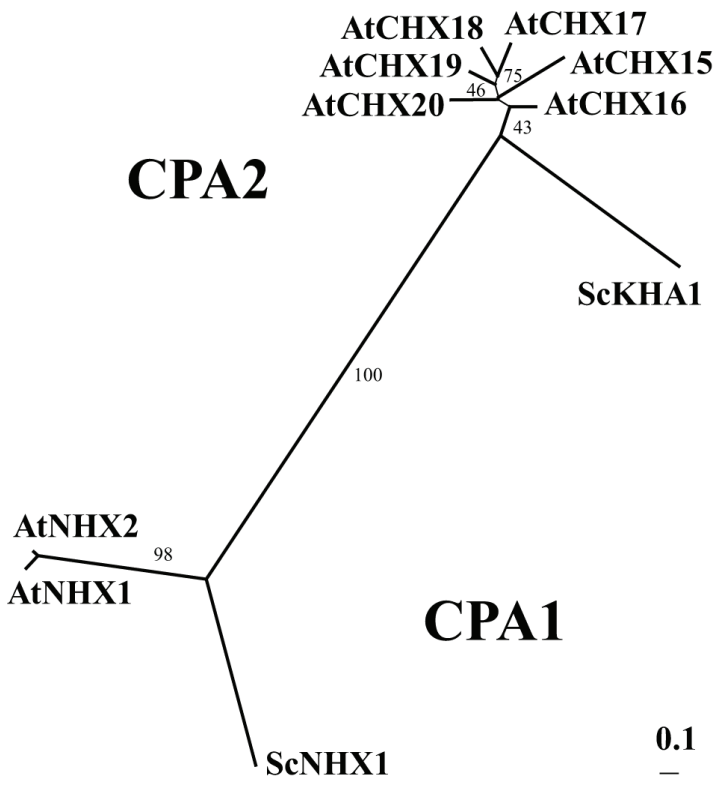

Fig. II-1. Arabidopsis CHX15-20 are homologs of yeast KHA1.

AtCHX15-20 and ScKHA1 (YJL094C) form a cluster within CPA2 family, and ScNHX1 (YDR456W), and AtNHX1-2 (At5g27150, At3g05030) cluster within CPA1 family. AtCHX genes identified by AGI no. At2g13620 (CHX15), At1g64170 (CHX16), At4g23700 (CHX17), At5g41610 (CHX18), At3g17630 (CHX19), and At3g53720 (CHX20) encode proteins of 86.9-91.5 kDa (Fig. A-II-1). Alignment was processed by Clustal X v.2.0. Values indicate the number of times (%) that each branch topology was found in 10,000 replicates in an unrooted tree.

D. RESULTS

D.1. Phylogenetic Relationship of AtCHX, ScKHA1 and NHX1

According to cDNA sequences, the deduced proteins of CHX15 to CHX20 have a hydrophobic domain with 12 transmembrane spans at the amino terminal half (427-433 residues) and a hydrophilic C tail of 372-409 residues (Fig. A-II-1) (Sze et al., 2004). Phylogenetic analysis has revealed that CHX15-20 are tightly clustered away from yeast KHA1 within the CPA2 family (Fig. II-1); however, the CHX cluster and ScKHA1 are both clearly separated from the CPA1 family represented by yeast and Arabidopsis NHX or $\underline{Na}^+/\underline{H}^+$ e<u>x</u>changers (Brett et al., 2005). Although ScKHA1 has only 38-41% overall similarity to CHX15-20, the transmembrane domain shared 60% homology (Fig. A-II-1, Table A-II-10). Thus, ScKHA1 is considered orthologous to AtCHX15-20.

D.2. AtCHX16-20 confer yeast growth at alkaline pH

I tested CHX15-20 function in a panel of yeast mutants variously defective in Na^+ extrusion and $K^+(Na^+)/H^+$ antiport (Fig. II-2A). Cation/proton antiporters maintain cellular pH homeostasis and growth in response to large perturbations in external pH. Thus, yeast strain KTA40-2 proliferated at pH 5.6, but failed to grow at pH 7.5. I showed that KTA40-2 expressing *CHX16*, *17*, *18*, *19* or *20* recovered tolerance to alkaline pH, similar to AXT3 strain that expresses the endogenous *ScKHA1* (Fig. II-2B, right). Similar results were obtained when *CHX17* or *CHX20* was expressed in single *kha1Δ* mutant at low K^+ (Fig. II-2E). Alterations in membrane potential and membrane trafficking significantly influence sensitivity to the cationic drug hygromycin B (Perlin et al., 1988; Banuelos et al., 2010). KTA40-2 was shown to be sensitive to HygB (100 μg/ml) at pH 5.6 (Fig. II-2B, middle). Interestingly, only CHX17, 18 or 19 conferred

Fig. II-2. Differential tolerance to alkaline pH and hygromycin B of yeast expressing CHXs and NHX1.

A) Yeast strains. Wild-type or disrupted genes are denoted as + and -, respectively. Genes and corresponding proteins are *ENA1-4*, PM Na^+-extrusion pumps; *NHA1*, PM Na^+/H^+ antiporter; *NHX1*, PVC Na^+/H^+ exchanger; *KHA1*, Golgi K^+/H^+ antiporter; *TRK1/2,* PM K^+ uptake pathways and *TOK1,* a K^+ channel.

B) Differential activities. Yeast strain KTA40-2 harboring pDR196-derived empty vector (EV*)* or vector with *CHX15-20* were normalized and 5 µl of each serial dilution were dropped on medium (far left) at pH 5.6 or 7.5, and incubated 3 d. KHA1 refers to strain AXT3. Hygromycin B (HygB) was 100 µg/ml.

C) pH and HygB. Yeast strain KTA40-2, AXT3 and LMB01 expressing pYES52-derived vector (EV) or vector with *CHX17* were prepared as above and tested at pH 6 or 7.5. ScNHX1 refers to strain LMB01. HygB was 125 µg/ml.

D) External pH and low K^+. Strain KTA40-2 and AXT3 expressing pDR196-derived vector (EV) or vector with *CHX17*, *CHX20*, *AtNHX1*, or *AtNHX2* were normalized, and tested on medium with 0.6 mM K^+.

E) Wild-type strain (KHA1) or *kha1* single mutant harboring pYES52-derived vector (EV) or vector with *CHX17* or *CHX20* were normalized with K^+-free YNB. Cells were spotted on medium containing 0.6, 10 or 100 mM K^+ at pH 5.8 or 7.5.

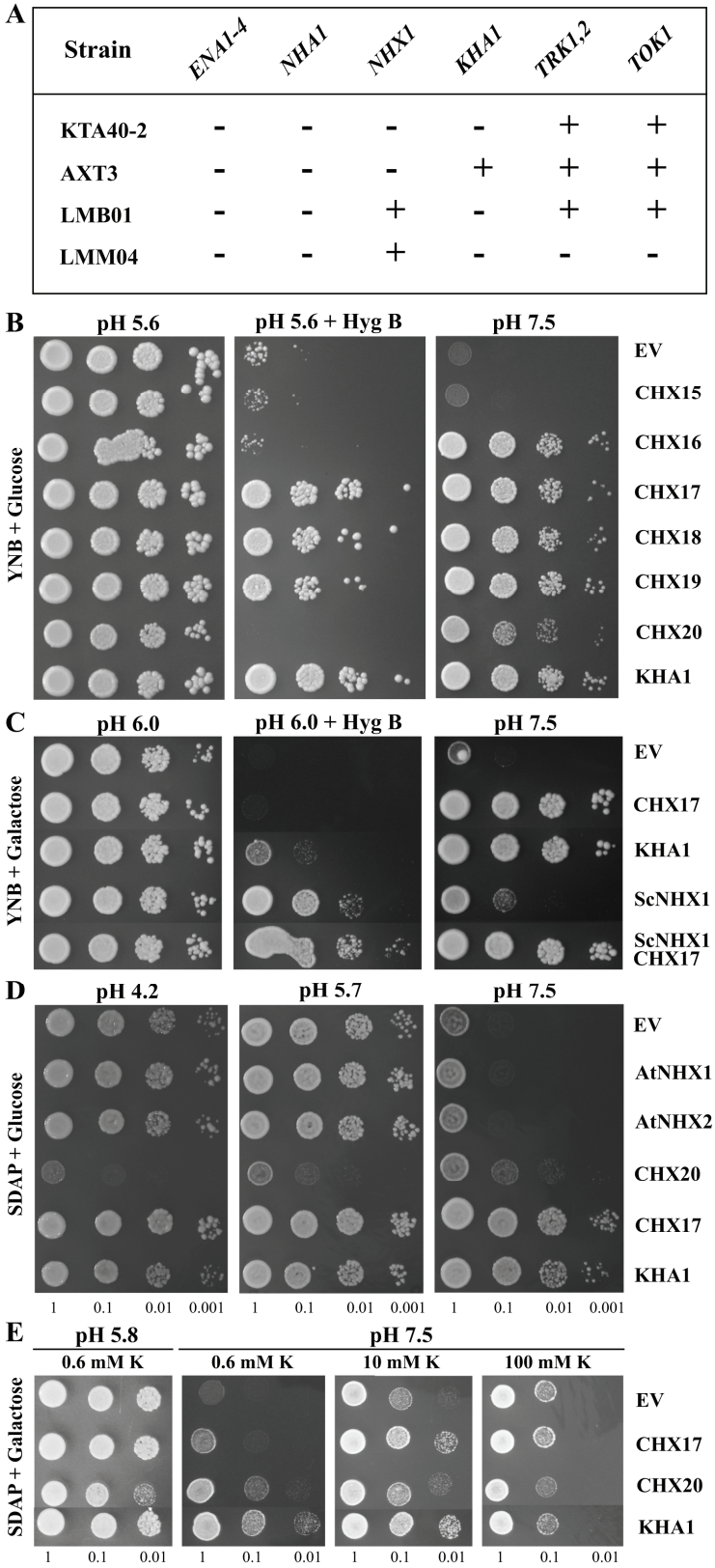
A
Strain
ENA1-4
NHA1
NHX1
KHA1
TRK1,2
TOK1
KTA40-2 - - - - + +
AXT3 - - - + + +
LMB01 - - + - + +
LMM04 - - + - - -
B
pH 5.6
pH 5.6 + Hyg B
pH 7.5
YNB + Glucose
EV
CHX15
CHX16
CHX17
CHX18
CHX19
CHX20
KHA1
C
pH 6.0
pH 6.0 + Hyg B
pH 7.5
YNB + Galactose
EV
CHX17
KHA1
ScNHX1
ScNHX1 CHX17
D
pH 4.2
pH 5.7
pH 7.5
SDAP + Glucose
EV
AtNHX1
AtNHX2
CHX20
CHX17
KHA1
1 0.1 0.01 0.001 1 0.1 0.01 0.001 1 0.1 0.01 0.001
E
pH 5.8
pH 7.5
0.6 mM K
0.6 mM K
10 mM K
100 mM K
SDAP + Galactose
EV
CHX17
CHX20
KHA1
1 0.1 0.01 1 0.1 0.01 1 0.1 0.01 1 0.1 0.01

resistance to HygB (Fig. II-2B), similar to ScKHA1, whereas CHX15, CHX16 and CHX20 did not. CHX15 was unable to restore growth under any of the conditions tested. These results suggest that multiple *CHX* genes share a role in pH homeostasis, although they differ in the ability to confer hygromycin B resistance.

D.3. AtCHX17 and AtNHX1 have distinct, yet overlapping, functions

Yeast strains with endogenous *ScNHX1* but lacking *ScKHA1* (LMB01) grew poorly on alkaline medium, compared to strains expressing either *AtCHX17* (in KTA40-2) or *ScKHA1* (AXT3) (Fig. II-2C, right). Furthermore, alkaline pH sensitivity of KTA40-2 could not be rescued by Arabidopsis *NHX1* or *NHX2* (Fig. II-2D). Thus, CPA2 transporters (AtCHX17 and ScKHA1) were more effective than CPA1 transporters (ScNHX1, AtNHX1, AtNHX2) in supporting yeast growth at alkaline pH. LMB01, expressing endogenous *ScNHX1,* clearly showed stronger resistance against HygB (Fig. II-2C, middle) compared to cells expressing *AtCHX17* or *ScKHA1*. Interestingly, cells expressing both *CHX17* and endogenous *ScNHX1* showed enhanced HygB resistance suggesting an additive or cooperative effect by these two activities. These results indicate that ScKHA1 (CPA2) and ScNHX1 (CPA1) are involved in separate functions in yeast and that AtCHX17 is a functional ortholog of ScKHA1.

D.4. Growth rescue by AtCHX16-20 of K^+ uptake-deficient mutant depends on pH_{ext}

LMM04, a K^+ uptake-deficient mutant, showed little or no growth on 8 mM K^+ (Fig. II-3A); though growth of *TRK1/2*- and *TOK1*-positive strains (KTA40-2 and LMB01) was vigorous (Fig. II-3C), suggesting a crucial role of K^+ uptake in restoring growth that was optimal at pH 5.6. Intriguingly, mutants expressing *CHX17*, *CHX18* or *CHX19* showed enhanced growth especially at pH 7.5 (Fig. II-3A). Furthermore, *CHX16*

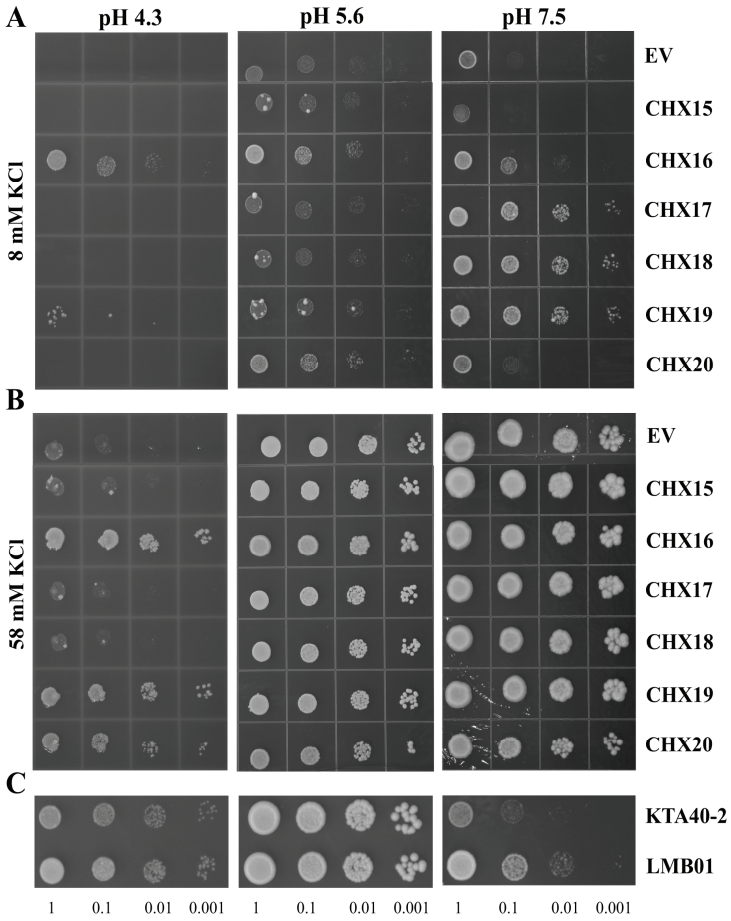

Fig. II-3. CHX restored growth of K^+ uptake-deficient yeast depends on external $[K^+]$ and pH.

Effect of pH and KCl at 8 mM (A) and 58 mM (B). K^+ uptake-deficient yeast strain LMM04 harboring pDR196-derived vector (EV), or vector with *CHX15-20*, were grown in YNB with 100 mM KCl, normalized, 5 µl of each serial dilution was dropped on medium at pH 4.3, 5.6 or 7.5, and incubated 5 d. C) K^+ uptake-proficient strain LMB01 and KTA40-2 growing on medium with 8 mM KCl at indicated pH's after 3 d.

expression improved mutant growth partially at 8 mM $[K^+]_{ext}$ at acidic or alkaline pH's, but growth was fully restored at pH_{ext} 4.3 at 58 mM K^+ (Fig. II-3B). Yet CHX19 rescued mutant growth at pH 7.5 under 8 mM K^+, and also at pH 4.3 when K^+ was 58 mM, but it was ineffective at pH 5.6. In contrast, CHX20 enhanced growth at pH 4.3 (58 mM K^+) and 5.6 (8 mM K^+) but not at pH 7.5 (Fig. II-3A). The differential effectiveness in supporting growth suggest that CHX17, 18 or 19 facilitated K^+ homeostasis under alkaline conditions, whereas, CHX16 or CHX20 was needed under an acidic environment.

D.5. CHX17 and CHX20 exert differential effects on cytosolic and vacuolar pH in yeast

A pH calibration curve shows that the responsive range of pHluorin (Miesenbock et al., 1998), is between pH 6.5 to pH 8.0 (Fig. II-4A) which agrees with the apparent pK_a of 7.6 for the superecliptic pHluorin (Schulte et al., 2006). Furthermore, yeast mutants co-expressing *pHluorin* and *CHX17* or *CHX20* retained their activity as shown by their ability to restore growth at alkaline pH (Fig. A-II-2B).

I tested whether acidic pH_{ext} and $[K^+]_{ext}$ might alter pH_{cyt}. Basal pH_{cyt} of yeast strain AXT3 carrying the wild-type *KHA1* or KTA40-2 strain disrupted in *kha1* was estimated to be pH 7.2 after 30 min incubation at pH 5.6 (Fig. II-4B). Expression of *CHX17* in KTA40-2 did not significantly change pH_{cyt}. However, pH_{cyt} in the mutant expressing *CHX20* was lowered to pH 7.06 suggesting acidification resulting from activity of CHX20. When the K^+ level was lowered to 0.1 or 0.8 mM, basal pH_{cyt} of *kha1* mutant dropped to about pH 6.9 and 7.1, respectively (Fig. A-II-3A, 3C).

Fig. II-4. CHX20 but not CHX17 altered cytosolic and vacuolar pH in yeast.

A) pH_{cell} calibration. Yeast strain KTA40-2, AXT3 and LMB01 harboring *pHluorin* in pYES52 derived- vector (EV) or vector with *CHX* were added to buffers with ionophores at indicated pHs. Results from four strains at 10, 20 and 30 min were similar and pooled. pHluorin fluorescent (F_{510}/F_{460}) is related to pH_{cell} 6.5-8. Bars represent SEM (n=72).

B) pH_{ext} 5.6 on cytosolic pH. Yeast strain KTA40-2, AXT3 and LMB01 harboring *pHluorin* in empty vector (EV) or vector with *CHX* were added to K^+-free YNB with 8 mM KCl at pH 5.6. F_{510}/F_{460} was recorded at 10, 30, and 50 min. Data are from three independent lines. Bars represent SEM (n=36).

C) pH_e 8.0 on cytosolic pH tested as in B.

D) pH_{in} calibration of BCECF signals. Cells loaded with BCECF were incubated in buffers at pH 5.0 to 7.5 containing CCCP. Fluorescence F_{ex492}/F_{ex460} is related to *in situ* pH_{in}. Data from four strains at 20, 30 and 40 min were pooled. Bars represent SEM (n = 36).

E) pH_{ext} 5.6 on vacuolar pH. KTA40-2 or LMB01, carrying ScNHX1 (ScNHX1), were transformed with empty vector (EV), *CHX17* or *CHX20*. KHA1 refers to strain AXT3. Cells loaded with 50 μM BCECF were added to K^+-free YNB with 8 mM KCl at pH 5.6. Fluorescence (F_{Ex492}/F_{Ex460}) were taken at 10, 30 and 50 min. Data are from two independent lines. Bars represent SEM (n=12).

F) pH_{ext} 8.0 on vacuolar and intracellular pH tested as in E.

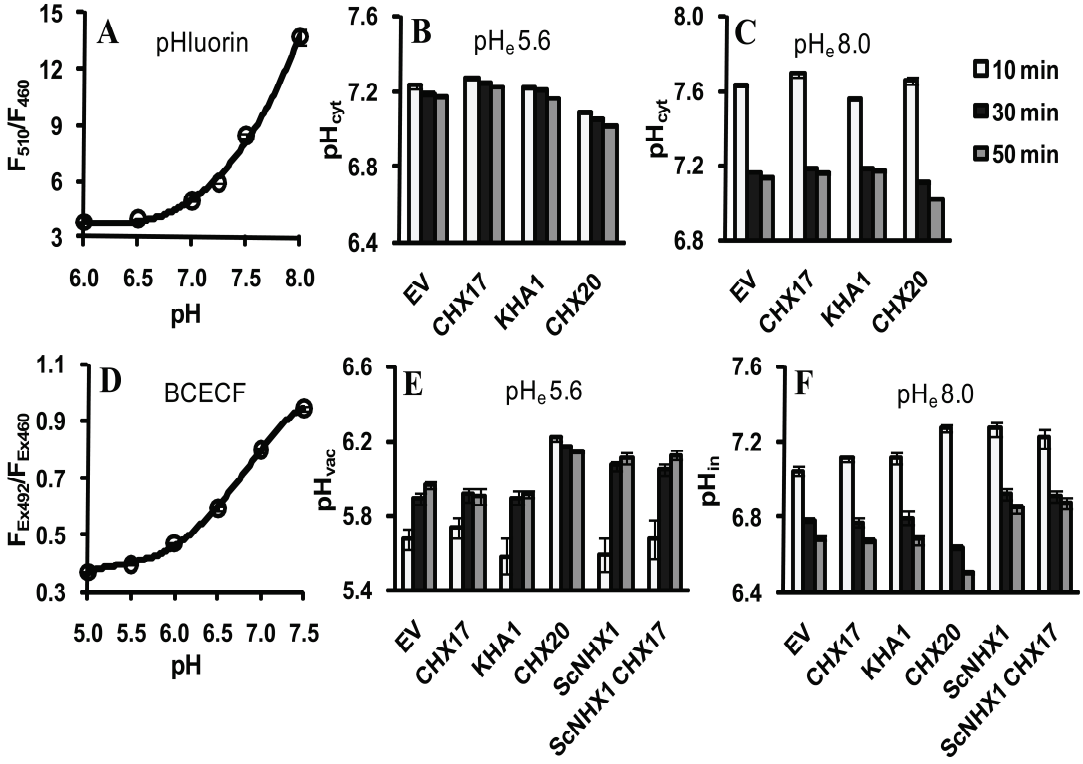
A
pHluorin
F_{510}/F_{460}
pH
B
pH_e5.6
pH_{cyt}
C
pH_e8.0
pH_{cyt}
10 min
30 min
50 min
EV
CHX17
KHA1
CHX20
D
BCECF
F_{Ex492}/F_{Ex460}
pH
E
pH_e5.6
pH_{vac}
F
pH_e8.0
pH_{in}
EV
CHX17
KHA1
CHX20
ScNHX1
ScNHX1 CHX17

Expression of either *KHA1*, *CHX17*, *NHX1* (LMB01 strain) or both *NHX1* and *CHX17* did not change pH_{cyt} significantly.

After cells were exposed to alkaline pH_{ext} (Fig. II-4C), the pH_{cyt} of all strains initially became basic (~pH 7.6); however within 30 min, the pH_{cyt} of most strains reached a steady pH of 7.16-7.18. Similar to the acid pH shift, the mutant expressing *CHX20* showed a slightly lower pH_{cyt} of pH 7.11 which dropped to pH 7.01 after 50 min (Fig. II-4C). However, at $[K^+]_{ext}$ of 0.1 or 0.8 mM, the pH_{cyt} dropped from ~7.4 to 7.05 and 7.15, respectively in all strains (Fig. A-II-3B, A-II-3D) except in mutants expressing *CHX20* which had a pH_{cyt} of 6.88 at 50 min (Fig. A-II-3B). Furthermore, only CHX20 significantly acidified pH_{cyt} in a single *kha1* mutant (Fig. A-II-11), suggesting that cytosolic acidification was directly mediated by CHX20. These results indicate that i) KHA1, CHX17, or NHX1 did not affect pH_{cyt} significantly at the external pH conditions tested; ii) *CHX20*-expressing cells consistently acidified their pH_{cyt} by up to 0.2 units especially when $[K^+]_{ext}$ was limiting; and iii) adequate levels (8 mM) of K^+ seemed critical for maintaining a steady pH_{cyt} homeostasis.

Vacuolar pH was estimated using BCECF, which accumulates within yeast endosomes and vacuole (Plant et al., 1999; Ali et al., 2004). BCECF fluorescence in H^+-permeabilized cells showed an apparent pK_a between pH 6.5 to 7.0 (Fig. II-4D), consistent with a previous report in yeast (Plant et al., 1999). At acidic pH_{ext}, the resting pH_{vac} of strains KTA40-2 and AXT3, except for *CHX20*-expressing cells, had reached a steady pH of 5.9 after 30 min (Fig. II-4E). Expression of *CHX17* or *KHA1* did not alter yeast pH_{vac}. However, expression of *NHX1* (LMB01 strain) significantly raised pH_{vac} to 6.1 (Fig. II-4E) as previously reported (Ali et al., 2004). Surprisingly, expression of

CHX20 also elevated pH_{vac} to 6.13 after 50 min. Unlike cytosolic pH, vacuolar pH was slightly altered by external K^+. When K^+ was 0.1 mM, basal pH_{vac} of *kha1* mutant remained at ~pH 5.9 (Fig. A-II-3E). Expression of *KHA1* or *CHX17* did not significantly change pH_{vac}. Remarkably, expression of *CHX20* further alkalinized pH_{vac} to 6.28 (Fig. A-II-3E) but this alkalinization was reduced in strain LMB01 as observed by pH_{vac} 6.03 at limiting K^+ concentration.

At alkaline medium, BCECF signal reflects the average intracellular pH (pH_{in}), as the dye was localized at both cytosol and vacuole. The pH_{in} of cells expressing *CHX17* or *KHA1* was pH 7.1 initially, but dropped to 6.6 after 1 h. Yet, expression of *NHX1* resulted in a pH_{in} of 0.2 units higher. As these strains maintained a similar pH_{cyt} (Fig. II-4C, A-II-3B, A-II-3D), the results infer that only NHX1, alkalinized pH_{vac}. The role of CHX20 in yeast is less certain, as it altered both pH_{cyt} and pH_{vac}. These results showed that CHX17 or KHA1 had no effect on regulating bulk vacuolar pH when pH_{ext} was either acidic or alkaline.

Together, the ability of CHX17 or KHA1 to confer yeast growth tolerance on alkaline medium was not accompanied by alteration of bulk cytosolic pH or vacuolar pH. NHX1 alkalinized vacuolar pH consistent with prior reports (Ali et al., 2004; Brett et al., 2005b). CHX20, however, differed as cells expressing this gene consistently showed a more acidic pH_{cyt} and a more basic pH_{vac}.

D.6. CHX17-mediated K^+ uptake in *E. coli*

I was unable to detect significant changes in K^+ ($^{86}Rb^+$) fluxes resulting from expression of *CHX17* or *CHX20* in yeast LMM04 cells at either pH 7.5 or pH 4.5 (Fig. A-II-4), therefore, I expressed *CHX17* and *CHX20* in *E. coli* strain LB2003 that is defective

Fig. II-5. CHX17 or CHX20 mediated K^+ uptake into *E. coli*.

A) Cell density at varied K^+ concentration. *E. coli* strain LB2003 harboring pPAB404 vector (EV), or vector with *CHX17*, *CHX20*, or *KAT1* were starved for K^+ in basal SGM medium at pH 6.6 for 2 h. Cells were added to SGM-MES-MOPS medium at pH 6.6 with 1-8 mM K^+ and incubated 14 h at 30°C.

B) pH_{ext} on cell growth at18 h . Same as A, except medium contained 2 mM K^+ at varied pH's. Bars represent SEM (n=4).

C) Time-course of Rb^+ uptake. IPTG was added to medium during K^+ starvation. Reaction mixture consisted of 2 mM RbCl at pH 6.2 and cells expressing vector (EV –x-), or vector harboring *CHX17* (X17, -●-), *CHX20* (X20, -▲-) or *KAT1* (-o-). An aliquot was filtered and washed at indicated times. Data are from two independent experiments.

D) Rb^+ uptake at pH 6.2 or 6.6. Reaction was similar to C. Uptake at 30 min is shown. Bars represent SEM (n=2). E) Cations reduced CHX17-dependent Rb^+ uptake. Cells expressing *CHX17* were prepared as in C and normalized. Reaction mixture consisted of 0.6 mM RbCl (0.5 μCi/ml ^{86}Rb) and ~$2.5x10^8$ cells/ml in SGM-MES-MOPS at pH 6.2 plus one cation-Cl (Li – Δ -, Na -○- , K -▲-, Rb -●-, Cs -■-, NH_4 -□-) at near 0,1, 3, 10, or 30 mM. ^{86}Rb uptake was measured at 30 min. Uptake without added cation (100%) was 0.8 nmol Rb^+ per 10^8 cells.

F) Cations on CHX20-dependent uptake. Method is same as E. Uptake without added cation (100%) was 2.4 nmol Rb^+ per 10^8 cells. Data are from 2 independent experiments. Bars represent SEM (n=2).

G) CCCP on Rb^+ uptake at pH 6.2 versus pH 7.2. Assays were similar to C, except cells were incubated with CCCP at 0-30 μM for 30 min. Data are from two independent experiments. Data of KAT1 is representative of three independent experiments. Bars represent SEM (n=2).

H) Ba^{2+} decreased *E. coli* growth supported by CHX17 or KAT1. Cells expressing vector only or *CHX17*, *CHX20* or *KAT1* were incubated in medium containing 5 mM K^+ at pH 6.6 plus 5 mM choline-Cl, 1.25 mM $BaCl_2$, or 5 mM CsCl for 18 h. Bars represent SEM (n=4).

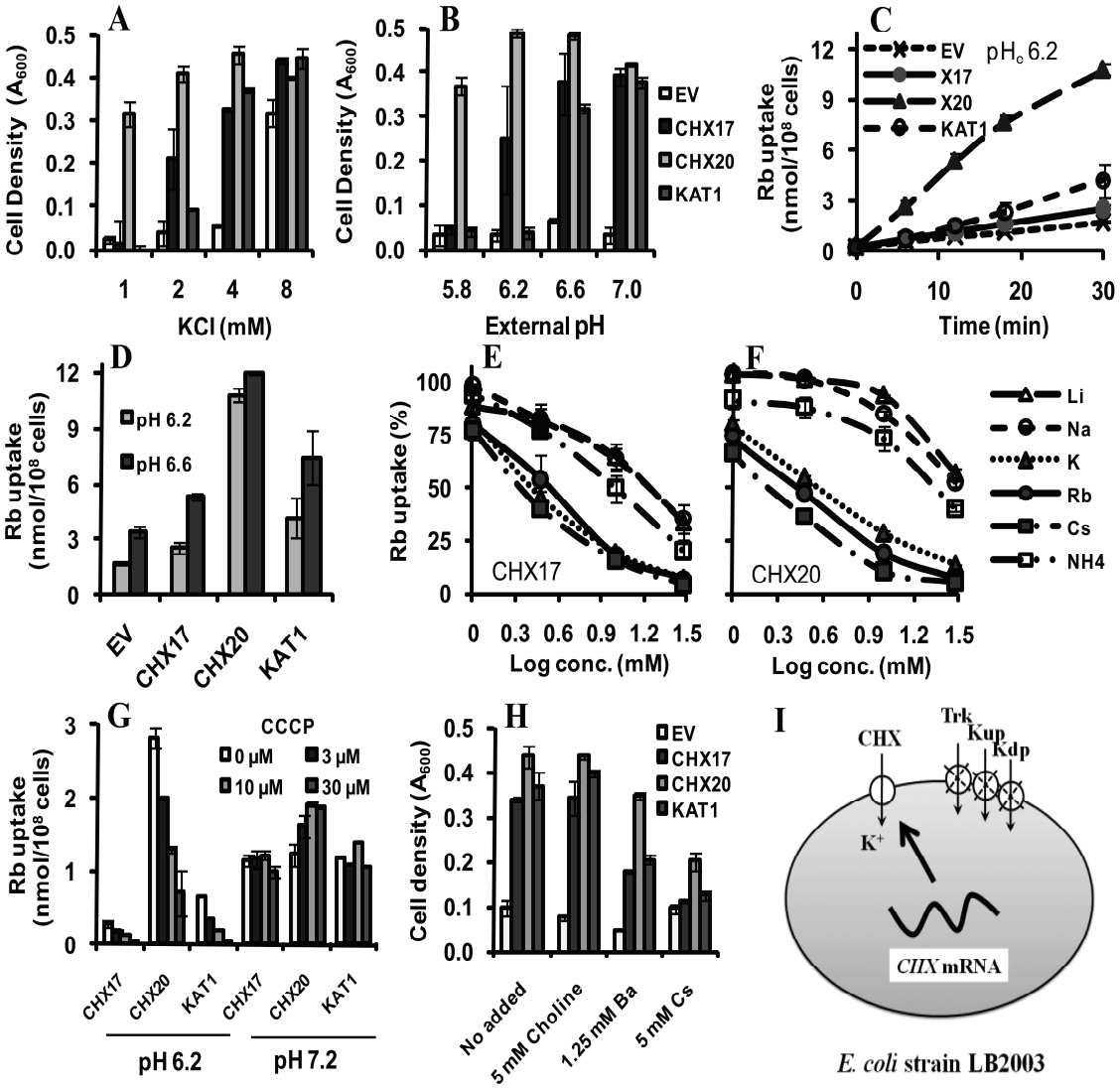
A
Cell Density (A600)
KCl (mM)
B
External pH
EV
CHX17
CHX20
KAT1
C
Rb uptake (nmol/10^8 cells)
pHo 6.2
X17
X20
KAT1
Time (min)
D
pH 6.2
pH 6.6
E
Rb uptake (%)
CHX17
Log conc. (mM)
F
CHX20
Li
Na
K
Rb
Cs
NH4
G
CCCP
0 µM
3 µM
10 µM
30 µM
pH 6.2
pH 7.2
H
No added
5 mM Choline
1.25 mM Ba
5 mM Cs
I
CHX
Trk
Kup
Kdp
K+
CHX mRNA
E. coli strain LB2003

in three K^+-uptake systems (Stumpe and Bakker, 1997). In this system, heterologously-expressed membrane protein would be inserted in the plasma membrane (Uozumi, 2001). Both CHX17 and CHX20 restored bacterial growth on YTM medium containing 1-4 mM K^+ at pH 6.6 (Fig. A-II-5A). Increasing concentrations of K^+ and Rb^+, but not Na^+, enhanced growth of cells harboring CHX17, CHX20 or KAT1 at pH 5.5 (Fig. A-II-5B), indicating that Rb^+ can partially substitute for K^+. KAT1 is an inward rectifying K^+ channel from Arabidopsis (Schachtman et al., 1992), and serves as a positive control.

Using SGM medium (synthetic-glycerol-mannitol) to better control K^+ levels, I showed that CHX17 restored growth of LB2003 strain at 2-4 mM K^+ similar to KAT1. CHX20 was more effective as it increased bacterial growth at 1 mM K^+ (Fig. II-5A). By 8 mM K^+, cells harboring empty vector grew as fast as others, indicating that K^+ is taken up via non-specific pathways. CHX20 rescued bacteria growth at all pHs tested (Fig. II-5B), though CHX17 or KAT1 enhanced growth was near optimal at pH 7.0. These results indicate that growth rescue by CHX17 and CHX20 is influenced differently by external K^+ and pH.

CHX20 mediated $^{86}Rb^+$ uptake at a faster rate than that facilitated by CHX17 or KAT1 at pH 6.2 and 6.6 (Fig. II-5C, II-5D). I chose pH 6.2 for further experiments to minimize non-specific Rb influx. These results demonstrated that CHX17 and CHX20 mediated K^+ uptake in a pH-dependent manner. K^+ or Rb^+ reduced CHX17-dependent ^{86}Rb uptake with an IC_{50} (half maximal inhibitory concentration) of about 2.6 mM, relative to a IC_{50} of 17-36 mM by Li^+ or Na^+ (Fig. II-5E, II-5F, A-II-10). The concentration of Cs^+, Rb^+ and K^+ required to inhibit CHX20-dependent Rb^+ flux (IC_{50}) was 1.5, 2.5 and 3.8 mM, respectively, indicating that CHX20 preferred $Cs^+ > Rb^+ > K^+$. KAT1 also showed a

Fig. II-6. Differential localization of CHX17-CHX20 in endomembranes.

A) Distribution of AtNHX1, CHX17, CHX20 and FM4-64 in yeast. Wt strain FY833 harboring *CHX17, CHX20* or *AtNHX1* fused with *GFP* at the C-terminus were grown in YNB, transferred to YPAD medium and incubated 4 h. Cells were observed after 10 min in 10 μM FM4-64. 'Merged' column shows images of GFP- (column 1) and FM4-64- (column 2) labeled cells shown in bright-field (right). Bar = 2 μm.

B) CHX17 localized to PVC. Plant protoplasts were co-transfected with *CHX17-GFP* or *CHX17-RFP* and a tagged marker. Markers used are Golgi ST-GFP, trans-Golgi network RFP-SYP41, PVC RFP-SYP21, and endosomes GFP-ARA7. Signals were observed at 18-24 h. 'Merged' signals from GFP and RFP are shown at bottom row. Bars = 5 μm.

C) CHX18 and CHX19 localized to PVC whereas CHX20 localized to ER. Protoplasts were co-transfected with *CHX18-GFP*, *CHX19-GFP*, or *CHX20-RFP*, and a marker as in B. CHX17-RFP, Syp22-GFP and HDEL-GFP served as markers for PVC, vacuole and ER, respectively. Bars = 5 μm.

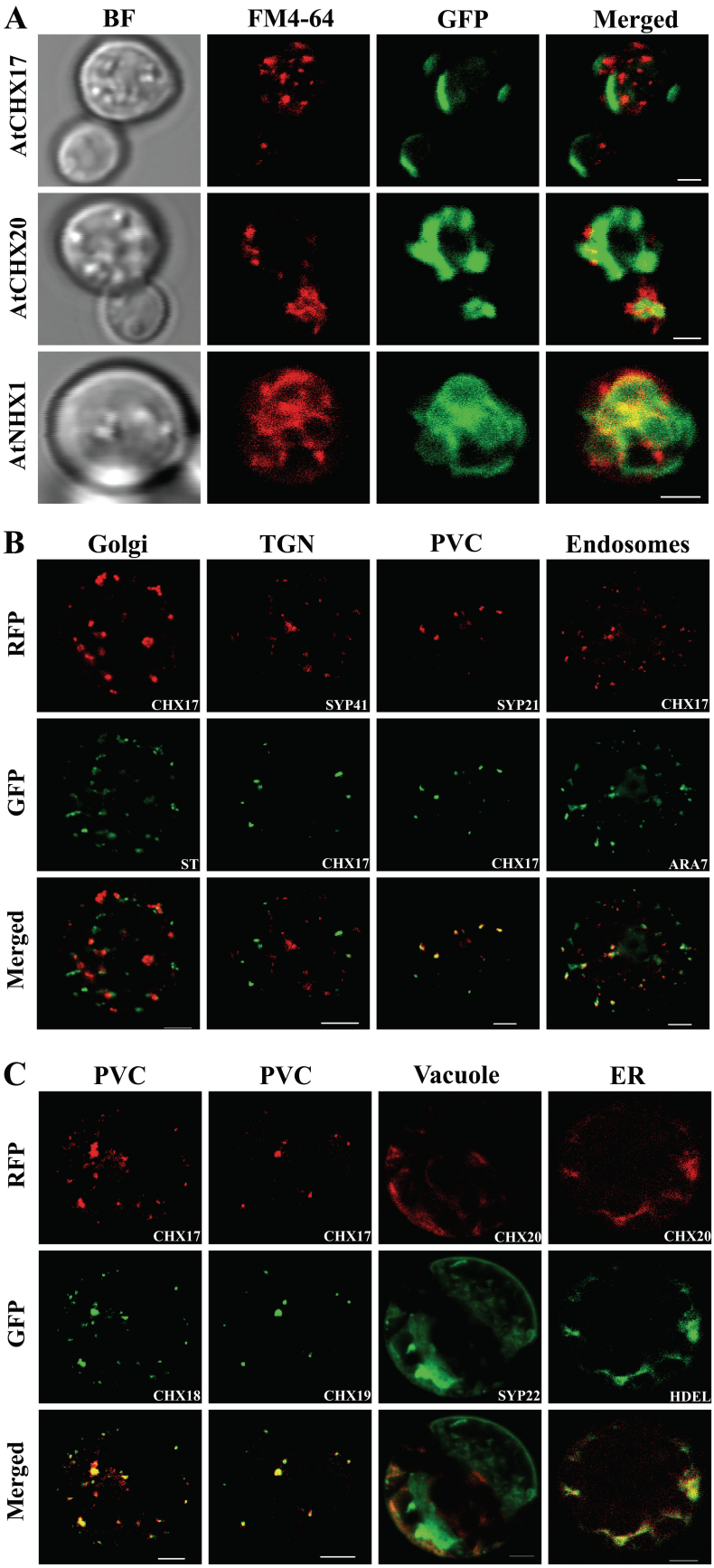
A
BF
FM4-64
GFP
Merged
AtCHX17
AtCHX20
AtNHX1
B
Golgi
TGN
PVC
Endosomes
RFP
GFP
Merged
CHX17
SYP41
SYP21
CHX17
ST
CHX17
CHX17
ARA7
C
PVC
PVC
Vacuole
ER
RFP
GFP
Merged
CHX17
CHX17
CHX20
CHX20
CHX18
CHX19
SYP22
HDEL

slight preference of K^+ over Rb^+ (Fig. A-II-10) based on the IC_{50} of 2.1 and 3.2 mM, respectively, consistent with the study by Uozumi et al. (1995). Thus, CHX17 and CHX20 are monovalent cation transporters with an apparent K_m for K^+ in the low mM range.

CCCP decreased Rb^+ uptake mediated by CHX17, CHX20 and KAT1 (Fig. II-5G) at pH 6.2. Curiously, an increase in Rb^+ uptake in cells harboring CHX20 was observed at pH 7.2 in the presence of CCCP. However, CCCP caused no change in Rb uptake mediated by CHX17 or KAT1. This result would suggest that CHX20-mediated K^+ transport is coupled to a pH gradient, whereas CHX17 dependent K^+ transport is not. Ba^{2+} at 1.25 mM reduced *E coli* growth dependent on CHX17 or KAT1 by 50% relative to the control. Yet Ba^{2+} reduced growth of cells harboring CHX20 by only 20% (Fig. II-5H). Moreover, Cs^+ at 5 mM inhibited CHX17- or KAT1-dependent growth though cells harboring CHX20 grew better than the control. Thus the mode of K^+ transport mediated by CHX17 or CHX20 might differ.

D.7. Localization of CHXs to endomembrane in yeast and in plant cells

All CHXs tagged at the carboxyl end to GFP were shown to restore growth of KTA40-2 mutants on alkaline medium (Fig. A-II-6). Furthermore, resistance to HygB was also retained in cells expressing *GFP*-tagged *CHX17*, *CHX18*, or *CHX19*. Cells expressing *CHX16-GFP* or *CHX20-GFP* were hypersensitive to HygB (Fig A-II-6, middle), as shown before for the untagged protein (Fig. II-2B). These results demonstrate that CHX16-CHX20 tagged at the C-terminal end with GFP retained their native activity.

In wild-type yeast (FY833), CHX17-GFP and CHX20-GFP fluorescence appeared on tubular and reticulate structures (Fig. II-6A). The GFP signal co-localized

poorly with that of FM4-64 (Fig. II-6A) indicating that CHX17 or CHX20 proteins were not associated with the PM, endosomes or vacuole. These patterns suggested that CHX17 and CHX20 were localized to distinct endomembranes. In contrast, AtNHX1-GFP labeled intracellular membranes that were mainly reticulate and partially overlapped with FM4-64.

In plant cells, CHX17-GFP alone showed a punctate pattern (Fig. A-II-7). CHX17 did not co-localize with sialyl transferase or syntaxin 41 (Fig. II-6B), suggesting that CHX17 was not associated with the Golgi or the *trans*-Golgi network (TGN). However, CHX17 co-localized very well with syntaxin 21 and partially with RabF2b or Ara7 (Fig. II-6B) suggesting that CHX17 was in prevacuolar compartments (PVC), a subset of endosomes. Moreover, CHX18 and CHX19 co-localized with CHX17 suggesting that these two proteins were also at the PVC (Fig. II-6C). In contrast, CHX20-RFP gave a reticulate pattern that co-localized with an ER marker (GFP-HDEL) but not with syntaxin 22 (Fig. II-6C). In addition, CHX16-GFP also showed a reticulate pattern (Fig. A-II-7) implying that CHX16 and CHX20 were associated with ER.

D.8. CHX17 or CHX20 altered efficiency of CPY sorting depending on pH_{ext}

I tested if CHX17 or CHX20 had a role in protein sorting. Carboxypeptidase Y (CPY) is normally trafficked from Golgi to the vacuole lumen via the prevacuolar/late endosomal compartment. Cells with the same density were cultured in medium at pH 5.7 or 7.3 and growth was monitored continuously using A_{600} (Fig. A-II-8). Extracellular CPY was determined, and normalized to cell density. The assay was validated with purified yeast CPY with or without yeast cells (LMB01) at pH 5.5 or pH 7.3. pH_{ext} had little to no effect on CPY detection without yeast cells (Fig. II-7A). Yeasts grown at pH

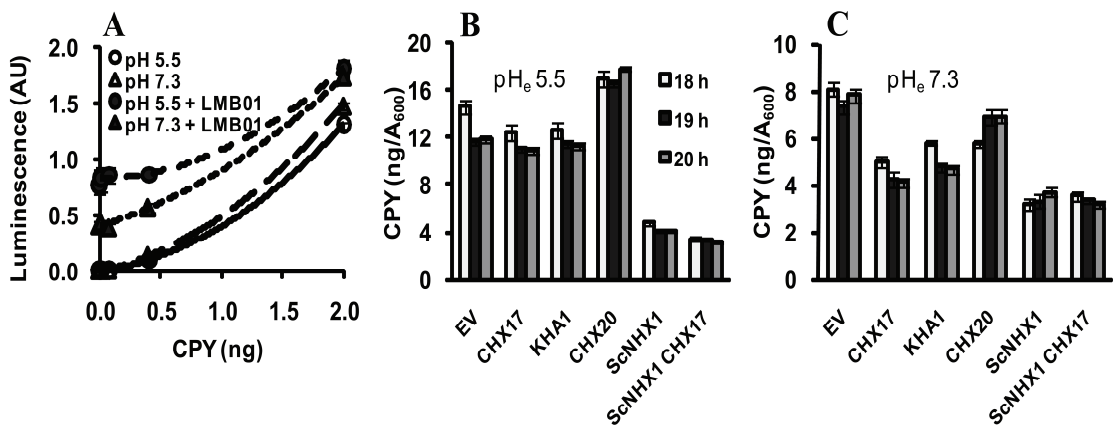

Fig. II-7. CHX17 reduced extracellular carboxypeptidase Y in yeast at alkaline pH.

A) Standard CPY. Purified CPY at indicated amount (ng) was added to an ELISA plate with or without yeast strain LMB01 at pH 5.5 (●, ○) or 7.3 (▲, Δ). After 20 h, cells were removed and CPY was detected by immuno-assay. AU, Arbitrary unit. Bars represent SEM (n=14).

B) Extracellular CPY of yeast at pH_{ext} 5.5. Yeast strain KTA40-2, AXT3 and LMB01 (Fig. II-2A) were transformed with pYES52-derived plasmid alone (EV) or vector with *CHX17 or CHX20*. KHA1 and ScNHX1 refer to strain AXT3 and LMB01, respectively. Yeast was grown in YNB, normalized to A_{600} 0.2 and added to K^+-free YNB with 2% galactose and 8 mM K^+ at pH 5.5. CPY on plate was detected at early log-phase (18-20 h). Signals were normalized to cell density (A_{600}), and converted to ng CPY/A_{600} cells. Data are from 7 replicates of two independent lines. Bars represent SEM (n=14).

C) Extracellular CPY of cells grown at pH 7.3. Experiment was conducted as in B, except the initial A_{600} was 0.8 and pH of the medium was 7.3. Bars represent SEM (n=14).

5.5 showed more CPY in the medium than cells grown at pH 7.3 (Fig. II-7A). This result shows that immuno-detected CPY in the medium is related with extracellular CPY in the medium.

Similar levels of extracellular CPY were detected in KTA40-2 mutants (11.8 ng/A_{600}), mutants expressing *CHX17* (11.0 ng/A_{600}) or *KHA1* (11.3 ng/A_{600}) at pH 5.5 (Fig. II-7B). However strains expressing *NHX1* (LMB01) alone or *NHX1* and *CHX17* showed minimal extracellular CPY (4.0 and 3.3 ng/A_{600}), supporting prior studies that NHX1 is critical for sorting proteins to the vacuole (Bowers et al., 2000; Mukherjee et al., 2006). Thus, CHX17 has little or no additional effect when NHX1 is present in cells growing in acidic medium. However, CHX20 resulted in enhanced secretion of CPY, indicating a perturbation of CPY trafficking.

At alkaline pH_{ext}, mutants expressing *CHX17* or *KHA1* showed reduced extracellular CPY (4.1 or 4.7 ng/A_{600}), relative to 7.8 ng/A_{600} of the KTA40-2 mutant (Fig. II-7C). Expression of *NHX1* with or without *CHX17* (in LMB01 cells) also decreased CPY levels (3.7 or 3.2 ng/A_{600}). These results suggest that protein sorting and membrane trafficking pattern are shifted in KTA40-2 mutants expressing *CHX17* or *KHA1*, resulting in reduced secretion in cells grown at alkaline pH. Thus, CHX17 or KHA1 are effective in altering trafficking patterns in cells in a pH-dependent manner. Curiously, cells expressing *CHX20* did not show a similar reduction in CPY secretion levels at alkaline pH_{ext}, suggesting that it may influence protein sorting in a differential manner.

E. DISCUSSION

E.1. Tolerance to alkaline pH: diversity among 5 CHXs

A striking phenotype of *AtCHX16-20* expressed in KTA40-2 yeast mutants is their ability to restore growth at alkaline pH. This was shown before for AtCHX20 (Padmanaban et al., 2007) and for AtCHX17 (Maresova and Sychrova, 2006); though the mechanistic basis was unknown. Here I show that Arabidopsis CHX17, 18 or 19 is most effective in conferring tolerance to alkaline pH of KTA40-2 mutants, similar to yeast KHA1. By contrast, CHX20 or CHX16 is less effective in conferring alkaline tolerance. Furthermore, cells expressing *CHX17*, *18* and *19* were resistant to hygromycin B, whereas cells expressing *CHX16* or *CHX20* were sensitive or hypersensitive. Importantly, the properties of CHX17 differed from those of ScNHX1 or AtNHX1. ScNHX1 was unable to restore growth of KTA40-2 mutant at alkaline pH; and was more effective in conferring HygB resistance than CHX17, as seen between ScNHX1 and ScKHA1 (Maresova and Sychrova, 2004). The variations observed among five AtCHX's cannot be attributed to unequivalent expression of protein levels:, as (i) the qualitative phenotypes are consistently observed in independent transformants; (ii) GFP-tagged CHX16 through CHX20 at the C terminus are active in conferring alkaline tolerance and are localized to intracellular membranes in yeast; and (iii) CHX17-GFP conferred HygB resistance whereas CHX20-GFP or CHX16-GFP did not. Thus, all five CHX proteins (CHX16 to CHX20) appear to function in pH homeostasis in yeast in a manner distinct from NHX1. Moreover CHX17, CHX18 and CHX19 diverge in activity from CHX16 and CHX20.

E.2. Importance of K^+ in pH homeostasis

Several observations pointed to a role of $[K^+]_{ext}$ in pH homeostasis and in growth of yeast mutants expressing *CHX*: i) CHX17 or CHX20-enhanced growth of single *kha1* mutant at alkaline pH was evident at 0.6-10 mM $[K^+]$ but not at 100 mM (Fig. II-2E); ii) CHX17-19 restored growth of K^+-uptake-deficient mutant LMM04 at pH 7.5 similar to yeast harboring K^+ uptake systems, Trk1/2 and Tok1 (Fig. II-3A, II-3C), and iii) whereas CHX16, CHX19 and CHX20 restored growth at pH 4.3 (Fig. II-3B). The increased growth of K^+-uptake deficient mutants by CHX17, 18 or 19 at alkaline pH suggests that intracellular K^+ is needed for growth and that these CHXs facilitated K^+ acquisition into cells. However, there was no increase in K^+ ($^{86}Rb^+$) flux at pH 7.5 or pH 4.5 into K^+-uptake deficient yeast (LMM04) expressing *CHX17* (Fig. A-II-4A, A-II-4B). Curiously, KTA40-2 strains expressing *CHX17* or *CHX20* took up less K^+ than in mutants with vector only, and cells grown at pH 7.5 took up 3-fold more K^+ than at pH 4.5 (Fig. A-II-4C, A-II-4D). As both CHX17 and CHX20 were localized to endomembranes in yeast, these results suggested that CHXs do not enhance net K^+ uptake into cells via the plasma membrane, though they may be important in cation uptake, sorting and/or cycling K^+ through certain endomembrane compartments and the cell. For example, uptake of K^+ by endocytosis could fill vesicular stores, which could then be released to the cytoplasm by CHX transporters (Fig. II-8A). This interpretation could also apply to yeast ScKHA1 which has been localized to Golgi (Flis et al., 2005; Maresova and Sychrova, 2006).

I provide direct evidence that CHX17 and CHX20 mediated K^+ transport as their expression in a K^+-uptake deficient *E. coli* strain stimulated K^+ uptake and cell growth on medium with 1-4 mM K^+. CHX20 enhanced *E. coli* LB2003 growth at acidic pH (pH

5.8-6.2) whereas cells expressing CHX17 or KAT1 showed optimal growth at pH 6.6-7. Cation competition studies showed that CHX17 preferred $K^+ = Rb^+ > Na^+$; whereas CHX20 showed specificity for $Cs^+ > Rb^+ > K^+ >> Na^+$. Thus, K^+ is the physiological substrate, and both CHX 17 and CHX20 transport K^+ with a K_m in the low mM range. Cs^+ blocked Rb^+ flux; this may be due to Cs^+ transport by CHX20, as Cs^+ accumulation trait was mapped to *AtCHX20* locus using quantitative trait loci (QTL) method (Kanter et al., 2010). Thus CHX17 and CHX20 are monovalent cation transporters with distinct properties, though their mode of transport and relationship to pH homeostasis is unclear (see section E.3 below).

E.3. Mode of K^+ transport mediated by CHX is ambiguous

Several observations suggested that CHX20 mediated H^+-coupled K^+ transport: i) K^+ influx into *E coli* is optimal when pH_{ext} is acidic; and ii) CCCP, a protonophore, inhibited K^+ uptake at pH 6.2 but not at pH_{ext} 7.2 when there is little or no pH gradient across the PM. However, at pH 7.2, increasing CCCP concentration enhanced CHX20-dependent Rb^+ uptake into cells. This finding is surprising, unless the protein has switched its mode of transport.

Transport properties of CHX17 mimicked that of KAT1, an inward-rectifying K^+ channel. They both showed optimal transport at neutral pH, and K^+ influx was not sensitive to the protonophore CCCP at neutral pH. Bacterial growth stimulated by both CHX17- and KAT1- is inhibited ~50% by 1.25 mM Ba^{2+}, a K^+ channel blocker (Schachtman et al., 1992, Wegner et al., 1994), whereas CHX20-supported growth is less sensitive. I propose that CHX20 behaves like a H^+-coupled K^+ symporter and CHX17 has channel-like properties. The differential mode of K^+ transport mediated by CHX20 and

by CHX17 suggested here will need to be rigorously verified. It is interesting that examples are emerging where channel properties exist in transporters (Defelice and Goswami et al., 2007). For example, KefC (a homolog of AtKEA1/2) has channel-like properties and cation/proton antiport activity when co-expressed with a peripheral protein, KefF (Fujisawa et al., 2007). In spite of the ambiguity, I postulate that K^+ transport mediated by CHX is likely coupled either directly or indirectly to a H^+ flux, which would change compartment pH or localized pH at an endomembrane.

E.4. Differential effects of CHX17 and CHX20 on intracellular pH

The inability to detect changes in cytosolic or vacuolar pH in yeast expressing *CHX17* or *ScKHA1*, could be due to the relatively weak or limited signal from small compartments or to pH changes restricted to KHA1-associated compartment, the Golgi (Flis et al., 2005; Maresova and Sychrova 2005; 2006). Intriguingly, K^+ and Cl^- transporters were implicated with cellular pH regulation in yeast. For example, plasma membrane K^+ transporters, TRK1 and TRK2, are involved in cytosolic pH regulation possibly as K^+-coupled H^+ gradient dissipators (Yenush et al., 2002). Moreover, a recent study in yeast revealed the role of the putative Cl^-/H^+ antiporter GEF1 in Golgi pH alkalinization (Braun et al., 2010). GEF1 and KHA1 potentially localize to the same compartment (Flis et al., 2005). Since either *gef1* mutant or *kha1* mutant showed sensitivity to HygB, it is likely that GEF1 and KHA1 affect endomembrane luminal pH regulation. Unlike GEF1 that alkalinizes luminal pH by a predicted antiport activity (Braun et al., 2010), it is possible KHA1 would acidify luminal pH by releasing K^+ as an counter ion required to balance electrogenic H^+ pumping by V-ATPase (see a working model on Fig. II-8). Considering that CHX17 is a close ortholog to KHA1, and CHX17

can rescue KHA1 function in yeast, I propose a model that CHX17, mediates K^+ release into the cytosol via a channel and thus it also regulates luminal pH of endomembranes.

In contrast, cells expressing *CHX20* alkalinized the vacuole and acidified the cytosol by about 0.2 units, indicating that the roles of CHX20 differed from that of CHX17. At limiting K^+ (0.1 mM; Fig S3E) pH_{vac} increased from 5.92 to 6.28 (~0.4 units) in cells-expressing *CHX20*; while *NHX1* alkalinized pH_{vac} by about 0.1 unit to pH 6.03. I previously showed that cells expressing *NHX1* had a slightly basic pH in vacuoles (pH 6.1) relative to pH 5.9 of vacuoles in KTA40-2 (*nhx1*Δ) (Fig. II-4E), consistent with the model that NHX1 alkalinizes vacuolar pH (Brett et al., 2005b). This result suggested that CHX20 and NHX1 show differential modes of transport. It was shown before that vacuolar K^+ concentration changed according to K^+ availability in the tissue (Walker et al., 1996). If so, K^+ transport into the vacuole via NHX1-mediated electroneutral K^+/H^+ exchange, would be reduced at low K^+; however, the increase in vacuolar alkalinization and cytosolic acidification seen in cells with CHX20 would favor a model of a H^+/K^+ symporter (see above).

These results suggest that tolerance to alkaline pH conferred by either CHX17 or CHX20 was not due largely to changes in pH_{cyt} or pH_{vac}. CHX17 and KHA1 rather mediated K^+ transport as a counter ion for pH gradient generation in the endomembranes, e. g. Golgi. On the other hand, CHX20 rendered HygB sensitivity and compromised growth at acidic pH (Fig. II-2B, 2D) as a result of intracellular pH alteration, possibly by CHX20-mediated H^+ coupled K^+ transport toward the cytosol. Since H^+ gradient is diminished at alkaline pHext, CHX20 might mediate K^+ transport as a channel similar to

CHX17 and KHA1 (Fig. II-5G) at this condition thereby rescuing the growth of *kha1* mutant.

E.5. Endosomal pH, protein sorting and membrane trafficking

How do transporters in intracellular membranes improve yeast growth on alkaline medium or low K^+? Based on studies of yeast, my results point to participation of CHX16-CHX20 transporters in compartment pH homeostasis, membrane trafficking and protein sorting. First, it is well-known that yeast mutants sensitive to alkaline pH are defective in genes important for endomembrane acidification, vacuolar protein sorting or vacuole biogenesis (Serrano et al., 2004). For instance, *vma* mutants defective in a H^+-pumping V-ATPase subunit fail to grow at pH 7.5 but proliferate normally on medium at pH 5.5 (Nelson and Nelson, 1990). Vacuoles of *vma4* mutants become acidic when grown in pH 5.5-buffer and change to pH 7 when exposed to pH 7.5 buffer, though vacuoles of wild-type cells remain acidic at pH 5.9 (Plant et al., 1999). Mutants lacking the vacuolar H^+ pump survive in acidic medium where they are thought to maintain compartment acidification by fluid phase endocytosis. Thus, cells proliferate as long as endolumenal compartments are acidic. Here I showed that the growth sensitivity to alkaline pH of single *kha1* mutant is reversed at acidic pH_{ext} (Fig. II-2E) similar to *vma* mutants. Moreover, I demonstrated that growth of *kha1* mutant or KTA40-2 strain was rescued at alkaline pH by CHX17 or ScKHA1 (Fig. II2B, 2E). Thus, my results suggest that CHX17 or ScKHA1 are involved in adjusting cation and pH of one or more endomembrane compartments and so promote cell proliferation.

Second, yeast mutant KTA40-2 expressing *CHX17* or *CHX20* secreted (37-39%) less CPY at pH 7.3 relative to that seen at pH 5.5 (100%) (Fig. II-7B, II-7C). *CHX17* and

ScKHA1 expression also reduced CPY secretion (52-60%) relative to KTA40-2 mutant alone at alkaline pH. CHX17 differed from that of ScNHX1 which reduced CPY secretion in LMB01 yeast at either acidic or alkaline external pH. My results are consistent with previous work (Bowers et al., 2000; Ali et al., 2004; Brett et al., 2005b) demonstrating that pH modulation of endosomal/PVC by NHX1 is important for sorting CPY from Golgi to vacuole. Expression of *CHX17*, on the other hand, partially lowered CPY secretion in yeast KTA40-2 strain disrupted in *nhx1* at alkaline pH_{ext}. These results suggest that CHX17 serves a similar role to ScNHX1, possibly by working at membrane compartments or domains other than the PVC in yeast. CHX17 (Fig. II-6) and ScKHA1 (Flis et al., 2005; Maresova and Sychrova, 2006) were localized to endomembranes resembling ER and Golgi in yeast. Thus I propose a model where modulation of cation and pH homeostasis in the ER, Golgi or both are also critical for proper protein sorting and membrane trafficking (Fig. II-8). CHX17 is localized to endosomes/PVC in plant cells suggesting a similar model of CHX17 in membrane trafficking.

Third, the ability of CHX17 and ScNHX1 to confer hygromycin B resistance in yeast could be related with vesicle trafficking. The cellular basis of aminoglycoside resistance in yeast is still debatable. Toxicity has been attributed to the relative transport of hygromycin B into the cytosol where it binds the 30S ribosome and blocks protein translation (Brodersen et al., 2000). Yeast grown under K^+-starved condition are sensitive, suggesting an increase in potential-driven uptake of $HygB^+$ (Perlin et al., 1988); yet *kha1* or *nhx1* mutants showed no change in membrane potential (Kinclova-Zimmermannova et al., 2006; Maresova et al., 2006). One study showed that gentamicin, another aminoglycoside, enters pig kidney cells (LLC-PK1) via endocytosis and is then

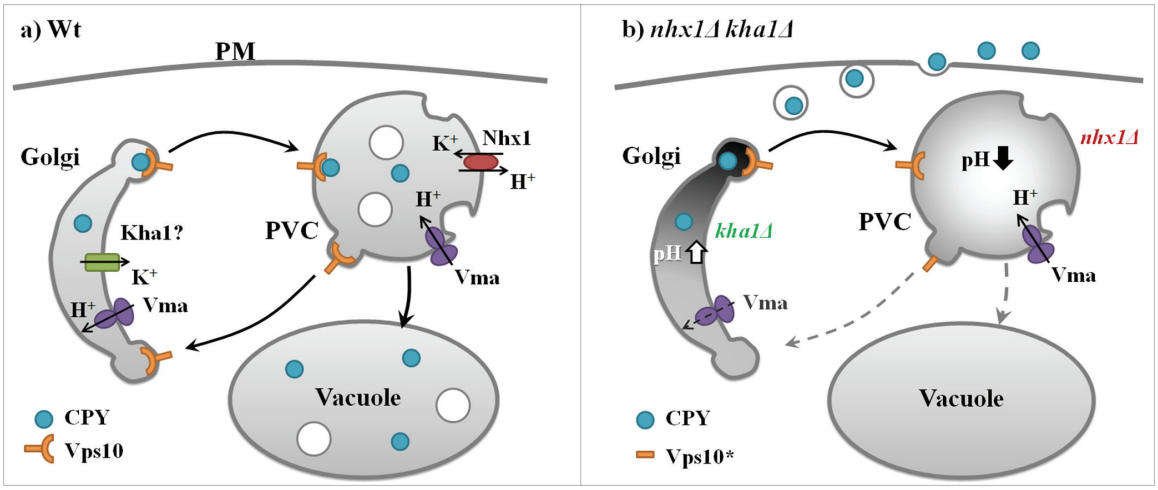

Fig. II-8. Roles of ScNHX1, ScKHA1 and AtCHX17 in membrane trafficking and protein sorting in yeast.

A) In *wild-type*, CPY is synthesized at the ER, processed at the Golgi and sorted to the PVC by vacuolar sorting receptor (Vps10) which cycles between late Golgi and PVC. CPY is then delivered to the vacuole.

B) In *nhx1Δ* mutant, PVC is acidified (Brett et al., 2005b) leading to degradation of Vps10* so CPY in late Golgi is secreted instead (Bowers et al., 2000). In *nhx1Δ kha1Δ* double mutant, it is postulated that luminal pH and K^+ balance in PVC and Golgi (Flis et al., 2005) are altered thereby enhancing CPY secretion. AtCHX17 appears to serve a role similar to ScKHA1 in yeast.

delivered by retrograde traffic to the vacuole and ER/Golgi, where its leakage into the cytosol poisons the cell (Sandoval and Molitoris, 2004). Furthermore, several gentamicin-sensitive yeast mutants are defective in genes associated with GARP (golgi-associated retrograde pathway) or HOPS (homotypic fusion and vacuolar protein sorting) (Wagner et al., 2006). Results suggest that gentamicin sensitivity in yeast is due to altered intracellular membrane trafficking. I also demonstrated that CHX17, KHA1 or NHX1 conferred both HygB and gentamicin resistance (Fig. A-II-9). Some mutants of *vma, vps* or *pep* genes are also sensitive to HygB. As Vps44 or NHX1 alkalinizes the vacuole (Brett et al., 2005b), and confers tolerance to HygB or gentamicin, I propose that NHX1 could influence sorting of the antibiotic into a compartment (e.g. vacuole) for degradation or inactivation. CHX17 confers an additive effect of HygB resistance on cells harboring wild-type NHX1 (Fig. II-2B), suggesting that CHX17-modulated pH or cation homeostasis of compartments that collaborate to facilitate retrograde transport leading to degradation or inactivation of the antibiotic. Furthermore, the inability of CHX20 to confer HygB resistance could be attributed to its different transport properties, its association with distinct endomembranes, or both, that interfere with antibiotic sorting and inactivation.

E.6. Summary

This study has revealed distinct properties of two Arabidopsis cation transporters, CHX17 and CHX20, after expression in yeast and *E. coli*. My findings point to a common role of CHXs in modulating cation and pH homeostasis of diverse endosomal compartments. Apart from the role of CHX20 in guard cell movement, phenotypic analyses of single or high-order mutants of CHX16 through CHX19 have been unremarkable so far. Mutant *chx17* plants grown under K^+ starvation showed reduced K^+ content supporting a role in K^+ homeostasis (Cellier et al., 2004). Increased expression of *CHX17* transcripts by K^+ starvation, ABA, or high salt (Cellier et al., 2004) would suggest additional roles in stress tolerance. My finding that endosomal-associated CHX17 alters vacuolar protein sorting in yeast supports a role in endomembrane trafficking. Whether it influences the anterograde or retrograde trafficking among ER, PVC and endosomes has yet to be established. It is clear that although the roles of NHX1 and CHX17 overlap, they are clearly distinct in yeast and possibly also in plants. Together, my studies provide the first indication that members of the CHX family are monovalent-cation transporters that play distinct and critical roles in controlling membrane trafficking patterns that ultimately could impact stress tolerance, development and growth of plants.

CHAPTER III

DUAL LOCALIZATION OF ARABIDOPSIS CHX17 IN PREVACUOLAR COMPARTMENTS AND PLASMA MEMBRANE

A. ABSTRACT

The importance of sorting proteins and cell wall components to their appropriate destination is critical for plant growth, development and rapid adaptation to environmental stress, though the molecular machinery regulating membrane trafficking is poorly understood. Endomembrane cation/proton transporters (AtCHX) that potentially modulate pH and cation homeostasis of compartments are emerging as important players. A previous study revealed their biochemical properties and localization in single cell hosts; though, their localization and specific roles in plants are mostly unclear. Analysis of *chx* null mutants indicated that CHX16, 17, 18 and 19 were not associated with K^+ nutrition, but had an unknown yet redundant function in reproduction. All four CHXs were localized to post-Golgi compartments and plasma membrane (PM) *in planta*, so CHX17 was selected for further study. The full-length *CHX17-GFP* was localized in prevacuolar compartments (PVC) and PM in root epidermis of transgenic plants. Truncation of the carboxyl terminus rendered CHX17(1-425) to be inactive in yeast and retained in the ER. However, CHX17(1-472) containing 47 residues after the last transmembrane domain retained activity and did exit ER to reach the Golgi; though the protein was not targeted to PVC and PM. Together, these results indicate that CHX17 and most likely CHX16, 18 and 19 are localized to dynamic endomembranes, trafficking between PVC and PM. In addition, results suggest that the long C tail of CHX17 is required for ER exit and targeting to PVC and PM. I propose that these CHXs might have a role in cell wall remodeling through regulation of cargo sorting and cell wall material modification in endosomal systems.

B. INTRODUCTION

The endomembrane system is a network of subcellular compartments required for the synthesis, processing and sorting of various secreted and membrane proteins to their designated targets. The secretory pathway refers to the membranes involved in the delivery of cellular materials to the plasma membrane (PM) from the endoplasmic reticulum (ER), through the Golgi and *trans*-Golgi network (TGN). This secretory or biosynthetic pathway is also known as anterograde transport. In contrast, retrograde transport refers to movement of materials in the opposite direction. For example misfolded or non-functional proteins, resident proteins and trafficking machineries are mostly processed to maintain quality control, organelle identity and membrane trafficking, respectively. Endocytosis is another major pathway associated with the endomembrane system. This pathway is crucial for internalization of extracellular materials and membrane proteins. Compartments formed by endocytosis from the PM are known as endosomes. These vesicular compartments are highly dynamic in nature. In plant cells, endocytosed proteins are normally transported via early and late endosomes to the vacuole. Early and late endosomes are defined mainly by their cargo and the trafficking machineries. In general, late endosomes are closely associated with the vacuole, also known as prevacuolar compartments (PVC). Due to the dynamic and heterogeneous properties of endosomes, their identity, function and regulation are poorly understood in plants. Studies in the past decade have revealed the roles of plant endosomes in protein sorting and in signaling (see review by Raikhel and Hicks, 2007; Geldner and Robatzek, 2008; Otegui and Spitzer, 2008; Robinson et al.., 2008; Irani and

Russinova, 2009), although the modulation of endosomal trafficking is still very poorly understood.

A striking example of the dynamic nature of endosomes is the specific distribution of PIN proteins involved in facilitating efflux of auxin (see review by Friml, 2010; Grunewald and Friml, 2010). PINs, auxin efflux facilitators, are delivered to the plasma membrane after initial synthesis. However, they are preferentially internalized and recycled back specifically at one face of the PM (Dhonukshe et al., 2008). The recycling of PIN1 is dependent on the GNOM ARF-GEF which is sensitive to brefeldin A (BFA) and localizes to endosomes (Geldner et al.., 2001; Geldner et al.., 2003, Klein-Vehn et al., 2008). PIN2 also recycles between endosomes and PM as demonstrated by its accumulation in BFA compartments and its return to PM after BFA removal (Klein-Vehn et al., 2008). The polar nature of auxin transport is thus maintained by the asymmetric distribution of the efflux facilitators.

Endosomes also play a critical role in the mechanism by which plants modulate B uptake under varying B levels in the environment. AtBOR1 was recently discovered as a boron exporter, which is required for xylem loading of boron (Takano et al., 2002). When external B is low (0.1 μM), BOR1-GFP is localized at the PM; however when B level is increased to 100 μM, BOR1-GFP disappeared from the cells. Evidence suggests BOR1 protein has been endocytosed and then moved to the vacuole for degradation during boron sufficiency (Takano et al., 2005; 2010). Intriguingly, BOR1 also showed polar localization at the inner PM face of xylem parenchyma cells (Takano et al., 2010). Thus plants can prevent uptake of excess B by removing and degrading BOR1 transporters that transfer B into the plant body.

Evidence that endosomes participate in signal transduction has emerged recently in plant cells. Upon binding of brassinosteroid ligand (BR) to its receptor BRI1, localized at the PM, BRI1 kinase is activated leading to the release of inhibitory protein BKI1 from the PM and the interaction of BAK1, an LRR receptor-like protein kinase, to interact with BRI1 (Nam and Li, 2002; Li et al., 2002; Wang and Chory, 2006). This activation leads to dephosphorylation of BES1 transcription factors controlling BR response (Yin et al., 2005; Vert and Chory, 2006). Interestingly, BFA increases endosomal localization of BRI1, a plant steroid receptor, and induces dephosphorylation of BES1 and other downstream activities (Gelner et al., 2007). Surprisingly, BR has no effect on BRI1 internalization, suggesting that BRI1 signal transduction is initiated through endosomal localization and is independent of ligand-mediated internalization pathway.

In spite of the critical roles of endosomes and membrane trafficking, it is unclear how the movement and directionality of secretory and endocytic pathways are modulated. A working hypothesis is that the particular environment of each intracellular compartment or domain is critical in modulating protein-protein associations and/or dissociations which facilitate vesicle transport, tethering, binding and fusion. Ion transporters are likely candidates that could alter the pH or ionic environment locally and transiently. Recently, several cation proton exchangers from the CPA2 subfamily in *Arabidopsis thaliana* were localized to endosomes and ER raising the possibility of their role in modulating intracellular pH and K^+ homeostasis (Padmanaban at al., 2007; Lu et al.., 2011; Chapter II). Importantly, the potential of CHX17 and CHX20 K^+ transporters in altering protein sorting was suggested in the model yeast cell (Chapter II).

The role of these CHX transporters in plant cells is still unclear. Here I focus on CHX16, 17, 18 and 19 which share high sequence homology, and show similar subcellular localization at the PVC or late endosomes. I provided evidence that these proteins can traffic between endosomes/PVC and PM in root epidermal cells of transgenic plants. I also tested the role of the long hydrophilic tail at the carboxylic terminus using CHX17 as a model, and demonstrate roles in activity and membrane targeting. Although no apparent phenotype was observed in single or double mutants of CHX16, 17, 18 or 19 in *Arabidospis*, further segregation analysis revealed the distortion of triple or quadruple mutant populations in the progeny suggesting a role of these CHXs in reproduction or seed development. Together, the studies suggest that these K^+ transporters do not have a role in K^+ nutrition as suggested before (Cellier et al., 2004). Instead I suggest that CHX modulate the ionic and pH environment of endosomes required for adaptation to environmental stress.

C. MATERIALS AND METHODS

C.1. Plant materials and growth condition

Wild-type *Arabidopsis thaliana* (ecotype Columbia-0), T-DNA insertion mutants (Table A-III-3, A-III-4) or transgenic plants (Table A-III-5) were grown in Miracle-Gro potting mix (Scotts) with 1/20 part of Miracle-Gro perlite (Scotts) in growth chamber (Percival). After sowing, seeds were vernalized in the dark at 4 ^oC for 2-3 days. Environmental conditions were constant at 21^oC, 65% relative humidity and 16-h photoperiod of 150 $\mu E\ m^{-2}\ s^{-1}$. Plants were watered three times a week.

For growth on solid medium, seeds were surface sterilized with 25% bleach and 0.05% Tween-20 then sown on half-strength (0.5X) Murashige and Skoog (MS) medium

prepared from salt mixture (Gibco #11117-058). 0.1% sucrose and 1 mM MES (2-(N-morpholino)ethanesulfonic acid; Sigma #M3671) were added to enhance germination and maintain optimal growth at pH 5.8, respectively. All solid media had 0.8% agar either from Difco granulated agar (BD #214510) or noble agar (BD #214230). The latter contains less salt content. Seeds were stratified, germinated and grown under the same condition as described above. In some cases, 7-d old seedlings were transferred to either 0.5X MS solid medium or Gibeaut (GB, Gibeaut et al., 1997) solid medium with some modification (Table A-III-16) as indicated in figure legend.

C.2. Genotyping and RNA expression

Genomic DNA was isolated from leaves of 2-4 wk old plants according to Edwards et al., 1991. In brief, leaves were ground in 400 µl of Edwards' buffer (0.2 M Tris HCl pH 8.0, 0.25 M NaCl, 25 mM EDTA, 0.5% SDS) in microfuge tubes using pestle and drill then centrifuged at 12000 rpm for 10 min. Supernatant was transferred to new microfuge tubes containing 400 µl of isopropanol, mixed thoroughly then centrifuged at 12000 rpm for 10 min. Pellets were washed with 500 µl of 70% ethanol and allowed to dry at room temperature then resuspended in 100 µl of water. Genotypes of *wild-type* and mutant plants were detected by PCR using gene-specific primers and T-DNA specific primers (Table A-III-10). Taq DNA polymerase (NEB, M0273L) was used to amplify corresponding DNA fragments with three-step cycling (denature at 94^{o}C for 20 sec, anneal at 55^{o}C for 30 sec and extend at 72^{o}C for 75 sec) for 30 cycles. Amplified products were run on 1% agarose gel electrophoresis with TAE buffer and visualized by fluorescence of intercalated ethidium bromide.

RNA was isolated from10-d old seedlings germinated on 0.5X MS solid medium. The protocol is based on Oñate-Sánchez and Vicente-Carbajosa, 2008. In brief, liquid-nitrogen frozen sample from 7 seedlings were ground in microfuge tubes using pestle and drill then 300 µl of lysis solution (2% SDS, 68 mM sodium citrate, 132 mM citric acid, 1 mM EDTA) was added. Tubes were briefly vortexed, mixed and left at room temperature for 5 min. 100 µl of precipitation solution (4 M NaCl, 16 mM sodium citrate, 32 mM citric acid) was added to the cell lysate, mixed and incubated on ice for 10 min then centrifuged at 12000 rpm for 10 min at 4^{o}C. Supernatant was transferred to new microfuge tubes containing 300 µl of isopropanol, mixed thoroughly then centrifuged at 12000 rpm for 5 min. Pellets were washed with 500 µl of 70% ethanol and allowed to dry at room temperature then resuspended in 88 µl of DEPC water. 10 µl of DNase 1 buffer and 2 µl of DNase 1 (Ambion #1906) were added to the RNA solution and incubated at 37^{o}C for 30 min. Then 50 µl of 7.5 M ammonium acetate and 400 µl of 100% ethanol were added to the RNA solution, mixed thoroughly and centrifuged at 12000 rpm at 4^{o}C for 30 min. RNA pellets were washed with 70% ethanol, air-dried at room temperature then suspended in 20 µl of DEPC water.

RNA expression was determined by reverse transcription PCR (RT-PCR). First, RNA was reverse transcribed to first-strand cDNA by SuperScript III First-Strand Synthesis System for RT-PCR (Invitrogen #18080-051) according to manufacturer's protocol. PCR to detect 5' and 3' regions of *CHX16-19* transcripts was performed and detected as described above based on the gene specific primers shown in Table A-III-11 and Fig. III-1A. *ACTIN11* was used to verify an equal amount of cDNA templates.

Relative expression of *CHX16-19* (Fig. A-III-1) was calculated from pixel density of Fig. III-1B using ImageJ (NIH) then normalized with *ACTIN11* transcripts.

C.3. Generation of multiple T-DNA insertion mutants

To generate double mutant plants, *chx17-4* mutants were crossed with *chx18-1*mutants or *chx19-2* mutants and *chx16-10a* mutants were crossed with *chx18-1* mutants. Heterozygous mutant plants were allowed to self-pollinate then double mutant plants of *chx17-4 chx18-1*, *chx17-4 chx19-2* or *chx16-10a chx18-1*genotypes were obtained from the progeny.

To generate triple mutant plants, *chx17-4 chx18-1* mutants were crossed with *chx17-4 chx19-2* mutants. Heterozygous *chx18-1 chx19-2* and homozygous *chx17-4* mutant plants were allowed to self-pollinate. Due to the lack of homozygous triple mutant observed in the progeny, heterozygous *chx18-1* and homozygous *chx17-4 chx19-2* mutants or heterozygous *chx19-2* and homozygous *chx17-4 chx18-1* mutants were selfed again to produce *chx17-4 chx18-1 chx19-2* mutant progenies.

To generate quadruple mutant plants, heterozygous *chx16-10a chx18-1* mutants were pollinated with pollen from *chx17-4 chx19-2* homozygous mutants. Plants harboring heterozygous *chx16-10a chx17-4 chx18-1 chx19-2* genotypes were scored from the progeny and allowed to self-pollinate. Only plants of heterozygous *chx17-4* and homozygous *chx16-10a chx18-1 chx19-2* or heterozygous *chx18-1* and homozygous *chx16-10a chx17-4 chx19-2* genotypes were obtained. Self-pollination of these plants produced *chx16-10a chx17-4 chx18-1 chx19-2* mutants in the progeny. Segregation analyses of double, triple or quadruple mutants were based on genotypes detected by PCR as describe above from genomic DNA isolated from F1 plants.

C.4. Bacterium, yeast and plant transformation

E. coli transformation Sub-cloning efficiency competent cells of *Escherichia coli* strain DH5α were purchased from Invitrogen (18265-017) and transformed according to the manual. In some cases, *E. coli* DH5α or Topten competent cells were prepared as described in Appendices section A.1.e; however, growth and generation of competent cells were done using LB medium. Cell culture was spread on solid LB with appropriate antibiotics (50 µg/ml Kanamycin, 100-200 µg/ml Ampicillin, 30 µg/ml Choramphenicol, 20 µg/ml Hygromycin or 100 µg/ml Spectinomycin) and incubated at 30^{o}C or 37^{o}C overnight. Solid medium was prepared by adding 1.5-2.0% w/v Difco granulated agar.

Agrobacterium transformation (based on protocol from DNA cloning service) *Agrobacterium tumefaciens* strain GV3103 was grown in 2 ml Luria-Bertani (LB) medium supplemented with 25 µg/ml gentamycin (MP Biomedicals #1405-41-0) at 30^{o}C and 200 rpm overnight then inoculated to 50 ml LB-gentamycin and incubated as above until A_{600} reached 0.5. Cell suspension was centrifuged at 3000xg and 4^{o}C for 5 min. Cell pellets were gently resuspended in 1 ml of ice-cold 20 mM $CaCl_2$ solution. Competent cells were instantly frozen in -80^{o}C ethanol bath in 100 µl aliquot. To transform *Agrobacterium*, 1-2 µl of binary vectors (Table A-III-5, A-III-15) were added to the frozen competent cells, incubated at 30^{o}C for 5 min and placed on ice for 30 min. Cell suspension was spread on solid LB-gentamicin medium supplemented with either 100 µg/ml spectinomycin or 100 µg/ml kanamycin corresponding to each binary vectors and incubated at 30^{o}C for 1-2 days. Solid medium was prepared by adding 1.5-2.0% w/v Difco granulated agar.

Yeast transformation *Saccharomyces cerevisiae* strain KTA40-2 (*ena1-4Δ, nha1Δ, nhx1Δ, kha1Δ*) were prepared and transformed as described in Appendices section A.1.b.

Arabidopsis transformation (floral dip method based on Zhang et al., 2006) *Arabidopsis thaliana* Wt (col-0) or T-DNA insertion mutants (Table A-III-3, A-III-4) were grown as described above for 4 weeks or more until there were a bunch of floral inflorescences. *A. tumefaciens* harboring corresponding binary vectors were grown overnight in 2 ml LB supplemented with appropriate antibiotics at 30^{o}C and 200 rpm then inoculated to 250 ml LB and incubated as above overnight. Cell suspension was centrifuged at 4000xg and 25^{o}C for 10 min. Cell pellets were gently resuspended in 250 ml 5% w/v sucrose then 50 µl of Silwet L-77 was added to the cell suspension. Arabidopsis inflorescences were submerged into *Agrobacterium* suspension for 5-10 sec with gentle swirling. Then the excess suspension was absorbed by placing Arabidopsis inflorescence horizontally on paper towel. Plants were covered with plastic wrap to maintain moisture and laid down overnight. After removing the wrap, plants were placed back in the growth chamber and grown for additional 4 wks or more until the siliques turned brown. Seeds were harvested, surface sterilized and germinated on 0.5X MS solid medium as described above. Medium was supplemented with appropriate antibiotics or chemicals (30 µg/ml Hygromycin, 50 µg/ml Kanamycin or 25 µg/ml Glufosinate ammonium (Crescent chemical company #CA14030000) for selection of transformants. In most cases, transformants, harboring Basta (Glufosinate) resistance, were selected on soil by spraying 1:1000 dilution of herbicide containing 5.78% Basta (Finale) every 2-3 days. At least 10 independent transformants were scored for further analysis.

Arabidopsis leaf protoplast transformation Leaf protoplasts were prepared and transformed as described in Appendices section A.1.g. Plasmids used for transformation are listed in Table A-III-7.

C.5. cDNA, promoter and genomic DNA cloning

cDNA cloning Full-length CHX16-19 were PCR amplified by Platinum Pfx DNA Polymerase (Invitrogen #11708-013) from cDNA using gateway compatible primers (Table A-III-8) and inserted into gateway donor vectors, pDONR221 (Invitrogen #12536-017), using BP clonase II enzyme mix (Invitrogen #11789-020). The resultants were gateway entry vectors (Table A-III-13). Several entry vectors had been described previously (Chapter II). These entry vectors were subsequently recombined with gateway destination vectors (Table A-III-14) using gateway LR clonase II enzyme mix (Invitrogen #11791-020). Expression vectors from this reaction were listed on Table A-III-15. Recombination procedures were performed according to manufacturer's protocols.

CHX17p::YFP CHX17 promoter driven YFP expression construct was generated using homologous recombination in yeast (Oldenburg et al., 1997; Nagano et al., 2007). In brief, 3 kb promoter region of CHX17 and yeast origin of replication (2μ), together with URA3 (Orotidine-5'-phosphate decarboxylase) as a selective marker in yeast, were PCR amplified by iProof High-Fidelity DNA Polymerase (Biorad #172-5301) from BAC clone (F9D16) and pYES-DEST52 destination vector (Invitrogen #12286-019), respectively, using homologous primers (Table A-III-9). PCR was three-step cycling (denature at 98^{o}C for 5 sec, anneal at 55^{o}C for 15 sec and extend at 72^{o}C for 90 sec) for 35 cycles. Yeast strain KTA40-2 was co-transformed as described above with two amplified products: i) *CHX17* promoter and *2μOri – URA* and ii) NcoI linearized

pBYWG-CHX17 expression vector. NcoI (NEB #R0193S) had two specific restriction cut sites (389 bp apart) in 35S promoter region of pBYWG-CHX17. At least 8 independent yeast transformants were scored for further plasmid isolation. Plasmids containing *CHX17* promoter followed by *YFP* construct (pBYUR-CHX17p) were confirmed by PCR using primers specific to the *CHX17* promoter and *YFP*, respectively (Table A-III-12). *E. coli* DH5α was then transformed with pBYUR-CHX17p for further plasmid preparation using a miniprep kit (Qiagen #27160). Recombinant binary vector, pBYUR-CHX17p, was verified by restriction cut and PCR, respectively.

Yeast plasmid isolation A protocol (Qiagen) was adapted from *E. coli* plasmid isolation using miniprep kit (Qiagen #27160). In brief, 5 ml of overnight-grown yeast in YNB medium was centrifuged at 2500xg for 5 min. Pellets were resuspended in 250 µl P1 buffer and transferred to microfuge tubes. 50-100 µl of Acid-washed glass beads (Sigma #G8772) were added to the cell suspension and vortexed vigorously for 5-10 min at 4^{o}C then supernatant was transferred to new microfuge tubes. After this step, regular procedure for *E coli* plasmid isolation was performed according to manufacture protocol.

CHX17p::gCHX17 CHX17 promoter driven native CHX17 constructs were generated by PCR amplifying genomic CHX17, including 3-kb upstream promoter region and open reading frame using gateway compatible primers (Table A-III-8) with BAC clone (F9D16) as a template. High-Fidelity DNA Polymerase iProof (Biorad #172-5301) was used in PCR with three-step cycling (denature at 98^{o}C for 5 sec, anneal at 55^{o}C for 30 sec and extend at 72^{o}C for 3 min) for 35 cycles. Amplified products were purified using illustra GFX PCR DNA purification kit (GE Healthcare #28-9034-71) and inserted into gateway donor vectors, pDONR221 (Invitrogen #12536-017), using BP clonase II

enzyme mix (Invitrogen #11789-020). The resultant gateway entry vector (pEp17gX17) was verified by restriction cut. The correct clone of entry vector was recombined to destination vector, pMDC107 (Curtis and Grossniklaus, 2003; Table A-III-14), using gateway LR clonase II enzyme mix (Invitrogen #11791-020). Due to the lack of a distinct selectable marker (both entry and destination vector harbor kanamycin resistant gene) and *E. coli* harboring pMDC107 was hygromycin B resistant, combination of kanamycin and hygromycin B was used to select for expression vector (pMDCp17gX17). Recombinant binary vector, pMDCp17gX17, was verified by PCR using specific primers to *CHX17* promoter region and open reading frame, respectively (Table A-III-11, -12).

Truncation of CHX17 Truncated CHX17 (TM(1-425), TM(1-475)) or CHX17 C-terminus (Ct(426-820), Ct(473-820)) were PCR amplified from pSMCHX17 template using gateway compatible primers (Table A-III-8). High-Fidelity DNA Polymerase iProof (Biorad #172-5301) was used in PCR with three-step cycling (denature at 98^{o}C for 10 sec, anneal at 60^{o}C for 30 sec and extend at 72^{o}C for 1 min) for 30 cycles. Amplified products were purified by PEG precipitation. In brief, 50 µl of PEG-$MgCl_2$ (30% PEG8000, 30 mM $MgCl_2$) was added to 100 µl of PCR products in TE then centrifuged at 12000 rpm for 10 min. Pellets were suspended in TE and used for BP reaction with gateway donor vectors, pDONR221 (Invitrogen #12536-017). The resultant gateway entry vectors (Table A-III-13) were verified by restriction cut. Entry vectors were subsequently recombined with destination vectors (Table A-III-14) to generate expression vectors (Table A-III-15).

C.6. CHX17 promoter YFP analysis

Tissue expression T2 seedlings of *chx17-4* mutants harboring pBYUR-CHX17p were grown in 0.5X MS solid medium for 14 days. Seedlings were then transferred and submerged in GB medium for 1 h before observation under confocal microscope (Zeiss LSM710). To observe *CHX17* expression in seeds, T2 seedlings of *chx17-4* mutants harboring pBYUR-CHX17p were grown in soil for 4-6 wks. Siliques from different stages were collected and cut open using a scalpel. The whole siliques or individual seeds were immediately submerged in water and observed with a fluorescence microscope (Nikon E600).

Quantitative analysis T2 seedlings of *chx17-4* mutants harboring pBYUR-CHX17p were grown in 0.5X MS solid medium for 7 days then transferred to modified GB solid medium (Table A-III-16) which had extremely low K^+ (< 0.01 mM). Therefore, 1.75 mM K^+ was normally added to compensate for the lack of K^+ in the medium otherwise indicated. To minimize high K^+ contamination from agar in solid medium, noble agar (BD #214230) was used. At 0.8% w/v of this agar, K^+ concentration was approximately 0.05 mM. Seedlings were allowed to grow in modified GB solid medium at different treatments (1.8 mM K^+, 0.05 mM K^+(no K^+ added), 100 mM NaCl, 200 mM Sorbitol) for 7 days before root-length measurement or fluorescence-intensity measurement.

To measure fluorescence intensity, seedlings were submerged in GB medium then immediately observed under fluorescence microscope (Nikon E600). Images were taken using SPOT software (Diagnostic Instruments) by fixing all parameters including, exposure time (411 msec), gain (1) and excitation intensity. Both bright filed and

fluorescent images were captured at the same time consecutively to locate root boundaries. Three images were taken per one root which was approximately 0-3, 4-6 and 7-9 mm away from the root tip, respectively. Images were analyzed using ImageJ (NIH). Fluorescence intensity superimposed to root boundaries from bright-field picture was measured for average fluorescence density (F) and normalized with area of measurement (pixel) to generate relative intensity (F/Mpixel).

C.7. Functional study in yeast

Yeast strain KTA40-2 (*ena1-4Δ, nha1Δ, nhx1Δ, kha1Δ*) was transformed with expression vector pDR196 (Table A-III-15). Transformants harboring empty vector, full-length CHX, truncated CHX17 (TM(1-425), TM(1-475)) or CHX17 C-terminus (Ct(426-820), Ct(473-820)) were grown in 1 ml YNB medium overnight. Cells were then diluted with 4 ml YNB without a carbon source and incubated for an additional 12-14 h. Cells were washed and normalized with water to A_{600} of 0.2 and diluted 10-fold serially. Five μl of each dilution was dropped on YNB medium supplemented with 20 mM MES adjusted to pH 5.6 or pH 7.5 with arginine. Yeasts were allowed to grow at 30^{o}C for 2 days before images were taken (Nikon Coolpix 995).

C.8. Confocal microscopy

Tissue expression Seedlings of *chx17-4* mutants harboring pBYUR-CHX17p submerged in GB medium were placed on slides with two spacers made from 0.5 mm wide parafilm and covered with cover glasses. Each slide was observed under LSM710 (Zeiss) with excitation at 514 nm. Emission of YFP was 520-574 and 639-685 nm for chlorophyll. Bright field images were concomitantly obtained from 514 nm light source.

Transient expression in protoplasts Protoplasts harboring expression vectors (Table A-III-11) were gently transferred to slides with spacers as described above and observed using LSM510 (Zeiss). The filter sets used for excitation (Ex) and emission (Em) were: GFP, 488 nm (Ex)/BP505-530 nm (Em); RFP, 543 nm (Ex)/BP560-615 nm (Em); chlorophyll 543 nm (Ex)/LP650 nm (Em); bright field 633 nm.

Guard cell plasmolysis Leaves from 3-wk old plants harboring GFP or GFP-tagged constructs (Table A-III-5) were infiltrated with 0.1X MS medium with or without 30% sucrose. Infiltration was done by vacuum and incubation in indicated medium for 1 h. Leaf samples were observed under LSM510 (Zeiss). The filter sets were GFP, 488 nm (Ex)/LP505 nm and NPT545 nm (Em); neutral red, 543 nm (Ex)/LP560 nm and NPT635 nm (Em); chlorophyll and neutral red 543 nm (Ex)/LP650 nm (Em); bright field 633 nm.

Localization in roots To determine localization of full-length CHX or truncated CHX *in planta*, transgenic plants harboring GFP fusion constructs were crossed with transgenic plants harboring RFP fusion constructs (Table A-III-6). 10-d old seedlings from F1 or F2 generation were submerged in 0.1X MS medium or GB medium for 1 h. Seedlings were transferred to slide and covered with cover glasses in the root region otherwise indicated. Fluorescent signals were observation under LSM710 (Zeiss). GFP was excited at 488 nm with emission between 494-555 nm. RFP was excited at 561 nm with emission between 580-694 nm.

Localization of native CHX17 fused with GFP at the C-terminus 7-d old seedlings harboring pMDCp17gX17 expression vector from T2 generation were grown in 0.5X MS solid medium. Seedlings were transferred to 0.05 mM K^+ GB solid medium (Table A-III-16) and grown for additional 3 days. 10-d old seedlings were submerged in

GB medium for 1 h then transferred to GB medium supplemented with 10 μM FM4-64 (Invitrogen #T-3166) and incubated for 10 min. FM4-64 was washed off by transferring seedlings to 3 ml GB medium three times then seedlings were placed on slides for immediate observation with LSM710 (Zeiss). GFP and FM4-64 were excited at 488 nm with emission between 490-556 nm and 611-741 nm, respectively.

Brefeldin A and wortmannin treatment 10-d old seedlings harboring pBFWG-CHX17 or pBFWG-TM(1-472) expression vectors (Table A-III-5) from T3 generation grown in 0.5X MS solid medium were submerged in 0.1X MS medium for 1 h. Seedlings were incubated with 0.1X MS medium supplemented with 10 μM FM4-64 for 10 min then transferred to 3 ml 0.1X MS medium twice. FM4-64 labeled seedlings were incubated 90-120 min further in 0.1X MS medium supplemented with 0.5% DMSO, 50 μM brefeldin A (BFA; Invitrogen #B-7450) or 33 μM wortmannin (wm; Biosource #PHZ1301). Seedlings were placed on slides and observed using LSM510 (Zeiss). The filter sets were GFP, 488 nm (Ex)/BP505-530 nm (Em) and FM4-64, 488 nm (Ex)/LP650 nm (Em). In some cases, transfected protoplasts harboring expression vectors (Table A-III-7) were prepared as described earlier. Before observation, DMSO or BFA were added to the incubating solution to the final concentration of 0.35% and 35 μM, respectively, and incubated for 60-90 min. Additional filter set for chlorophyll was 543 nm (Ex)/LP650 nm (Em).

In some experiments, F2 transgenic plants harboring GFP and RFP fusion constructs (Table A-III-6) were grown in 0.5X MS solid medium for 10 days. Seedlings were submerged in GB medium for 1 h then transferred to GB medium supplemented with 1.5% DMSO or 150 μM BFA and incubated for additional 3 h. Seedlings were

placed on slides and observed under LSM710 (Zeiss). GFP was excited at 488 nm with emission between 494-555 nm. RFP was excited at 561 nm with emission between 580-694 nm.

Localization in yeast Yeast strain KTA40-2 was transformed with expression vector pGWFDR196 (Table A-III-15). Transformants harboring GFP-tagged full-length CHX17, TM(1-472) or TM(1-425) constructs were grown overnight in 1 ml YNB media then centrifuged at 2000 x g for 2 min. Cell pellets were resuspended in 1 ml YPAD medium and then incubated further for 3 h at 30^{o}C. Just before observation, the final concentration of 1 μM FM4-64 was added to the cell suspension in YPAD medium and incubated for 10 min at room temperature. Cells were then washed with 2% sucrose, allowed to settle down for 10 min then resuspended in 0.05% agarose. Yeast cells were observed under LSM510 (Zeiss). The filter sets were GFP, 488 nm (Ex)/BP505-530 nm (Em) and FM4-64, 488 nm (Ex)/LP650 nm (Em).

C.9. Tissue preparation and immunolocalization for transmission electron microscopy

Samples for immunolocalization were fixed in 0.1% glutaraldehyde and 4% paraformaldehyde in 100 mM phosphate buffer (pH 7.0) for 4 hour at 4°C. After rinsing three times with phosphate buffer, glycerol was gradually added in samples until its concentration was up by 25%. The samples were rapidly frozen in nitrogen slush, then immediately transferred to Lecia EM AFS (Automatic Freeze Substitution) at -160°C for 10 min. Freeze substitution was performed in anhydrous ethanol. The samples were kept at -85°C for 3 days, -60°C for 1 day, at -20°C for 1 day, at 0°C for 12 hours, at 4°C for 12 hours, and then changed to room temperature. Samples were infiltrated and embedded

with LR White resin; polymerization was performed at 60°C for 1 day. Ultrathin sections, 100-120 nm, were cut by Reichert Ultracut S (Leica, Vienna, Austria) and collected on 50 or 100 mesh nickel grids.

For immunogold labeling, the individual grids were floated on blocking solution A [blocking reagent (Roche Applied Science, Mannheim, Germany) 0.5% in buffer 1 (100 mM Tris-HCl, 15 mM NaCl and 0.3 % Tween-20 (pH 7.5)] for 30 min, and then on blocking solution B (1% BSA, 0.3% Triton X 100 in buffer 1) for 40 min at room temperature. Grids were floated on drops of the primary monoclonal antibodies to GFP (diluted 1:5 in buffer 1, Roche Applied Science) at room temperature for 1 hr. After being washed 5 times with ddH_2O, the grids were floated on an excess amount (1:20 dilution) of 18 nm colloidal goat anti-mouse IgG (Jackson Immuno Research, West Grove, PA, USA) at room temperature for 30 min. Then the grids were washed sequentially with 3 droplets of buffer 1, followed by three times washes with ddH_2O. After immunogold labeling, the sections were stained with 5% uranyl acetate in water for 10 min and 0.4% lead citrate for 6 min. Sections were observed using a Philips CM 100 Transmission Electron Microscope at 80 KV. (From Dr. Guang-Yuh Jauh, Institute of Plant and Microbial Biology, Academia Sinica, Taiwan)

D. RESULTS

D.1. T-DNA insertional mutants of CHX16 to CHX19

To study the function of CHX in plants, I obtained five *chx* T-DNA insertional mutants named *chx16-10a*, *chx17-1, chx17-4*, *chx18-1*and *chx19-2* as shown in Fig. III-1A. *Wild-type* siblings were verified using gene-specific primers flanking the T-DNA insertion site and single homozygous mutants were tested with a T-DNA left border (LB)

Fig. III-1. Arabidopsis *CHX16-CHX19* gene organization, T-DNA insertions and partial transcripts in mutants.

A) Genome organization of *AtCHX16-AtCHX19* and T-DNA insertion mutants used in study. *chx16-10a*, *chx17-4*, *chx18-1* and *chx19-2* mutants correspond to SALK_138136, SALK_033417, SALK_001563 and SALK_100047, respectively. Boxes represent exons. Scale bar = 200 bp.

B) Absence of full-length transcripts in single, double, and quadruple mutants. RNA extracted from 10-d old seedlings was reverse transcribed and PCR amplified. Forward (F) and reverse (R) primers used for RT-PCR in are denoted as RTn (5'-region) and RTc (3'-region) for each gene as shown in A). Amplified products for the 5'-upstream region and the 3'-downstream region are shown for *Wild type* (Wt) , single mutant *chx17-4*, double mutants *chx17-4/chx19-2* and *chx17-4/chx18-1*, quadruple mutant *chx16/17/18/19* and *Wt* plants over-expressing *CHX17* (Wt *35Sp*::*CHX17*). All 5'-region primer pairs spanned an intron, so a band of larger size seen for *CHX18* and *CHX19* may be products of unspliced transcripts. *Actin11* was amplified as a loading control. Result is representative of two experiments.

A

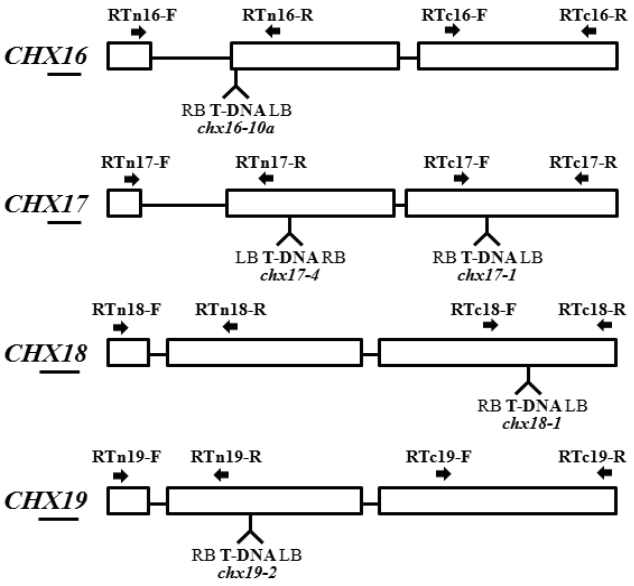
RTn16-F
RTn16-R
RTc16-F
RTc16-R
CHX16
RB T-DNA LB
chx16-10a
RTn17-F
RTn17-R
RTc17-F
RTc17-R
CHX17
LB T-DNA RB
chx17-4
RB T-DNA LB
chx17-1
RTn18-F
RTn18-R
RTc18-F
RTc18-R
CHX18
RB T-DNA LB
chx18-1
RTn19-F
RTn19-R
RTc19-F
RTc19-R
CHX19
RB T-DNA LB
chx19-2

B

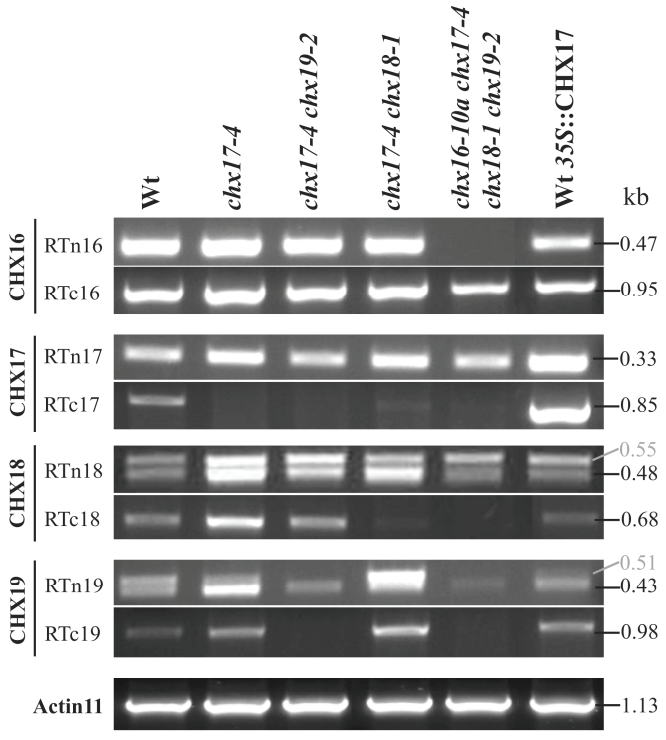
Wt
chx17-4
chx17-4 chx19-2
chx17-4 chx18-1
chx16-10a chx17-4
chx18-1 chx19-2
Wt 35S::CHX17
kb
CHX16
RTn16
RTc16
CHX17
RTn17
RTc17
CHX18
RTn18
RTc18
CHX19
RTn19
RTc19
Actin11
0.47
0.95
0.33
0.85
0.55
0.48
0.68
0.51
0.43
0.98
1.13

primer and one gene-specific primer. Primer sequences are listed in Table A-III-10. Analyses of single *chx17* mutants (*chx17-1* and *chx17-4*) showed little to no difference in root growth relative to *wild-type* (col-0) grown at pH 5.75 to 7.0 (Fig. A-III-2). Therefore, I generated double, triple and quadruple mutants.

To test if these T-DNA insertions resulted in null mutants, RNA was extracted from seedlings, reverse transcribed and the first strand cDNA was used for PCR analysis. F1 seedlings from selfing of single homozygous parents were subject to RNA extraction and reverse transcription to generate cDNA. First-strand cDNA was then used as a template for PCR analysis. Two sets of primer pairs (Table A-III-11) per *chx* mutant, corresponding to the 5'- and 3'- end, were used to test for transcripts upstream and downstream of each insertion site, respectively. Relative transcript level was estimated using actin as a control. RNA isolated from Wt seedling showed transcripts at both the 5'- and the 3'- end, suggesting that full-length transcripts were present for CHX16, 17, 18 and 19 (Fig. III-1B, lane 1). In mutant seedlings, all of them showed partial transcripts. For example, transcripts at the 5' end were detected, however transcripts corresponding to the 3' end were not detected in *chx17-4* allele (Fig. III-1B, lane 2-5), *chx18-1* allele (Fig. III-1B, lane 4,5) and *chx19-2* allele (Fig. III-1B, lane 3,5). *chx17-4* and *19-2 alleles* were likely null mutants, as the T-DNA insertions disrupted the TM domain (1-~450 residues), which is usually important for transport function (Table A-III-3). Allele *18-1* carries a T-DNA insertion within the hydrophilic C tail, so it is less certain if this mutant is a null. Although *chx16-10a* did not produce transcripts at the 5'-end probably because primers flanked the insertion site (Fig. III-1A; III-1B, lane 5); the insertion at residue 80 would disrupt the TM domain, so this mutant is likely a null. Curiously, potentially

Table III-I. Segregation ratio of the progeny of *chx16-19* triple or quadruple mutants.

Parent (selfed)				Segregation in progeny						
Genotypes				Genotypes				Observed	Expected	χ^2
chx16	*chx17*	*chx18*	*chx19*	*chx16*	*chx17*	*chx18*	*chx19*	(n = 40)	(n = 40)	p 0.05 = 5.99
+/+	-/-	+/-	-/-	+/+	-/-	+/+	-/-	9	10	
				+/+	-/-	+/-	-/-	29	20	10.55
				+/+	-/-	-/-	-/-	2	10	
+/+	-/-	-/-	+/-	+/+	-/-	-/-	+/+	16	10	
				+/+	-/-	-/-	+/-	20	20	7.2
				+/+	-/-	-/-	-/-	4	10	
-/-	+/-	-/-	-/-	-/-	+/+	-/-	-/-	15	10	
				-/-	+/-	-/-	-/-	23	20	9.35
				-/-	-/-	-/-	-/-	2	10	
-/-	-/-	+/-	-/-	-/-	-/-	+/+	-/-	17	10	
				-/-	-/-	+/-	-/-	20	20	9.8
				-/-	-/-	-/-	-/-	3	10	

+/+, +/- and -/- represent gene-specific- homozygous *Wt*, heterozygous mutant and homozygous mutant, respectively.There is significantly different from the Mendelian's segregation ratio when $\chi^2 > 5.99$ at *p value* = 0.05 (df = 2).

unspliced transcripts were observed in *chx18-1* allele and *chx19-2* allele (Fig. III-1B, row 5,7 in grey) as it was not detected in *chx17-4* allele. Thus, mutants *chx16*, *chx17* and *chx19* are mostly likely nulls.

Interestingly, I noticed some changes in the relative transcript level in single or double mutants (see quantitative results in Fig. A-III-2). Transcripts of both *CHX18* and *CHX19* were slightly increased in *chx17* mutants relative to the Wt, suggesting *CHX18* and *CHX19* are up-regulated when *chx17* is not functional (Fig. III-1B, lane 2). Consistently, *CHX18* transcript was higher in *chx17-4 chx19-2* double mutant (Fig. III-1B, lane 3) and *CHX19* transcript was enhanced in *chx17-4 chx18-1* double mutant (lane 4) when compared to *Wt* (lane 1). In contrast, Wt transgenic lines expressing *35Sp::CHX17* showed increased *CHX17* transcripts relative to Wt and other mutants (Fig. III-1B, row 3,4). Furthermore, over expression of *CHX17* was accompanied by reduction of *CHX16* transcript but not other *CHXs*. These results suggest that CHX17, 18 and/or 19 might compensate for one another functionally.

D.2. Higher order mutants of *chx17*, *chx18* and *chx19* led to segregation distortion

To test whether the progeny of heterozygous double, triple or quadruple mutants showed Mendelian's segregation, 40-157 individual plants were genotyped using PCR. Fortunately, the five genes, *CHX16* (At1g64170), *CHX17* (At4g23700), *CHX18* (At5g41610) and *CHX19* (At3g17630), were located on different chromosomes, therefore the law of independent assortment could be applied to this study. Statistical analysis using chi-square ($\chi 2$) test was then performed to assess the segregation distortion probability at 95% (p value = 0.05).

Selfing of two double heterozygous mutants, *chx17-4*$^{+/-}$ *chx18-1*$^{+/-}$ or *chx17-4*$^{+/-}$ *chx19-1* $^{+/-}$ produced the progeny with the expected segregation ratio ($\chi 2 < 15.51$, Table A-III-1, exp i and ii). Surprisingly, a triple mutant containing homozygous *chx17-4*$^{-/-}$ and heterozygous *chx18-1*$^{+/-}$ *chx19-1* $^{+/-}$ failed to produce any triple mutant plant out of 144 progenies analyzed (Table A-III-2, exp i). I further tested the progeny of a double homozygous mutant and one heterozygous mutant, *chx17-4*$^{-/-}$ *chx18-1*$^{-/-}$ *chx19-1*$^{+/-}$ or *chx17-4*$^{-/-}$ *chx18-1*$^{+/-}$ *chx19-1*$^{-/-}$. Among 40 progenies analyzed, the ratio of segregation observed was lower than that expected in either set of parents (Table III-1, exp i and ii) ($\chi 2 > 5.99$,). Triple mutants were obtained even though the numbers were about 2-5-fold less than that from expected segregation.

I recovered very few or no quadruple mutants of *chx16*, *17*, *18* and *19*. When quadruple heterozygous *chx16-10a*$^{+/-}$ *chx17-4*$^{+/-}$ *chx18-1*$^{+/-}$ *chx19-1* $^{+/-}$ plant was selfed, homozygous quadruple mutants were not recovered from 157 F_1 plants genotyped. Due to the limited population and large number of possible genotypes, I was unable to obtain any quadruple mutant and to assess $\chi 2$ properly. Interestingly, only 1 out of 9 F_1 plants harboring *chx17-4* $^{-/-}$ *chx18-1* $^{-/-}$ genotype was recovered from this screen (Table A-III-2, exp ii). When, *chx16-10a*$^{-/-}$ *chx17-4*$^{+/-}$ *chx18-1*$^{-/-}$ *chx19-1*$^{-/-}$ or *chx16-10a*$^{-/-}$ *chx17-4*$^{-/-}$ *chx18-1*$^{+/-}$ *chx19-1*$^{-/-}$ plants were selfed, segregation distortion was consistently observed in F_1 from both parents (Table III-1, exp iii and iv) ($\chi 2 > 5.99$,). Quadruple mutants were recovered at a frequency of 3-5 fold less than expected.

No obvious morphological or growth changes were observed in vegetative growth of triple homozygous and quadruple homozygous mutants relative to *Wt* plant on soil. However, the reduction of expected triple or quadruple mutant in the F1 population

would suggest that CHX17, 18, and 19 could have overlapping functions in plant reproduction and/or seed development.

D.3. CHX17 is expressed in developing seeds, stipules and roots

To monitor *CHX17* expression in live tissue, a 3-kb region upstream of the *CHX17* open-reading frame was cloned into the binary vector, pBYWG-CHX17 using homologous recombination in yeast. The resultant construct, *CHX17p*$_{3\ kb}$*::YFP*, in pBYUR-CHX17p vector was introduced into *chx17-4* mutant by *Agrobacterium*-mediated transformation. T2 seedlings or plants were examined for YFP fluorescence.

In mature plants grown on soil, YFP signals were observed consistently in developing seeds at the micropylar, chalazal endosperm or hilum region (Fig. III-2A, III-2B) at the pre-globular stage to the mature stage. I frequently observed the YFP signals from senescing cells in leaves and in areas surrounding a wound caused by insect or mechanical injury (data not shown). In seedlings cultured on 0.5X MS solid medium, I observed YFP signals in the stipules (Fig. III-2C). However, the most prominent YFP signals were observed in roots at the maturation zone, and sometimes at the root-shoot junction (Fig. III-2D). In the maturation zone, YFP signals were prominent in the epidermis as seen by the parallel fluorescent signals along the root (Fig. III-2E, top right) and at the surface of the mature lateral root (Fig. III-2E, bottom left). Fluorescence decreased towards the elongation zone and no fluorescence was detected at the root tip (Fig. III-3A-ii). These results are consistent with those obtained from microarray analyses of specific root cells isolated by cell sorting (Birnbaum et al., 2003) and promoter-gus reporter gene (Cellier et al., 2004; Sze et al. 2004). These results suggest a role of CHX17 in mature roots.

Fig. III-2. CHX17 promoter activity in developing seeds, stipules and mature roots of live plants.

CHX17p::*YFP* transgenic plants were grown on soil (A-B) or 0.5X MS solid medium (C-E). YFP fluorescent signals were observed under epifluorescent microscope (A-B) or confocal microscope (C-E). Scale bar = 50 um. Images were taken from 14-d old seedlings unless otherwise stated. Images are representatives of at least three independent transgenic lines of *chx17-4*, *CHX17p*::*YFP* plants.

A-B) *CHX17* promoter-driven YFP fluorescence in developing seeds. Epifluorescence (A) and DIC (A') images of developing seeds attached to the funiculus. Enlarged view of one seed showing YFP flourescence at the micropylar or chalazal end (B). Images were taken from seeds at mature green stage.

C) Stipules with YFP and seen by bright-field (C') are merged in C".

D-E) Root-shoot junction showed *CHX17* promoter-driven YFP activity (D), and as seen under bright field (D') are merged in D", including epidermis and root hair cells in mature region.

E) Epidermis of the main root (upper right) and of a lateral root (left) show CHX17 promoter activity. Epifluorescence (E) and bright field (E') images are merged in E".

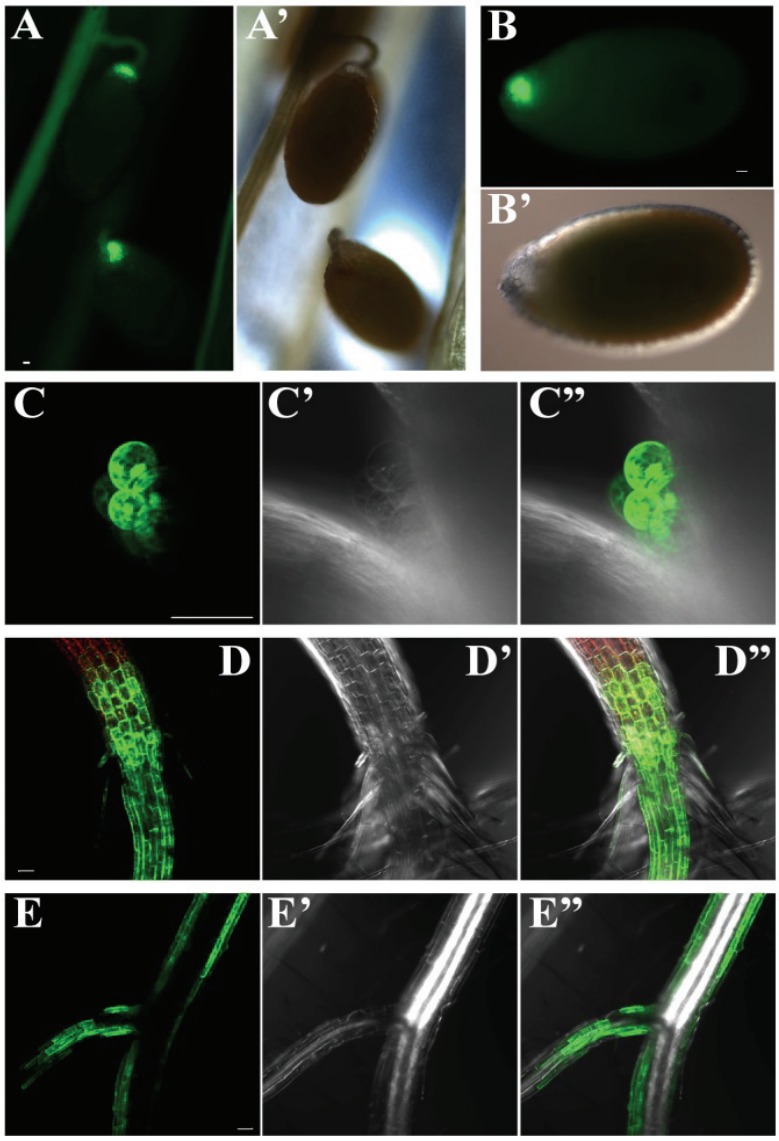
A
A'
B
B'
C
C'
C"
D
D'
D"
E
E'
E"

D.4. K^+ starvation enhances *CHX17* expression in roots

To test the effect of limited K^+, salt and osmotic stress on *CHX17* expression, YFP signals in roots of transgenic plants harboring *CHX17p$_{3\ kb}$::YFP* were monitored. Seedlings were grown in 0.5X MS solid medium for 1 week before transferring to modified Gibeaut (GB) solid medium (Gibeaut et al, 1997) where K^+ concentration was adjusted. To reduce K^+, I used noble agar which contains about 0.05 mM K^+, whereas regular GB medium contains about 1.8 mM K^+.

Very strong YFP signals were observed in mature root epidermis of seedlings grown in 0.05 mM K^+ compared to 1.8 mM K^+. To make comparisons of fluorescent signals, I focused on the root tip. As seen before, no YFP signals were observed at the root tip in seedlings grown with 1.8 mM K^+ (Fig. III-3A-ii). In contrast, YFP signals were clearly enhanced in plants grown at limiting K^+ (0.05 mM), (Fig. III-3A-iv). The root tip region was arbitrarily divided into three segments, at 0-3, 3-6 or 6-9 mm from the tip, and the relative fluorescent signals were compared by fixing the exposure time and camera sensitivity. No significant change in YFP signals were observed in seedlings treated with 100 mM NaCl or 200 mM sorbitol relative to 1.8 mM K^+ (Fig. III-3B). Also, no significant change in YFP signals was observed in seedlings grown at pH 7.0 instead of pH 5.8 (data not shown). Only, 0.05 mM K^+ caused a 25-fold increases in YFP flourescence compared to that seen with 1.8 mM K^+ (Fig. III-3B). This result agrees with a previous study (Cellier 2004). Interestingly, limiting K^+ in the growth medium appeared to induce many short root hairs with increased *CHX17* promoter activity near the root tip region.

Fig. III-3. *CHX17* promoter activity was up-regulated when K^+ was limiting.

All plants were germinated in 0.5X MS solid medium for 7 d and then transferred to GB solid medium with indicated concentration of K^+, Na^+ or sorbitol at pH 5.8. Growth or fluorescence was determined after 7 d.

A) *CHX17* expression at the root tip is induced by limiting K. Single *chx17-4* mutant seedlings expressing YFP under the control of the *CHX17* promoter were grown in medium containing 1.8 mM K (i-ii) or 0.05 mM K (iii-iv). Bright field (i, iii) and corresponding epifluorescence (ii, iv) images are shown. Images are representative of two independent transgenic lines. Scale bar = 50 μm.

B) *CHX17* promoter activity is enhanced by limiting K^+ but not by osmotic stress. Seedlings of *chx17-4* mutant expressing *YFP* under the native *CHX17* promoter were grown in medium containing adequate (1.8 mM) or limiting (0.05 mM) KCl, 100 mM NaCl or 200 mM sorbitol. Roots were separated into 3 sections as measured from the tip: 0-3, 3-6 and 6-9 mm. Fluorescent intensity (F) was measured at a fixed exposure time of 411 msec and a gain of 1. Result is representative of two experiments with two transgenic lines per experiment. n = 20, bars = SD

C) Root length was unaltered in mutants relative to wild-type plants. Transgenic or mutant seedlings were grown in medium containing 1.8 mM or 0.05 mM K. Root length was determined 7 d later. Plants tested include: i) *wild-type* with *35S*::*GFP* (Wt); ii) *chx17-4* mutant expressing *CHX17p*::*YFP* (chx17); iii) single *chx17-4 mutant* expressing *35S*::*CHX17-GFP* (chx17/CHX17); iv) double *chx17-4/chx18-1* expressing *35S*::*GFP* (*chx17/chx18*); and v) quadruple *mutant chx16-10a, chx17-4, chx18-1, chx19-2* expressing *35S*::*GFP* (quadruple). Data are from two independent siblings or transgenic lines, n = 20-28, bar = SD.

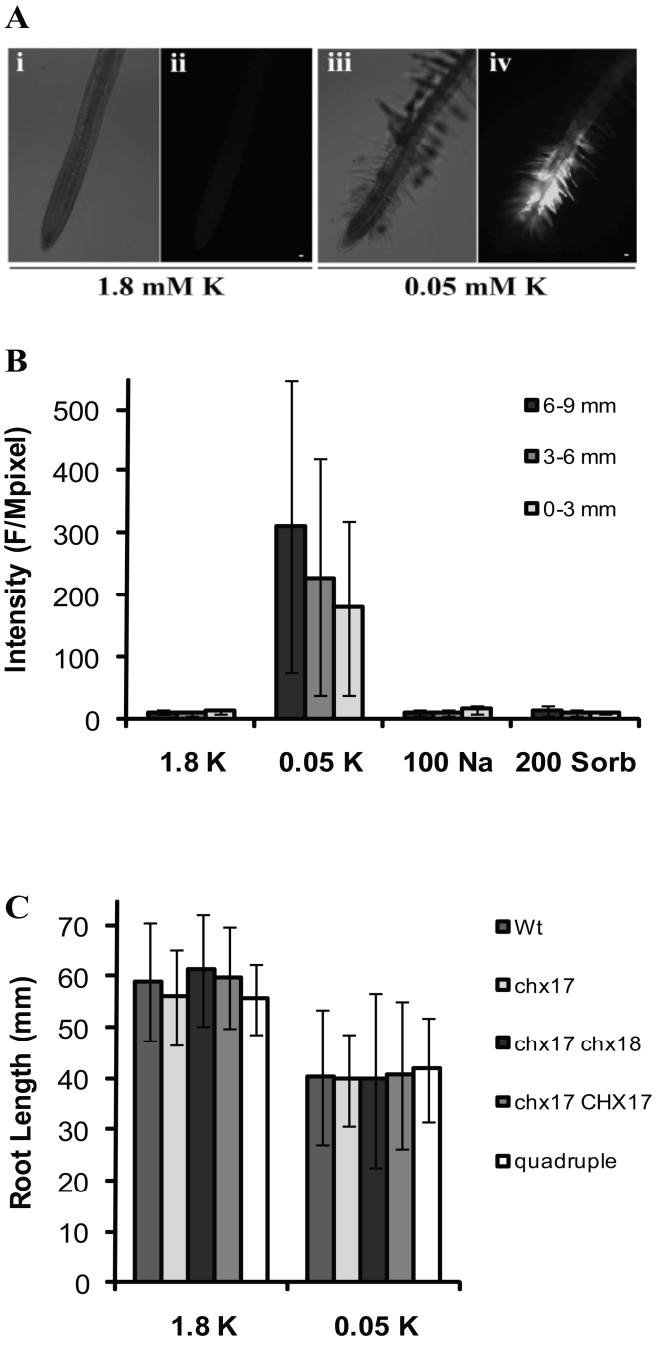
A
i
ii
iii
iv
1.8 mM K
0.05 mM K
B
Intensity (F/Mpixel)
500
400
300
200
100
0
6-9 mm
3-6 mm
0-3 mm
1.8 K
0.05 K
100 Na
200 Sorb
C
Root Length (mm)
70
60
50
40
30
20
10
0
Wt
chx17
chx17 chx18
chx17 CHX17
quadruple
1.8 K
0.05 K

In spite of the altered *CHX17* promoter activity, there was no obvious differences in root length between the Wt, and *chx17-4* single mutant, *chx17-4, chx18-1* double mutant, quadruple mutant or with plant lines over-expressing *CHX17* at 1.8 mM K^+ or 0.05 mM K^+ (Fig. III-3C). Growth was partially impaired in all plants cultured on medium with 0.05 mM K^+ relative to 1.8 mM K^+. This result suggested that CHX16, 17, 18 or 19, nonetheless, did not play a major role in K^+ nutrition.

D.5. CHX16, 17, 18 and 19 localize to PM and post-Golgi compartment in plants

To determine the subcellular distribution of CHX16 to CHX19, transgenic plants harboring *GFP*-tagged *CHX* under the control of the *35S* promoter were generated. GFP-tagged to the carboxyl terminus of CHX proteins were functionally active as shown by their ability to restore growth of alkaline-pH sensitive yeast mutant on pH 7.5 medium (Fig. A-II-6). Surprisingly, I observed CHX16, 17, 18 and 19-GFP at the cell periphery of the intact roots in addition to puncta that had been verified as PVC in protoplasts previously (Chapter II).

To test whether the signals observed from the cell periphery were PM, cells were plasmolyzed by incubating leaves of transgenic plants with 30% sucrose. In plasmolyzed cells, the PM forms strand-like structures, known as Hechtian strands, due to the shrinkage of cytosol while PM is attached to points of the cell wall (Lang et al., 2004). I observed fluorescence from CHX16, 17, 18 or 19-GFP at Hechtian strands in guard cells. However, free GFP or GFP-KDEL, representing cytosol or luminal ER, respectively, localized entirely to the oval structure after plasmolysis (Fig. III-4A). No strand-like structure was observed. Likewise, CHX15-GFP which most likely localized to ER membrane (Fig A-III-3A) showed no strand-like structure after plasmolysis (Fig. III-4B).

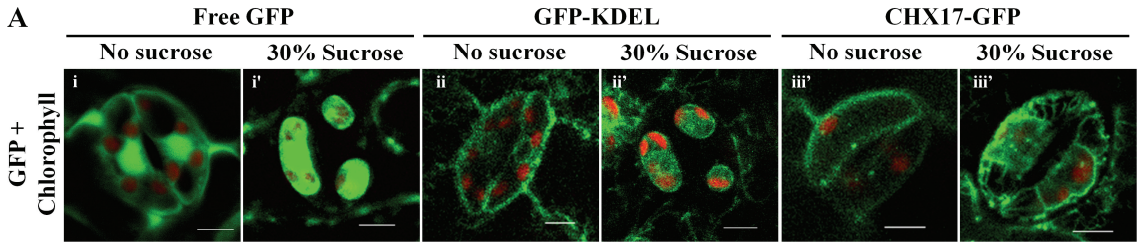

Fig. III-4. GFP–tagged CHX16 to CHX19 are localized to Hechtian strands after cell plasmolysis.

A) Plasmolysis of cells treated with 30% sucrose revealed Hechtian strands. Transgenic plants harboring (i) free GFP, (ii) GFP-KDEL or (iii) CHX17-GFP under the control of the *35SCaMV* promoter were cultivated for 3 weeks. Leaves were infiltrated with 0.1X MS medium alone (no sucrose) or with 30% sucrose for 1 h. Leaves were washed and submerged in 0.1X MS medium with 30% sucrose. Guard cells were observed by microscopy. Scale bars = 5 μm.

i) Soluble GFP (i', cytosol and nucleus) in control (no sucrose) cells labeled the peripheral cytosol and the nucleus, and was concentrated in reduced areas after sucrose treatment.

(ii) GFP-KDEL (ii', ER marker) labeled the cell periphery and the perinuclear region in control cells, and converged into few smaller compartments in sucrose-treated cells. Plastids as shown by red fluorescence were dispersed in the cytoplasm in control cells became localized after treatment with sucrose.

(iii) CHX17-GFP fluorescence distributed in the peripheral cytoplasm of control cells, appeared in Hechtian strands and at the boundary of the plasmolyzed cells.

Fig. III-4. B) Localization of GFP-tagged CHX15 to ER, and of CHX16, CHX17, CHX18 and CHX19 to the plasma membrane and punctate structures. Transgenic plants harboring *CHX15-GFP* (i), *CHX16-GFP* (ii), *CHX17-GFP* (iii), *CHX18-GFP* (iv) or *CHX19-GFP* (v) constructs under the *35S* promoter were grown in soil for 3 wks. Leaves were infiltrated with 0.1X MS medium only (no sucrose) (column 6) or with 30% sucrose and 4 μM neutral red, and incubated for 1 h. Leaves were washed and submerged in 0.1X MS medium with 30% sucrose. Guard cells were observed by bright field (column 5) or by confocal microscopy for GFP (column 1), red emission over 650 nm, chlorophyll and neutral red (column 2), or 560-635 nm for neutral red only (column 3) and images were merged in column 4. Column 6 shows merged images of GFP and chlorophyll (505-405 nm and over 650 nm, respectively) fluorescence in control cells.

i) CHX15-GFP labeled reticulate and perinuclear regions of control cells (column 6). After plasmolysis, GFP was confined inside reduced oval areas containing chloroplasts (chlorophyll fluorescence) and vacuole as represented by neutral red fluorescence (column 3).

ii-v) CHX16-GFP to CHX19-GFP labeled punctate and peripheral fluorescence in unplasmolyzed cells (ii-v, column 6), and the boundary of plasmolyzed cells as well as Hechtian strands (column 1 and 4). Chlorophyll fluorescence (column 2) and neutral red (column 3) are enclosed within the boundary of the plasmolyzed compartments. Bright field images (column 5) show the reduced area of the plasmolyzed cytoplasm within the guard cells.

Fluorescent signals were observed under confocal microscope (GFP: Ex 488 nm/Em 505-545 nm, chlorophyll: Ex 543 nm/Em > 650 nm, neutral red: Ex 543 nm/Em > 560 nm). Images are representative of two experiments. At least 3 leaves from two transgenic lines were used in each experiment. Scale bars = 5 μm.

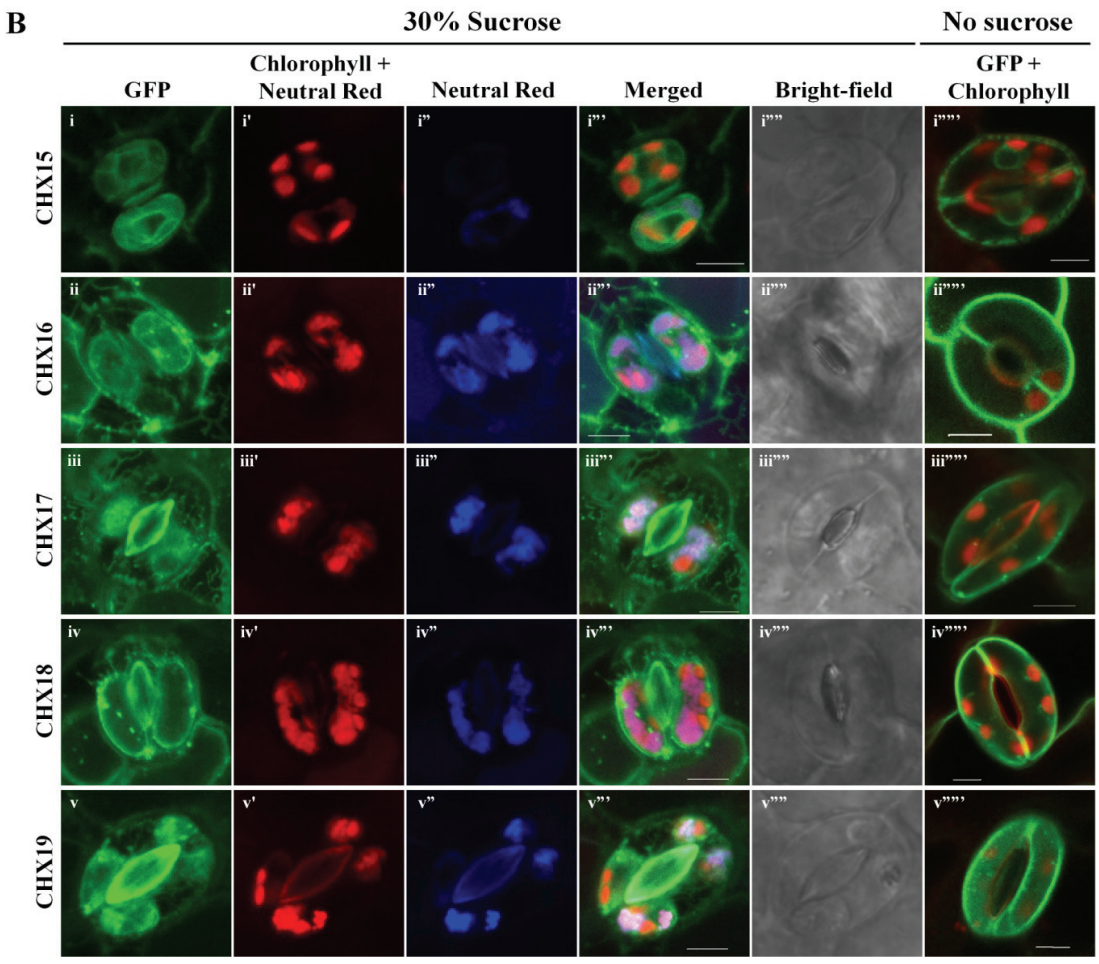
B
30% Sucrose
No sucrose
GFP
Chlorophyll + Neutral Red
Neutral Red
Merged
Bright-field
GFP + Chlorophyll
CHX15
CHX16
CHX17
CHX18
CHX19
i
i'
i"
i"'
i""
i""'
ii
ii'
ii"
ii"'
ii""
ii""'
iii
iii'
iii"
iii"'
iii""
iii""'
iv
iv'
iv"
iv"'
iv""
iv""'
v
v'
v"
v"'
v""
v""'

Therefore, the oval structures observed after plasmolysis represented the shrunken protoplasts as shown by the presence of cytosol, ER, chloroplasts, vacuole and part of PM (Fig. III-4B). Furthermore, I did not observe association of CHX16, 17, 18 or 19-GFP with acidic compartments which accumulated neutral red (Fig. III-4B). Therefore, CHX16, 17, 18 or 19-GFP were localized to PM but not to the vacuolar membrane.

To verify the location of CHX16 to CHX19, a PM marker tagged with the red fluorescence protein was introduced by crossing transgenic plants harboring *CHX-GFP* with plants carrying *AtPIP2-RFP*. F1 plants were examined by confocal microscopy. Accordingly, fluorescent signals at the cell periphery derived from CHX16-, 17-, 18- or 19-GFP co-localized well with AtPIP2-RFP in root epidermis from the division zone (Fig. III-5A). Curiously, CHX16-GFP which previously showed reticulate pattern in protoplasts (Fig. A-II-7) displayed punctate pattern in intact root (Fig III-5A-i).

To test if the puncta observed in roots of CHX16, 17, 18 and 19-GFP transgenic plants might be Golgi, transgenic plants harboring *CHX-GFP* were crossed with plants expressing a Golgi marker, *GmMAN1-RFP*. CHX16-GFP showed both punctate and reticulate pattern in root epidermis from the maturation zone of F1 progeny (Fig. III-5B-i). However, the fluorescent puncta observed in CHX16-GFP transgenic plants did not co-localize with GmMAN1-RFP. Intriguingly, CHX16-GFP showed mainly punctate localization only at the root epidermis in the division zone (Fig. III-5A-i) and leaf epidermis (data not shown). In root maturation zone, CHX16-GFP showed substantial reticulum labeling indicating localization at the ER. I also observed reticulate pattern in epidermis of root maturation zone in transgenic plants expressing *CHX17*-, *CHX18*- or *CHX19-GFP* though the frequency of green puncta was dominant (Fig. III-5B-ii, -iii, -iv).

Fig. III-5. CHX16, 17, 18 and 19 localized to the PM and post Golgi compartments in planta.

Trangenic lines (*Wt col-1* background) co-expressing *GFP* and *RFP* fusion constructs were obtained from a cross between plants expressing *35Sp*::*CHX-GFP* and *35Sp*::*AtPIP2-RFP* (A) or *35Sp*::*GmMAN1-RFP* (B). F1 seeds were germinated in 0.5X MS solid medium for 10 d before observation or treatment. Fluorescent signals were observed under confocal microscopy. Images are representative of at least two independent transgenic lines. Scale bar = 5 μm.

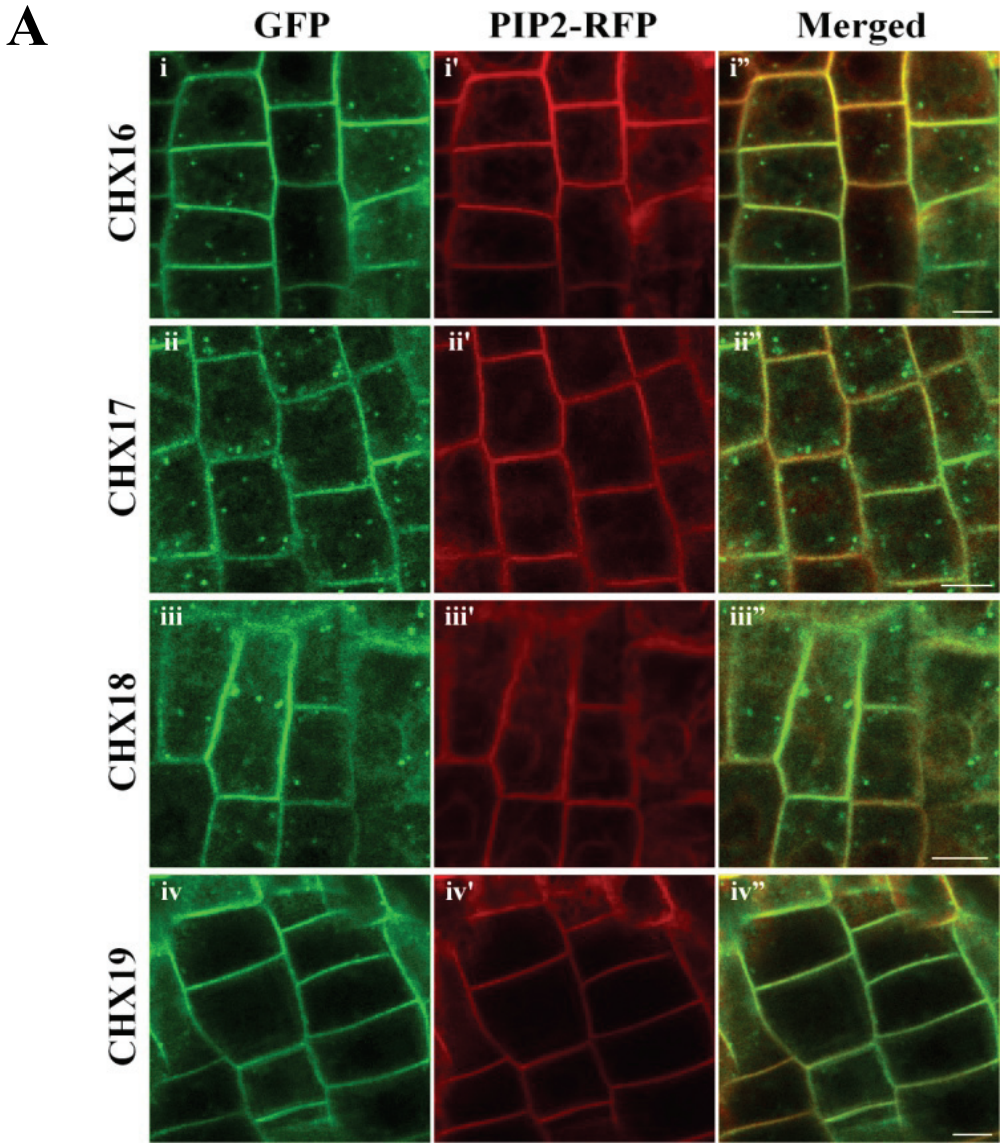

Fig. III-5. A) GFP-tagged CHX16, 17, 18 or 19 co-localized with PIP2 at the PM. GFP signals were observed in puncta and the cell periphery. AtPIP2-RFP (PM marker) co-localized with GFP at the cell periphery as seen in merged images. Cells are from the root epidermis near the root tip of 10-d old seedlings at the division zone. Result is representative of at least two independent observations. Scale bars = 5 μm.

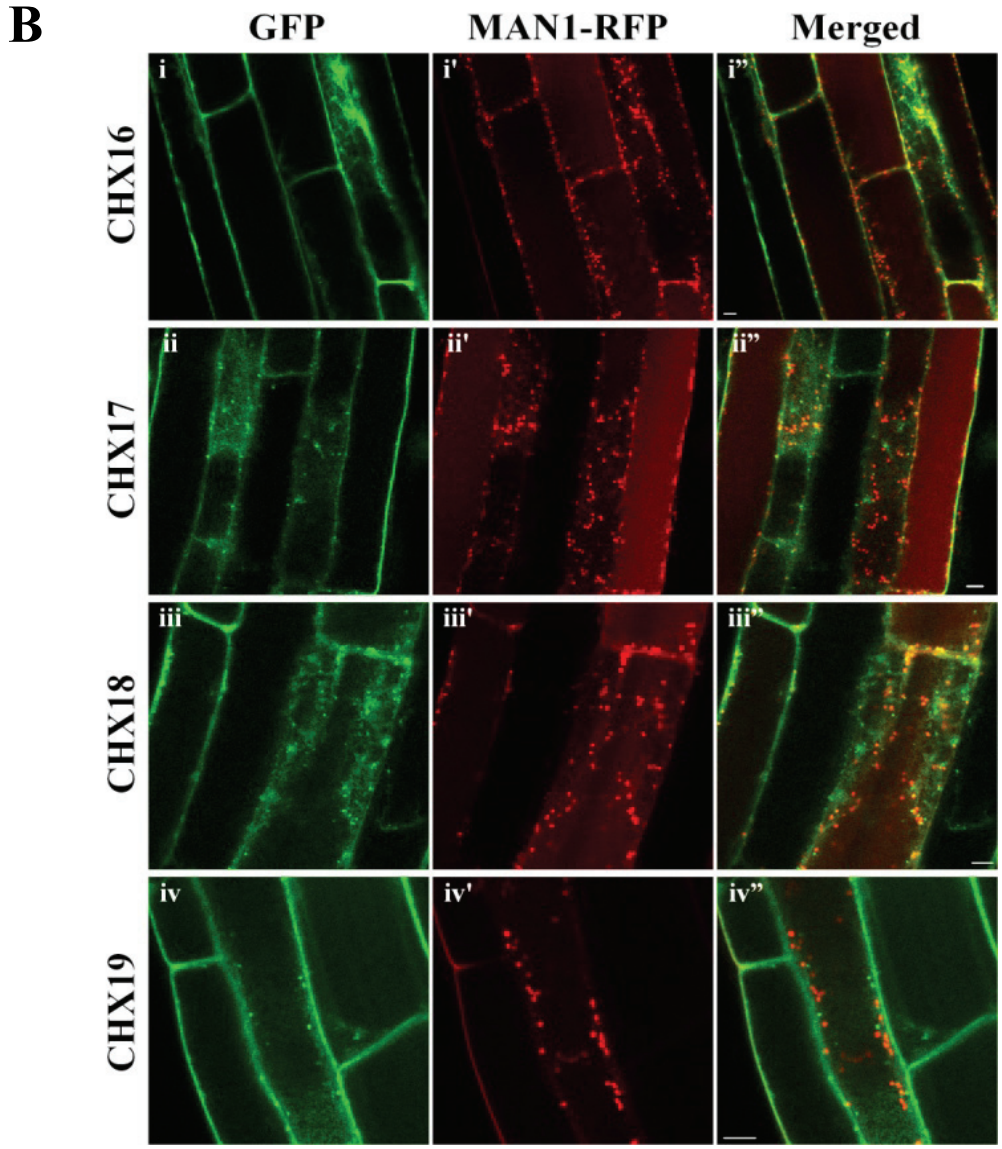

Fig. III-5. B) GFP-tagged CHX16, 17, 18 and 19 were localized to puncta that did not co-localize with a Golgi marker. Transgenic seedlings co-expressing *CHX(16, 17, 18, 19)-GFP* and *GmMAN1-RFP* were imaged. Root epidermal cells from the mature zone are shown. Result is representative of at least two independent observations. Scale bars = 5 μm.

Fig. III-5. C) CHX17-GFP driven by its native promoter localized to the PM and to puncta that were not Golgi or TGN. GFP (left) and FM4-64 (middle) signals were merged at the right column. Scale bars = 5 μm.

(i) CHX17-GFP did not co-localize with GmMAN1-RFP in root epidermis at the mature zone. Transgenic plants harboring genomic *CHX17-GFP* fusion under the control of its native promoter and *35Sp*::*GmMAN1-RFP* as in B were grown in 0.5X MS solid medium for 7 d then transferred to GB medium with low K^+ (0.05 mM) for 3 d.

(ii) CHX17-GFP co-localized with FM4-64 at the cell periphery but not at endocytic compartments in root epidermis at the mature zone.. Roots of transgenic plants expressing CHX17-GFP under its native promoter were grown as in C-i, and incubated with 10 μM FM4-64 for 10 min then washed and submerged in GB medium with 1.75 mM K^+.

(iii) CHX17-GFP localized at the puncta within and outside the confined compartments in cells near the division zone. Roots of plants as in C-ii. No co-localization was observed with FM4-64 either at the cell periphery or endocytic compartments.

C

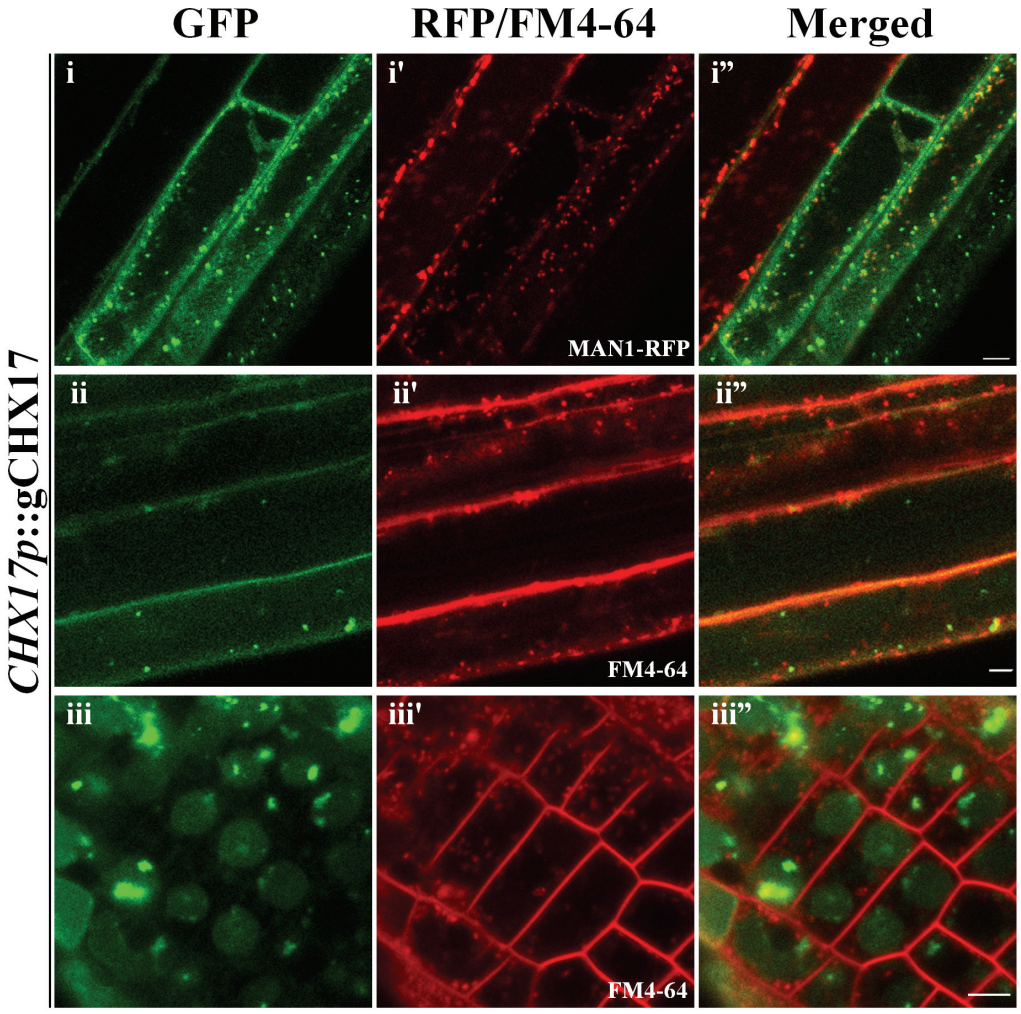
GFP
RFP/FM4-64
Merged
CHX17p::gCHX17
i
i'
i"
MAN1-RFP
ii
ii'
ii"
FM4-64
iii
iii'
iii"
FM4-64

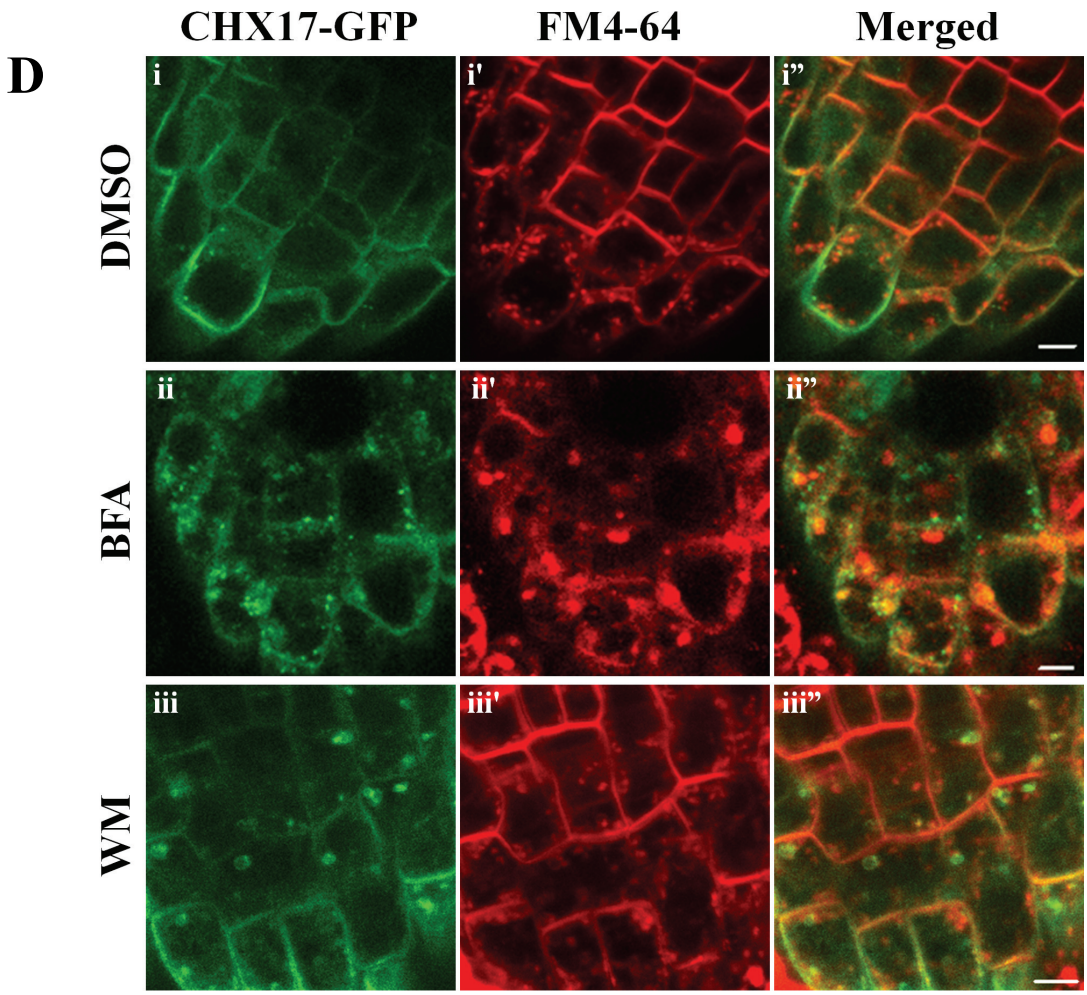

Fig. III-5. D) Wortmannin caused formation of ring-like structures labeled by CHX17-GFP. *Wt* seedlings harboring *35S*::*CHX17-GFP* were incubated with 10 μM FM4-64 for 10 min, then washed and treated with 0.5% DMSO, 50 μM BFA or 33 μM wortmannin (Wm) in 0.1X MS medium for 90-120 min. (Top) DMSO-treated cells. CHX17-GFP was observed at the puncta and cell periphery. (Middle) CHX17-GFP signals did not co-localize with FM4-64 signals from Brefeldin A (BFA) compartments. (Bottom) CHX17-GFP localizing compartments formed ring-like structures after Wm treatment. FM4-64 labeled membranes were unaffected by Wm. Cells are from root epidermis at the division zone. Result is representative of two experiments. Scale bars = 5 μm.

Nevertheless, the puncta from CHX17, 18 or 19-GFP did not colocalize with those from GmMAN1-RFP in root epidermis from the maturation (Fig. III-5B) or division zone (data not shown). Together, these results indicated that CHX16, 17, 18 and 19 localized to PM and to post-Golgi compartment, but not Golgi.

To examine CHX17 expression under its native promoter, transgenic plants expressing genomic *CHX17-GFP* (gCHX17) driven by its native promoter were generated. As shown with a constitutive promoter, green fluorescence signals were consistently observed at the cell periphery and in puncta of transgenic plants harboring *CHX17p*::*gCHX17-GFP* (Fig. III-5C). When these transgenic plants were crossed with plants expressing a Golgi marker, *GmMAN1-RFP*, I observed no co-localization between gCHX17-GFP and GmMAN1-RFP in root epidermis from maturation zone of F1 plants (Fig. III-5C-i''). These results further verified that gCHX17-GFP associated with post-Golgi compartments. Further analysis showed that FM4-64 did not overlap with gCHX17-GFP at the puncta but displayed superimposed signals at the cell periphery (Fig. III-5C-ii''), indicating that gCHX17-GFP localized to the PM but not the TGN or early endosomes.

Interestingly, fluorescence from gCHX17-GFP was observed in root epidermis at the division zone when transgenic plants harboring *CHX17p*::*gCHX17-GFP* were grown in K^+-limited medium (0.05 mM) for 3 days (to induce CHX17 expression). Under this condition, fluorescent puncta were observed in the vacuole and the signals from cell periphery disappeared (Fig. III-5C-iii). Moreover, FM4-64 which labeled PM and TGN did not co-localize with gCHX17-GFP at all (Fig. III-5C-iii"). The appearance of gCHX17-GFP in the vacuole and the absence from the PM would suggest that gCHX17-

GFP was endocytosed and delivered to the vacuole in cells at the root tip. The presence of CHX17-GFP inside the vacuole, PM and the post-Golgi compartments that are not associated with TGN or early endosomes implies that gCHX17-GFP indeed localized to PM and late endosomes (PVC). It is likely that GFP signals observed in reticulate structures (Fig. III-5B) reflect newly-synthesized CHX at the ER due to over-expression by the 35S promoter.

D.6. Effect of BFA and wortmannin suggest CHX17 is localized to PVC *in planta*

To verify the distribution of CHX17 *in planta*, I tested the effect of brefeldin A (BFA) or wortmannin (Wm) on the status of CHX17-GFP-labeled compartments. BFA interferes with vesicle budding and membrane trafficking resulting in accumulation of 'BFA' compartments by targeting ADP-ribosylation factor (ARF-GEF), thus blocking the exchange of GTP onto ARF (Donaldson et al, 1992). Wortmannin, a fungal metabolite, is an inhibitor of phosphoinositide 3-kinases (PI3K, Arcaro & Wymann, 1993). This enzyme (PI3K) produces phosphatidylinositol 3-phosphate (PtdIns3P) which binds ring finger FYVE and Phox (PX) domains of protein effectors and recruits them to endosomes, especially proteins involved in trafficking of late endosomes (PVC). Wortmannin causes a depletion of PtdIns3P, thus it prevents membrane trafficking in PVC causing an enlargement of these compartments.

Before BFA treatment, CHX17-GFP localized to puncta and the cell periphery (Fig. III-5D-i) at the root epidermis from the division zone. There was no co-localization between CHX17-GFP and FM4-64 at the puncta (Fig. III-5D-i") indicating that CHX17-GFP did not localize to the TGN. However, both CHX17-GFP and FM4-64 co-localized well at the cell periphery (Fig. III-5D-i"), indicating CHX17 association with the PM.

With BFA treatment, I observed large puncta labeled with FM4-64 often referred to as 'BFA compartments' (Fig. III-5D-ii'). No co-localization between FM4-64 and CHX17-GFP was observed (Fig. III-5D-ii"). This result indicated that CHX17-GFP-labeled punctate structures were unaffected by BFA. Intriguingly, the signals at the cell periphery from both FM4-64 and CHX17-GFP were diminished after BFA (Fig. III-5D-ii"), suggesting that BFA inhibited the trafficking of both FM4-64 and CHX17-GFP to the PM. Furthermore, after prolonged BFA treatment (2 h and at higher dosage), I observed co-localization of CHX17-GFP and FM4-64 at 'BFA compartments' (data not shown). These result suggested that CHX17-GFP-labeled compartments are less sensitive to BFA than FM4-64-labeled compartments.

In contrast, I observed that wortmannin caused CHX17-GFP labeled puncta to form ring-like structures (Fig. III-5D-iii); though it had little or no effect on FM4-64-labeled punta (Fig. III-5D-iii') which represented the TGN. Yet, both CHX17-GFP and FM4-64 remained at the cell periphery (Fig. III-5D-iii) after wortmannin treatment, suggesting that this inhibitor did not block trafficking of CHX17-GFP and FM4-64 to the PM. As Wm causes dilation of the PVC and blocks trafficking to the vacuole; the evidence would support the idea that CHX17-GFP was localized at the PVC, and not at the TGN.

This idea is further supported by immuno-electron microscopy. Transgenic seedlings expressing *CHX17*-tagged to *GFP* were fixed, sectioned and probed with anti-GFP linked to gold. Gold particles were observed at the PM, PVC (P), inside the vacuole (V) and ER (Fig. III-6). Interestingly, no gold particles were observed at the Golgi. This result further confirmed that CHX17-GFP was localized to the PVC and PM.

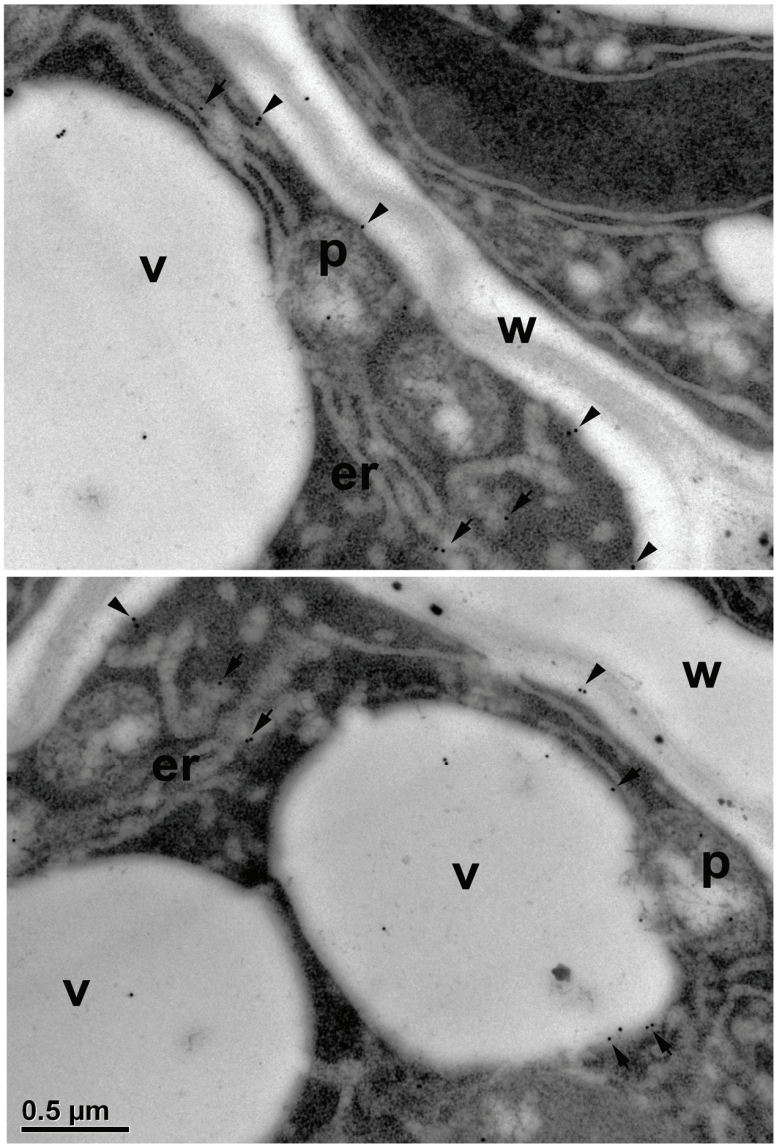

Fig. III-6. Immuno-EM localization of CHX17-GFP to the PM and PVC in plants. Roots of *Wt* transgenic seedlings expressing *35S*::*CHX17-GFP* were fixed, embedded in LR white and sectioned. Sections were incubated with antibodies against GFP followed by secondary antibody conjugated to gold particles. Gold particles was mainly localized at the PM and the PVC. P, prevacuolar compartment PVC; ER endoplasmic reticulum, V vacuole and W, cell wall. Scale bar = 0.5 µm. (Jauh GY)

D.7. A truncated CHX17 lacking the C-terminal tail is active

To test the role of the hydrophilic carboxyl tail, constructs lacking C tail or transmembrane (TM) domain of CHX17 were tested for activity in yeast mutant KTA40-2 (Fig III-7A). All yeast transformants grew well on medium at pH 5.6. However at pH 7.5, yeast harboring empty vector failed to grow whereas the full-length CHX17 rescued growth (Fig III-7A) as shown before (Chapter II). A truncated CHX17-TM(1-425) lacking the last TM domain failed to restore growth at alkaline pH, whereas a truncated CHX17-TM(1-472) containing the entire TM domain was partially effective. Yeast strains expressing the hydrophilic C tail alone, CHX17-Ct(473-820), or C tail with TM11, CHX17-Ct(426-820), grew poorly at pH 7.5 (Fig. III-7A) similar to those harboring the empty vector. These result suggested that the complete TM domain of CHX17, TM(1-472), was necessary for activity.

The CHX17-TM(1-472)-GFP was localized in yeast to different compartments when compared to the full-length transporter. The full-length CHX17-GFP localized to tubular structures at the cell periphery (Fig. 7B-i) that did not co-localize with FM4-64 (Fig. III-7B-i"). The truncated CHX17-TM (1-472)-GFP localized to reticulate and to perinuclear structures (Fig. III-7B-ii). The signals from CHX17-TM (1-472)-GFP did not overlap with that of FM4-64 (Fig. III-7B-ii"). However, a short truncated CHX17-TM(1-425)-GFP showed dim diffuse signals on some puncta (Fig. III-7B-iii) that partially overlapped with FM4-64 (Fig. III-7B-iii"). Thus, the non-functional form, TM (1-425)-GFP, appeared to be localized and degraded in the endosomes and vacuole, respectively. These results also suggested that the functional forms of truncated CHX17-TM(1-472)-

Fig. III-7. Truncated CHX17 TM(1-472) was functionally active and localized to yeast endomembranes.

A) Yeast expressing truncated *CHX17-TM(1-472)* or full-length *CHX17 (1-820)* showed growth at alkaline medium. Yeast strain KTA40-2 (*ena1-4Δ, nha1Δ, nhx1Δ, kha1Δ*) harboring empty pDR196 vector (EV), or vector with full-length (FL) or truncated *CHX17* containing *TM(1-425)*, *TM(1-472)*, *Ct(426-820)*, or *Ct(473-820)* were grown in YNB-Glucose overnight. Cells were then diluted 5 fold with YNB without carbon source and incubated for an additional 12-14 h. Cells were washed and normalized with water to A_{600} 0.2 and diluted 10-fold serially. Five μl of each dilution was dropped on YNB-MES-Glucose medium at pH 5.6 or pH 7.5.

B) C-tail truncated CHX17-TM(1-472) and full-length CHX17 localized to endomembrane in yeast. Yeast strain KTA40-2 (*ena1-4Δ, nha1Δ, nhx1Δ, kha1Δ*) harboring pGWFDR196 vector with full-length *CHX17*, or C-tail truncated *CHX17-TM(1-472)* or *TM(1-425)* fused to *GFP* were grown in YNB-Glucose overnight then replaced with YPAD medium and incubate for 3 h. Cells were given FM4-64 at a final concentration of 1 μM for 10 min, washed and suspended in 2% sucrose and 0.05% agarose. Fluorescent signals were observed by confocal microscopy. Images were taken 10-30 min after washing. Scale bars = 2 μm.

A

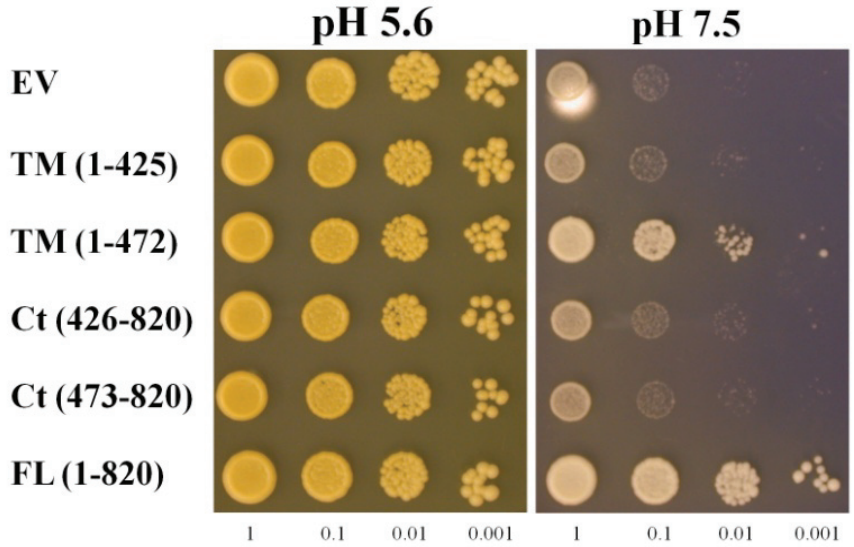
pH 5.6
pH 7.5
EV
TM (1-425)
TM (1-472)
Ct (426-820)
Ct (473-820)
FL (1-820)
1
0.1
0.01
0.001
1
0.1
0.01
0.001

B

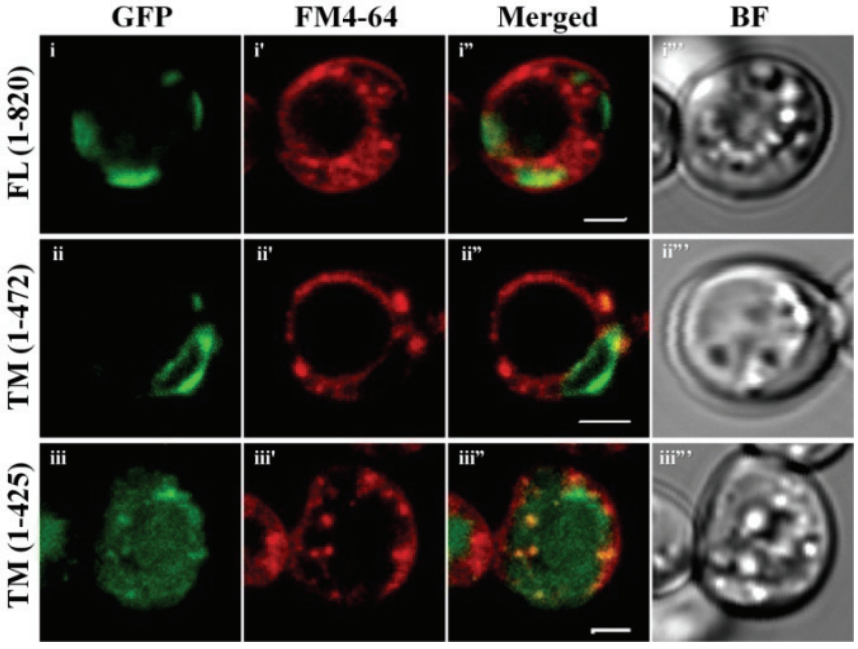
GFP
FM4-64
Merged
BF
FL (1-820)
TM (1-472)
TM (1-425)
i
i'
i"
i"'
ii
ii'
ii"
ii"'
iii
iii'
iii"
iii"'

GFP, and full-length CHX17-GFP were likely localized to different domains in ER or endomembrane in yeast.

D.8. C-tail of CHX17 is required for trafficking out of the ER in plant

To test the role of the hydrophilic C tail on membrane distribution in plants, *Arabidopsis* protoplasts were transfected with vectors harboring CHX17-truncated constructs fused with *GFP* at the 3' end (Fig. III-8A). The full-length CHX17-GFP was localized to small puncta (Fig. III-8B-vi, A-III-3B-i), resembling PVC as seen before. The truncated CHX17-TM (1-425)-GFP, which lacks the entire hydrophilic carboxyl tail and the last TM11, showed solely a reticulate pattern (Fig. III-8B-ii) similar to ER marker, GFP-HDEL (Fig. A-III-4D-i). In contrast, a truncated CHX17-TM(1-472)-GFP, which had complete TM domain, was localized to reticulum and to the puncta (Fig. III-8B-iii). Interestingly, the fragment thought to be the hydrophilic C tail and the last TM domain, CHX17-Ct (426-820)-GFP, showed reticulate pattern (Fig. III-8B-iv) similar to signals from GFP-HDEL (Fig. A-III-4D-i) and free GFP (cytosol and nucleus marker, Fig. III-8B-i). In contrast, the hydrophilic C tail only, CHX17-Ct(473-820)-GFP displayed diffuse localization solely in cytosol and nucleus similar to soluble free GFP. Thus, CHX17-Ct(426-820)-GFP was likely associated with ER, cytosol and nucleus. Together, these results suggest that, the truncated TM domain, CHX17-TM(1-425)-GFP was localized to the ER, whereas, the entire TM domain, CHX17-TM(1-472)-GFP was localized to other compartments in addition to ER. These results imply that the last TM domain of CHX17 could have a role in sorting.

To identify the puncta labeled by CHX17-TM (1-472)-GFP, protoplasts were co-transfected with TM (1-472)-GFP and PVC markers, RFP-ARA7 or CHX17-full length-

RFP as shown before (Chapter II). Signals from CHX17-TM(1-472)-GFP did not overlap with that of RFP-ARA7 (Fig. III-8C-i", A-III-4A-i") or CHX17-RFP (Fig. III-8C-ii"), indicating that CHX17-TM(1-472)-GFP was not localized to the PVC. To test whether these puncta are associated with Golgi, transgenic plant harboring *35Sp*::*CHX17-TM(1-472)-GFP* (Fig. III-8A) were crossed with *GmMAN1-RFP* expressing plants. Fluorescent signals from CHX17-TM(1-472)-GFP overlapped well with GmMAN1-RFP at the small puncta (Fig. III-8E) in epidermis from the root-shoot junction of F1 plants, suggesting localization of CHX17-TM(1-472)-GFP at the Golgi.

To determine whether CHX17-TM(1-472)-GFP was also associated with ER, transgenic plants co-expressing *RFP-HDEL* and full-length or truncated *CHX17-GFP* were generated by crossing. The lines co-expressing both red and green fluorescence were selected from the F1 plants. Truncated CHX17(1-425)-GFP co-localize well with ER marker (Fig. III-8D-i") confirming that reticulum observed in Fig. III-8B-ii was ER. Intriguingly, CHX17-TM (1-472)-GFP also overlapped well with RFP-HDEL (Fig. III-8D-ii") in reticulate network, however, signals from small and large punctate structures did not co-localize with ER marker. In addition, the full-length CHX17 seen at the puncta did not co-localize with RFP-HDEL (Fig. III-8D-iii"). Furthermore, the green and red fluorescence that appeared to overlap at the cell periphery displayed different patterns. GFP signals were smooth but RFP-HDEL signals were discontinuous, suggesting PM and ER, respectively, as shown in Fig. A-III-3A-ii, v. Together, these results indicated that CHX17 (1-425)-GFP was entirely localized to ER whereas CHX17-TM(1-472)-GFP was localized to ER, Golgi and as yet undefined compartments.

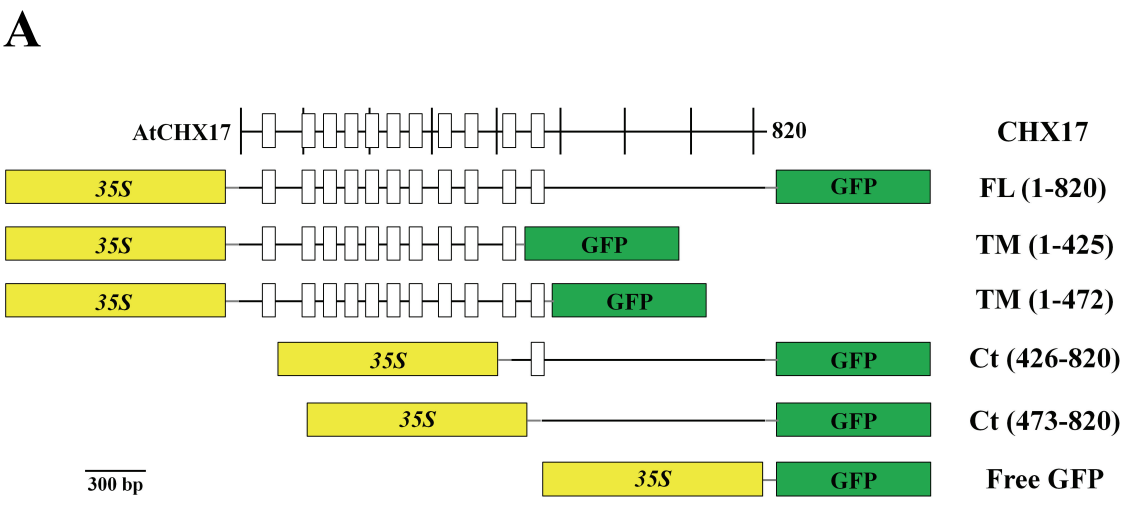

Fig. III-8. Role of the CHX17 carboxyl hydrophilic tail in sorting to PVC and PM.

A) Constructs encoding full-length and truncated *CHX17* fused to *GFP*. Truncated sequences encoding *CHX17-TM(1-425)*, *CHX17-TM(1-472)*, and two hydrophilic carboxyl tail (Ct) of *CHX17-Ct(426-820)* and *CHX17-Ct(473-820)* were PCR-amplified using the full length CHX17, FL (1-820) cDNA. The sequences were recombined into Gateway p2GWF7 and pB7FWG2 (*GFP* fusion at the 3' end) destination vectors for expression in protoplasts and plants, respectively. Scale bar = 300 bp.

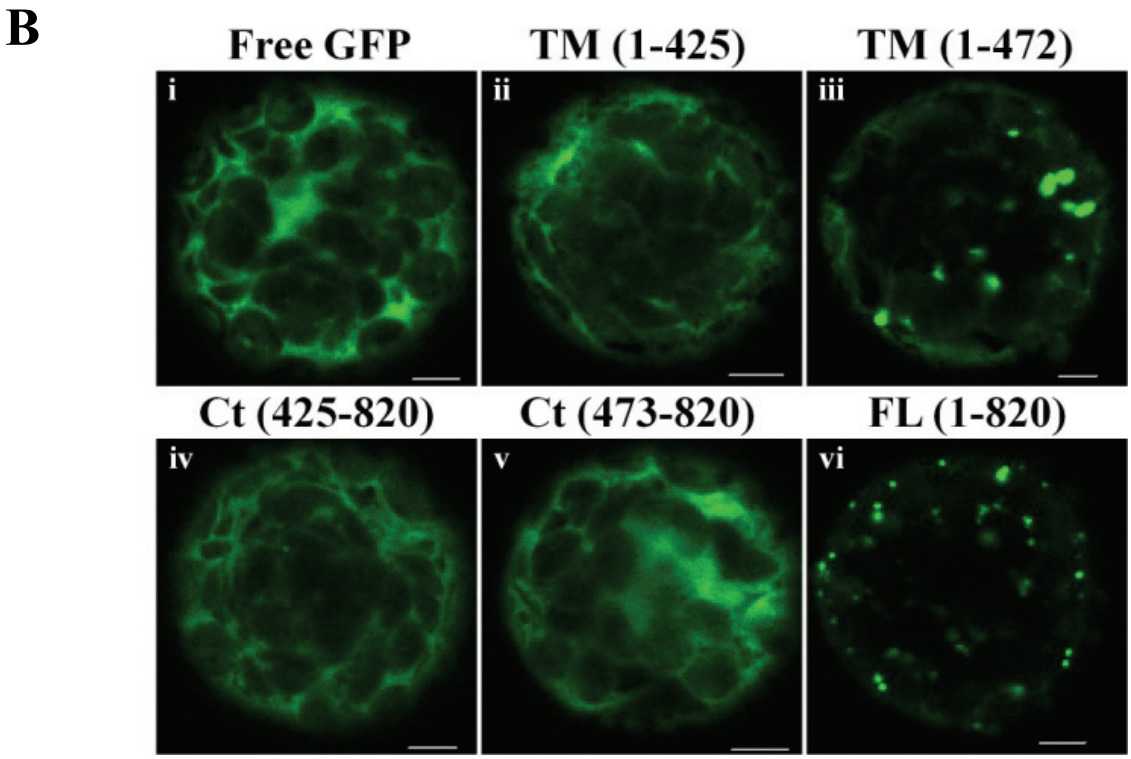

Fig. III-8. B) Truncated CHX17-GFP protein lacking the C tail is missorted. Protoplasts from *Wt col-1* were transfected with plasmids harboring each construct shown in A), and incubated for 18 h. Cells expressing green fluorescence were visualized: (i) GFP alone, ii) CHX17-TM(1-425)-GFP showed reticulate pattern, iii) CHX17-TM(1-473)-GFP displayed a mixture of reticulate and punctate, iv) CHX17-Ct (473-820)-GFP (v) CHX17-Ct (426-820)-GFP and vi) Full-length CHX17 (1-820)-GFP were punctate. At least 5 transfected protoplasts displaying GFP signals were observed in each experiment. Results are representative of three independent experiments. Scale bars = 5 μm.

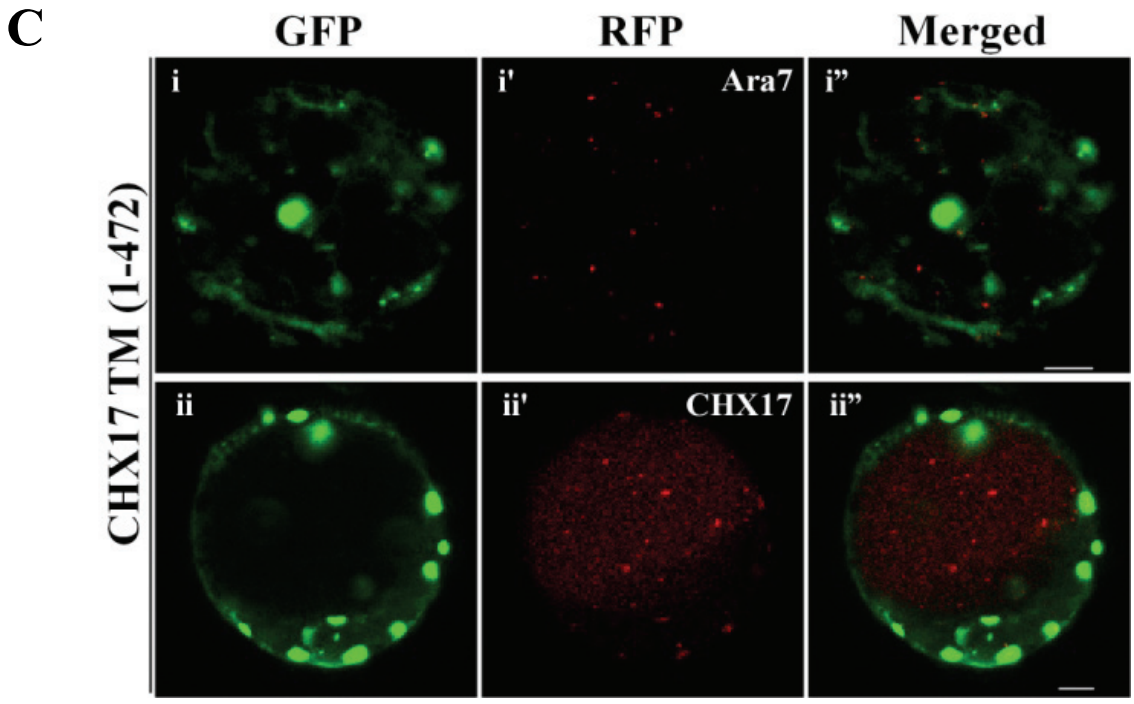

Fig III-8. C) CHX17-TM(1-472) did not localize to PVC.

Protoplasts from *Wt col-1* were co-transfected with *CHX17-TM(1-472)-GFP* and *RFP-Ara7* (i') or full-length *CHX17-RFP* (ii') and incubated as in B. Large puncta observed in cells expressing *TM(1-472)-GFP* (i and ii) did not co-localize with Ara7 (i', late endosome marker), or full-length CHX17 (ii') as shown in merged images (i", ii"). Results are representative of at least 3 transfected protoplasts displaying both GFP and RFP signals from two independent experiments. Scale bars = 5 μm.

Fig. III-8. D-E) Residue 426-472 of CHX17 is important for ER exit. Trangenic plants harboring *TM(1-425)*, *TM(1-472)* or Full-length *CHX17* constructs as shown in A were crossed with plant expressing *35S*::*RFP-HDEL* (ER marker) or *35Sp*::*GmMAN1-RFP* (Golgi marker). F1 seeds were germinated in 0.5X MS solid medium for 10 d. Seedlings displaying both GFP and RFP signals were selected for observation. Result is representative of at least two observations from three independent transgenic lines.

D) CHX17-TM(1-425)-GFP was retained in the ER.

(top) CHX17-TM(1-425)-GFP (i) and RFP-HDEL (i') showed reticulate pattern that overlapped in cells at the center (i").

(middle) CHX17-TM(1-472) displayed reticulum, punctate and aggregate patterns (i), though only the reticulum GFP signal co-localized with RFP-HDEL (ii"). Tubular structures observed in RFP-HDEL (ii') and aggregate structures in CHX17-TM(1-472) (ii) did not co-localize well with each other (ii").

(bottom) Full-length CHX17 localized to puncta (iii) that did not co-localized with RFP-HDEL reticulum pattern (iii"). Signals observed at cell pheriphery from RFP-HDEL (iii') were not continuous as seen in Full-length CHX17 (iii). Images were taken from the mature root epidermis of 10-d old seedlings. Scale bars = 5 μm.

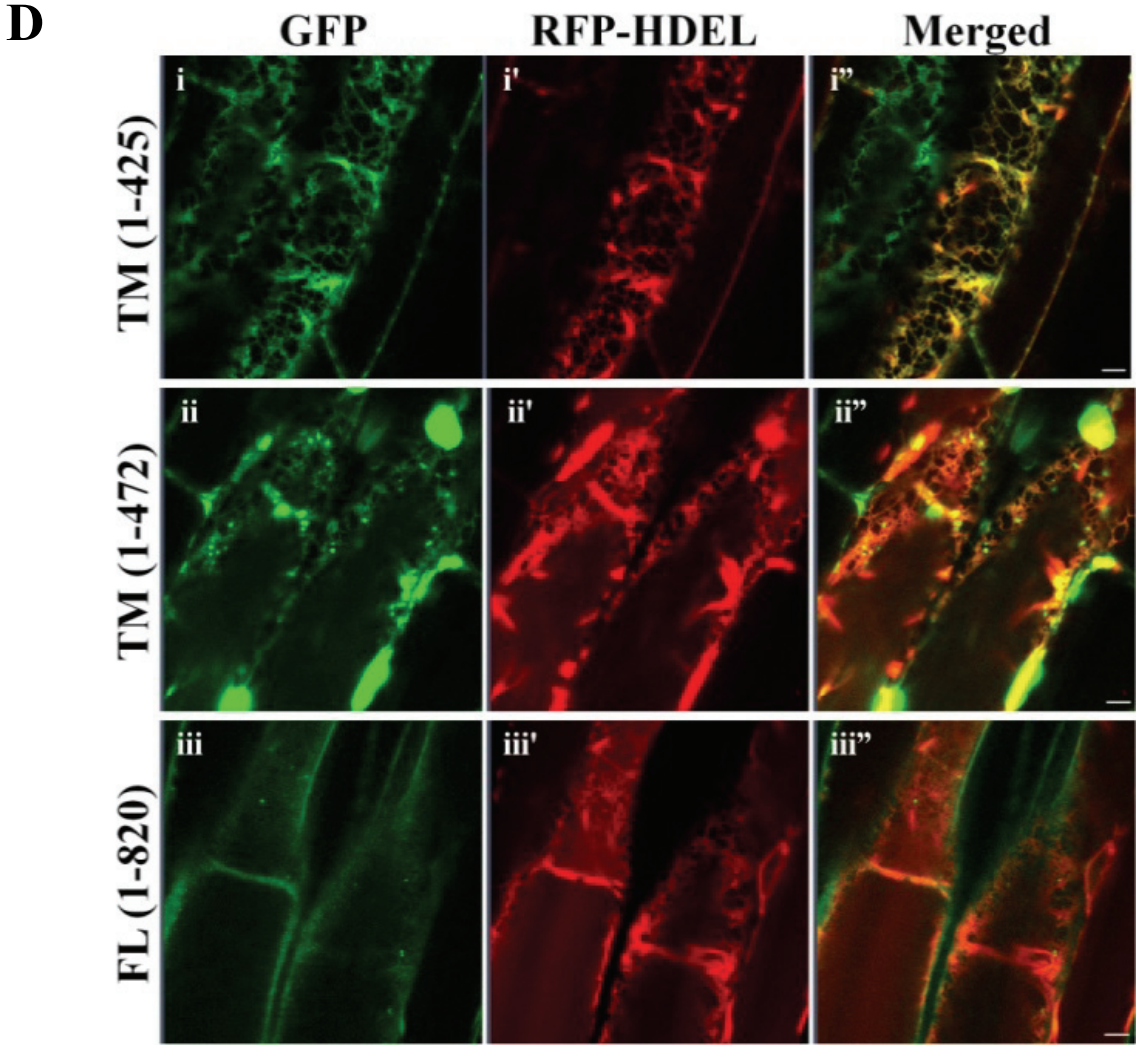
D
GFP
RFP-HDEL
Merged
TM (1-425)
TM (1-472)
FL (1-820)
i
i'
i"
ii
ii'
ii"
iii
iii'
iii"

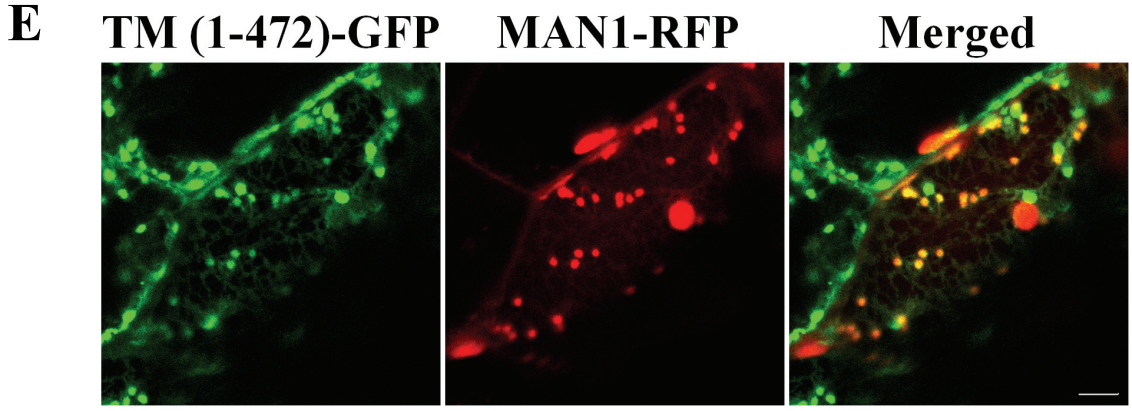

Fig. III-8. E) CHX17-TM(1-472)-GFP trafficks out of the ER to Golgi and unknown aggregates. CHX17-TM(1-472)-GFP co-localized with GmMAN1-RFP at the small puncta but not at the large puncta or aggregates. Chlorophyll autofluorescence from ~ 4-μm chloroplasts was also observed in the red channel with MAN1-RFP. Images were taken from the root-shoot junction epidermis of 10-d old seedlings. Scale bars = 5 μm.

Fig. III-8. F) CHX17-TM(1-472) did not localize to endosomes. Transgenic plants harboring CHX17-TM(1-472) were grown in 0.5X MS solid medium for 10-d and incubated in 0.1X MS medium with 10 μM FM4-64 for 10 min. Washed seedlings were treated with 0.5% DMSO, 50 μM BFA or 33 μM WM in 0.1X MS medium for 90-120 min. Cells are from the root epidermis at the division zone. Result is representative of two experiments. Scale bars = 5 μm.

(Top) DMSO, CHX17-TM(1-472)-GFP (i) and FM4-64 (i') signals did not co-localize (i").

(Middle) Brefeldin A (BFA) did not alter CHX17-TM(1-472)-GFP signal (ii) but FM4-64 signal formed BFA compartment (ii'). CHX17-TM(1-472)-GFP did not co-localize with BFA compartments (ii").

(Bottom) Wortmannin (WM) did not alter CHX17-TM(1-472)-GFP signal (iii) or FM4-64 label (iii'). No co-localization observed between CHX17-TM(1-472) and FM4-64 in merged image (iii").

F

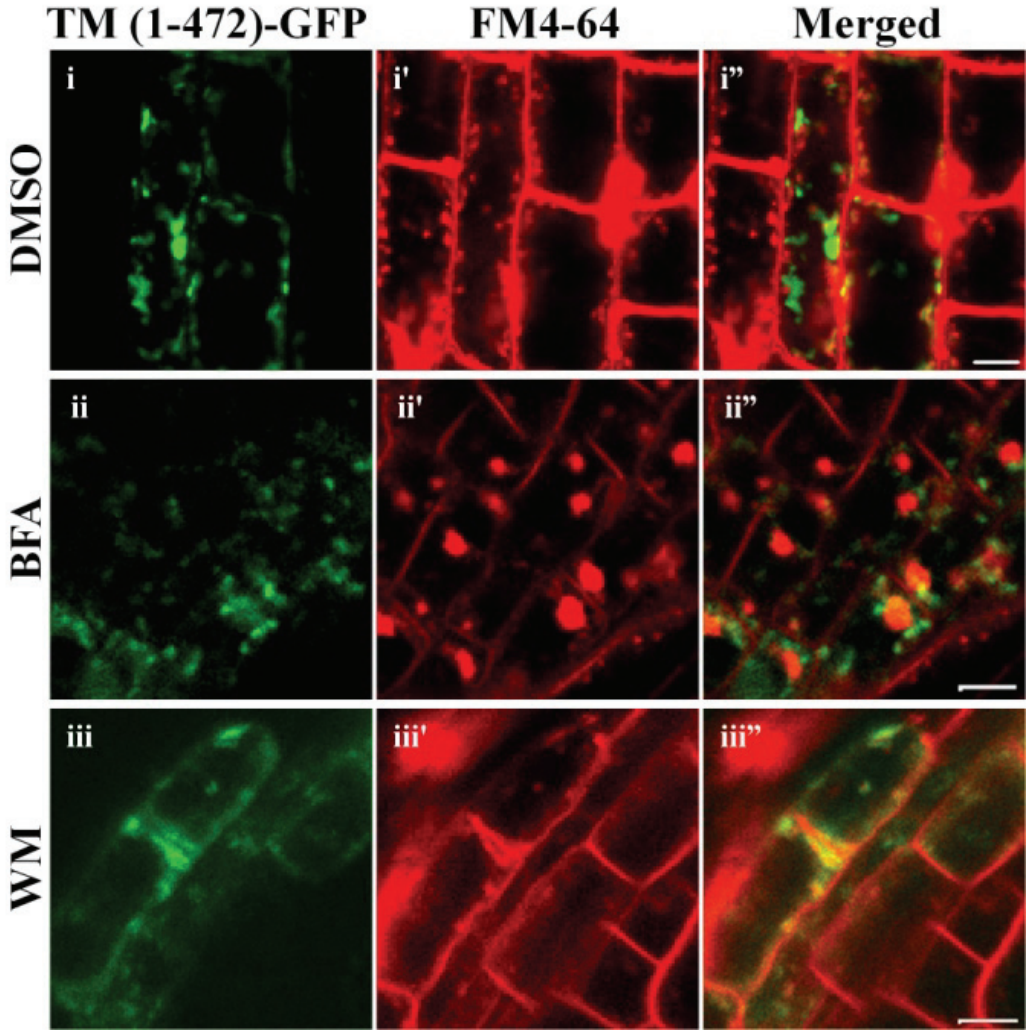

To test whether CHX17-TM(1-472)-GFP might be associated with endosomes in plants, I used endosomal membrane trafficking inhibitors, brefeldin A and wortmannin. In untreated seedlings, CHX17-TM(1-472)-GFP localized to tubular structures (Fig. III-8F-i) similar to GFP-HDEL (Fig. A-III-4F-i). FM4-64 labeled PM at the cell periphery and early endosomes or TGN (Robinson et al., 2008) at the puncta (Fig. III-8F-i'). No green fluorescence was observed from the cell periphery indicating that CHX17-TM(1-472)-GFP was not localized to PM and TGN. After BFA treatment, the morphology of TM(1-472)-GFP-labeled structures appeared unchanged (Fig. III-8F-ii, A-III-4A-ii, A-III-4E-ii). Besides, signals from CHX17-TM(1-472)-GFP did not overlap with 'BFA' compartments labeled by FM4-64 (Fig. III-8F-ii", A-III-4E- ii"). Moreover, morphology of CHX17-TM(1-472)-GFP and FM4-64 labeled compartments were unchanged with wortmannin (Fig. III-8F-i, -iii). These results indicated that CHX17-TM(1-472)-GFP was not localized to endosomes and PM.

Curiously, I noticed the formation of large GFP-HDEL puncta in BFA-treated protoplasts (Fig. A-III-4D-ii) resembled the distribution of CHX17-TM(1-472)-GFP expressed in protoplasts (Fig. A-III-4A). It is possible that the accumulation of GFP-HDEL at the large puncta after BFA treatment is due to an inhibition of the retrograde movement of HDEL to the ER or vice versa as BFA binds the Golgi-associated ARF-GEF (Robinson et al, 2008). If so, then the ER-Golgi derived GFP-HDEL puncta observed in BFA-treated protoplasts might overlap with TM(1-472)-GFP localized puncta. To test this idea, transgenic lines co-expressing both *CHX17-(1-472)-GFP* and *RFP-HDEL* were treated with BFA for 3 h. In control (DMSO) treatment, CHX17-TM(1-472)-GFP localized to reticulum and puncta (Fig. A-III-4G-i) whereas RFP-HDEL

localized to reticulum and tubular-like structures (Fig. A-III-4G-i'). After BFA treatment, most of RFP-HDEL signals changed from reticulum to puncta (Fig. A-III-4G-ii). There was no overlap between RFP-HDEL and CHX17-TM(1-472)-GFP at all (Fig. A-III-4G-ii"). Moreover, the large puncta appeared to be multi-layered membrane aggregates (Fig. A-III-4H). These results would point to the localization of the large puncta, derived from CHX17-TM(1-472)-GFP containing compartments, at structures other than the ER-Golgi interface.

Altogether, the presence of CHX17-TM(1-472)-GFP at ER, Golgi and unknown multi-layered membrane compartments compared to ER only of TM(1-425)-GFP suggests that the last TM11 of CHX17 is critical for trafficking out of the ER whereas PM and PVC targeting signals are embedded in the hydrophilic C tail.

E. DISCUSSION

E.1. CHX16, 17, 18 and 19 are expressed in tissues/cells with active endomembranes

Expression of CHX genes in plant tissues and in response to environmental cues provided valuable insights of their roles. For instance, CHX17 promoter-activity in transgenic plants was seen in mature root epidermis, stipules and developing seeds at the hilum region. Furthermore, expression of CHX16 and CHX18 were observed in hydathodes, stipules, emerging lateral roots and central cylinder of roots using promoter GUS analyses (Hong Zhao, unpublished data). These results are supported by Affymetrix microarray analyses where CHX genes are expressed in root cell types (Birnbaum et al., 2003) and in distinct part of developing seeds (Le et al., 2010). Many of these cell types expressing *CHX17* are known to have active endomembrane systems.

CHX17 expression in particular is up-regulated by environmental stresses, such as salt stress, acid pH stress, or K^+ starvation as shown before (Cellier et al., 2004). Moreover, abscisic acid, a stress-induced hormone, enhanced CHX17 expression as shown by RT-PCR (Cellier et al., 2004; S Padmanaban, unpublished data). However, salt (100 mM Na^+) or osmotic (200 mM sorbitol) stress did not cause any significant up-regulation of *CHX17* using promoter-driven *YFP* analysis. In contrast, very strong expression of *CHX17* in the root was observed when seedlings were transferred to medium with limited K^+ at 0.05 mM K^+ (Fig III-3A, III-3B). These results suggested that K^+ starvation, rather than Na^+ or osmotic stress, was the major stress that enhanced *CHX17* expression.

In spite of the increased CHX17 expression, I did not observe any growth differences between wild-type versus single, double or quadruple mutants of *chx16, 17, 18 and 19* during K^+ limitation (Fig. III-3C). Thus, even though CHX17-mediated K^+ transport (Chapter II), it is unlikely to play a major role in K^+ acquisition into whole plants as suggested before (Cellier et al., 2004). Kinetic studies of K^+ transport mediated by CHX17 in *E. coli* showed that CHX17 had specificity for K^+ with a K_m of 1-3 mM (Chapter II). Affinity for K^+ at the low millimolar range would not be effective in mediating K^+ uptake when external K^+ is limiting. In contrast, AKT1 and HAK5 are candidates for high-affinity K^+ transport in root exposed to K^+ below 100 nM and 10 nM, respectively (Pyo et al, 2010; Rubio et al, 2010). Furthermore, CHX16-19 were localized to endomembranes like PVC and ER. One exception is AtCHX13 which also mediated K^+ transport and was localized to the PM (Zhao et al 2008). It remains to be established whether CHX13 plays a direct role in enhancing K^+ uptake into plants or whether the

effect is indirect possibly via a signaling role. Considering the up-regulation of *CHX17* after K^+ limitation and other findings, I consider the possibility that CHX16, 17, 18 or 19, plays an indirect role in K^+ uptake in roots when external K^+ is limited.

Other results suggest K^+ transport of CHX is linked to pH regulation as a result of K^+-coupled H^+ transport, or modulation of membrane potential. In chapter II, I showed that CHX20 can modify cytosolic and vacuolar pH in yeast. CHX20 is localized to endomembranes in yeast and to the ER in plants. This observation suggested the potential role of CHXs in pH regulation through K^+ homeostasis in endomembrane systems. Although CHX17 did not change bulk vacuolar or cytosolic pH in yeast, the implication of CHXs on local pH of endosomes is considered in plants.

E.2. CHX16, 17, 18 and 19 are associated with endosomes and PM *in planta*

Surprisingly, this study showed that CHX17 is localized to the plasma membrane in intact plant cells, in addition to association with endomembranes. In transiently transfected leaf protoplasts, I showed that AtCHX17-GFP was predominantly localized to PVC (Chapter II). However, fluorescent-tagged *CHX16, 17, 18* or *19,* expressed under a constitutive promoter in transgenic plants, labeled punctate structures as well as the cell periphery. Using plasmolysis and co-localization with PM markers, I demonstrated that CHX17-GFP at the cell periphery was associated with PM (Fig. III-4B, III-5A), and that fluorescence at the puncta was not associated with the Golgi (Fig. III-5B). Moreover, CHX17-GFP expressed under its native promoter confirmed that CHX17 labeled PM in transgenic plants. This conclusion is independently supported by the finding that a phosphorylated CHX17 was found in a PM–enriched fraction (Hem et al., 2007).

Punctate structures labeled by CHX17-GFP were not marked by FM4-64, an impermeable fluorescent molecule that can be taken into cells by endocytosis and then trafficked via TGN to the vacuole (Bolte et al., 2004). Thus, CHX17-labeled puncta is not associated with membranes of the TGN. Brefeldin A (BFA) and wortmannin (Wm), are commonly used to dissect and distinguish between sub-populations of 'early endosomes' or TGN versus 'late endosomes' (PVC or MVB), respectively (see review by Robinson et al., 2008). After BFA treatment for 90 min, CHX17-GFP signals were absent at the cell periphery and did not co-localize with FM4-64 fluorescence in BFA compartments (Fig. III-5D). This observation suggested that BFA blocked CHX17 trafficking to PM.

Nevertheless, it is unknown whether the blockage is caused by BFA inhibition of recycling endosomes (RE) trafficking (Geldner et al., 2003) or inhibition of ER/Golgi trafficking (see above, section D.8), thereby reducing secretion of the newly synthesized proteins. To distinguish between these two pathways, a protein synthesis inhibitor, cycloheximide, could be applied concomitantly. Since my primary purpose was to use membrane trafficking inhibitors to verify the location of CHX17, no further experiment using cycloheximide was performed.

On the other hand, wortmannin had no effect on PM-associated CHX17-GFP, but it caused the formation of ring-like structures (Fig III-5D) similar to that seen for ARA7-labeled structures in *gnom* mutants (Geldner et al., 2003) or in wortmannin-treated plants (Robinson et al., 2008). As ARA7 co-localized with CHX17 (Chapter II), the results strongly suggested that CHX17 was localized to PVC. Furthermore, immuno-electron-microscopy revealed CHX17 at ER, PM, PVC and inside the vacuole (Fig. III-6), but not

in the Golgi. Therefore, I conclude that CHX17 at the puncta and cell periphery in cells of intact plants were localized to PVC and PM, respectively.

Interestingly, CHX16, 17, 18 or 19 showed similar patterns at the plasma membrane (Fig. III-5A) and at post-golgi compartments (Fig. III-5B), most likely PVC as shown before in protoplasts (Chapter II). Taken together, several lines of evidence suggest that CHX16, 17, 18 and 19 were localized to two membranes. Additionally, the results also indicate that membranes carrying one of these CHXs are able to traffick to and/or from PVC and PM.

E.3. Role of C-tail of CHX17 in trafficking and targeting

Nothing is known about the long hydrophilic C tail of CHX proteins, although it is proposed to perform regulatory roles and to interact with other proteins as shown for animal NHEs (Donowitz et al., 2009). Preliminary studies of truncated CHX17 suggested that the hydrophilic tail C tail was important for localization while the TM domain (1-472) is critical for activity. Truncated CHX17-TM(1-472), but not CHX17-TM(1-425), restored partial growth of alkaline-sensitive yeast compared to full-length CHX17. However, truncated versions of CHX17 were not localized to the PM or PVC. In transgenic plant, TM(1-425)-GFP localized to the ER (Fig III-8Di), whereas TM(1-472)-GFP localized to both reticular and punctate structures that were not endosomes and PVC (Fig III-8C). I demonstrated that, CHX17-TM(1-472) was partially localized to the Golgi at the small puncta *in planta* (Fig. III-8E) and as yet unknown large puncta (Fig A-III-4H).

CHX17-TM(1-472)-GFP was not localized to post-golgi compartment, as in control cells and those treated with BFA or Wm, FM4-64 did not overlap with CHX17-

TM(1-472)-GFP nor was the size of CHX17-TM(1-472)-GFP-associated compartments (Fig III-8A) changed. If CHX17-TM(1-472)-GFP was associated at the Golgi and unknown compartments, I hypothesize that the last TM sequence (residue 426-472), as predicted by SOSUI v.1.1 (Fig. A-III-5), is crucial for function and required for trafficking out of ER to the Golgi, whereas the hydrophilic C-tail is important for targeting CHX17 to PVC and PM.

I looked for a potential ER exit motif. Oddly, I was unable to find the conventional diacidic motifs, D/E-X-D/E or D/E-X-X-D/E, that are crucial for exit of membrane proteins from the ER (Hanton et al., 2005; Mikosch et al., 2006; Chatre et al., 2009). However, the topological diagram of CHX17-TM(1-472) revealed the proximity of three acidic residues, D_{437}, E_{444} and E_{455} between TM10–TM11 (Fig. A-III-5) that together with the last TM (TM11) might serve as an ER exit signal. Furthermore, the short amino acid sequence (Y_{427}-K_{451}) before the last TM of CHX17 is rich in poly basic amino acid (H, K, R) (Fig. A-II-1, A-III-5). Interestingly, it was demonstrated before that the poly positively-charged domain immediately adjacent to the TM domain was sufficient to target membrane protein to peroxisomes (Mullen and Trelease, 2000; Karnik and Trelease, 2007). Furthermore, over-expression of these proteins fused with GFP facing the cytosolic side caused aggregation of peroxisomes, mitochondria and/or plastids which led to the formation of reticular or circular compartments (Lisenbee et al., 2003; Fig. A-III-3v). Lisenbee *et al.* demonstrated nicely that oligomerization of GFP at the cytosol was the culprit for the sticky aggregation. Interestingly, I also observed similar structures from the large puncta containing CHX17-TM(1-472)-GFP (Fig. A-III-4H). Moreover, BFA treatment at high concentration (150 μM), which was shown previously

to collapse the Golgi to ER trafficking (Robinson et al., 2008b), did not collapse the large puncta containing CHX17-TM(1-472)-GFP but caused the formation of small puncta containing RFP-HDEL (Fig. A-III-4G), an indication of ER/Golgi trafficking inhibition. Even though the similar size of large puncta containing CHX17-TM(1-472)-GFP and large puncta containing RFP-HDEL generated by BFA was observed (Fig. A-III-4A, A-III-4D, respectively), no overlap of both markers at the large puncta existed (Fig. A-III-4G). This result confirmed the aggregate was out of ER and Golgi boundaries. Therefore, I speculate that the aggregation of the membrane in the large puncta is caused by an over-expression of CHX17-TM(1-472)-GFP which is probably mislocalized to peroxisomes, mitochondria and plastids after leaving ER and/or Golgi due to the lack of PVC or PM sorting signals at the C-terminus.

These results give clues about CHX17 topology. If aggregation and mislocalization of GFP fusion transmembrane proteins with poly-basic amino acid signals occur only when the fused GFP protein is localized in the cytosol (Lisenbee et al., 2003), my results would imply that CHX17 hydrophilic C tail faces the cytosolic side. Thus, the prediction of 11 TM by SOSUI version 1.11 would suggest that the N-terminus of CHX17 faces the luminal side (outside). This prediction is also supported by GFP-tagged CHX17 or CHX20 at the N-terminus localized at puncta in yeast (Fig. A-V-4), possibly the Golgi or peroxisomes, as the GFP fusion at the C-terminus of these proteins, although retains their original activity, causes the formation of the tubular aggregates (Fig. II-6A) as discussed above. Collectively, I could infer from this indirect evidence that CHX17 or CHX20 has an N-terminus facing the luminal side and C-terminus in the cytosolic side.

E.4. CHX and cell wall remodeling

Single and double mutants failed to show any obvious growth changes; however the low recovery of triple or quadruple mutants suggested a role in reproduction and/or seed development. Furthermore, quadruple-mutant plants cultured in hydroponic culture were small in size relative to triple-mutant, double-mutant or wild-type plants at 3 weeks or later (Fig. A-V-14). This phenotype suggests a potential role of CHX16, 17, 18 and 19 genes in cation homeostasis and osmoregulation during vegetative growth.

Interestingly, mutation of two redundant $Na^+(K^+)/H^+$ exchangers, NHX5 and NHX6, led to small growth phenotype which was significant after 3 weeks (Bassil et al, 2011). Both NHX5 and NHX6 were localized to endosomal compartments associated with TGN and Golgi and thought to be important for vesicle trafficking toward the vacuole. Interestingly, microarray analysis in *nhx5 nhx6* double mutants revealed the up-regulation of stress response genes, vesicular-trafficking related genes and down-regulation of cell-wall related genes (Bassil et al, 2011). I also observed that ScNHX1 conferred strong hygromycin B resistance in yeast mutants compared to the moderate resistance mediated by ScKHA1 or CHX17 (Maresova and Sychrova, 2005; Chapter II). The cellular basis underlying hygromycin B sensitivity in yeast mutants is likely associated with vesicular trafficking defects as demonstrated by enhanced CPY secretion in *nhx1* and/or *kha1* mutants though the latter was only observed at alkaline pH (Chapter II). Therefore, the similarity in phenotype but difference in degree of severity in mutant plants possibly suggested the role of CHX16, 17, 18 and 19 in vesicular trafficking that is different from NHX5 and NHX6, most likely due to the localization at different compartments and differential modes of transport (discussed below).

Several lines of evidence suggested that CHXs potentially play roles in cell wall modification. First, CHX homologs exist in organisms that produce cell walls, including cyanobacteria, fungi and plants. No CHX homolog has been annotated in animals to date (Brett et al.., 2005). Secondly, majority of CHXs in plant are expressed in pollen (Sze et al., 2004). It has been demonstrated that pollen development and pollen tube growth are controlled by cell wall-modifying enzymes (Campanoni and Blatt, 2007; Krichevsky et al., 2007). Thirdly, several CHXs, including *CHX16*, *17*, *18* and *19* are preferentially expressed in abscission zone, mature zone and specific tissues, including hydathodes, stipules and vessels (Fig. III-2 and data not shown). These locations are places where most of the cell wall modification occurs as seen by the similar expression patterns in pectate lyase-like (*PLL*) gene family (Sun and Nocker, 2010) and *Daisy* gene (Suberin biosynthesis; Franke et al., 2009). The latter is expressed in root exodermis, endodermis, and wound periderm (Schreiber, 2010). Lastly, CHX16, 17, 18 and 19 traffick between post-golgi compartments, most likely PVC as represented by CHX17, and plasma membrane (Fig. III-4B, III-5A, III-5B).

Interestingly, membrane trafficking and cargo sorting to the PM has a profound effect on wall-modifying enzymes as shown in mutants of PVC/endosomal Ca^{2+}/Mn^{2+} pump AtECA3 (Li et al., 2008). Plant peroxidases are also known to play an important role in reinforcement of cell wall and lignification (Passardi et al., 2005; Almagro et al., 2009; Marjamaa et al., 2009). Moreover, Ca^{2+}-pectate binding peroxidase from Arabidopsis has been identified, emphasizing the role of plant apoplastic peroxidase, calcium and pectin in cell wall remodeling (Penel and Greppin, 2004). Intriguingly, activity of pectin methylesterase (PME), which modifies plant cell wall by removing

methyl group from pectin polymer generating pectate (Pelloux et al., 2007; Jolie et al., 2010), was influenced by salt and pH *in vitro* as demonstrated by differential pectate gel formation (Yoo et al., 2003). Pectate gelation was induced by K^+ at pH 5.0 but it was induced by Na^+ at pH 7.0 although no gelation was observed with Li^+ (Yoo et al., 2003). The results from my studies of CHX16, 17, 18 and 19 are consistent with a role in cell wall remodeling either by regulating endosomal membrane trafficking that affects cell wall modification or regulating activity of cell wall-modifying enzymes through K^+ and pH modulation.

IV. CONCLUSION AND FUTURE PROSPECTS

A. CONCLUSIONS

The significant findings of this study are i) CHXs, plant specific transporters from the cation proton antiporter-2 family, are K^+ transporters; ii) Five related CHXs show diverse biochemical activities under varied environmental conditions; and iii) they are localized on trafficking membranes, such as endosomes and plasma membrane . Instead of serving roles for plant K^+ nutrition, I propose a new model that CHXs influence the type and extent of cell wall remodeling through their activities affecting localized K^+ and pH homeostasis.

A.1. CHX16, 17, 18, 19 and CHX20 have differential properties distinct to CHX family

CHX form the largest subfamily of the cation proton antiporter (CPA) superfamily that is poorly understood (Sze et al., 2004). I have demonstrated for the first time that members of CHX family from *Arabidopsis*, including CHX17 and CHX20, mediate K^+ transport. Even though the mode of K^+ transport is still ambiguous, several lines of evidence point to CHX17 and CHX20 behaving as a K^+ channel and a H^+-K^+ symporter, respectively. This is surprising because CHX17 and CHX20 are phylogenetically close. However, several members of cation proton antiporter-2 family do not behave solely as $Na^+(K^+)/H^+$ antiporters as seen in Gern from *Bacillus cereus* (Southworth et al., 2001), NhaS4 in *Synechocystis spp* (Inaba et al., 2001), and KefC from Escherichia coli (Fujisawa et al., 2007). The finding of my research supports the recent concept that modes of transport are changeable

depending on regulatory domains as seen in KefFC where KefF is an auxiliary protein modulating KefC in antiport mode (Fujisawa et al., 2007).

Although several CHXs belong within a subclade, the activities of CHX15 to CHX20 differ. Functional analyses in yeast reveal that each CHX isoform had different optimal external pH required for rescuing growth of K^+ uptake-deficient yeasts. Although CHX15 had no activity observed in yeast, preliminary study showed that it rescued growth of K^+ uptake-deficient *E. coli*. In general, CHX16-20 improve growth of yeast *kha1* mutant (KHA1 is a CHX homolog in yeast), at alkaline pH; however, there is no correlation between this phenotype and intracellular pH change. Interestingly, the ability to confer hygromycin B resistance in yeast separates these CHXs roughly into two groups i) CHX17-19 conferred HygB resistant and ii) CHX16 and CHX20 caused more HygB sensitivity. Furthermore, a recent study mapped CHX16 and CHX20 loci on Cs^+ accumulation trait in Arabidopsis (Kanter et al., 2010), emphasizing the differential function among these two groups in plants.

In addition to revealing plant CHX function in yeast, my study also provided a detailed characterization of yeast endogenous KHA1. It is obvious that AtCHX and ScNHX serve different roles in yeast, and most likely in plants. Therefore, this study provides further evidence that CHX most likely serves unique roles that is not redundant with other cation/proton exchangers such as NHX1 or NHX2, in plants. This alone would answer one fundamental question on why plants evolve to have multiple copies of CHXs. I suggest that multiple CHXs are necessary to carry out fine-tuned functions that might be subtle; however, suitable for diverse circumstances in a multicellular plant body with specific organs and tissues.

A.2. CHX16, 17, 18 and 19 traffick between endosomes and plasma membrane

Another novel finding in this study is that CHX16-19 are localized in both endosomes and plasma membrane. This is unlikely due to an artifact caused by over-expression, as CHX17-driven by its native promoter also localized to both late endosomes (PVC) and PM. Furthermore, I have demonstrated that targeting to the PM of CHX17 is blocked by brefeldin A, which causes accumulation of recycling proteins in endosomes, indicating that CHX16-19 can traffic to or from endosomes and PM. This trafficking might also imply their biological function. For instance, it has been shown that localization of several transporters are controlled by vesicular trafficking, including AtBOR1 for Boron transport (Takano et al., 2005; 2010) and AtKAT1 for K^+ transport (Sutter et al., 2006), depending on when and where they are needed.

Since endosomes are compartments responsible for protein sorting and membrane trafficking, it is conceivable that endosomal CHXs would likely play a role in membrane trafficking. I showed in yeast that CHX17 affects carboxypeptidase Y secretion at alkaline pH, corresponding well with the growth phenotype. Even though it has been shown previously that NHX1 from both yeast and plants have a role in membrane trafficking (Bower et al., 2000; Ali et al., 2004; Mukherjee et al., 2006; Wagner et al., 2006; Hernandez et al., 2010), this is the first time for CHX family that suggests the role of CHX17 and yeast KHA1 in regulating yeast protein sorting, perhaps through luminal pH and K^+ modulation. Nevertheless, this role has yet to be verified in plants.

In this study, I have also demonstrated for the first time, by using CHX17 as a model, that the carboxylic tail of CHX is important for its activity and for its trafficking and membrane targeting *in planta*. ER exit signal for CHX17 is not a conventional di-acidic motif as described previously in KAT1 (Sieben et al., 2008), but this signal could be either aspartate and double glutamate after TM 10 or the last TM of CHX17. Furthermore, PM and PVC (late endosomes) targeting signals are likely embedded in the hydrophilic C tail. Although these signals are still poorly characterized, a few have been found in plants (Banerjee et al., 2010; Wywial et al., 2010), e. g. FYVE domains (conserved domains appear in Fab1, YOTB, Vac1 and EEA1; Stenmark et al., 2002) and PX domains (Phox-homology; Ellson et al., 2002). These domains bind to phosphatidylinositol-3-phosphate (PI3) enriched in endosomes (reviewed by Lindmo and Stenmark, 2006). Inhibition of PI3 kinase results in swollen endosomes containing intraluminal vesicles (multivesicular body, MVB or prevauolar compartment, PVC) in both animals and plants (Fernandez-Borja et al., 1999; Katzmann et al., 2002; Robinson et al., 2008). This is consistent with the observation of ring-like structures labeled by CHX17-GFP after treating with PI3-kinase inhibitor, wortmannin (Davidson, 1995).

The recycling of CHX17 to PM, which is inhibited by BFA, raises the question on how proteins destined to the PVC or late endosomes recycle to PM. This question remains unclear in plants although several lines of evidence indicate that this mechanism could be mediated through trans-Golgi network or early endosomes or undefined recycling endosomes where GNOM localizes (Viotti et al., 2010). Nevertheless, it has been acknowledged in animals for such a direct exocytosis of

MVB, called exosomes (Pelchen-Matthews et al., 2004). This process is important in cell immunity, cell and tissue polarity, and reproduction of animals (Pilzer et al., 2005; Lakkaraju and Rodriguez-Boulan, 2008; Mincheva-Nilsson and Baranov, 2010). Evidence is emerging that plants also secrete exosomes derived from PVC during defense against pathogen invasion (An et al., 2006; 2007) though more data are required to support this hypothesis. If CHX17 traffick directly from PVC to PM, this could be another evidence to support the existence of this pathway.

A.3. Emerging role of CHX16, 17, 18 and 19 in cell wall remodeling

Determining the biological function of CHXs in plants has been challenging partly due to genetic redundancy, and in part due to lack of a clear working model. Even though there is no major apparent phenotype in multiple *chx* mutants in *Arabidopsis*, segregation distortion was observed in the progeny of triple or quadruple mutants. These mutants are: *chx17 chx18 chx19* triple mutant and *chx16 chx17 chx18 chx19* quadruple mutant. Up-regulation gene expression of each corresponding CHX in single or double mutants highlights the genetic redundancy of these CHXs in plants. Curiously, although CHX17 is expressed in roots and up-regulated by K^+ starvation, no phenotype related to root growth is observed in single or multiple mutants of *chx16-19* when grow in low K^+ medium. These results suggest that the major role of CHX16-19 is not for K^+ nutrition (uptake) in plants.

Unexpectedly, I discovered that *chx16-19* quadruple mutants showed growth retardation after 3 weeks in hydroponic systems but not in soil. Since K^+ did not enhance growth of mutants and this only occurred when quadruple mutants were

grown in aqueous solution at the mature rosette stage, it is likely that the defect came from roots that fail to control osmotic pressure. In plants, cell wall is very critical for controlling turgor pressure, therefore I propose a new idea that CHX16-19 have a function in cell wall remodeling.

CHX16, 18 and 19 genes are expressed in stipules, hydathode, lateral root initiation, and vessels whereas CHX17 is expressed at stipules, mature root epidermis and cortex, and abscission zone eg. wounding area, hilum in seeds, and vessels in receptacle. Moreover, CHX17 and 19 are also expressed in pollen. These cells or tissues are rich in endomembrane vesicles and possibly active in cell wall modification.

The following results would be consistent with the role of CHX17 in cell wall remodeling. First, under its native promoter, CHX17-GFP localizes to intracellular compartments containing aggregates in mature root epidermal cells (Fig. A-V-6 and A-V-7). These aggregates potentially contain cell wall materials internalized from the PM. Secondly, CHX17 is specifically expressed in guard cells (Fig. A-V-8) incubated in hypo-osmotic condition, which will likely induce changes of the cell wall. Third, single *chx17* mutants show a reduction of dark-induced stomata closure at alkaline pH in hypotonic solution (Fig. A-V-10). Fourth, hypo-osmotic condition, which induces protoplasts to burst, enhances the localization of CHX17-GFP to the cell periphery (Fig. A-V-13). Taken together, these results suggest a working idea: under extreme hypo-osmotic condition, CHX17 might play a role in strengthening cell wall by modifying internalized cell wall materials in endosomes and delivering them to the wall by exocytosis when needed.

Interestingly, phylogenetic analyses suggest that *CHX* is initially transferred to fresh-water green algae (charophytes), the sister of land plants (Wodniok et al., 2011). During the evolution of marine green algae (chlorophytes) to fresh-water charophytes, marine algae have to adapt to hypo-osmotic environment and reduced availability of Na^+. It is possible that, at this time, CHX becomes essential for them. Reports from charophytes, especially *Spirogyra spp.*, indicated that they produced special cell wall components. For instance, they secreted materials that formed temporary cell wall when the filament was cut (Inoue et al., 2002), they had slime-like substances between the cell wall layers where some of these materials were derived from post-Golgi compartments (Jordan, 1970). Recently, it was demonstrated that charophytes produced pectin which forms the cell wall matrix in land plants (Domozych et al., 2007; Sorensen et al., 2010; Popper et al., 2011). In plants, it has been shown that slime excreted from the root cap is a modified form of pectin to provide a hydrated protective coating around the root tip (Wright and Northcote, 1974). Curiously, since pectin is thought to originate in charophyte at the same time as CHX genes, it is possible that CHX function and pectin metabolism, are related.

Pectin modifying enzymes in plants are highly redundant as shown by the large family comprising between 20-60 members per lineage. Interestingly, members of the *PECTATE LYASE-LIKE* genes are expressed in the tissue similar to CHX16-20, including pollen, receptacle, hilum, lateral root initiation, stipules and guard cells (Sun and Nocker, 2010). Pectin is also known to be critical for pollen development and pollen tube growth (Bosch and Hepler, 2005; Tian et al., 2006; Pelloux et al., 2007; Krichevsky et al., 2007; Chae and Lord, 2011). Moreover, stomata cell walls

are also rich in pectins (Majewska-Sawka et al., 2002) and they are required for proper stomata movements (Jones et al., 2003). Recently it has been shown that CHX20 has a role in light-induced stomata opening (Padmanaban et al., 2007) whereas CHX21 and CHX23 play a role in pollen tube guidance (Lu et al., 2011). The presence of pectin and pectin modifying enzymes in specific tissues where CHXs are expressed and exert similar biological effect supports the notion that CHX function is associated with pectin metabolism.

Pectin is known to be synthesized in the Golgi and secreted as esterified form which then is modified further at the cell wall (Harholt et al., 2010). However, this notion began to change lately since it has been shown that pectin is actively internalized in root apex cells and cross-linked with calcium and boron in endosomes, especially through PVC (Hudak et al., 1993; Baluska et al., 2002; Yu et al., 2002; Samaj et al., 2004; Baluska 2005). Interestingly, these processes are notably in osmotically-stressed cells (Ciamporova and Mistrik, 1993) and chilling-stressed cells (Stefanowska et al., 2002). It has been proposed that a pool of internalized pectin serves as a ready supply of cell wall materials, especially during rapid turnover in guard cells movement, rapid papilla formation during pathogen invasion, and rapid tip growth in root tip and pollen tubes.

Recent *in vitro* study on pectate gel formation, de-esterification of pectin to form pectate, indicates that pH and K^+ or Na^+ (but not Li^+) are important for activity of pectin-modifying enzymes (Yoo et al., 2003). This result implies that localized condition, e.g. pH and ionic strength, is pivotal for pectin modification. Taken together, I propose a model that CHXs play a role in regulation pH and K^+

Fig. IV-I. Role of CHX17 in pectin modification and trafficking in the endosomal system.

Esterified pectin is synthesized in the Golgi and secreted to plasma membrane (PM) through secretory vesicles (top left). During plant growth and development, pectin can be modified at the cell wall by pectin methylesterase (PME) and the resultant pectate can be cross-linked by Ca salt bridges. Pectin at the wall can also be internalized to early endosomes (TGN) and late endosomes (PVC), respectively, and then modified inside these compartments (middle). The pH and cation concentration of endosomes, modulated by transporters such as V-ATPases and CHX17, provide conditions that activate or reduce pectin-modifying enzymes. In response to signals, cells would exocytose modified pectin from the PVC either directly, via TGN or recycling endosomes (top right). PM CHX17 would also locally affect activity of PME and other modifying enzymes in the apoplast. To down-regulate function, PM-bound CHX17 or pectin is internalized and delivered to TGN, and PVC for degradation in the vacuole (lower right). BFA and Wm refer to brefeldin A and wortmannin, which inhibit endosomal trafficking. Blue, red and purple arrows indicate secretory pathway, endocytosis and exocytosis, respectively. [Figure is modified from Grunewald and Friml, 2010]

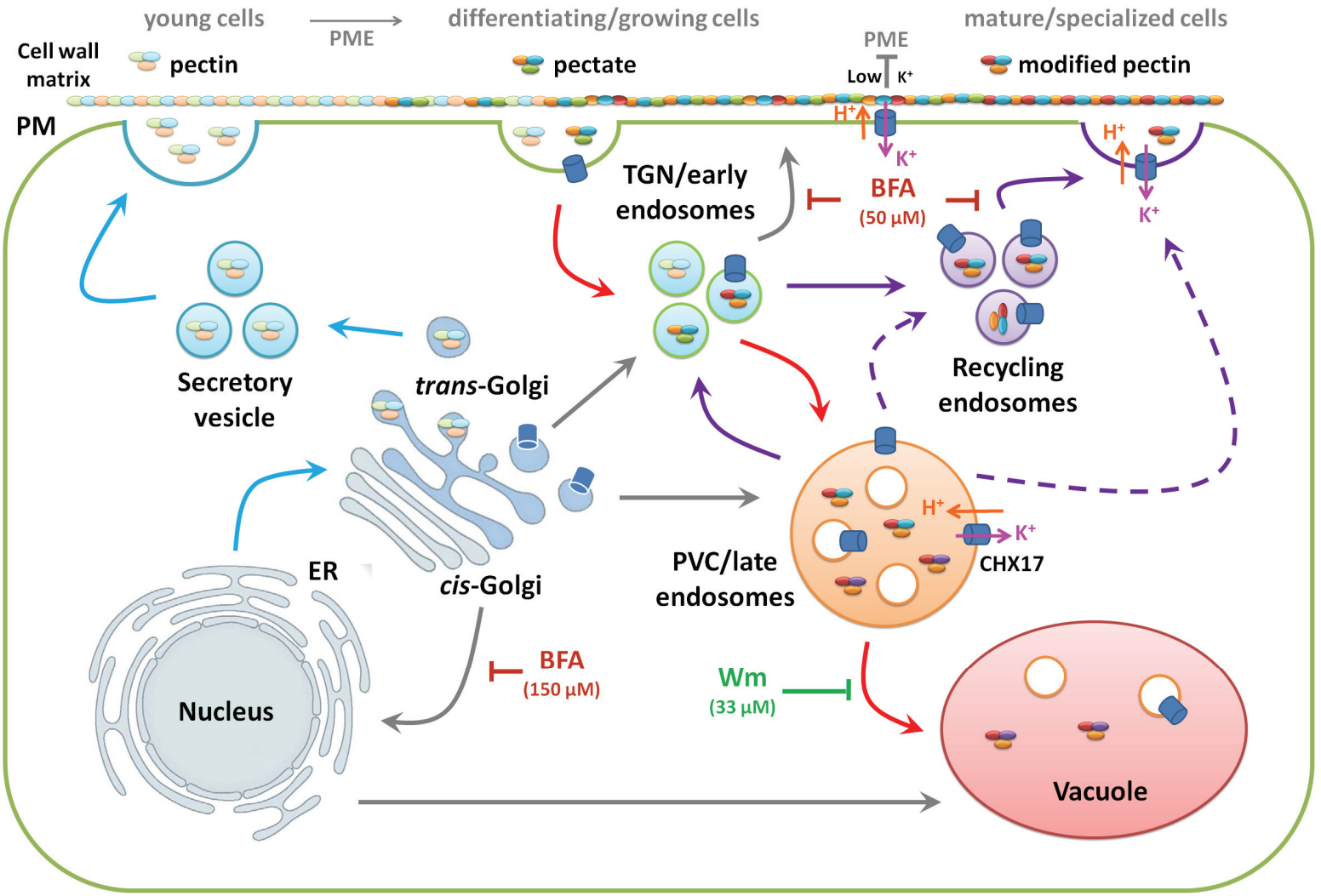
young cells
PME
differentiating/growing cells
PME
mature/specialized cells
Cell wall matrix
pectin
pectate
Low K+
modified pectin
PM
H+
K+
H+
K+
TGN/early endosomes
BFA (50 µM)
Secretory vesicle
trans-Golgi
Recycling endosomes
ER
cis-Golgi
PVC/late endosomes
H+
K+
CHX17
BFA (150 µM)
Wm (33 µM)
Nucleus
Vacuole

concentration suitable for differential pectin modification during pectin internalization and recycling back to the PM (Fig. IV-1). However, I could not rule out the possibility that CHXs can also regulate trafficking of pectin between PM and PVC.

B. FUTURE DIRECTIONS

This work has revealed for the first time the complexity of a novel family of cation/proton exchangers of unknown biological functions in plants, and tantalizing clues to their potential roles in osmoregulation via remodeling of cell walls. CHX expression in many cell-types, and their roles in guard cell movement and pollen tube guidance have led us to a new working hypothesis. 'CHXs play a role in affecting enzymatic modification of pectin during their internalization and recycling to the wall by modulating the pH and K^+ concentration of the microenvironment of endosomes.' One approach to test this idea is to elucidate the role of CHXs in cell wall remodeling, especially through pectin metabolism.

Pectin is a major plant component that affects growth and development, including root development, pollen tube growth, guard cell movement, and fruit ripening. It also has economical value, such as food additives (gelling agent, thickener, and stabilizer), medicine (laxative, moisturizer), polymers (film, coating materials) and agriculture (fruit texture). Therefore, CHX is a promising candidate for controlling pectin modification. A few experiments to test the importance of CHX on pectin metabolism and trafficking are given.

B.1. Determine pectin components in the cell walls of *wild-type* and *chx* mutant plants using histochemical stains

Hypothesis: CHX activity will affect the amount and type of pectin in cell wall.

The major step in pectin modification is demethylesterification generating pectate (carboxyl group rich pectin), methanol and protons (Moustacas et al., 1991). Pectate then becomes available to either form ionic bonds with Ca^{2+} promoting the formation of "egg-box" model structure representing by the gel formation, or be modified or degraded by pectin-degrading enzymes resulting in changes in the texture and rigidity of the cell wall (Pelloux et al., 2007). Changes in de-esterification of pectin can be monitored by ruthenium red staining as its binding site requires two negative charges 0.42 nm apart present in pectate form of pectin (Sterling, 1970). In contrast, hydroxylamine-$FeCl_2$ has been used to stain esterified form of pectin which is based on the ability of alkaline hydroxylamine-$FeCl_2$ to react with methyl-ester groups of pectin releasing the products that form reddish-brown precipitate with ferric ions (Reeve, 1959). These two methods have successfully demonstrated that only methyl-esterified pectin predominates in wound periderm where lateral root initiation occurs (Sabba and Lulai, 2002). Therefore, I propose to visualize pectin in cell walls of single or multiple *chx* mutants and *wild-type* plants as a first step to test the effect of CHX function in cell wall remodeling.

Different types of pectin can be quantitated to confirm the differential pectin metabolism that is potentially associated with CHX function. Recent technology in

mass spectrometry allows the high-through-put analyses of cell wall properties, including pectin (Ralet et al., 2009).

B.2. Determine internalized pectin in *wild-type* and *chx* mutant plants with monoclonal antibodies

Hypothesis: CHX activity will change the modification and delivery of pectins in endosomes and walls due to altered internalization and recycling of pectin and pectin-modifying enzymes.

Pectin was recently shown to be internalized and recycled to the PM in plants (Baluska et al., 2005). However, only certain forms of pectin undergo internalization, distinct from other pectins in the Golgi (Hudak et al., 1993; Baluska et al., 2002; 2005; Yu et al., 2002). Different forms of pectin can be detected by specific monoclonal antibodies, such as JIM7 versus JIM5. Pectin species that are internalized and recycled back to the PM in *wild-type* and *chx* mutant plants can be tested using immuno-EM or with fluorescence microscopy. This immuno-detection method might allow quantification of pectin species in a microplate reader using ELISA. Application of BFA, and wortmannin, together with the use of native CHX-GFP fusion will also help to dissect the role of CHX in pectin trafficking. These studies will shed light on whether CHX activity alters pectin trafficking and metabolism.

B.3. Test the effect of CHX on pH and K^+ homeostasis and pectin metabolism *in vitro* and *in vivo*

Hypothesis: CHX controls pectin modification through changes in the local pH and K^+ environment.

I have proposed that CHXs activity modulates the K^+ and pH homeostasis, yet there is no direct evidence that endosomal pH or K^+ content is affected. I propose to use pH sensitive variants of GFP, pHluorins, targeted to PVC or fused with CHX to allow real-time monitor of pH change *in vivo*. CHX20 altered guard cell movement (Padmanaban et al., 2007) and CHX17 also changed stomata closure in alkaline pH (Fig. A-V-10), so guard cells can be used as a model. However, it might be relatively difficult to manipulate this in plants. Alternatively, if a genetic tool is available, it is possible to use fresh water green algae as a model because they potentially have only a single CHX homolog closely related to CHX15-20 in plants. Even though measuring compartmental K^+ is challenging, it is possible that one can analyze the effect of K^+ or other cations on internalized pectin metabolism in *wild-type* and *chx* mutant plants. By coupling to the visualization of pectin species in endomembrane, these approaches would show if pH and K^+ homeostasis by CHX is connected to the modulation of internalized pectin modification.

B.4. Understand how CHX is integrated with signaling networks that determine wall pectin modification

Hypothesis: CHX is regulated by interacting with signaling proteins, pectin or pectin-modifying enzymes.

To address the question on how CHX is regulated, it is essential to understand biochemical properties of CHX in detail. I have demonstrated what CHX transports and how pH affects K^+ transport mediated by CHX. The next step is to identify the domains that regulate CHX activity. A molecular approach using gene mutation will answer this question by creating CHX mutant constructs and expressing them in *E. coli* or yeast then assessing their function compared to the function of the *wild-type*. The second approach is to determine the domains that interact with vesicular trafficking machineries, pectin modifying enzymes or pectin itself. One strategy would be to pull-down of proteins that interact with CHXs using available *CHX-GFP* constructs, and then identify proteins using mass spectrometry. For interaction with pectin, the same strategy will be used but focus on the detection of pectin polymer. These studies could provide support for the model linking pectin metabolism and trafficking to endosomal transporters that alter localized K^+ and pH homeostasis.

V. APPENDICES

TABLES OF CONTENTS

LIST OF APPENDIX TABLES

Supplemental tables for Chapter II

LIST OF APPENDIX TABLES (continued)

LIST OF FIGURES

Supplemental figures for Chapter II

LIST OF FIGURES (continued)

LIST OF FIGURES (continued)

Other supplemental figures

A. SUPPLEMENTAL INFORMATION FOR CHAPTER II

A.1. Methods

A.1.a. cDNA cloning

Cloning AtCHX cDNA. Total RNA was isolated from seedlings and first strand cDNA was synthesized using reverse transcriptase. *AtCHX15*, *16*, *17*, *18* and *19* CDSs were amplified from cDNA using primers indicated in Table A-II-2. Only *AtCHX17* CDS was amplified from pSMCHX17. PCR were performed using Platinum Pfx DNA polymerase (Invitrogen 11708-013) with three step cycling (denature at 94^{o}C for 15 sec, anneal at 55^{o}C for 30 sec and extend at 68^{o}C for 2-3 min) for 30-35 cycles. PCR-amplified *AtCHXs* were purified by QIAquick Gel Extraction Kit (Qiagen 28704). Purified *AtCHXs* fragments were cloned into Gateway donor vector, pDONR221 (Invitrogen) using Gateway BP Clonase II Enzyme Mix (Invitrogen 11789-20), generating entry vectors listed on Table A-II-3. Empty vector control was derived from the insertion of a 90-bp oligonucleotide to Gateway pENTR/D-TOPO (Invitrogen), generating an entry vector shown in Table A-II-3. These entry vectors and destination vectors listed on Table A-II-4 were recombined using Gateway LR Clonase II Enzyme Mix (Invitrogen 11791-100), generating expression vectors listed on Table A-II-5 and A-II-9.

Cloning AtCHXs into E. coli expression vector. *AtCHX17* and *CHX20* coding sequences were amplified from gateway entry vectors pECHX17 and pECHX20 (Table A-II-3), using primers with additional restriction site KpnI:XbaI and KpnI:BglII, respectively (Table A-II-6). PCR products were amplified using Iproof DNA polymerase

(Biorad 172-5331) with three step cycling (denature at 98^{o}C for 10 sec, anneal at 65^{o}C for 30 sec and extend at 72^{o}C for 30 sec) for 30 cycles. PCR-amplified *CHX17* was restriction cut at KpnI and XbaI (NEB R0142S and R0145L) and PCR-amplified *CHX20* was cut at KpnI and BglII (NEB R0144S) sites. Sticky-end PCR fragments were agarose-gel purified by Illustra GFX purification kit (GE Healthcare 28-9034-71). For linearized vector preparation, pPAB404 plasmids were digested with KpnI and XbaI or KpnI and BamHI (NEB R0136S) corresponding to *CHX17* and *CHX20* PCR fragments, respectively. To prevent self ligation, the 5' phosphate of linearized plasmids was removed by adding alkaline phosphatase (NEB M0290S) prior to gel purification. Processed-*CHX17* or -*CHX20* fragments and linearized-pPAB404 were then ligated using the quick ligation kit (NEB M2200S) and transformed to *E coli* strain NEB10β (NEB C3019H). The transformed cells harboring pPAB404-derived vectors were selected on solid LB medium containing 50 μg/ml Ampicillin.

A.1.b. Yeast transformation and functional assays

Yeast transformation. Yeast strains were originally grown in YPAD medium (1% yeast extract, 2% peptone, 0.01% adenine, 2% glucose) prior to transformation. Transformation protocol was based on Geitz & Schiestl (2007) with some modification. Yeasts were grown in 10 ml YPAD overnight, diluted with 10 ml YPAD and incubated for additional 4-8 h to early log phase. Cell cultures were centrifuged at 2000 x g for 5 min, washed with 10 ml sterile water then suspended in FCC solution (5% v/v glycerol, 10% v/v DMSO) to A_{600} of 100 and stored at -70^{o}C. For transformation, 12.5 μl of cells was mixed with 77 μl of 40% PEG 3350 (Fluka 88276), 9 μl of 1.0 M lithium acetate (Sigma L-6883), 2.5 of μl 10 mg/ml Salmon Sperm DNA (Invitrogen 15632-011), and

1.5 µl of plasmids. The mixtures were incubated at 42°C for 1-2 h, centrifuged at 5000 x g for 1 min. Then supernatants were removed using pipet and suspended in 200 µl sterile water prior to plating on selective YNB medium supplemented with amino acid required for growth. All selective media contained 0.1 g/L of adenine. After 2-3 d, 4-12 single colonies were sub-cultured onto selective YNB plates to generate independent-transformed lines.

Functional assays. Yeasts were grown in YNB medium overnight. The regular carbon source for YNB is glucose and pH is 5.8-6.0 unless mentioned otherwise. Cell cultures were then diluted with YNB without carbon source, and incubated for 12-14 h to synchronize cell growth. Cells were washed three times and normalized using sterile water or (K^+ free) YNB without carbon source to A_{600} of 0.2. Yeast suspension was 10-fold serially diluted, and 5 µl of each dilution was spotted onto YNB or SDAP media supplemented with either 2% glucose for yeast strains harboring pDR196-derived vectors, containing constitutive *PMA1* promoter, or 2% galactose for yeast strains harboring pYES52-derived vectors, containing inducible *GAL1* promoter. All media for drop tests were made with 20 mM MES (2-(N-morpholino)ethanesulfonic acid) and adjusted to alkaline pH of 7.5 using arginine and to acidic pH using glutamic acid. KCl was used to adjust K^+ concentration. Hygromycin B (Calbiochem 400052) was added to autoclave-sterilized medium. Plates were incubated at 30°C for 3-5 d before images were taken (Nikon Coolpix 995). List of media used and their components are shown in Table A-II-7A.

A.1.c. pH_{cyt} and pH_{vac} determination

Introducing pHluorin gene into yeast by homologous recombination. A pH-sensitive GFP variant, superecliptic pHluorin (GenBank #AY533296) was provided by Dr. Miesenbock (Yale University). We generated expression vectors harboring *pHluorin* using *in vivo* homologous recombination in yeast (Oldenburg et al., 1997). *pHluorin* was amplified from pGEX-2T-derived plasmid using Platinum Pfx DNA polymerase with three step cycling (denature at 94^{o}C for 15 sec, anneal at 55^{o}C for 30 sec and extend at 68^{o}C for 1 min) for 35 cycles. *PMA1* promoter was amplified from pDR196 using the same condition. Homologous primers used for PCR are shown in Table A-II-8. Amplified-PCR fragments containing *pHluorin* or *PMA1* promoter flanking with 20-bp homologous sequences listed on Table A-II-8 were purified by PEG precipitation. In brief, 30% PEG8000 and 30 mM $MgCl_2$ were added to PCR reaction to a final concentration of 10% PEG8000 and 10 mM $MgCl_2$. The mixture was centrifuged at 10,000 x g for 15 min at room temperature, then the supernatant was discarded and the pellet was suspended in 50 μl TE buffer pH 8.0. Yeast was transformed with purified PCR fragments and linearized pYES52-derived plasmids as described earlier. ClaI and NheI (NEB R0197S and R0131S, respectively) linearized pYES52-derived plasmids by cleaving between *URA3* and *2μ* origin of replication as shown in Fig. A-II-2A. After 2-3 d, colonies expressing *pHluorin* were confirmed by the presence of green fluorescent signals and selected under fluorescence microscope (Nikon E600). At least 12 independent transformants were selected, cultured and verified for activity of *CHX* genes. Plasmids were isolated from verified transformants, and *E. coli* was re-transformed to

amplify plasmids. New *pHluorin* containing expression vectors were named pDYpH as shown in Table A-II-5.

Cytosolic pH measurement. Yeast cells were grown in YNB medium overnight then YNB-Galactose medium was added on day 2 to induce gene expression. Cells were washed with K^+-free YNB-Galactose three times and normalized to A_{600} of 20. Aliquot of 20 μl was added to 96-well, flat bottom, tissue culture plate (Falcon 3078) loaded with 180 μl of YNB media varied in pH and K^+ concentration. For each strain, a single line of yeast without *pHluorin* (pYES52) served as a background control and three independent transformants harboring *pHluorin* (pDYpH) were used for fluorescent intensity measurements. Immediately after adding yeast suspension to the media (final A_{600} of 2), the plate was inserted into a multimode plate reader (BMG FLUOstar Optima model, BMG Labtechnologies) set to 30°C. Then plate was shaken for 15 sec and fluorescence was read for 3 min in each cycle for a total of 3 cycles (approximately 10 min). For time-course analysis, the time interval for each measurement was 20 min. Emission fluorescent intensity at 460 nm (F_{460}) and 510 nm (F_{510}) was read using excitation at 400 nm. The ratio of F_{510}/F_{460} was converted to pH units using the pH calibration curve (Fig. II-4A). An *in situ* pH calibration curve was generated by adding yeast cells to buffers with ionophores instead of YNB medium. The buffer mixture with slight modification was similar to that used by Brett et al. (2005b). The solution contained 50 mM MES, 50 mM HEPES, 25 mM BTP, 50 mM KCl, 50 mM NaCl, 10 mM NaN_3, 10 mM 2-deoxyglusoe, 200 mM ammonium acetate, 75 μM monensin, and 10 μM nigericin. CCCP is unsuitable due to its fluorescence after excitation at 400 nm (Brett, 2005b). Buffers were adjusted to pH 6.0, 6.5, 7.0, 7.5 and 8.0 using NaOH or HCl. There were 6 replicates per

line at each pH. Fluorescence was read after 10, 20 or 30 min. Fluorescent intensity were measured and processed through OPTIMA software version 2.0 provided by the manufacturer. Background fluorescence was subtracted from all fluorescent readings in Microsoft Excel to generate pHluorin-dependent fluorescent intensity. The calibration curve was generated from the mean ratio F_{510}/F_{460} at each pH and fitted to the regression of polynomial of order 3 (cubic equation) using Microsoft Excel.

Vacuolar pH measurement. We used the dual-excitation ratiometric pH indicator BCECF to measure vacuolar pH in yeast (Plant et al., 1999). Yeasts were prepared as above; however cells were normalized to A_{600} of 40 then loaded with 50 μM BCECF-AM (2′,7′-Bis(2-carboxyethyl)-5(6)-carboxyfluorescein acetoxymethyl ester; Sigma B8806) by adding an equal volume of 100 μM BCECF-AM in YNB-Galactose adjusted to pH 4.5 with tartaric acid and incubated for 25 min at 200 rpm and 30^{o}C. BCECF-loaded cells were washed three times with K-free YNB-Galactose to remove extracellular BCECF and normalized to A_{600} of 20. Aliquot of 20 μl was added to 96-well, flat bottom, tissue culture plate (Falcon 3078) loaded with 180 μl of YNB media varied in pH and K^+ concentration. For each strain, two independent lines of yeasts were assayed. Each BCECF-loaded line was added to 6 wells to make 6 replicates, and 1 well for yeast without BCECF served as background control. Immediately after yeast was added to the reaction media, the 96-well plate was inserted into a multimode plate reader set to 30^{o}C, shaken for 15 sec and fluorescence was read for 3 min in each cycle for a total of 3 cycles (approximately 10 min). The mixture was incubated for 10 to 150 min at 20 min intervals. We determined the ratio $F_{ex\ 492}/F_{ex\ 460}$ with emission fixed at 530 nm. The excitation ratio of F_{ex492}/F_{ex460} was converted to pH units using a pH calibration

curve (Fig. 4D). An *in situ* pH calibration curve was generated by incubating yeast with pH-controlled buffers. The buffer with slight modification to that used by Plant et al. (1999) contained 50 mM MES, 50 mM MOPS, 50 mM KCl, 50 mM NaCl, 10 mM NaN_3, 10 mM 2-deoxyglusoe, 200 mM ammonium acetate and 50 μM CCCP. Buffers were adjusted using NaOH or HCl. Background fluorescence from yeast without BCECF was subtracted. The calibration plot was generated from the mean ratio F_{ex492}/F_{ex460} at pH 5.0, 5.5, 6.0, 6.5, 7.0, 7.5 and fitted to the regression of polynomial of order 4 (quartic equation) using Microsoft Excel.

A.1.d. Measuring Carboxypeptidase Y Secretion.

Yeast growth. Yeast strains harboring pYES52-derived plasmids were grown in YNB medium overnight then YNB-Galactose medium was added on day 2 to induce gene expression. Cells were washed with K^+ free YNB without carbon source three times before normalizing to A_{600} of 0.2 or 0.8. Twenty μl aliquot was added to white opaque 96-well ELISA plate (Pierce 15042) containing 180 μl of YNB-Galactose medium pH 5.5 supplemented with 4 mM K_2SO_4 or 8 mM KOH (pH 7.3). To measure growth by cell density, flat bottom 96-well ELISA plate immulon 1(Dynatech 0110103350) was used. The starting cell density was approximately 0.01 for pH 5.5 and 0.04 for pH 7.3 at A_{600} read by a multimode plate reader. For each strain, two independent lines of yeasts were tested. Each line was added to 7 wells to make 7 replicates, one well with media alone served as a background control. Plates were incubated at 30^oC for 18-20 h to early log phase, and then extracellular CPY was measured.

Extracellular CPY measurement. General procedure for enzyme immunoassay was performed directly. Growth was terminated by removing the cells. Extracellular proteins, including CPY adheres to the surface of the wells. Briefly, plates were washed three times with PBS buffer and blocked with 1%BSA-PBS. Plates were washed twice with PBS-T solution (PBS buffer, 0.05% TWEEN-20) prior to addition of 100 µl of PBS-T with mouse anti-CPY (Invitrogen A-6428) at 1:1000 dilution (0.25 µg anti-CPY/ml) to each well and incubated at 30^{o}C for 1 h. Plates were washed four times with PBS-T solution before addition of 100 µl of PBS-T with goat anti-mouse conjugated to IgG horseradish peroxidase (Thermo Scientific 31430) at 1:10,000 dilution (0.04 µg anti-mouse IgG/ml) and incubated at 30^{o}C. After 1 h, plates were washed four times with PBS-T solution. Horseradish peroxidase activity was measured by chemiluminescence (Haan and Behrmann, 2007). Briefly, luminol (3-Aminophthalhydrazide, 5-Amino-2,3-dihydro-1,4-phthalazinedione, Sigma A8511) and 4-IPBA (4-Iodophenylboronic acid, Aldrich 471933) were used as substrate and enhancer, respectively. Substrate solution (100 mM Tris/HCl pH 8.8, 2.5 mM luminol, 0.4 mM 4-IPBA) was prepared fresh from stock solution and kept in the dark. After the plate was washed thoroughly, 30% hydrogen peroxide was added to the substrate solution yielding 2.6 mM H_2O_2. The reaction mixture (100 µl) was then added to each well, and incubated for 5 min. The opaque ELISA plate was inserted into a multimode plate reader set to 30^{o}C, shaken for 2 sec and luminescence was read for 90 sec in each cycle for a total of 10 cycles (approximately 15 min). Luminescence signals collected from 10 cycles were pooled. Background luminescence was subtracted. Relative luminescence units were normalized to cell density measured at A_{600} on clear ELISA plates at indicated times. To demonstrate

that CPY measured by immunoassay represented differential extracellular CPY secreted by yeasts, purified yeast CPY at 0-2 ng was added to a 96-well ELISA plate with or without yeast strain LMB01 at pH 5.5 or 7.3. After 20 h, CPY on the plate was detected by immunoassay as described above. The calibration plot was generated from the mean luminescence and fitted to the regression of polynomial of order 2 (quadratic equation) using Microsoft Excel. Extracellular CPY was converted from arbitrary unit (AU) to ng CPY and then normalizing with cell density (A_{600}) as shown in Fig. 7B and 7C.

A.1.e. *E. coli* strain LB2003 transformation and growth assays

E. coli strain LB2003 transformation. Competent cell preparation and transformation were conducted as described by Maeder et al. (2009), except YTMK medium was used instead of LB medium. In brief, a single colony of *LB2003* was inoculated to 2 ml of YTMK and incubated in a shaker at 30^{o}C overnight. The next day, 1 ml of cell culture was added to 50 ml YTMK supplied with 15 mM $MgCl_2$, then incubated further for 2-3 h until A_{600} reach 0.4-0.6. Cells were pelleted at 3000 x g for 10 min at 4^{o}C. Pellets were suspended in sterile iced-cold solution A (50 mM $CaCl_2$, 10 mM MES, 15% Glycerol, 10 mM $MnCl_2$ pH 6.3) and incubated on ice for 30 min. Competent cells were instantly frozen in -80^{o}C ethanol bath and stored at -80^{o}C. To transform cells, frozen competent cells were thawed on ice for 15 min. An aliquot (1-2 µl) of pPAB404-derived plasmids were added to 50 µl of competent cells and incubated on ice for 5 min. Cells were heat-shocked at 42^{o}C for 2 min then cooled down on ice for another 2 min. Then, 250 µl of YTMK or SGM-KN media (Table A-II-7B) was added to the cell suspension then incubated on a shaker at 30^{o}C for 1-2 h. Cell cultures were spread on

solid YTMK or SGM-KN media supplemented with 50 μg/ml ampicillin and incubated at 30°C for 1-2 days. Only fresh transformed cells were used.

Growth assay. Each fresh transformant was grown in 500 μl SGM-KN medium overnight. Cell cultures were pelleted and resuspended in 750 μl SGM-KN then incubated at 30°C, 250 rpm for additional 3 h. Log-phase grown cells were washed with 1 ml basal SGM pH 6.6 (Table A-II-7B) five times then normalized to A_{600} of 0.5 and incubated for additional 2 h. In each well in a 96-well plate, 20 μl of normalized cell suspension was added to 180 μl SGM-MESMOPS (Table A-II-7B). All test media were supplemented with 50 μg/ml ampicillin, 0.5 mM IPTG (Isopropyl β-D-1-thiogalactopyranoside) and varied concentration of KCl and pH. In some experiments, cations at indicated concentration were added to the medium. The 96-well plate was inserted into a multimode plate reader set to 30°C, shaken for 15 sec and measured A_{600} every 15 min for upto 24 h. Growth of each transformant (cell density) was represented by an increase in A_{600} at any given time point. Background A_{600} measured from medium-only was subtracted from the A_{600} from each strain at each time point.

A.1.f. ^{86}Rb (K^+) transport

Yeast Yeast strains harboring pDR196 plasmids were grown in YNB medium at 30°C for 18 h. For K^+ uptake-deficient strain (LMM04), the medium was supplemented with 100 mM KCl. Cells were washed three times and suspended in SDAP medium for K^+ starvation then grown for additional 4 h at 30°C. Cells were washed three times with SDAP medium and normalized to A_{600} of 5.33. Transport reaction mixture (4 ml) comprised of 20 μM KCl, ^{86}Rb 0.75 μCi/ml (Perkin Elmer NEZ072), yeast at $1x10^7$ cells/ml (A_{600} 1.0) and SDAP medium adjusted to pH 4.5 or 7.5 using glutamic acid or

BTP, respectively. Aliquot of 750 µl was taken at 0, 5, 10, 15 and 30 min, mixed with 3.25 ml ice-cold wash solution, and filtered. The wash solution consisted of 1.75 mM RbCl in SDAP medium at pH 4.5 or pH 7.5. Yeasts filtered through 0.45 µm nitrocellulose membrane (Millipore HAWP304F0) was rinsed twice with 3.25 ml cold wash solution. Each filter was placed into a vial after drying.

E. coli Fresh transformed cells were grown in SGM-KN medium with 50 µg/ml ampicillin overnight at 30^{o}C and 250 rpm. The next day, cell cultures were pelleted at 3000xg for 10 min and suspended in the same volume of SGM-KN medium. Cells were allowed to grow for additional 2 h. Cells were pelleted again and suspended in 1 ml basal SGM medium pH 6.2. Cells were washed five times and normalized to A_{600} of 2.1 (for time course) or 3.2 (for cation inhibition) then incubated at room temperature for 2 h.

i) Time-course A 4-ml reaction contained cells at A_{600} of 0.4 (~2.5x10^{8} cells/ml), 0.5 mM IPTG, 2 mM RbCl , ^{86}Rb 0.5 µCi/ml, in SGM-MESMOPS medium pH 6.2 or 6.6. Aliquot of 750 µl was taken at 0, 5, 10, 15 and 30 min, mixed with 3.25 ml wash solution (4 mM H_3PO_4, 0.4 mM $MgSO_4$, 0.1 mM $CaCl_2$, 1.75 mM RbCl, 80 mM glycerol, 50 mM mannitol, 20 mM KCl, adjust to pH 6.2 or 6.6 using KOH), and filtered through 0.45 µm nitrocellulose membrane (Whatman Protran BA85). Retained cells on nitrocellulose membrane were washed for additional 2 times before placing into a vial.

ii) Cation inhibition. A 750-µl reaction contained cells at A_{600} of 0.4 (~2.5x10^{8} cells/ml), 0.5 mM IPTG, 0.6 mM RbCl, ^{86}Rb 0.5 µCi/ml, and cation as indicated concentration, in a quarter strength basal SGM medium with the final concentration of 80 mM glycerol, 10 mM MES and 10 mM MOPS, pH 6.2. Mannitol was used to balance the same osmolarity in each treatment. Cell suspension was added to the reaction mixture

first followed by ^{86}Rb solution after 30 s. After 30 min of incubation at room temperature, 3.25 ml of wash solution (pH 6.2) was added to the mixture, filtered and washed as above.

iii) CCCP. Procedure is similar to cation inhibition assay except assays contained CCCP in DMSO or DMSO alone and 60 mM mannitol to adjust osmolarity. Reaction was performed at pH 6.2 and pH 7.2.

Each vial was filled with 3 ml of Bio-Safe II scintillation cocktail (Research Products International Corp 111-195) and counted in the scintillation counter (Beckman Coulter). Each sample was counted for 3 min 2-3 times. For each time-course reaction mixture, 20 μl was counted to relate dpm with nmole Rb.

A.1.g. Transfection of Arabidopsis Mesophyll Protoplasts

Protoplast preparation. Plasmids carrying genes tagged with a fluorescent marker was transiently expressed in leaf protoplasts according to published protocols (Li et al. 2008; Umemura et al., 2004; Yoo et al., 2007) with some modification**.** In brief**,** Arabidopsis leaves from approximately 3 week-old plants were cut into small strips and digested in 2.5 ml of enzyme solution for 3 h. The digestion solution consisted of 1.3% cellulose R10, 0.25% macerozyme R100 (Yakult, Tokyo, Japan), 0.4 M mannitol, 20 mM KCl, 20 mM MES at pH 5.7, 10 mM $CaCl_2$, 0.1% fetal bovine serum (Sigma #F6178), and 2.5 mM β-mercaptoethanol. Protoplasts were filtered through 70 μm nylon mesh, centrifuged at 100 xg for 2 min. The pellets were washed twice in W5 solution containing 0.35 M mannitol, 125 mM $CaCl_2$, 5 mM KCl, 5 mM glucose, 2 mM MES at pH 5.7 by centrifuge at 100 x g for 1 min. Protoplasts were resuspended in MMg solution (0.4 M mannitol, 15 mM $MgCl_2$, 4 mM MES pH 5.7) prior to transfection. Plasmids were

purified by miniprep kit (Qiagen #27160) or plasmid midi kit (Qiagen #12143) and suspended in 0.4 M mannitol. The plasmids used in this study are shown in Table A-II-9.

PEG-mediated transfection. For each transfection, 10 μl of protoplast suspension (1-2 x 10^4 cells) was added to a mixture of 40 μl plasmids (5-10 μg per plasmid) listed in Table A-II-9, 5 μl M10Mg solution (0.4 M mannitol, 150 mM $MgCl_2$, 40 mM MES) and 55 μl PEG-Ca solution (40% PEG4000 (Fluka #81240), 0.2 M mannitol, 100 mM $CaNO_3$). After incubation at room temperature for 20-30 min, transfection mixture was diluted with 700 μl W5 solution and centrifuged at 100 x g for 45 sec. After supernatant removal, protoplasts were resuspended in 300 ul WI solution (0.5 M mannitol, 8 mM K_2HPO_4, 2 mM MES) and 400 μl MS solution (0.45 M mannitol, 1X MS salt mixture (GIBCO #11117-058), 1X Gamborg's vitamin solution (Sigma #G1019), 2% sucrose, 2 mM MES, 100 μg/ml ampicillin), respectively. Transfected protoplasts were incubated in the dark at room temperature for 18-24 hr. In general, the transformation efficiency of a single gene is 50% or higher; however, efficiency is lower in co-transfection due to differences in fluorescent signals and expression level of each gene.

A.2. Tables of materials and results

Table A-II-1. *Saccharomyces cerevisiae* strains.

Name	Genotype	Source/ Reference
FY833	MATa *his3Δ200 ura3-52 leu2Δ1 lys2Δ202 trp1Δ63 GAL2+*	Ramirez et al., 1998
Kha1	MATa *his3Δ200 ura3-52 leu2Δ1 lys2Δ202 trp1Δ63 GAL2+* kha1Δ::His5+	Ramirez et al., 1998 (Antonio Pena)
KTA40-2	MATa ade2-*1 can1-100 his3-11,15 leu2-3,112 trp1-1 ura3-1 mall0 ena1Δ::HIS3::ena4Δ nha1Δ::LEU2 nhx1Δ::TRP1 kha1Δ::kanMX*	Maresova & Sychrova, 2005
AXT3	MAT α ade2-*1 can1-100 his3-11,15 leu2-3,112 trp1-1 ura3-1 mall0 ena1Δ::HIS3::ena4Δ nha1Δ::LEU2 nhx1Δ::TRP1*	Quintero et al., 2000
LMB01	MATa ade2-*1 can1-100 his3-11,15 leu2-3,112 trp1-1 ura3-1 mall0 ena1Δ::HIS3::ena4Δ nha1Δ::LEU2 kha1Δ::kanMX*	Maresova & Sychrova, 2005
LMM04	MATa ade2-*1 can1-100 his3-11,15 leu2-3,112 trp1-1 ura3-1 mall0 ena1Δ::HIS3::ena4Δ nha1Δ::LEU2 trk1Δ::LEU2 tra2Δ::HIS3 kha1Δ::kanMX:tok1Δ*	Maresova & Sychrova, 2005

Table A-II-2. Primers used to clone CHX cDNA into Gateway vectors. Bases in lower case denote recombination sequence, *AttB*. Forward (F) primers show the first codon ATG (underlined), except for CHX20cF where bases in grey were not in the primer. Reverse (R) primers do not contain a stop codon.

Name	Primer Sequence	Template
CHX15cF	ggggacaagtttgtacaaaaaagcaggctTCGAAAAAATGGCGACAAGTGAAGAAC	Cdna
CHX15cR	ggggaccactttgtacaagaaagctgggtcACGTGGATTCTCTAAACCATATGTG	cDNA
CHX16cF	ggggacaagtttgtacaaaaaagcaggctTCATGGGTACTTTGGTCAACGGTACT	cDNA
CHX16cR	ggggaccactttgtacaagaaagctgggtcTGGCGTCTCCACCACCGGGACAGA	cDNA
CHX17cF	ggggacaagtttgtacaaaaaagcaggctTCAGCATGGGAACAAACGGTACAACAT	pSM_X17
CHX17cR	ggggaccactttgtacaagaaagctgggtcAGGACTCTCAGAATCCTCAACCAGC	pSM_X17
CHX18cF	ggggacaagtttgtacaaaaaagcaggctAGTCTGCAAGGATGGCTACAAAT	cDNA
CHX18cR	ggggaccactttgtacaagaaagctgggtcTTTATCCGTAGAAGTCAATACC	cDNA
CHX19cF	ggggacaagtttgtacaaaaaagcaggctTCTCCACTAGGATGGCAAGCACCAAC	cDNA
CHX19cR	ggggaccactttgtacaagaaagctgggtcGGCAGTTAAGTCTGAAATATCTCTG	cDNA
CHX20cF	ggggacaagtttgtacaaaaaagcaggctCGTCGATAAGAGAGTCCTTTGAAATCCCCAAAATG	cDNA
CHX20cR	ggggaccactttgtacaagaaagctgggtcTCCGTTAATACTTAGAGAAGACTC	cDNA

Table A-II-3. Entry vectors of PCR-amplified CHX sequence, and a 90 bp insert for the empty vector control.

Vector Name	Description	Source
pECHX15	full length AtCHX15 CDS without the stop codon	This work
pECHX16	full length AtCHX16 CDS without the stop codon	This work
pECHX17	full length AtCHX17 CDS, without the stop codon	This work
pECHX18	full length AtCHX18 CDS, without the stop codon	This work
pECHX19	full length AtCHX19 CDS, without the stop codon	This work
pECHX20	full length AtCHX20 CDS, without the stop codon	Padmanaban et al., 2007
pEempty	90-bp insert from primer annealing TCGTCTCAAGTGGTTTAAAGACCAATGTTGCGACG ATCCAAGGAGCTCAGTCTTGGGGTCTTCTGGTTTT AGTCACCGCCACAGCTTGTT	This work

Table A-II-4. Destination vectors used to create expression vectors.

Vector Name	Description	Source
pYES-DEST52	GAL1 promoter, V5 epitope, 6xHis, URA+, Amp R, Gateway	Invitrogen
pYES-DR196	PMA1 promoter, V5 epitope, 6xHis, URA+, Amp R, Gateway	Li et al., 2008
pFGW-DR196	PMA1 promoter, EGFP at N terminal, URA+, Amp R, Gateway	Li et al., 2008
pGWF-DR196	PMA1 promoter, EGFP at C terminal, URA+, Amp R, Gateway	Li et al., 2008

Table A-II-5. Expression vectors. Sequences in pDY plasmids are driven by the GAL1 promoter and those in pDR are under the control of the PMA1 promoter. (Continue on next page)

Vector Name	Description	Source
pDYempty	GAL1 promoter, 90 bp insert (45 bp if transcribed)	This work
pDYCHX15	GAL1 promoter , AtCHX15, V5 epitope, 6xHis	This work
pDYCHX16	GAL1 promoter, AtCHX16, V5 epitope, 6xHis	This work
pDYCHX17	GAL1 promoter, AtCHX17, V5 epitope, 6xHis	This work
pDYCHX18	GAL1 promoter, AtCHX18, V5 epitope, 6xHis	This work
pDYCHX19	GAL1 promoter, AtCHX19, V5 epitope, 6xHis	This work
pDYCHX20	GAL1 promoter, AtCHX20, V5 epitope, 6xHis	This work
pDRempty	PMA1 promoter, 90 bp insert (45 bp if transcribed)	This work
pDRCHX15	PMA1 promoter, AtCHX15, V5 epitope, 6xHis	This work
pDRCHX16	PMA1 promoter, AtCHX16, V5 epitope, 6xHis	This work
pDRCHX17	PMA1 promoter, AtCHX17, V5 epitope, 6xHis	This work
pDRCHX18	PMA1 promoter, AtCHX18, V5 epitope, 6xHis	This work
pDRCHX19	PMA1 promoter, AtCHX19, V5 epitope, 6xHis	This work
pDRCHX20	PMA1 promoter, AtCHX20, V5 epitope, 6xHis	This work
pFGWDRempty	PMA1 promoter, EGFP-90 bp insert, V5 epitope, 6xHis	This work
pFGWDRCHX15	PMA1 promoter, EGFP-AtCHX15, V5 epitope, 6xHis	This work
pFGWDRCHX16	PMA1 promoter, EGFP-AtCHX16 , V5 epitope, 6xHis	This work
pFGWDRCHX17	PMA1 promoter, EGFP-AtCHX17 , V5 epitope, 6xHis	This work
pFGWDRCHX18	PMA1 promoter, EGFP-AtCHX18 , V5 epitope, 6xHis	This work

Vector Name	Description	Source
pFGWDRCHX19	PMA1 promoter, EGFP-AtCHX19 , V5 epitope, 6xHis	This work
pFGWDRCHX20	PMA1 promoter, EGFP-AtCHX20 V5 epitope, 6xHis	This work
pGWFDRempty	PMA1 promoter, 90 bp insert (45 bp if transcribed)	This work
pGWFDRCHX15	PMA1 promoter, AtCHX15-EGFP , V5 epitope, 6xHis	This work
pGWFDRCHX16	PMA1 promoter, AtCHX16-EGFP , V5 epitope, 6xHis	This work
pGWFDRCHX17	PMA1 promoter, AtCHX17-EGFP , V5 epitope, 6xHis	This work
pGWFDRCHX18	PMA1 promoter, AtCHX18-EGFP V5 epitope, 6xHis	This work
pGWFDRCHX19	PMA1 promoter, AtCHX19-EGFP, V5 epitope, 6xHis	This work
pDYpHempty	GAL1 promoter, 90 bp insert and pHluorin driven by PMA1	This work
pDYpHCHX15	AtCHX15 driven by GAL1 promoter, pHluorin driven by PMA1	This work
pDYpHCHX16	AtCHX16 driven by GAL1 promoter, pHluorin driven by PMA1	This work
pDYpHCHX17	AtCHX17 driven by GAL1 promoter, pHluorin driven by PMA1	This work
pDYpHCHX18	AtCHX18 driven by GAL1 promoter, pHluorin driven by PMA1	This work
pDYpHCHX20	AtCHX19 driven by GAL1 promoter, pHluorin driven by PMA1	This work
pDR196-NHX1	PMA1 promoter, AtNHX1	ABRC
pDR196-NHX2	PMA1 promoter, AtNHX2	ABRC
pDR195-NHX1-GFP	PMA1 promoter, AtNHX1-GFP	IRNA-CSIC (Pardo JM via Cubero B)

Table A-II-6. **Primers used to clone CHX cDNA into *E. coli* expression vector.** Bases underlined denote start (ATG) or stop codon, restriction site is shown in bold.

Name	Primer Sequence	Template
PC-KpnIX17-F	CCC**GGTACC**ATGGGAACAAACGGTACAACATG TCCA	pECHX17
PC-XbaIX17-R	CCC**TCTAGA**CTAAGGACTCTCAGAATCCTCAAC CAGCGA	pECHX17
PC-KpnIX20-F	CCC**GGTACC**ATGCCCTTCAACATAACCTC	pECHX20
PC-BglIIX20-R	CCC**AGATCT**TCATACATTTGTGTCTCCGTTAA	pECHX20

Table A-II-7A. Media for yeast growth.

Name	Main component (per litre)		Catalog number
YPAD	Yeast extract	10 g	Fluka 70161
	Peptone	20 g	BD 211677
	Adenine	0.1 g	Sigma A8626-25G
	Dextrose (glucose)	20 g	BDH 0230-2.5KG
YNB	Yeast Nitrogen Base without amino acids	6.7 g	Difco 0919-07
	Glucose or Galactose	20 g	
SDAP (Synthetic Dextrose Arginine Phosphate)	500X Vitamins	2.0 ml	Based on YNB supplement
	200X Trace Elements	5.0 ml	
	$MgSO_4.7H_2O$	0.5 g	Fisher M63-500
	$CaCl_2$	0.1 g	Sigma C4901
	85% H_3PO_4	0.5 ml	Baker 0260-01
	Glucose or Galactose	20 g	
	Adjust pH with arginine base	varied	Fisher BP2505500
K^+-free YNB	500X Vitamins	2.0 ml	Based on YNB supplement
	200X Trace Elements	5.0 ml	
	$MgSO_4.7H_2O$	0.5 g	Fisher M63-500
	$CaCl_2$	0.1 g	Sigma C4901
	NaCl	0.1 g	Fisher S271-10
	$(NH_4)_2SO_4$	4.0 g	Fisher A938-500
	$(NH_4)_2HPO_4$	1.0 g	Baker 0784-01
	Adjust pH with H_2SO_4	varied	EMB SX1247-1

Table A-II-7B. Media for *E. coli* growth.

Name	Main component (per litre)		Catalog number
YTMK	Yeast extract	5 g	Fluka 70161
	Tryptone	10 g	IBI scientific IB49181
	Mannitol (50 mM)	9.1	Sigma M-4125
	KCl (30 mM)	2.2	Baker 3040-01
SGM (Synthetic Glycerol Mannitol)	4000X Vitamins	250 ul	Based on YNB supplement
	4000X Trace Elements	250 ul	
	1 M $MgSO_4.7H_2O$ (0.4 mM)	400 ul	Fisher M63-500
	1 M $CaCl_2$ (0.1 mM)	100 ul	Sigma C-4901
	85% H_3PO_4 (4 mM)	275 ul	Baker 0260-01
	10 mM $FeSO_4$.citrate (10 uM)	1 ml	Aldrich 21542-2 Baker 1-0110
	Thiamine Hydrochloride (1 mM)	0.34 g	Sigma T-4625
	Glycerol (80 mM)	6 ml	Sigma G-7757
	Mannitol (100 mM)	18.2 g	Sigma M-4125
	Adjust pH with arginine base	varied	Fisher BP2505500
SGM-KN	SGM with 50 mM mannitol	9.1 g	Sigma M-4125
	NH_4Cl (5 mM)	0.3 g	Fisher A-661
	KCl (30 mM)	2.2 g	Baker 3040-01
SGM-MESMOPS	SGM with 60 mM mannitol	11 g	Sigma M-4125
	MES (11 mM)	2.1 g	Sigma M-3671
	MOPS (11 mM)	2.1 g	Sigma M-1254

Table A-II-8. Primers used in homologous recombination of pHluorin. Bases in lower case denote sequences homologous to 2μ (origin of replication), SpH (superecliptic pHluorin), PMA (PMA1 promoter) and Ura (uracil synthesis enzyme). P (upper case) refers to primer.

Name	Sequence	Template
PH-**PMA**-2u-F	tttgacagcttatcatcgatCAAGCTTCCTGAAACGGAG A	pYES-DR196
PH-**PMA**-SpH-R	agttcttctcctttactcatGCTGGGGTATATTTTTTTTC	pYES-DR196
PH-**SpH**-PMA-F	gaaaaaaaatataccccagcATGAGTAAAGGAGAAGA ACT	pGEX-2T
PH-**SpH**-URA-R	aattgaattgaaaagctagcTTATTTGTATAGTTCATCC ATG	pGEX-2T

Table A-II-9. Plasmids used in transient expression in *Arabidopsis* protoplasts.

Parental Plasmid	Gene	Vector Name	Description	Reference
p2GWF7	AtCHX16	P2GWF-CHX16	*35S*::CHX16-EGFP	This work
p2GWF7	AtCHX17	P2GWF-CHX17	*35S*::CHX17-EGFP	This work
p2GWF7	AtCHX18	P2GWF-CHX18	*35S*::CHX18-EGFP	This work
p2GWF7	AtCHX19	P2GWF-CHX19	*35S*::CHX19-EGFP	This work
p2GWF7	AtCHX20	P2GWF-CHX20	*35S*::CHX20-EGFP	Padmanaban et al., 2007
P2GWR7	AtCHX16	P2GWR-CHX16	*35S*::CHX16-mRFP	This work
p2GWR7	AtCHX17	P2GWR-CHX17	*35S*::CHX17-mRFP	This work
p2GWR7	AtCHX18	P2GWR-CHX18	*35S*::CHX18-mRFP	This work
pUC18	mRFP-AtSYP21	-	*35Sp*, PVC marker	Uemura et al., 2004
pUC18	GFP-AtSYP22	-	*35Sp*, Vacuolar marker	Uemura et al., 2004
pUC18	mRFP-AtSYP41	-	*35Sp*, TGN marker	Uemura et al., 2004
pHTS13	GFP-AtRabF2b	-	*35Sp*, Endosomes marker	Ueda et al., 2001
pBSK	Rat-ST-GFP	-	*35Sp*, Golgi marker	Lee et al., 2002
pBSK	spGFP-HDEL	-	*35Sp*, ER marker	Hawes et al., 2001

Table A-II-10. Identity & similarity among AtCHX15-20 and ScKHA1 proteins. Clustal X version 2.0 was used to create protein alignment based on the Gonnet series protein weight matrix. Similarity among AtCHX and ScKHA1 is defined by amino acid substitution groups. Identity represents % of exact match in residues. Similarity table was generated using Genedoc version 2.6.002 (Nicholas and Nicholas, 1997).

Protein	**CHX15**	**CHX16**	**CHX 17**	**CHX 18**	**CHX 19**	**CHX 20**
A. Full	% Identity (Similarity)					
KHA1	20 (40)	20 (41)	20 (41)	20 (40)	20 (40)	19 (38)
CHX 15		41 (62)	43 (65)	46 (66)	45 (66)	42 (61)
CHX 16			56 (73)	53 (70)	51 (69)	43 (62)
CHX 17				60 (76)	57 (74)	45 (65)
CHX 18					61 (78)	47 (65)
CHX 19						49 (65)
B. TM	% Identity (Similarity)					
KHA1	32 (60)	33 (60)	34 (62)	32 (59)	35 (61)	33 (59)
CHX 15		52 (74)	53 (78)	55 (76)	53 (76)	52 (74)
CHX 16			68 (85)	68 (83)	67 (83)	58 (77)
CHX 17				73 (87)	71 (88)	61 (81)
CHX 18					74 (87)	62 (80)
CHX 19						64 (81)

A.3. Figures

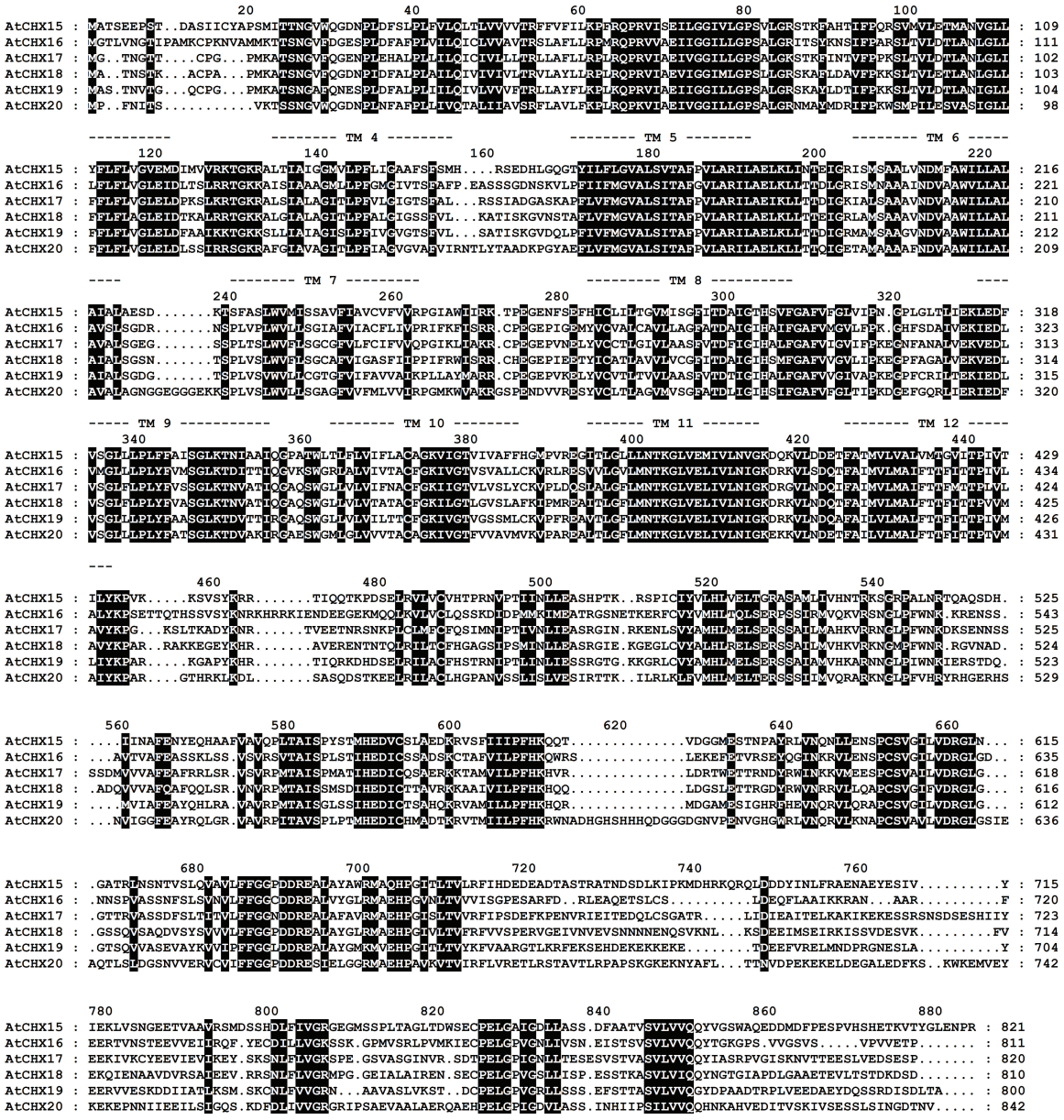

Fig. A-II-1. Alignment of *Arabidopsis* CHX15-20.

Sequence alignment and phylogenetic tree analysis shown in Fig. II-1 were performed using Clustal X version 2.0 (Larkin et al., 2007). Aligned sequences were reproduced by Genedoc version 2.6.002 (Nicholas et al., 1997). Conserved sequences among AtCHX15-20 are labeled in black. TM indicates predicted transmembrane region.

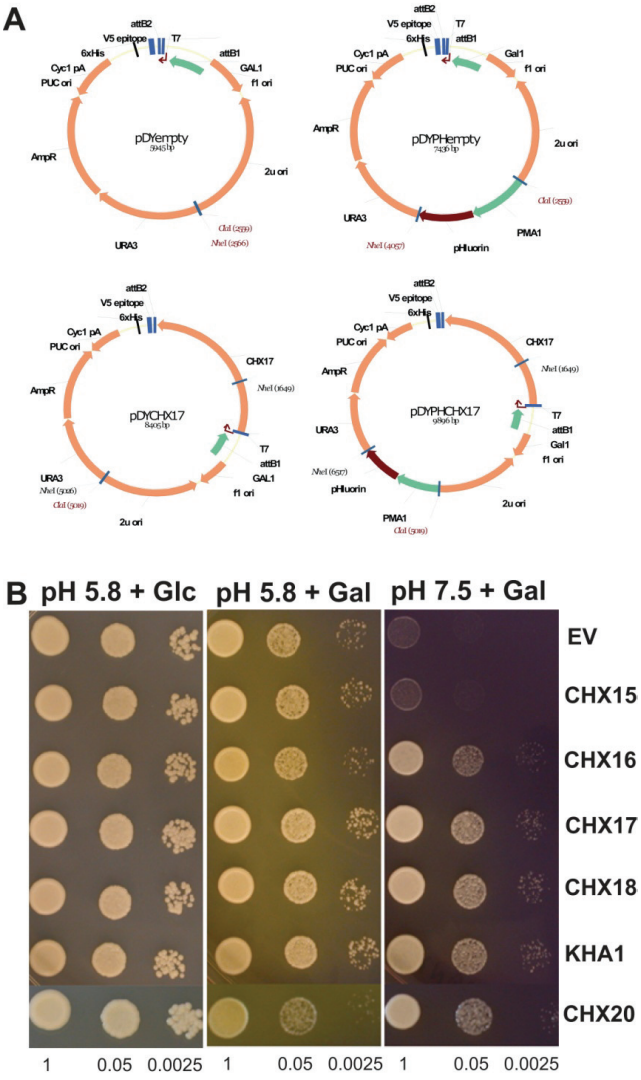

Fig. A-II-2. CHX in yeast co-expressing pHluorin is functionally active.

A) Constructing plasmids with pHluorin. pYES-DEST52-derived expression plasmids were linearized with ClaI and NheI prior to recombination. pDYempty or pDYCHX17 vectors before recombination are shown at left, and pDYPHempty or pDYPHCHX17 with pHluorin after recombination are shown at right. Empty vector contains the *GAL1* promoter driving random short transcripts (top). Vector harboring a *AtCHX* with a V5 epitope and 6x-His at the C-terminus driven by the *GAL1* promoter is shown below.

B) CHX conferred alkaline tolerance to yeast expressing *pHluorin*. Yeast strains KTA40-2 and AXT3 harboring *pHluorin* and one *CHX* were grown in YNB-Glucose overnight. Cells were diluted 10-fold with YNB containing 0.44% galactose to induce expression and incubated for 14-16 h. Washed cells were normalized with K^+-free YNB to an A_{600} of 1 and diluted 20-fold serially. Five µl of each dilution was dropped on to YNB-MES supplemented with glucose (Glc) or galactose (Gal) at pH 5.8 or 7.5 and incubated for 3 d. KTA40-2 strain expressing *pHluorin* and *CHX16-20* grew at pH 7.5 similar to *KHA1*.

Fig. A-II-3. Effect of CHX on pH_{cyt} or pH_{vac} in yeast strains grown under low K^+.

A-D) Cytosolic pH. Yeast strains KTA 40-2, AXT3, and LMB01 harboring *pHluorin* and empty vector (EV), *CHX17* or *CHX20* were prepared as Fig. A-II-2B except [K^+] was lowered to 0.1 or 0.8 mM. After incubation for 10, 30 or 50 min, relative fluorescent intensity was collected. Three independent lines of the same strain were used and twelve replicates were assayed per line at each condition (N=3, n=36). Bars = SEM.

A-B) Acidification of pH_{cyt} in strains grown at 0.1 mM K^+. CHX20 caused acidification of cytosol by ~0.2 unit at either pH_{ext} 5.6 (A) and pH_{ext} 8.0 (B) regardless of the external K^+ (see Fig. II-4B and II-4C).

C-D) pH_{cyt} in yeast expressing KHA1, NHX1 or NHX1 and CHX17 was not altered at low [K+]. Basal pH_{cyt} of all strains incubated at 0.8 mM K at either pH_{ext} 5.6 (C) or pH_{ext} 8.0 (D) was 0.1 lower than cells grown at 8 mM K (see Fig. II-4B and II-4C).

E-F) Vacuolar pH. Yeast strains KTA 40-2, AXT3, and LMB01 harboring empty vector (EV), *CHX17* or *CHX20* were prepared as above (A-D). After normalization, cells were loaded with 50 μM BCECF for 25 min, and then washed before starting the experiment. After incubation for 10, 30, 50 or 70 min, relative fluorescent signals were collected. Two independent lines of the same strain were used and six replicates were assayed per line at each condition (N=2, n=12). Bars = SEM.

E) Effect of 0.1 mM K^+ and external pH 5.6 on vacuolar pH. CHX20 and ScNHX1 caused vacuolar alkalinization. CHX17 and KHA1 had no effect on pH_{vac}. Compared to 8 mM K^+ (Fig II-4E), CHX20 increased pH_{vac} ~0.1 pH unit while ScNHX1 alkalinized pH_{vac} 0.1 pH unit lower at 0.1 mM K^+. No change in pH_{vac} was observed in yeast strain KTA40-2 expressing *EV*, *CHX17* or *KHA1* at 0.1 or 8.0 mM K^+.

F) Effect of 0.1 mM K^+ and external pH 8.0 on intracellular pH (pH_{cyt} + pH_{vac}). Yeasts harboring *ScNHX1* (LMB01) showed pH_{in} higher than strain KTA40-2 expressing *EV*, *CHX17*, *KHA1* or *CHX20*. Only CHX20 acidified pH_{in} further 0.2 pH unit at 0.1 mM K^+ when compared to at 8 mM K^+ (Fig 4F). No pH_{in} alteration was observed in yeasts expressing *EV*, *CHX17* or *KHA1* at 0.1 or 8.0 mM K^+.

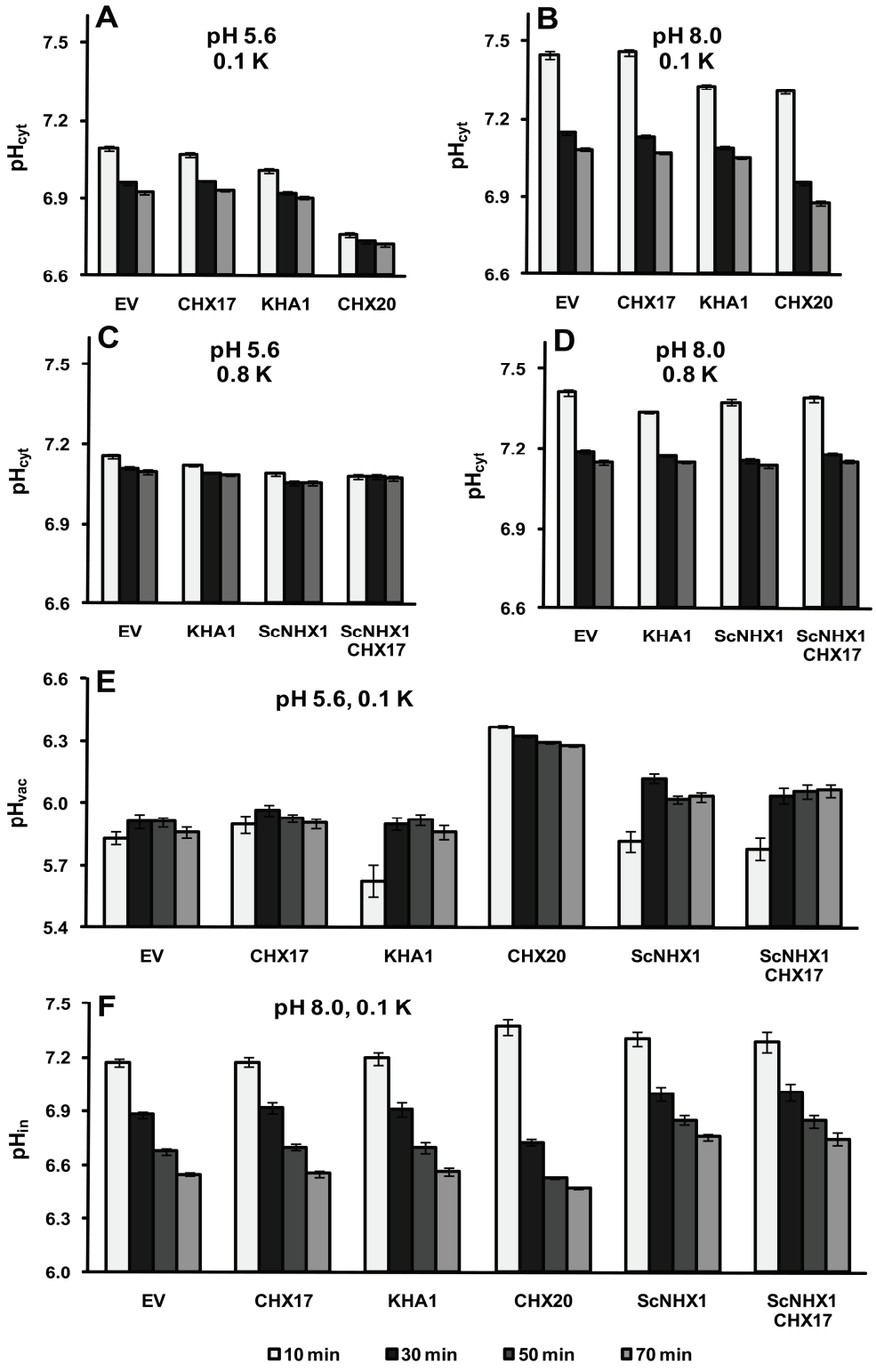
A
pH 5.6
0.1 K
B
pH 8.0
0.1 K
C
pH 5.6
0.8 K
D
pH 8.0
0.8 K
E
pH 5.6, 0.1 K
F
pH 8.0, 0.1 K
pHcyt
pHvac
pHin
7.5
7.2
6.9
6.6
6.3
6.0
5.7
5.4
EV
CHX17
KHA1
CHX20
ScNHX1
ScNHX1 CHX17
10 min
30 min
50 min
70 min

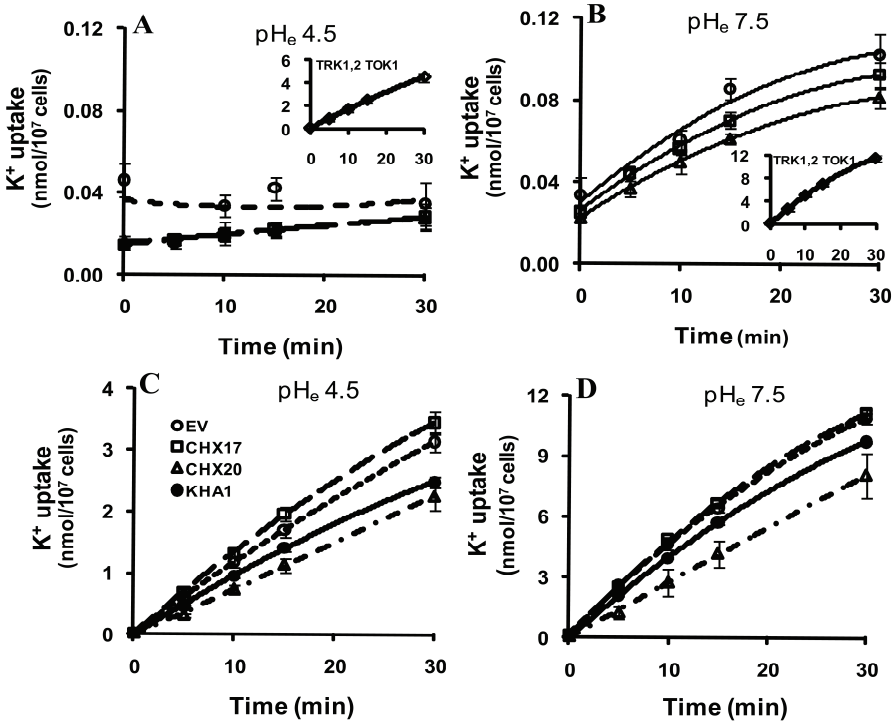

Fig. A-II-4. K^+ ($^{86}Rb^+$) uptake was unchanged in yeast expressing CHX17 or CHX20.

Strains LMB01, LMM04, KTA40-2, and AXT3 harboring pDR196 alone (EV) or vector with *CHX17* or *CHX20* were grown overnight in YNB medium. In experiment with K^+ uptake-deficient strain LMM04, medium was supplemented with 100 mM KCl. Yeast cell culture was then diluted 20-fold with the same medium and incubated for 14-16 h. Cells were washed five times and K+-starved for 4 h in SDAP medium and normalized to A_{600} of 5.33. K^+ uptake mixture consisted of SDAP medium, 2% glucose, 0.02 mM KCl, 0.75 µCi/ml 86Rb, and 10^7 cells/ml. At indicated times, 750 µl of cells was filtered and washed with 1.25 mM RbCl. Data are from four experiments. Bars represent SEM (n=4).

A-B) Time-course of K^+ (^{86}Rb) transport into K^+-uptake deficient yeast at pH_e 4.5 (A) or 7.5 (B). Flux was measured in LMM04 mutant expressing *EV* (○),*CHX17* (□), or *CHX20* (Δ). Inset show K^+ uptake into LMB01 cells that harbor *wild-type TRK1,2* and *TOK1* (◊).

C-D) Time-course of K^+ transport into KTA40-2 and AXT3 strain at pH 4.5 (C) or 7.5 (D). Flux was measured in KTA40-2 cells expressing *empty vector* (○), *CHX17* (□), *CHX20* (Δ), or in AXT3 cells carrying *wild-type KHA1* and *empty vector* (●).

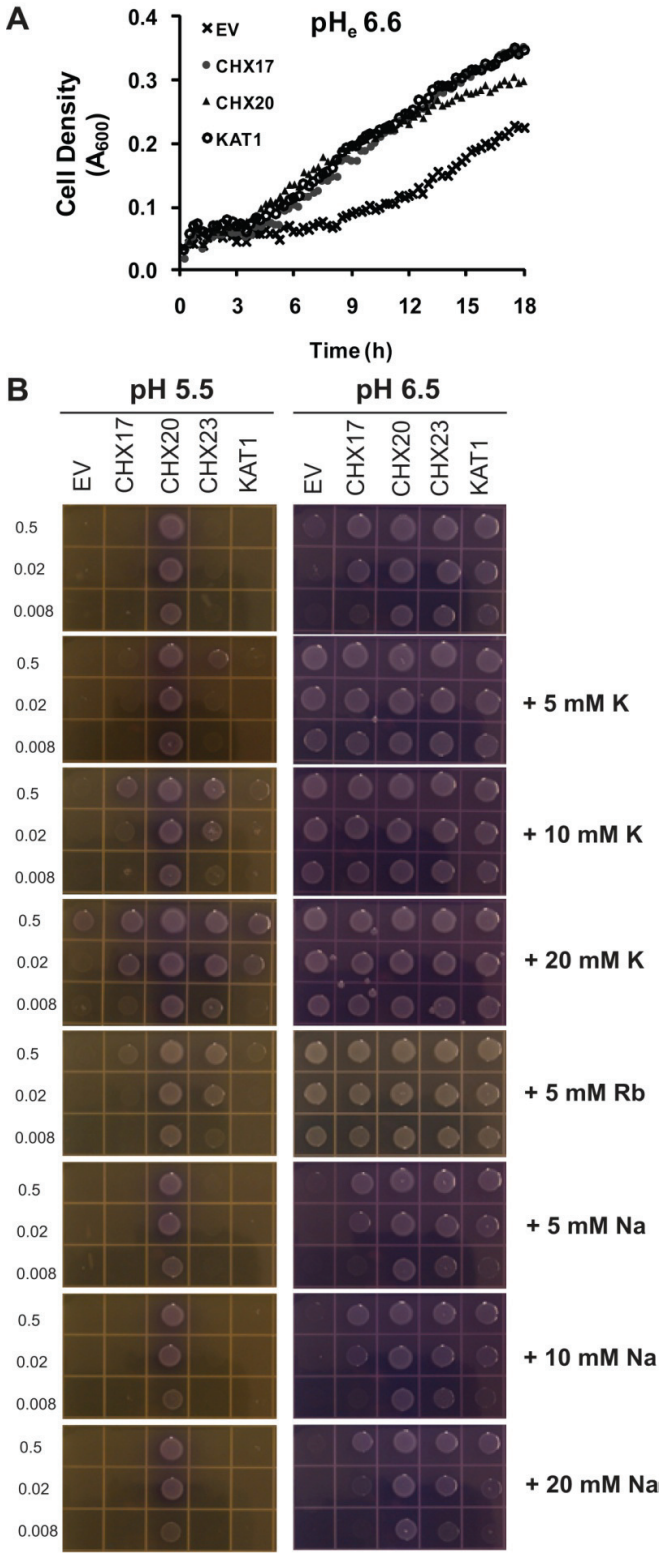

Fig. A-II-5. CHX rescued growth of K^+-uptake deficient *E. coli*. *E. coli* strain LB2003 (*trkAΔ, kup1Δ, kdpABCDEΔ*) harboring pPAB404 vector only (EV), Arabidopsis CHX17, CHX20, or KAT1 were grown overnight in YTM medium supplied with 30 mM KCl at pH 7.2. Cell cultures were replenished and grown for 2-3 h, and then washed with the same medium (YTM). Cells were normalized to an A_{600} of 0.5, 0.02 and 0.008 for plate assay, and 0.5 for liquid assay.

A) CHX17, KAT1 or CHX20 expression rescued *E. coli* LB2003 growth. Twenty µl of cell suspension normalized to A_{600} of 0.5 was added to 180 µl YTM medium at pH 6.6 and incubated at 30°C for 18 h with shaking. A_{600} was monitored every 15 min in 96-well microplate reader. All test YTM medium contained ~4 mM K, plus 50 µg/ml ampicillin, 0.5 mM IPTG, 10 mM MES and 10 mM MOPS at pH 6.6. Graph represents an average of A_{600} observed from 2 independent transformants and 2 replicates for each strain (n=4).

B) CHX20, CHX23 and CHX17 rescued E coli growth differentially on medium containing varying levels of K and Rb. Five µl of cell suspension normalized to 0.5, 0.2 or 0.008 was spotted on solid YTM supplemented with cations as indicated at pH 5.5 or pH 6.5, and incubated for 20 h at 30°C. The relative effectiveness of growth at 10 mM K was : CHX20 >> CHX23 > CHX17 = KAT1 at pH 5.5.

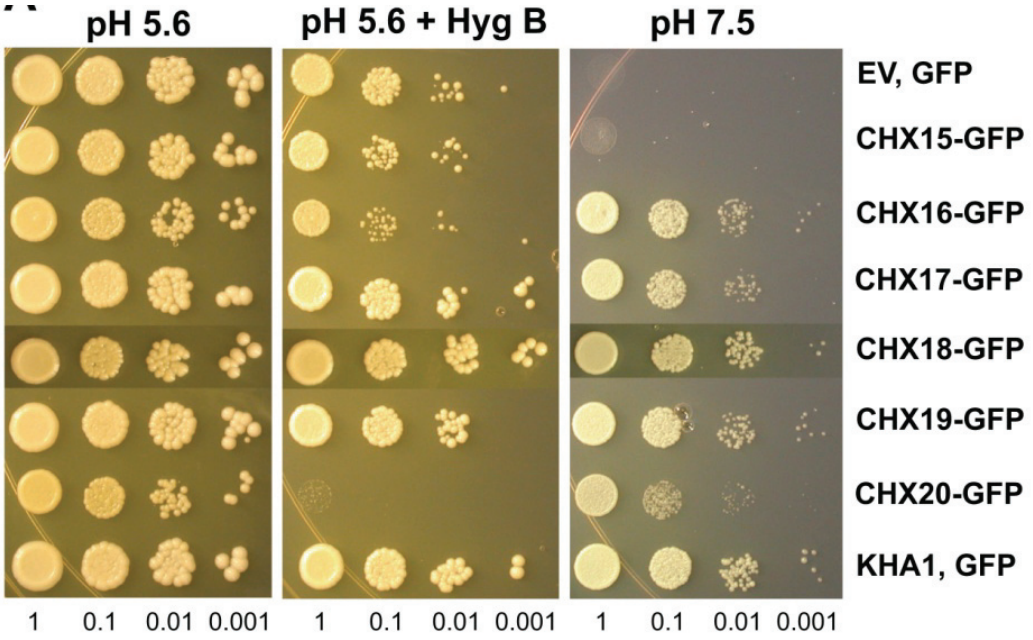

Fig. A-II-6. CHX16-CHX20 tagged with GFP at the C-terminus retained activity.

Yeast strains KTA40-2 and AXT3 harboring *GFP* alone or *CHX* fused with *GFP* at the C-terminus were grown in YNB-Glucose overnight, diluted 5-fold with YNB without carbon source, and incubated for 12-14 h. Cells were washed, normalized to A_{600} of 0.2, and serially diluted 10-fold. Five µl was dropped on to YNB-MES-Glucose medium at pH 7.5 or pH 5.6 with or without 150 µg/ml HygB. After 3 d, KTA40-2 strain expressing *CHX16-20* fused at the C-terminus with *GFP* grew at pH 7.5. CHX16 and CHX20 tagged at the C-terminus with GFP caused Hyg B sensitivity similar to CHX alone (see Fig. II-2B)

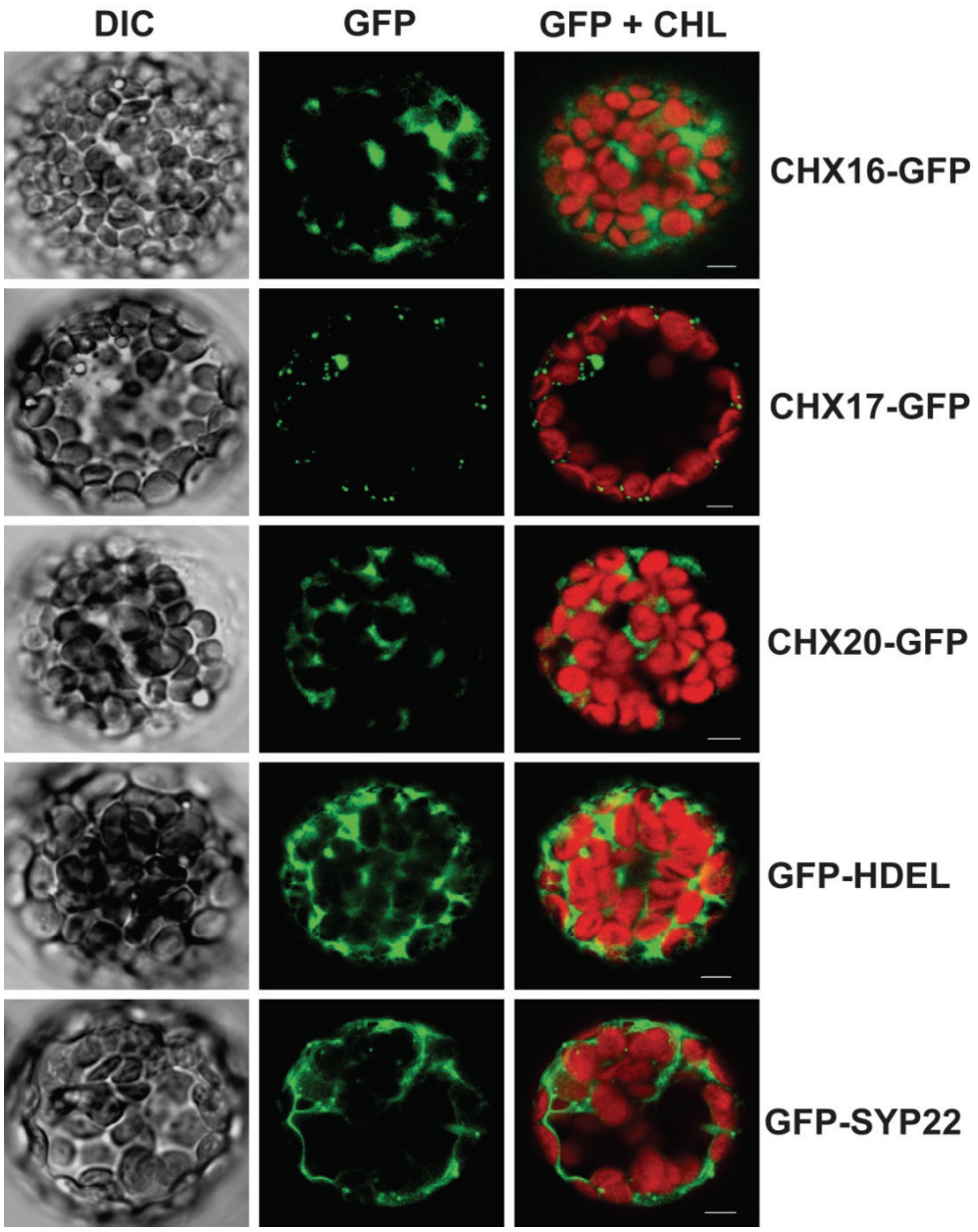

Fig. A-II-7. Localization of CHX17-GFP to punctate and of CHX16-GFP and CHX20-GFP to reticulate structures in protoplasts.

Arabidopsis leaf protoplasts were transfected with *CHX16-GFP*, *CHX17-GFP*, *CHX20-GFP*, ER lumen marker *GFP-HDEL* or vacuole membrane marker *GFP-SYP22* as described in section A.1.g. After 18 to 24 h, fluorescent signals were observed using LSM 510 confocal microscope. DIC images of cell is at left and chlorophyll fluorescence (CHL) is shown at right with GFP. Bars = 5 µm.

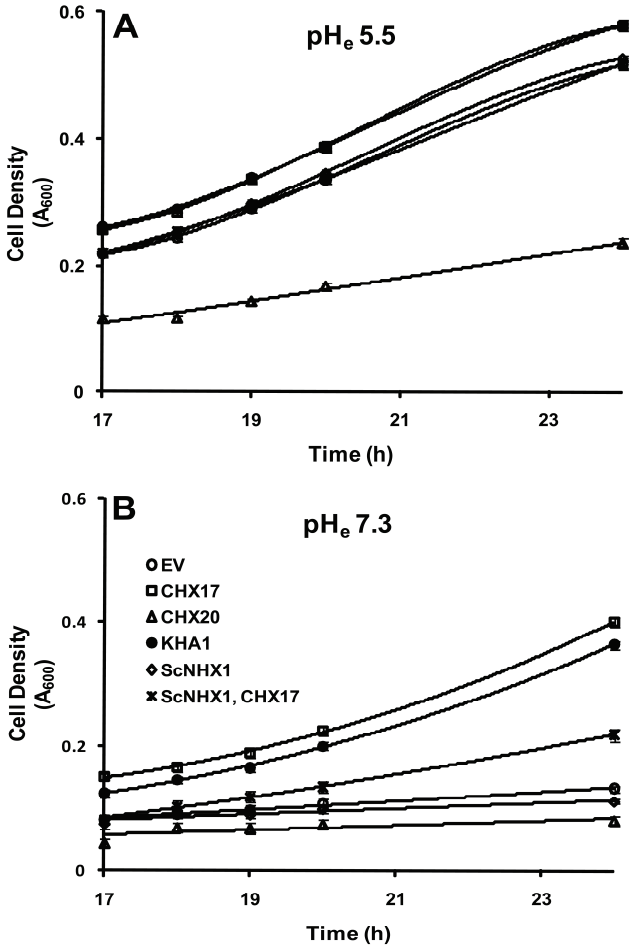

Fig. A-II-8. Effect of pH 5.5 or 7.3 on growth of yeast strains expressing different cation transporters.

Yeast strain KTA40-2, AXT3, and LMB01 transformed with pYES52-derived expression vector (EV), or vector harboring *CHX17 or CHX20* were grown in YNB-Glucose overnight. Cells were then diluted 10-fold with YNB containing 0.44% galactose and incubated for 14-16 h. Cells were washed and normalized to A_{600} of 0.2 or 0.8 with K^+-free YNB medium without carbon source. Then 20 µl of yeast suspension were added to 180 µl of K^+-free YNB with 2% galactose and 8 mM K^+ at pH 5.5 (A) or 7.3 (B) in 96-well ELISA plates. Plates were incubated at 30^{o}C and A_{600} was measured for 24 h. The effect of pH on extracellular CPY was determined on a separate microplate at early log phase (17-20 h) . Bars represent SEM (n=14).

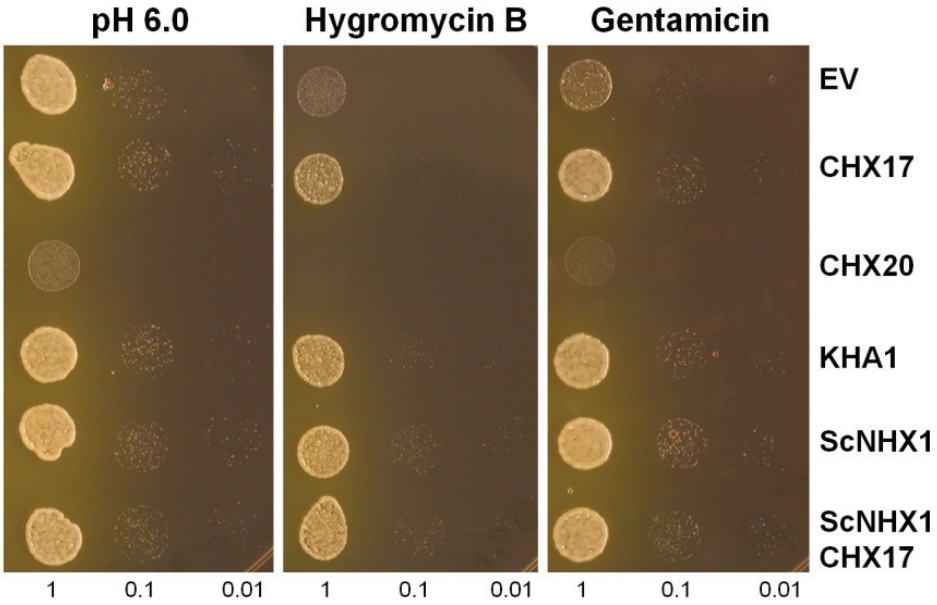

Fig A-II-9. Gentamicin resistance is enhanced in yeast expressing CHX17, KHA1 or ScNHX1.

Yeast strain KTA40-2, AXT3 (*KHA1*), and LMB01 (*NHX1*) harboring pYES52 derived expression vector (EV), or vector harboring *CHX17* or *CHX20* were prepared as Fig. A-II-8. Cells were normalized to an A_{600} of 0.15 and diluted 10 fold serially. Five µl of each serial dilution was dropped on to YNB-MES supplemented with galactose at pH 6.0, and incubated for 2 d. Images represent one of the two independent transformants. Mutants expressing *ScNHX1*, *CHX17* or *KHA1* enhanced resistance to hygromycin B (50 µg/ml) and gentamicin (200 µg/ml; MP biomedicals, 1405-41-0). KTA40-2 strain expressing *CHX20* was hyper-sensitive to gentamicin and hygromycin B similar to Fig II-2B.

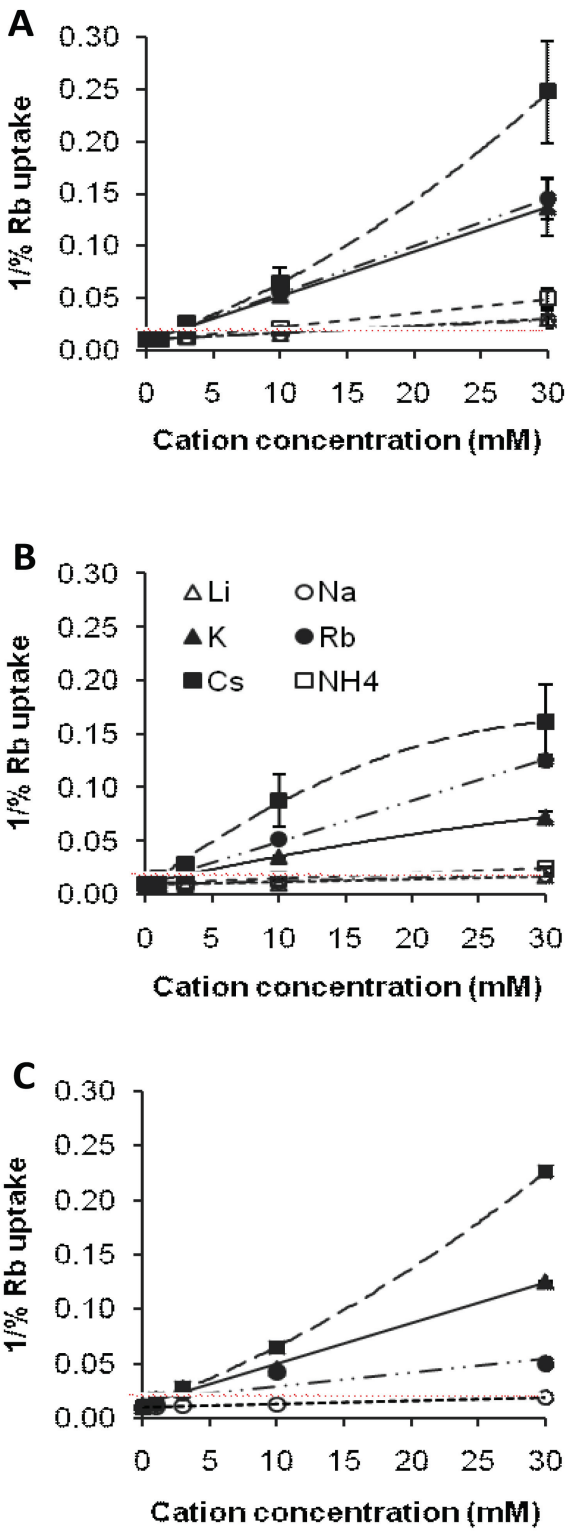

Fig. A-II-10. Reciprocal plot of cation-inhibited Rb^+ uptake data.

E. coli LB2003 **c**ells harboring pPAB404 alone (EV) or vector with *CHX17*, *CHX20* or *KAT1* were induced by IPTG during K^+ starvation. Reaction mixture consisted of 0.6 mM RbCl (0.5 µCi/ml ^{86}Rb) and ~$2.5x10^8$ cells/ml in SGM-MES-MOPS at pH 6.2 plus one cation-Cl (Li Δ, Na ○, K▲, Rb ●, Cs ■, NH_4 □) at near 0,1, 3, 10, or 30 mM. ^{86}Rb uptake was measured at 30 min by subtracting EV background uptake. 1/ Rb uptake % was plot against cation concentration. IC_{50} (half maximal inhibitory concentration) was estimated from concentration where 1/50% Rb uptake = 0.02 and was correlated with an initial slope.

A) CHX17-dependent Rb uptake was inhibited by $Cs^+ > Rb^+ = K^+ >> Na^+$. Uptake without added cation (100%) was 0.8 nmol Rb^+ per 10^8 cells.

B) CHX20-dependent Rb uptake was inhibited by $Cs^+ > Rb^+ > K^+ >> Na^+$. Uptake without added cation (100%) was 2.4 nmol Rb^+ per 10^8 cells.

C) KAT1-dependent Rb uptake was inhibited by $Cs^+ > K^+ > Rb^+ >> Na^+$. Uptake without added cation (100%) was 0.85 nmol Rb^+ per 10^8 cells.

Data are from 2 independent experiments except a single experiment in C. Bars represent SEM (n=2). Red line indicates IC_{50}, 1/50% Rb uptake = 0.02.

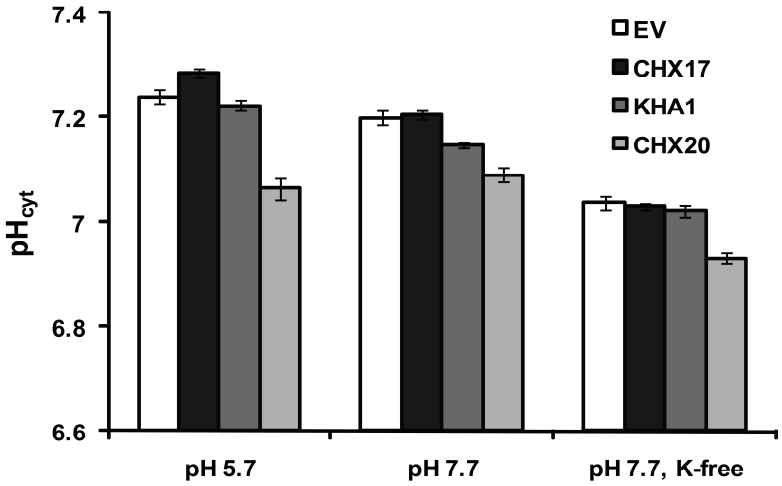

Fig. A-II-11. Effect of CHX on cytosolic pH of a single *kha1* mutant.

Yeast strain Kha1 (a single *kha1* deletion) and FY833 (*Wild-type*) harboring *pHluorin* pYES52 derived - *empty vector* (EV), *CHX17 or CHX20* were grown in YNB-Glucose overnight. Cells were diluted 10-fold with YNB containing 0.44% galactose to induce expression and incubated for 14-16 h. Cells were washed and normalized with SDAP-Galactose medium pH 6.0 to A600 of 20. Aliquot of 20 µl was added to a 96-well plate loaded with 180 µl of SDAP-MES-TRIS media at pH 5.7 or 7.7 supplemented with 2.5 mM KCl. In some experiements, addition of KCl was omitted (K-free). After incubation for 20 min, relative fluorescent intensity was collected. Three independent lines of the same strain were used and six replicates were assayed per line at each condition (N=3, n=18). Bars = SEM. Only *kha1* mutant harboring CHX20 demonstrated significant acidification of cytosolic pH about 0.2 unit. Basal cytosolic pH of *kha1* mutant, mutant expressing *CHX17* and *Wild-type* was about pH 7.2 which was lowered to about pH 7.0 when no KCl was added.

B. SUPPLEMENTAL INFORMATION FOR CHAPTER III

B.1. Tables of materials and results

Table A-III-1. No segregation distortion of progeny genotypes observed during double-mutant plant generation.

i) Parent: *chx17-4* $^{+/-}$ *chx18-1* $^{+/-}$ x self

Genotypes		Observed	Expected
chx17	***chx18***	(n = 50)	(n = 50)
+/+	+/+	2	3.125
+/+	+/-	9	6.25
+/-	+/+	1	6.25
+/-	+/-	13	12.5
+/+	-/-	2	3.125
+/-	-/-	7	6.25
-/-	+/+	1	3.125
-/-	+/-	12	6.25
-/-	-/-	3	3.125
		χ^2= 13.28	

ii) Parent: *chx17-4* $^{+/-}$ *chx19-2* $^{+/-}$ x self

Genotypes		Observed	Expected
chx17	***chx19***	(n = 30)	(n = 30)
+/+	+/+	2	1.875
+/+	+/-	6	3.75
+/-	+/+	2	3.75
+/-	+/-	6	7.5
+/+	-/-	0	1.875
+/-	-/-	6	3.75
-/-	+/+	1	1.875
-/-	+/-	3	3.75
-/-	-/-	4	1.875
		χ^2= 8.67	

+/+, +/- and -/- represent gene-specific- homozygous *Wt*, heterozygous mutant and homozygous mutant, respectively.

There is significantly different from the Mendelian's segregation ratio when $\chi^2 > 15.51$ at *p value* = 0.05 (df = 8).

Table A-III-2. Lack of homozygous triple or quadruple mutant genotypes observed during triple-mutant and quadruple-mutant plant generation.

i) Parent: *chx17-4* $^{-/-}$ chx18-2 $^{+/-}$ *chx19-2* $^{+/-}$ x self

Genotypes		Expected	Observed
chx18	***chx19***	(n = 144)	(n = 144)
-/-	+/+	9	13
-/-	+/-	18	17
+/-	-/-	18	11
+/+	-/-	9	9
-/-	-/-	9	0
+/-	+/-		
+/-	+/+		
+/+	+/-	81*	94*
+/+	+/+		
		χ^2= 15.64	

+/+, +/- and -/- represent gene-specific- homozygous *Wt*, heterozygous mutant and homozygous mutant, respectively.

There is significantly different from the Mendelian's segregation ratio when $\chi^2 > 11.07$ at *p value* = 0.05 (df = 5).

* represents number of plants from the combination of 4 genotypes

Table A-III-2.

ii) Parent: *chx16-10a* $^{+/-}$ *chx17-4* $^{+/-}$ *chx18-1* $^{+/-}$ *chx19-2* $^{+/-}$ x self

Genotypes				Expected	Observed
chx16	***chx17***	***chx18***	***chx19***	(n = 157)	(n = 157)
+/0	+/0	+/0	+/0	49.7	60
+/0	+/0	+/0	-/-	16.6	10
+/0	+/0	-/-	+/0	16.6	21
+/0	+/0	-/-	-/-	5.5	5
+/0	-/-	+/0	+/0	16.6	18
+/0	-/-	+/0	-/-	5.5	7
+/0	**-/-**	**-/-**	+/0	5.5	1
+/0	**-/-**	**-/-**	-/-	1.8	0
-/-	+/0	+/0	+/0	16.6	15
-/-	+/0	+/0	-/-	5.5	4
-/-	+/0	-/-	+/0	5.5	6
-/-	+/0	-/-	-/-	1.8	2
-/-	-/-	+/0	+/0	5.5	6
-/-	-/-	+/0	-/-	1.8	2
-/-	**-/-**	**-/-**	+/0	1.8	0
-/-	**-/-**	**-/-**	-/-	0.6	0
				χ^2= 15.18 < 25.00	

+/0 represents gene-specific homozygous *Wt* or heterozygous mutant.

-/- represents gene-specific homozygous mutant.

There is significantly different from the Mendelian's segregation ratio when χ^2 > 25.00 at *p value* = 0.05 (df = 15).

Table A-III-3. Single T-DNA insertion mutants.

Mutant	SALK#	T-DNA insertion (after base #)	Observed transcript (rel. to insert)	Protein (if translated)
chx16-10a	SALK_138136	767 (exon 2)	downstream	Truncated TM2
chx17-1	SALK_060180	2259 (exon 3)	no data	Complete TM to R_{546}
chx17-4	SALK_033417	996 (exon 2)	upstream	Between TM4 and 5
chx18-1	SALK_001563	2070 (exon 3)	upstream	Complete TM to G_{636}
chx19-2	SALK_100047	619 (exon 2)	upstream	Truncated TM5

Table A-III-4. Multiple T-DNA insertion mutants and corresponding *Wt* siblings.

Mutant/Wt sibling	Parent	Note
chx16 chx18	*chx16-10a* x *chx18-1*	Double mutant
chx17 chx18	*chx17-4* x *chx18-1*	Double mutant
chx17 chx19	*chx17-4* x *chx19-2*	Double mutant
chx17 chx18 chx19	*chx17 chx18* x *chx17 chx19*	Triple mutant
chx16 chx17 chx18 chx19	*chx16 chx18* x *chx17 chx19*	Quadruple mutant
Wt_4 (CHX17 CHX18)	*chx17-4* x *chx18-1*	Wt sibling
Wt_3 (CHX17 CHX19)	*chx17-4* x *chx19-2*	Wt sibling

Table A-III-5. List of transgenic plants. (Continue on next page)

Background	Plasmids	Description	Vector reference
Wt (col-0)	pBWGF-empty	*35Sp*::EGFP	This work
Wt (col-0)	pBWGY-empty	*35Sp*::EYFP	This work
Wt (col-0)	pBFWG-CHX15	*35Sp*::CHX15-EGFP	This work
Wt (col-0)	pBFWG-CHX16	*35Sp*::CHX16-EGFP	This work
Wt (col-0)	pBFWG-CHX17	*35Sp*::CHX17-EGFP	This work
Wt (col-0)	pBYWG-CHX17	*35Sp*::CHX17-EYFP	This work
Wt (col-0)	pBFWG-X17TM(1-425)	*35Sp*::CHX17TM(1-425)-EGFP	This work
Wt (col-0)	pBFWG-X17TM(1-472)	*35Sp*::CHX17TM(1-472)-EGFP	This work
Wt (col-0)	pBWG2D-X17Ct(473-820)	*35Sp*::CHX17Ct(473-820) and *rolDp*::EGFP-KDEL	This work
Wt (col-0)	pBFWG-CHX18	*35Sp*::CHX18-EGFP	This work
Wt (col-0)	pBFWG-CHX19	*35Sp*::CHX19-EGFP	This work
Wt (col-0)	pFGC-ER-RB	*35Sp*::mCherry-HDEL	Luminal ER marker, Nelson et al, 2007.

Background	Plasmids	Description	Vector reference
Wt (col-0)	pFGC-G-RB	*35Sp*::GmMan1-mCherry	*cis*-Golgi marker, Nelson et al, 2007.
Wt (col-0)	pFGC-PM-RB	*35Sp*::PIP2A-mCherry	PM marker, Nelson et al, 2007.
Wt_4 (CHX17 CHX18)	pBWGF-empty	*35Sp*::EGFP	This work
chx17-1	pBWG2D-CHX17	*35Sp*::CHX17 and *rolDp*::EGFP-KDEL	This work
chx17-4	pBWGF-empty	*35Sp*::EGFP	This work
chx17-4	pBWGY-empty	*35Sp*::EYFP	This work
chx17-4	pBFWG-CHX17	*35Sp*::CHX17-EGFP	This work
chx17-4	pBYUR-CHX17p	*CHX17p*::EYFP	This work
chx17-4	pMDC-p17gX17	*CHX17p*::gCHX17-GFP6	This work
chx17 chx18	pBWGF-empty	*35Sp*::EGFP	This work
chx16 chx17 chx18 chx19	pBWGF-empty	*35Sp*::EGFP	This work

Table A-III-6. List of transgenic plants harboring *RFP* and *GFP* fusion constructs

Transgenic plant	GFP construct	RFP construct
Wt-CHX16G-PIP2R	*35Sp*::CHX16-EGFP	*35Sp*::PIP2A-mCherry
Wt-CHX16G-MAN1R	*35Sp*::CHX16-EGFP	*35Sp*::GmMan1-mCherry
Wt-CHX17G-PIP2R	*35Sp*::CHX17-EGFP	*35Sp*::PIP2A-mCherry
Wt-CHX17G-MAN1R	*35Sp*::CHX17-EGFP	*35Sp*::GmMan1-mCherry
Wt-CHX18G-PIP2R	*35Sp*::CHX18-EGFP	*35Sp*::PIP2A-mCherry
Wt-CHX18G-MAN1R	*35Sp*::CHX18-EGFP	*35Sp*::GmMan1-mCherry
Wt-CHX19G-PIP2R	*35Sp*::CHX19-EGFP	*35Sp*::PIP2A-mCherry
Wt-CHX19G-MAN1R	*35Sp*::CHX19-EGFP	*35Sp*::GmMan1-mCherry
Wt-CHX17G-ERR	*35Sp*::CHX17-EGFP	*35Sp*::mCherry-HDEL
Wt-X17TM(1-425)G-ERR	*35Sp*::CHX17-TM(1-425)-EGFP	*35Sp*::mCherry-HDEL
Wt-X17TM(1-472)G-ERR	*35Sp*::CHX17-TM(1-472)-EGFP	*35Sp*::mCherry-HDEL
Wt-X17TM(1-472)G-MAN1R	*35Sp*::CHX17-TM(1-472)-EGFP	*35Sp*::GmMan1-mCherry

Table A-III-7. Plasmids used for transient expression in protoplasts. All plasmids contain Amp^R for selection in *E coli*. (Continue on next page)

Parental Plasmid	Gene cassette	Gene info.	Description	Reference
p2FGW7	GFP	Free GFP	*35S*::EGFP	Chanroj et al, MS1
p2GWF7	CHX15-GFP	CHX15	*35S*::CHX15-EGFP	This work
p2GWF7	CHX17-GFP	CHX17	*35S*::CHX17-EGFP	Chanroj et al, MS1
p2GWR7	CHX17-GFP	CHX17	*35S*::CHX17-mRFP	Chanroj et al, MS1
pUC18	GFP-AtSYP21	Syntaxin 21	*35Sp*, PVC marker	Uemura et al, 2004
pUC18	GFP-AtSYP22	Syntaxin 22	*35Sp*, Vacuolar marker	Uemura et al, 2004
pUC18	GFP-AtSYP41	Syntaxin 41	*35Sp*, TGN marker	Uemura et al, 2004
pHTS13	GFP-Ara7	RabF2b	*35Sp*, Endosomes marker	Ueda et al, 2001
pBSK	ST-GFP	Rat sialyltransferase	*35Sp*, Golgi marker	Lee et al, 2002
pBSK	spGFP-HDEL	ER retention signal	*35Sp*, ER marker	Hawes et al, 2001
No data	sGFP-CPK9	calmodulin-domain protein kinase 9	*35S,* PM marker	Lee,J-Y, from Harper,JF

Parental Plasmid	Gene cassette	Gene info.	Description	Reference
No data	sGFP-APX	36 aa residues of cottonseed per-oxisomal APX	*35Sp*, peroxisome marker (APX, ascorbate peroxidase)	Lee,J-Y, from Harper,JF
pUC18	mRFP-AtSYP21	Syntaxin 21	*35Sp*, PVC marker	Uemura et al, 2004
pHTS13	mRFP-Ara7	RabF2b	*35Sp*, Endosomes marker	Ueda et al, 2001

Table A-III-8. Primers used to clone CHX cDNA or gDNA into Gateway vectors. Bases in lower case denote recombination sequence, *AttB*. Forward (F) primers show the first codon. Reverse (R) primers do not contain a stop codon. For cDNA cloning of CHX15-CHX19 and empty vector, see section A, Table A-II-2 and Table A-II-3.

Name	Primer Sequence	Template	Amplifying
CHX17a 001F	ggggacaagtttgtacaaaaaagcaggctccATG GGAACAAACGGTACAACA	pSM_X17	CHX17-TM(1-425) or CHX17-TM(1-472)
CHX17a 425R	ggggaccactttgtacaagaaagctgggtgTGC CAGAACTAGAGGAGTCGT	pSM_X17	CHX17-TM(1-425)
CHX17a 472R	ggggaccactttgtacaagaaagctgggtgTAT GAGGTTGACGATCGTGG	pSM_X17	CHX17-TM(1-472)
CHX17a 426F	ggggacaagtttgtacaaaaaagcaggctccatgG TGTACAAACCGGGTAAATCC	pSM_X17	CHX17-Ct(426-820)
CHX17a 473F	ggggacaagtttgtacaaaaaagcaggctccatgG AAGCATCCCGAGGCATA	pSM_X17	CHX17-Ct(473-820)
3KBX17 gen-F	ggggacaagtttgtacaaaaaagcaggctccAAT ATTTGTTTCGGATTCCAATTAGA	F9D16 (BAC clone)	CHX17 3Kb promoter and genomic region
CHX17a 820R	ggggaccactttgtacaagaaagctgggtgAGG ACTCTCAGAATCCTCAACC	pSM_X17 or F9D16 (BAC clone)	CHX17-Ct(426-820), CHX17-Ct(473-820), or CHX17 3Kb promoter and genomic region

Table A-III-9. Primers used in homologous recombination of *CHX17p::YFP* construct. Bases in lower case denote sequences homologous to RB (right border), URA (uracil synthesis enzyme), PX17 (CHX17 .3Kb promoter region), and YFP. ORI refers to yeast 2μ origin of replication.

Name	Sequence	Template	Amplifying
RBURAORI-F	aacgacaatctgatccaagctcaagctaagct GGGTAATAACTGATATAATT AAATTGAA	pYES-DEST52	URA3 and 2μ Origin of replication
PX17ORIURA-R	tgattttctaattggaatccgaaacaaatattCA TTGCGAATACCGCTT	pYES-DEST52	URA3 and 2μ Origin of replication
ORIPX17-F	gtttgtggaagcggtattcgcaatgAATAT TTGTTTCGGATTCCAATTAG	F9D16 (BAC clone)	CHX17 3Kb promoter region
YFPPX17-R	acagctcctcgcccttgctcaccatGCTTT AAAGATCTGACAAATGATGA	F9D16 (BAC clone)	CHX17 3Kb promoter region

Table A-III-10. Gene-specific primers used for genotyping.

Name	Sequence	Amplifying region
chx16-10a-LP	TCTTGTCATTCTTCAGATTTGCCTTG	CHX16 exon 1
chx16-10a-RP	AGTATTCTCGCCAAAACTCCGAAAG	CHX16 exon 2
chx17-1TLP	GCTAACGCCTCACGATCATCATT	CHX17 exon 3
chx17-1TRP	CAGTCCTAGTTTCCCTTTACTGCAAAGTT	CHX17 exon 2
chx17-4TLP	AACTTTGCAGTAAAGGGAAACTAGGACTG	CHX17 exon 2
chx17-4TRP	TGAGTTTTATATTGTGGTTTTAGGGTGGA	CHX17 intron 1/exon 2
chx18-1TLP	ATTCTACCAACCAAAAACAAATTGCTC	CHX18 exon 3
chx18-1TRP	AGAAGAGCGAAGAAAGAAGGAGAATACAA	CHX18 exon 3
chx19-2LP	TGTAAGTAGATCTCCACTAGGATGGCAAG	CHX19 5' upstream
chx19-2RP	CACGGTTAGAGTGACACAAACATAGAGTT	CHX19 exon 2
LB-b13	ATTTTGCCGATTTCGGAAC	T-DNA left border

Table A-III-11. Primers for reverse transcription PCR.

Name	Sequence	Detection
RTn16-F	TCTTGTCATTCTTCAGATTTGCCTTG	CHX16 5’ transcript
RTn16-R	AGTATTCTCGCCAAAACTCCGAAAG	CHX16 5’ transcript
RTc16-F	AGAACCGCAAACATAGACGCAAGAT	CHX16 3’ transcript
RTc16-R	CTGGACACTCTATCTTCATAACCGGT	CHX16 3’ transcript
RTn17-F	GCTTTTCTCCTCCGTCCTCT	CHX17 5’ transcript
RTn17-R	TGCGGAGAGCAAAAGAAGTT	CHX17 5’ transcript
RTc17-F	ATCAGTCTACGCGATGCATCTTATG	CHX17 3’ transcript
RTc17-R	CGTGTCGCTTCTTACGTTTATCCCT	CHX17 3’ transcript
RTn18-F	CTCCGATGAAAGCAACCTCT	CHX18 5’ transcript
RTn18-R	CACACCCATGAAGACGAGAA	CHX18 5’ transcript
RTc18-F	CTTGATGGTTCGTTAGAGACTACAC	CHX18 3’ transcript
RTc18-R	TATCCGTAGAAGTCAATACCTCCGT	CHX18 3’ transcript
RTn19-F	TTCGCGCTTCCTCTTATCAT	CHX19 5’ transcript
RTn19-R	AAGGCAACACCCATGAAGAC	CHX19 5’ transcript
RTc19-F	GATCGAATCATCAAGAGGAACAGGC	CHX19 3’ transcript
RTc19-R	CTGAAATATCTCTGGAAGACTGATCG	CHX19 3’ transcript
Actin11-S	ATGGCAGATGGTGAAGACATTCAG	Actin transcript
Actin11-AS	GAAGCACTTCCTGTGGACTATTGA	Actin transcript

Table A-III-12. Primers used for verifying genes or sequences.

Name	Sequence	Detection
pCHX17-F	TCCGTGAGTATCGCCTCTTT	CHX17 promoter region
G-YFP-F	GACGTAAACGGCCACAAGTT	GFP or YFP
G-YFP-R	GAACTCCAGCAGGACCATGT	GFP or YFP
BAR-F	GACAAGCACGGTCAACTTCC	Basta resistance gene
BAR-R	ACCCACGTCATGCCAGTT	Basta resistance gene
35S-F	ATACAGTCTCAGAAGACCAAAGGGC	35S promoter region
35S-R	GTGCGTCATCCCTTACGTCAGT	35S promoter region

Table AIII-13. Entry vectors of PCR-amplified CHX or genomic sequences. For entry vectors of CHX15-CHX19 and empty vector, see section A, Table A-II-3.

Name	Description
pEX17TM(1-425)	Truncated CHX17, base position 1 to 1275, no stop codon
pEX17TM(1-472)	Truncated CHX17, base position 1 to 1416, no stop codon
pEX17Ct(426-820)	Truncated CHX17, base position 1276 to 2460, no stop codon
pEX17Ct(473-820)	Truncated CHX17, base position 1417 to 2460, no stop codon
pEp17gX17	CHX17 3Kb upstream and genomic region, no stop codon

Table A-III-14. Destination vectors used to generate expression vectors. For pYES-DR196 and pGWF-DR196, see section A, Table A-II-4.

Name	Description	References
p2GWF7	Transient expression, 35S promoter, EGFP at 3' end	Karimi et al, 2002
p2FGW7	Transient expressionr, 35S promoter, EGFP at 5' end	Karimi et al, 2002
p2GWR7	Transient expression, 35S promoter, mRFP at 3' end	Karimi et al, 2002
pB7FWG2	Binary vector, 35S promoter, EGFP at 3' end	Karimi et al, 2002
pB7WGF2	Binary vector, 35S promoter, EGFP at 5' end	Karimi et al, 2002
pB7YWG2	Binary vector, 35S promoter, EYFP at 3' end	Karimi et al, 2002
pB7WGY2	Binary vector, 35S promoter, EYFP at 5' end	Karimi et al, 2002
pB7WG2D	Binary vector, 35S promoter, *rolDp*::EGFP-KDEL for visualization	Karimi et al, 2002
pMDC107	Binary vector, GFP6 at 3' end	Curtis et al, 2003

Table A-III-15. List of expression vectors. See section A, Table A-II-5 for additional vectors that are previously described.

Name	Description
p2GWF-CHX15	*35Sp*::CHX15-EGFP, transient expression vector
pBFWG- X17TM(1-425)	*35Sp*::CHX17TM(1-425)-EGFP, binary vector
pBFWG- X17TM(1-472)	*35Sp*::CHX17TM(1-472)-EGFP, binary vector
pBWGF-empty	*35Sp*::EGFP, binary vector
pBYWG-CHX17	*35Sp*::CHX17-EYFP, binary vector
pBWGY-empty	*35Sp*::EYFP, binary vector
pBWG2D- CHX17	*35Sp*::CHX17, *rolDp*::EGFP-KDEL, binary vector
pBWG2D- X17Ct(473-820)	*35Sp*::CHX17Ct(473-820), *rolDp*::EGFP-KDEL, binary vector
pBYUR-CHX17p	*CHX17p*::EYFP, binary vector
pMDCp17gX17	*CHX17p*::gCHX17-GFP6, binary vector
pDR-X17TM(1-425)	*PMA1p*::CHX17TM(1-425), yeast expression vector
pDR-X17TM(1-472)	*PMA1p*::CHX17TM(1-472), yeast expression vector
pDR-X17Ct(426-820)	*PMA1p*::CHX17Ct(426-820), yeast expression vector
pDR-X17Ct(473-820)	*PMA1p*::CHX17Ct(473-820), yeast expression vector
pGWFDR-X17TM(1-425)	*PMA1p*::CHX17TM(1-425)-EGFP, yeast expression vector
pGWFDR-X17TM(1-472)	*PMA1p*::CHX17TM(1-472)-EGFP, yeast expression vector

Table A-III-16. Modified Gibeaut's medium. This medium, GB (Gibeaut et al., 1997), was mainly used for hydroponic and limited K^+ experiment in which K_2SO_4 was omitted. For all experiment 1 mM MES was regularly added otherwise indicated. The final pH was adjusted with Tris base or NH_4OH (to enhance growth, see Cramer's solution at www.ag.unr.edu/cramer/hydroponic.html) to pH 6.0 before autoclave.

Macronutrients	**FW**	**[Stock]**	**stock (g/L)**	**mL per 1 L**
$Ca(NO_3)_2$ x $4H_2O$	236.15	1M	236.2	1.50
HNO_3	63.01	1M	62.9	1.25
$Mg(SO_4)$ x $7H_2O$	246.48	1M	246.5	0.75
H_3PO_4 (85%)	98.00	1M	67.6 (ml)	0.50
NaFe-EDTA	367.10	0.072 M	26.4	1.00
K_2SO_4	174.26	0.5 M	87.1	1.75
Micronutrient	-	-	-	1.00
NH_4Cl	53.49	50mM	2.674	-
$MnSO_4$ x H_2O	169.01	10mM	1.690	-
$CuSO_4$	159.61	1.5mM	0.240	-
$ZnSO_4$ x $7H_2O$	287.54	2mM	0.575	-
H_3BO_3	61.83	50mM	3.092	-
$(NH_4)_6Mo_7O_{24}$	1235.9	0.075mM	0.093	-

B.2. Figures

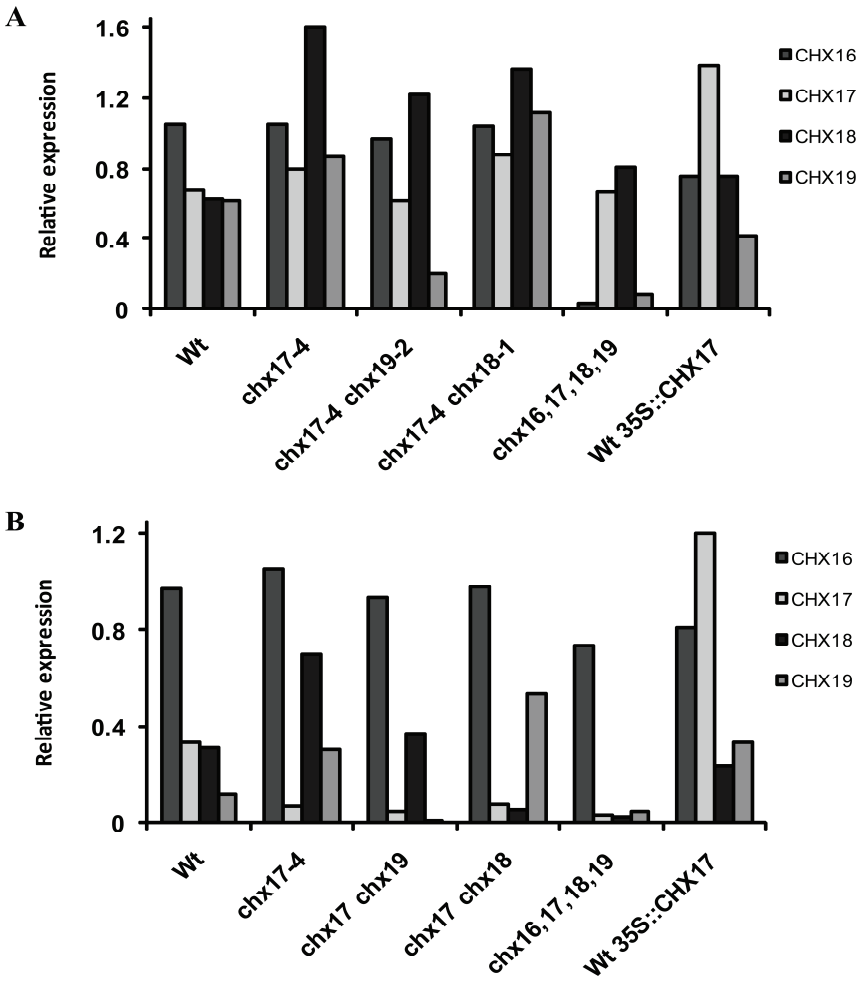

Fig. A-III-1. Semi-quantitation of *CHX16*, *17*, *18* and *19* transcripts.

RNA extracted from 10-d old seedlings was reverse transcribed and PCR amplified. Amplified products were run on 1% agarose gel electrophoresis with TAE buffer. Fluorescent intensity from each band was measured by ImageJ software (NIH) and normalized to fluorescent intensity from *Actin11*. After normalization, relative expression of *CHX* transcripts from 5' region (A) or 3' region (B) of the T-DNA insertion was shown. Position of primers used to amplify *CHX* transcripts and corresponding bands used for analyzing were shown in Figure III-1A and III-1B, respectively.

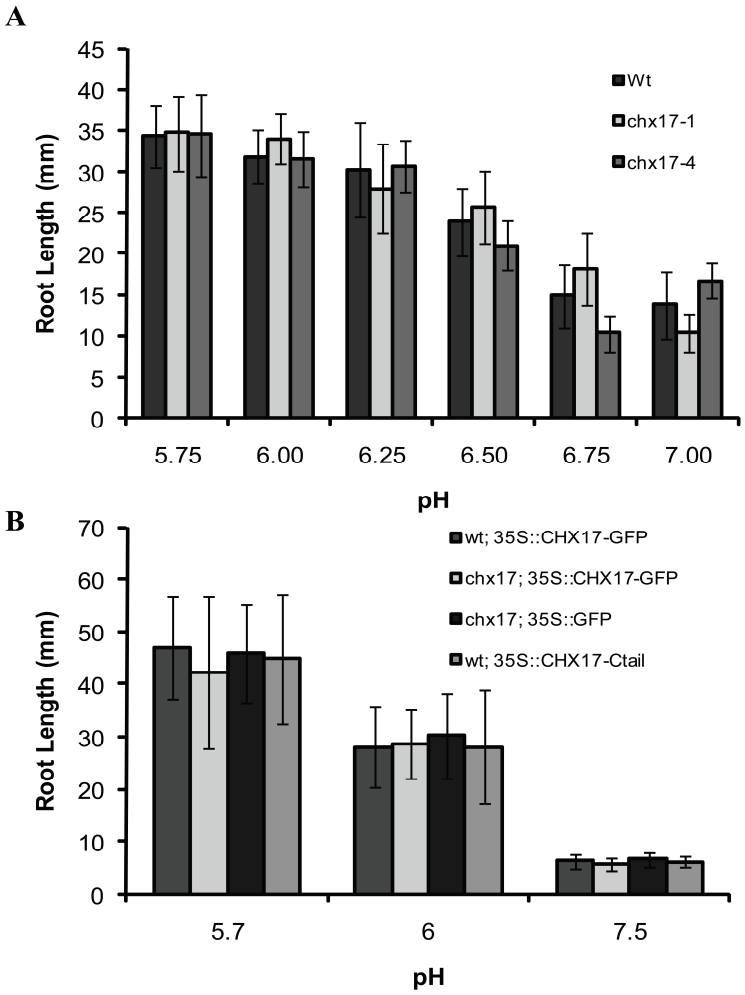

Fig. A-III-2. Single *chx17* mutant showed similar root growth as *Wt* plants.

A) Effect of pH on *Wt* and *chx17* mutant root lengths. *Wt col-1, chx17-1* and *chx17-4* seedlings were germinated and grown in 0.5X MS solid medium buffered with 5 mM MES-MOPS-BTP and Tris at indicated pHs for 11 d. n = 20-30 seedlings, bars = SD

B) Root growth in transgenic plants over-expressing full-length *CHX17* or its C-tail. All transgenic plants were germinated in 0.5X MS solid medium for 7 d and then transferred to 0.5X MS solid medium buffered with 10mM MES-Tris or HEPES-Tris at pH 5.7, 6 or 7.5. After 7 d, root length was measured. Transgenic plants were as follows: i) *wt* plant harboring *35Sp*::*CHX17-GFP*; ii) *chx17-4* mutant harboring *35Sp*::*CHX17-GFP*; iii) *chx17-4* mutant harboring *35Sp*::*GFP*; iv) *wt* plant harboring *35Sp*::*CHX17-Ct(473-820)* and *rolDp*::*GFP-KDEL*. n = 20-50 seedlings, bars = SD.

Fig. A-III-3. Localizing GFP-tagged marker proteins in protoplasts.

Arabidopsis leaf protoplasts were transfected with either *CHX15-GFP* , *CHX17-GFP* or various markers, including *GFP-HDEL* (ER), free *GFP* (cytosol and nucleus), *GFP-SYP22* (vacuolar membrane), *CPK9-GFP* (PM), *GFP-SYP21* (PVC), *GFP-SYP41* (TGN), *ST-GFP* (Golgi) and *GFP-APX* (peroxisome) as described in section A.1.g. After 18 to 24 h of incubation, fluorescence was observed using LSM 510 confocal microscope. Chlorophyll fluorescence from chloroplasts is shown in red. Results are representative of at least 10 protoplasts from at least two independent experiments, Bars = 5 μm.

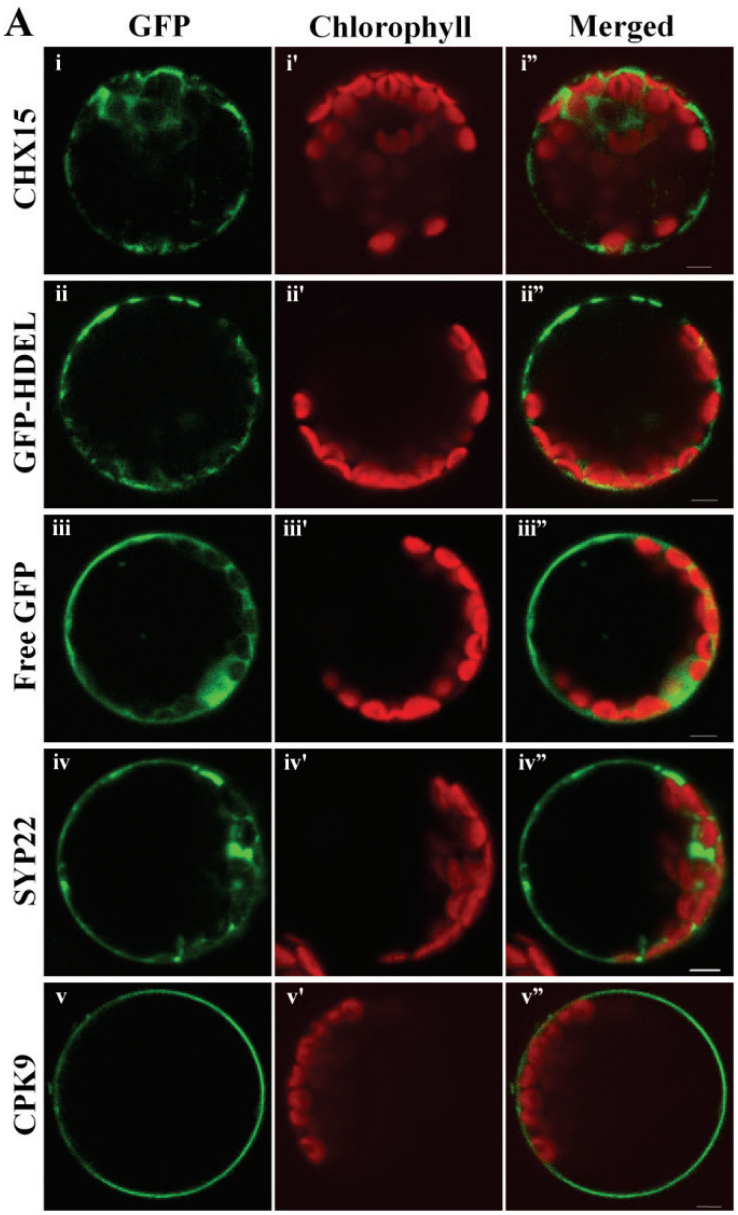

Fig. A-III-3. A) CHX15-GFP appeared to localize to ER. The pattern of CHX15-GFP (i) was similar to GFP-HDEL fluorescence (ii) as the signal from cell periphery was not smooth and reticular structures were observed in both cases (i, ii).

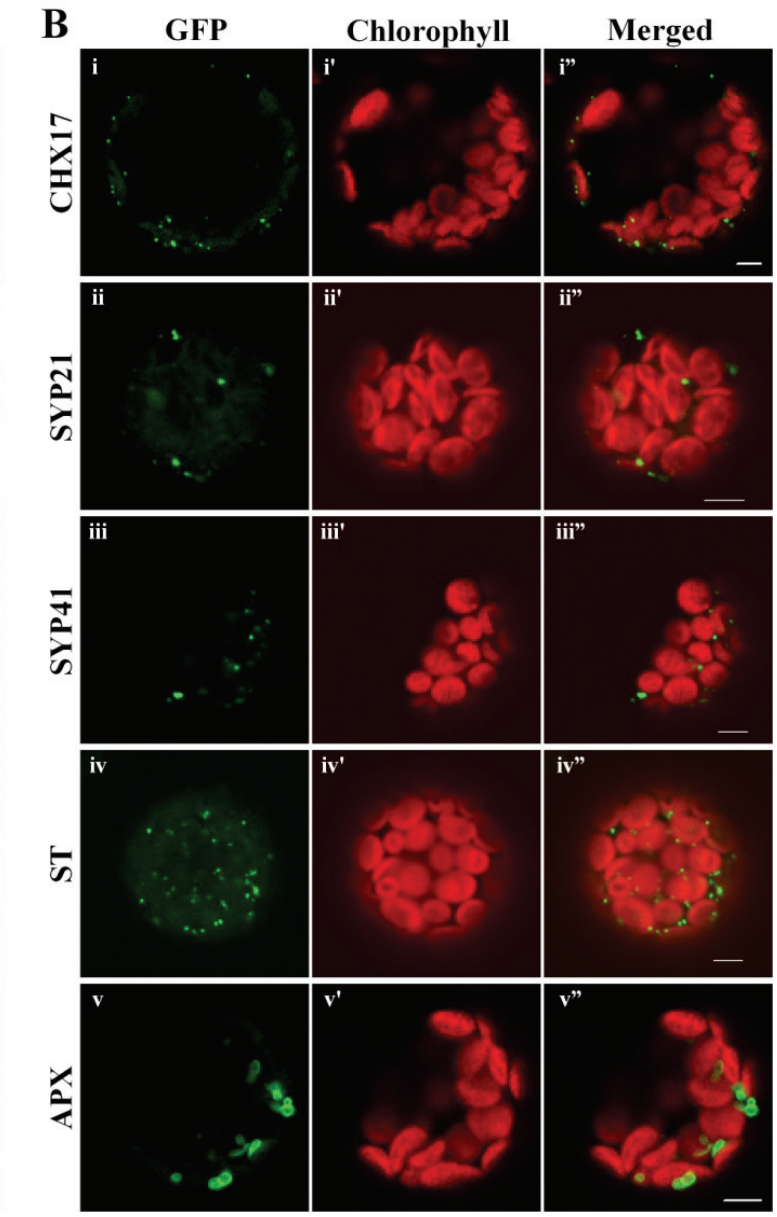

Fig. A-III-3. B) CHX17-GFP localized to puncta resembling PVC, TGN or Golgi. CHX17-GFP (i) showed localizing patterns similar to GFP-SYP21 (ii), GFP-SYP41 (iii) and ST-GFP (iv). GFP-APX fluorescence showed ring-like structures representing peroxisomes.

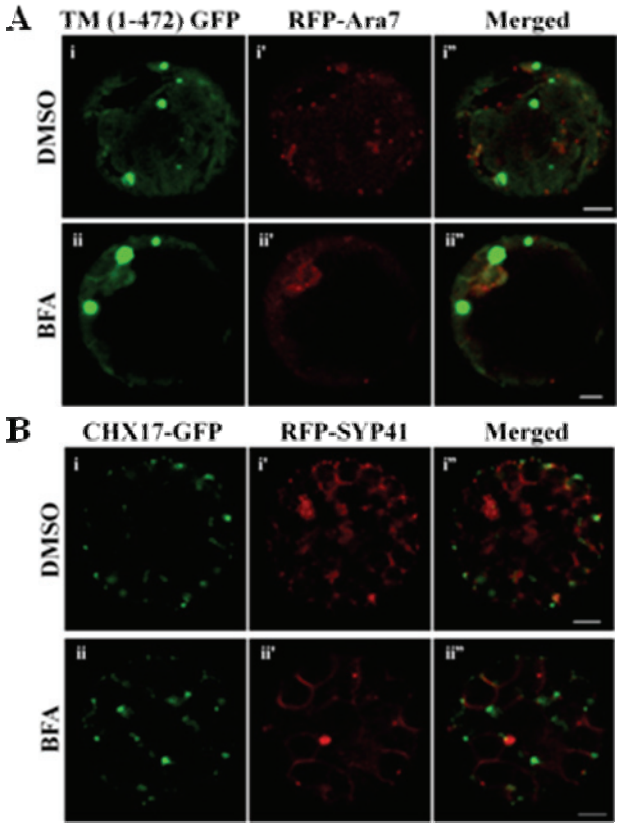

Fig. A-III-4. Punctate and aggregate localization of CHX17-TM(1-472) were unaffected by BFA.

A-B) BFA treatment altered the localization of SYP41 in protoplasts. *Arabidopsis* leaf protoplasts were co-transfected with A) *CHX17-TM(1-472)-GFP* and *RFP-Ara7*, a late endosome marker, or B) a full-length *CHX17(1-820)-GFP* and *RFP-SYP41*, a TGN marker as described in section A.1.g. After 18 h incubation, cells were treated with 0.35% DMSO or 35 μM BFA for 60-90 min, and observed by confocal microscopy (GFP: Ex 488 nm/Em 505-545 nm, RFP: Ex 543 nm/Em 560-615 nm). Results were representative of at least 8 protoplasts from two independent experiments. Scale bars = 5 μm.

A) Truncated CHX17-TM(1-472)-GFP localized to reticulum and a large puncta (i) that did not co-localized with RFP-Ara7-labeled structures (i"). BFA treatment did not significantly altered localization of TM(1-472)-GFP (ii) nor RFP-Ara7 (ii').

B) Full-length CHX17-GFP labeled puncta (i) did not co-localized with RFP-SYP41-labeled spots (i"). BFA treatment resulted in larger red puncta (BFA compartment) of RFP-SYP41 (ii') while no structural change was observed in CHX17-GFP (ii). No co-localization between CHX17-GFP and RFP-SYP41 were observed after BFA treatment (ii").

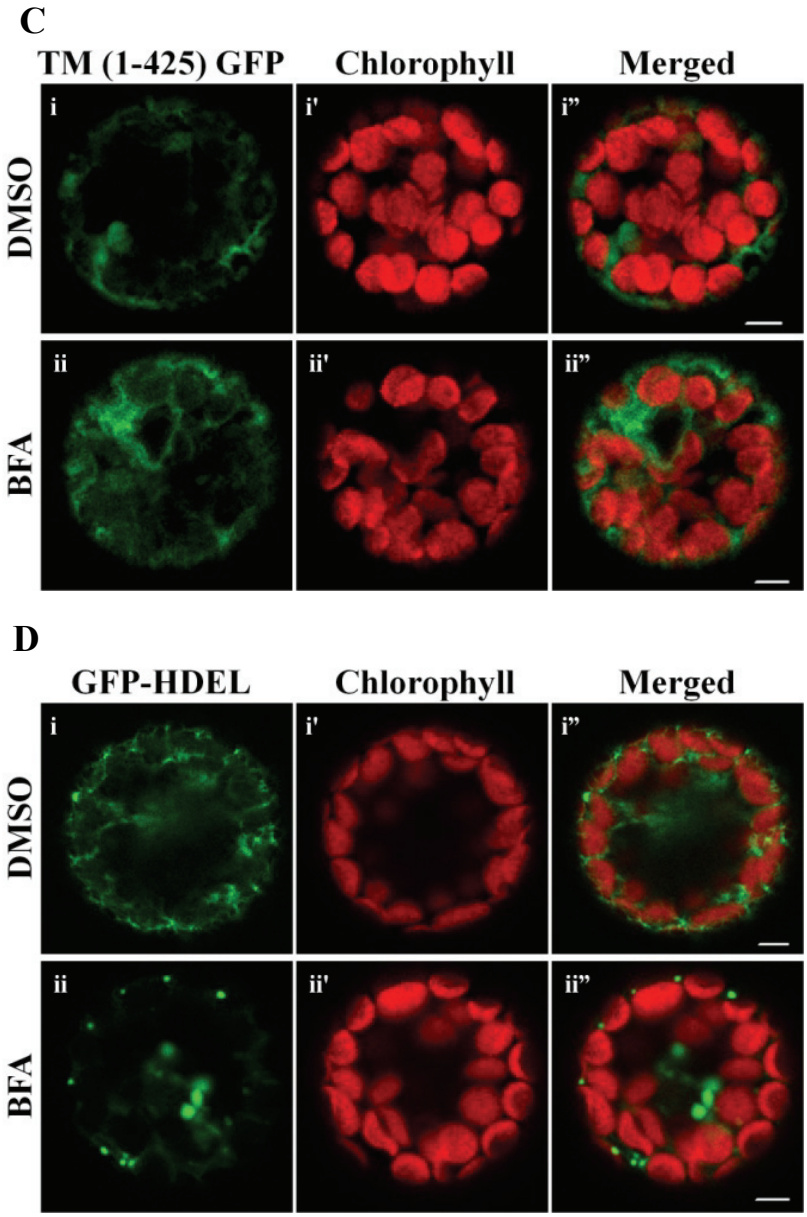

Fig. A-III-4. C-D) BFA treatment altered the localization of GFP-HDEL in protoplasts. Arabidopsis leaf protoplasts were transfected with *CHX17-TM(1-425)-GFP* (C) or *GFP-HDEL* (D, luminal ER marker) as described in section A.1.g. After 18 h of incubation, cells were treated with 0.35% DMSO (i) or 35 µM BFA(ii) for 60-90 min, and observed by confocal microscopy (GFP: Ex 488 nm/Em 505-545 nm, chlorophyll: Ex 543 nm/Em > 650 nm). Results were representative of at least 10 protoplasts from two independent experiments. Scale bars = 5 µm.

C) CHX17-TM(1-425)-GFP was localized to reticulate structures (i) resembling ER (D) with or without BFA treatment (ii).

D) GFP-tagged HDEL labeled reticulate structures, ER, (i) in control cells; however, luminal-ER GFP-HDEL appeared in puncta after BFA treatment (ii).

Fig. A-III-4. E-F) BFA treatment caused differential alteration of FM4-64, CHX17-TM(1-472)-GFP and GFP-HDEL localization. *Wt* transgenic seedlings harboring either *35Sp*::*CHX17-TM(1-472)-GFP* or *rolDp*::*GFP-KDEL* were incubated with 10 μM FM4-64 for 10 min, then washed and treated with 0.5% DMSO or 50 μM BFA in 0.1X MS medium for 90-120 min. Images were taken from root epidermis from maturation zone (E) or the division zone (F). Fluorescent signals were observed under confocal microscope (GFP: Ex 488 nm/Em 505-545 nm, FM4-64: Ex 488nm/Em > 650 nm). Results are representative of two independent experiments with two independent transgenic lines per experiment. Scale bars = 5 μm.

E) CHX17-TM(1-472)-GFP localized to reticulate structures and large puncta (i) that did not co-localized with FM4-64 labeled compartment (i', TGN and PM). After BFA treatment, FM4-64 labeled compartment showed accumulated signals (ii') that did not co-localized with the large puncta shown by TM (1-472)-GFP (ii').

F) BFA altered localization of GFP-HDEL from tubular structures or reticulum to puncta. Before BFA treatment, GFP-HDEL (luminal ER marker) localized to reticulate and tubular structures (i) where cell boundaries were labeled by FM4-64 at the PM (i'). After BFA treatment, GFP-HDEL changed localizing pattern towards puncta (ii) whereas FM4-64 accumulated in BFA compartments (ii'). No co-localization was observed between GFP-HDEL localizing puncta and FM4-64 labeled BFA compartments (ii") before or after BFA treatment.

E

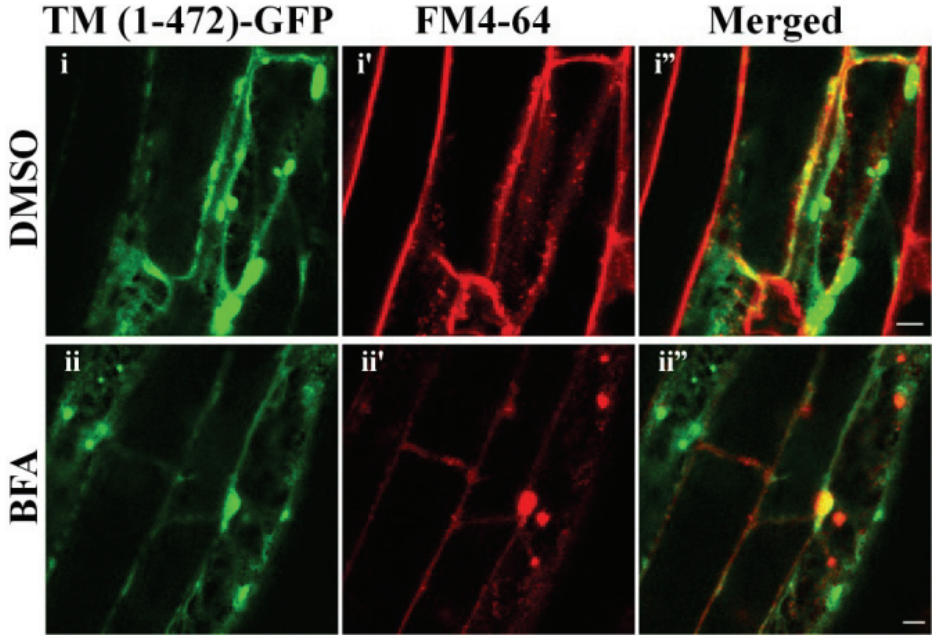
TM (1-472)-GFP
FM4-64
Merged
DMSO
BFA
i
i'
i"
ii
ii'
ii"

F

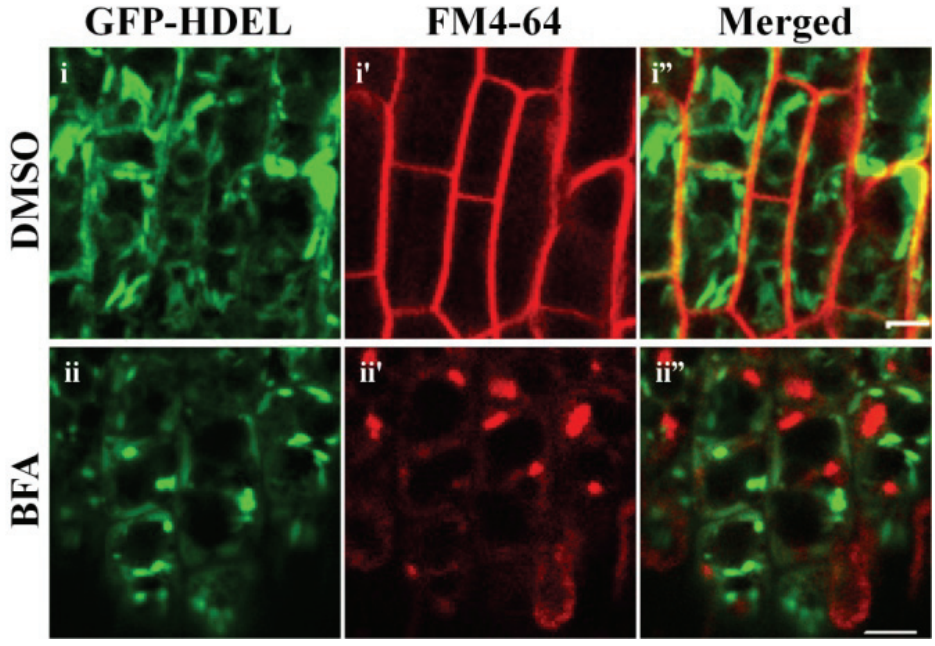
GFP-HDEL
FM4-64
Merged
DMSO
BFA
i
i'
i"
ii
ii'
ii"

G

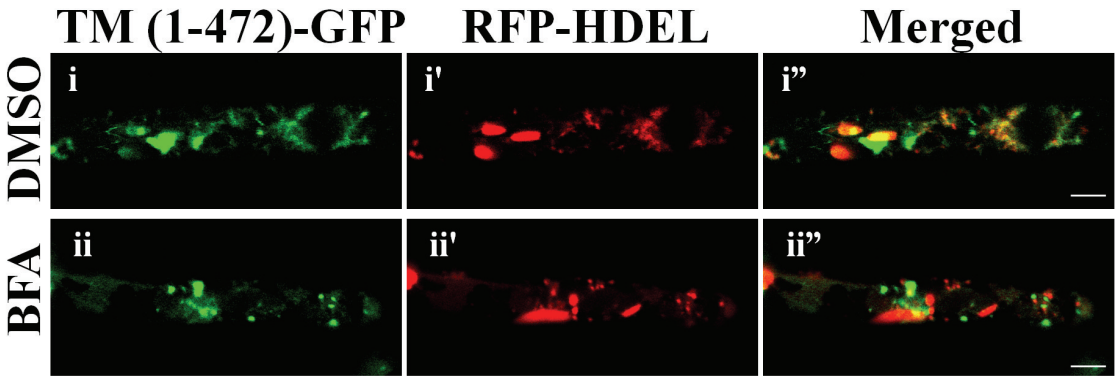

Fig. A-III-4. G) BFA-induced RFP-HDEL puncta did not co-localize with TM(1-472)-GFP-labeled puncta.

Transgenic plants harboring *35Sp*::*CHX17-TM(1-472)-GFP* were crossed with *35S*::*RFP-HDEL* (ER marker). F1 seeds were germinated in 0.5X MS solid medium for 10 d. Seedlings were treated with 0.5% DMSO or 50 μM BFA in 0.1X MS medium for 90-120 min. TM(1-472)-GFP localized to both reticulate and punctate structures after DMSO (i) or BFA treatment (ii). RFP-HDEL showed reticulate pattern (i') but became more punctate after BFA treatment (ii'). No co-localization was observed between TM(1-472)-GFP and RFP-HDEL (luminal ER) in the puncta after BFA treatment (ii'). Fluorescent signals were observed using confocal microscope (GFP: Ex 488 nm/Em 505-545 nm, FM4-64: Ex 488nm/Em > 650 nm). Images were taken from root-hair cells. Result is representative of at least two observations from three independent transgenic lines. Scale bars = 5 μm.

H

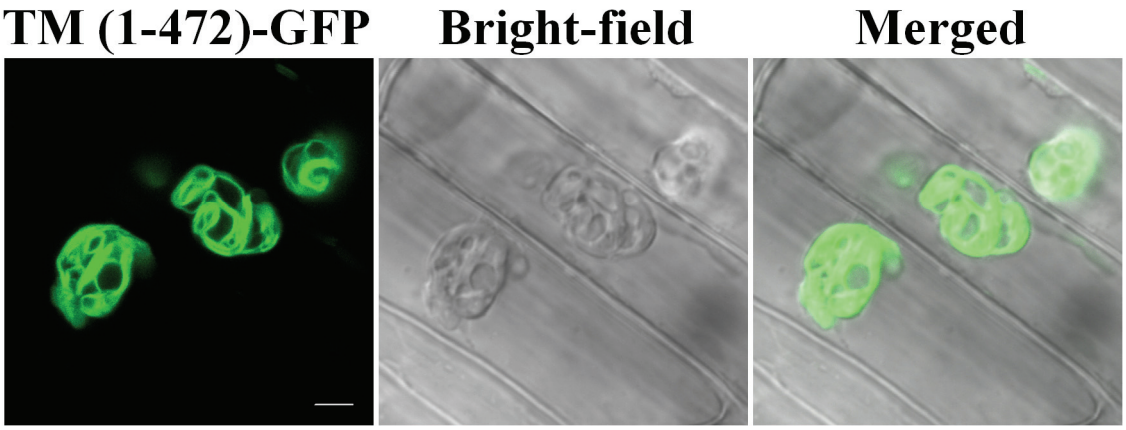

Fig. A-III-4. H) CHX17-TM(1-472)-GFP localized to aggregate membrane. Trangenic plants harboring *35Sp*::*CHX17-TM(1-472)-GFP* were germinated in 0.5X MS solid medium for 14 d. Seedlings were submerged in 0.1X MS medium for 3 h before observation. CHX17-TM(1-472)-GFP signals (left) were overlapped with the unknown multi-layered membrane compartments visualized by bright-field images (middle and right). (GFP: Ex 488 nm/Em 505-545 nm). Images were taken from mature root epidermis near the root-shoot junction. Result is representative of at least three observations from two independent transgenic lines. Scale bars = 5 μm.

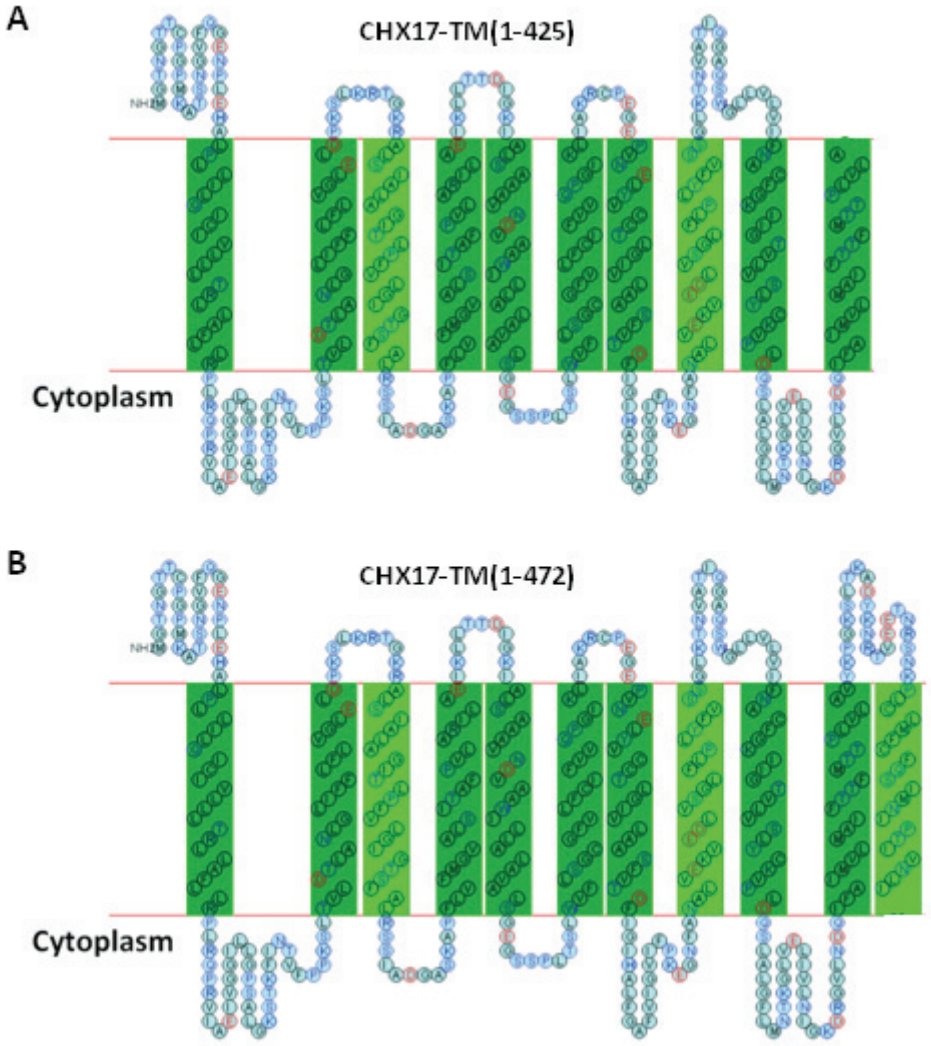

Fig. A-III-5. Predicted topology of truncated CHX17 proteins.

A) CHX17-TM(1-425) was predicted to have 10 TM domains lacking the last TM domains and the C tail. B) CHX17-TM(1-472) was predicted to have all 11 TM domains without C tail. Figures were obtained and modified from SOSUI version 1.11 (http://bp.nuap.nagoya-u.ac.jp/sosui/). The full-length CHX17 protein is shown in Chapter I, Fig. I-2.

C. OTHER SUPPLEMENTAL INFORMATION

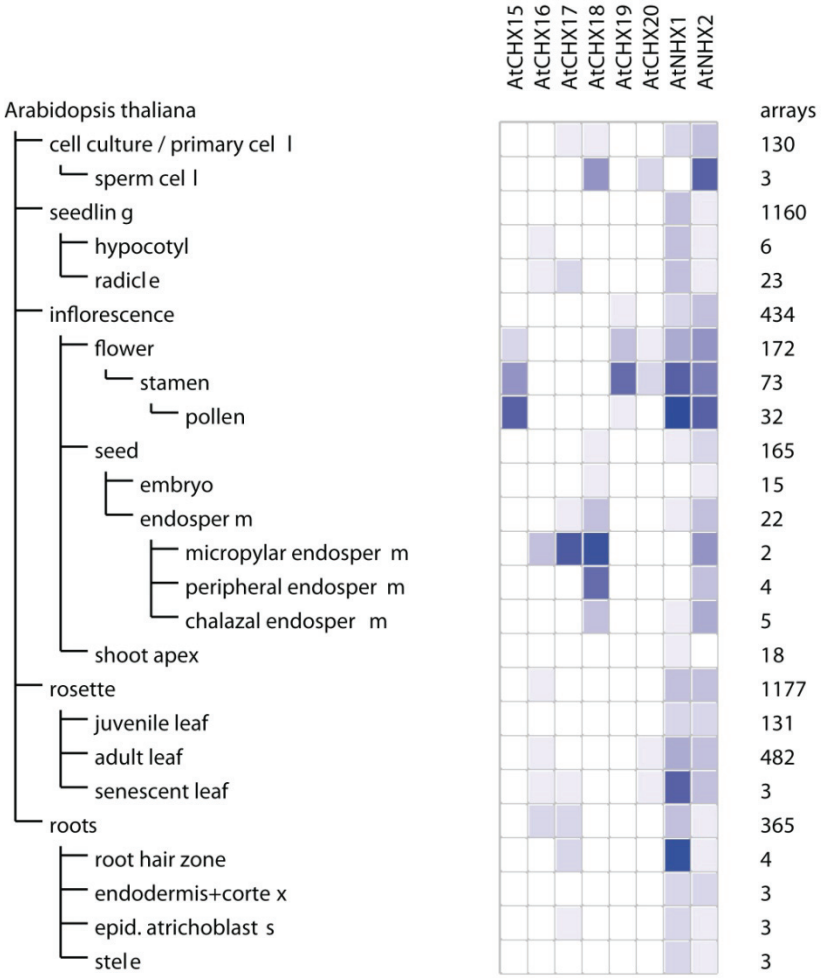

Fig. A-V-1. Tissue expression profiles of AtCHX15-20 and AtNHX1-2 from public microarrays.

Heat map represents normalized signal values relative to the expression potential (EP) of each gene according to the average of the top 1% signal values of the probe set across all arrays. The darkest color corresponds to the EP value referred to as the highest level of expression. Number refers to arrays that are included in each analysis. The figure was created by the web-based software tool, Genevestigator V3 (Hruz et al, 2008).

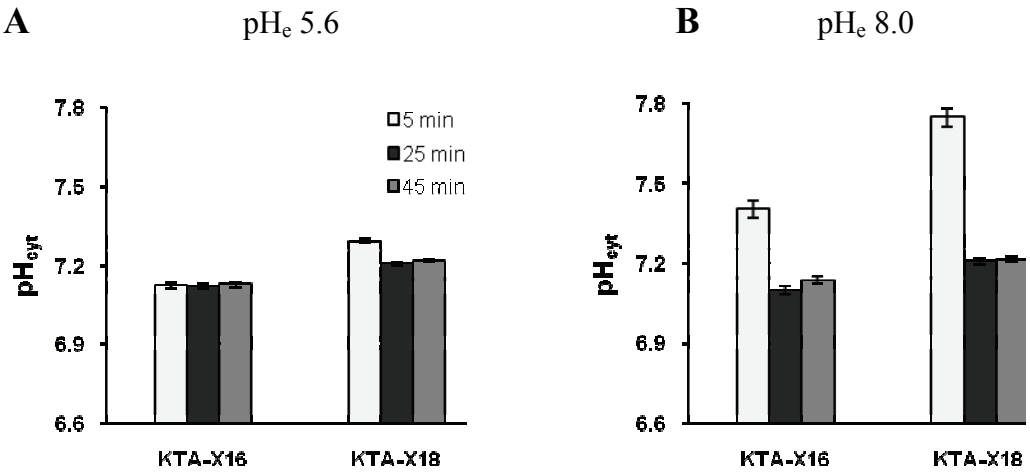

Fig. A-V-2. Cytosolic pH in yeast expressing CHX16 or CHX18.

CHX16 lowered pH_{cyt} by about 0.15 unit at both pH 5.6 (A) and pH 8.0 (B). Yeast strain KTA40-2 harboring *pHluorin* in empty vector (EV), vector with *CHX16* or *CHX18* were grown and normalized to OD_{600} of 20. For pH_{cyt} measurement, 20 µl of yeast suspension was added to 180 µl of K^+-free YNB with 2% glucose in 96-well plates. Test media were adjusted to pH 5.6 or 8.0 and 2.5 mM K^+ using arginine and KCl. After 5, 25 or 45 min incubation, fluorescent ratio at F_{510}/F_{460} nm were collected and converted to pH_{cyt} using a calibration curve shown in Fig. II-4A. Data are from three independent lines of the same strain and six replicates were assayed per line at each condition (N=3, n=18). Bars = SD.

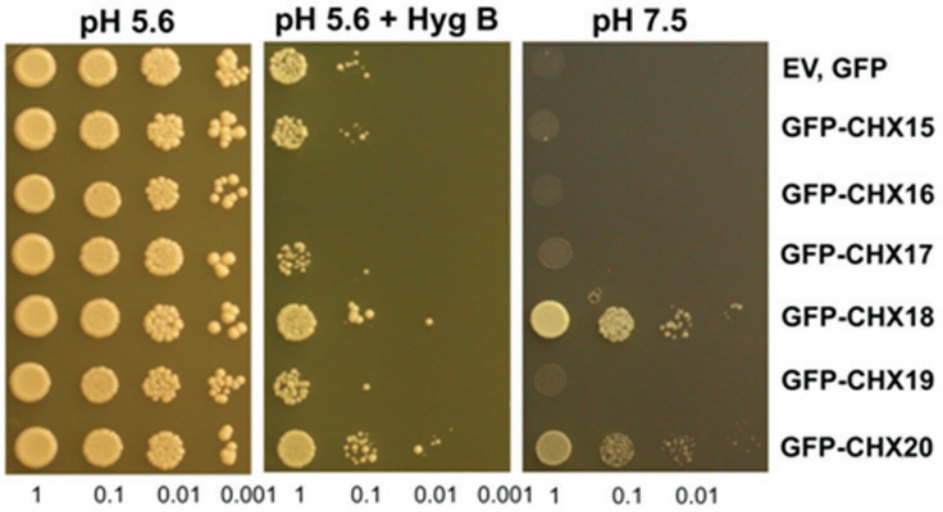

Fig. A-V-3. GFP-tagged at the N-terminal abolished or altered CHX function in yeast.

Yeast strains KTA 40-2 (*ena1-4Δ, nha1Δ, nhx1Δ, kha1Δ*) and AXT 3 (*ena1-4Δ, nha1Δ, nhx1Δ*) harboring *GFP* alone or *CHX* fused with *GFP* at the 5' end were grown in YNB-Glucose overnight, diluted 5 fold with YNB without carbon source, and incubated for an additional 12-14 h. Cells were washed, normalized with water to A_{600} of 0.2, and serially diluted 10 fold. Five ul was dropped on to YNB-MES-Glucose medium at pH 7.5, pH 5.6 or pH 5.6 with 150 µg/ml hygromycin B. CHX16, CHX17 and CHX19 can no longer rescue growth neither at pH 7.5 nor at150 µg/ml Hygromycin B, pH 5.6. In contrast, fusion at the N-terminus of CHX20 caused functional alteration by being resistant to hygromycin B.

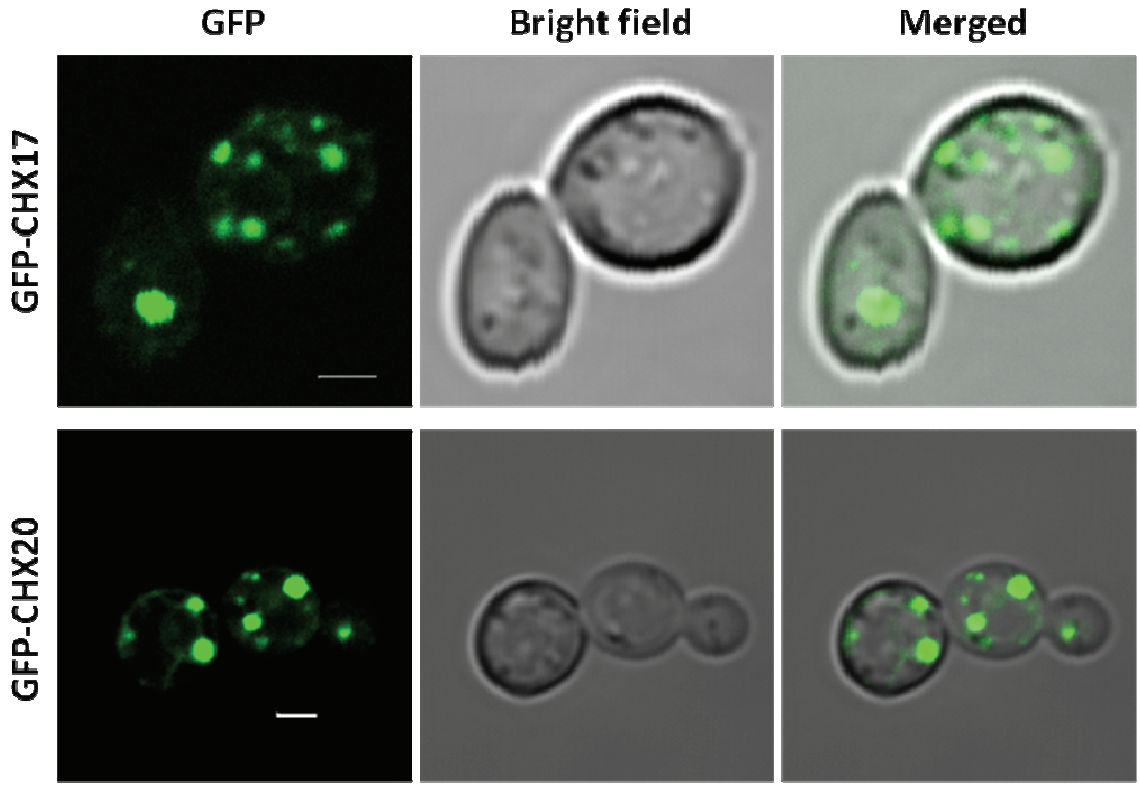

Fig. A-V-4. Localization of GFP-CHX17 and GFP-CHX20 at the puncta in yeast.

Yeast strains KTA 40-2 (*ena1-4Δ, nha1Δ, nhx1Δ, kha1Δ*) harboring *CHX* fused with *GFP* at the 5' end were grown in YNB overnight and YPAD for additional 4 h. Cells were washed with 2% sucrose and suspended in 0.05% agarose. Both GFP-CHX17 and GFP-CHX20 were localized to similar punctate structures in yeast. Scale bars = 2 μm.

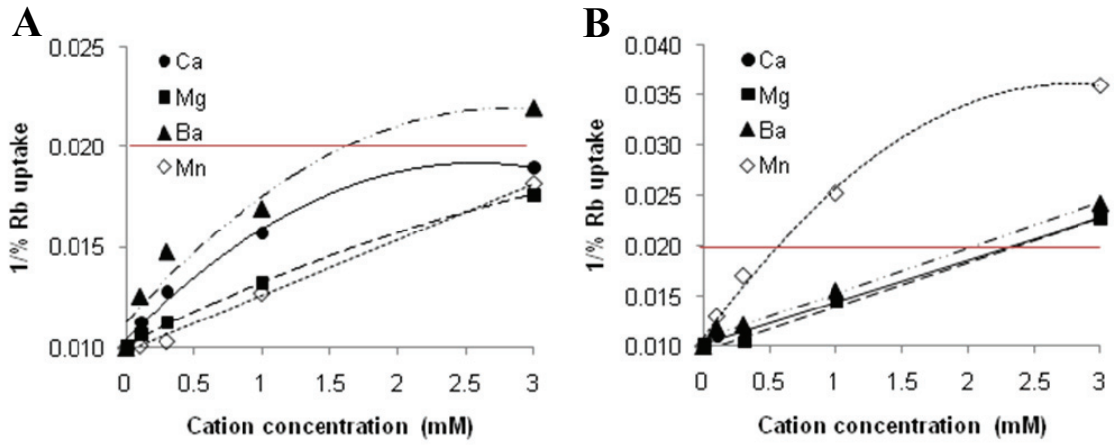

Fig. A-V-5. Reciprocal plot of divalent cation-inhibited Rb^+ uptake data.

E. coli LB2003 **c**ells harboring pPAB404 alone (EV) or vector with *CHX17*, *CHX20* or *KAT1* were induced by IPTG during K^+ starvation. Reaction mixture consisted of 0.6 mM RbCl (0.5 µCi/ml ^{86}Rb) and ~$2.5x10^8$ cells/ml in SGM-MES-MOPS at pH 6.2 plus one divalent cation-Cl_2 (Ca ●, Mg ■, Ba ▲, Mn ◊) at near 0, 0.1, 0.3, 1.0, or 3.0 mM. ^{86}Rb uptake was measured at 30 min by subtracting EV background uptake. 1/Rb uptake % was plot as a function of cation concentration. IC_{50} (half maximal inhibitory concentration) was estimated from concentration where 1/50% Rb uptake = 0.02 and was correlated with an initial slope.

A) CHX17-dependent Rb uptake was inhibited by $Ba^{2+} > Ca^{2+} >> Mg^{2+} = Mn^{2+}$. Uptake without added cation (100%) was 0.5 nmol Rb^+ per 10^8 cells.

B) CHX20-dependent Rb uptake was inhibited by $Mn^{2+} >> Ba^{2+} = Ca^{2+} = Mg^{2+}$. Uptake without added cation (100%) was 2.2 nmol Rb^+ per 10^8 cells.

Data are from 2 independent experiments. Bars represent SEM (n=2). Red line indicates IC_{50}, 1/50% Rb uptake = 0.02.

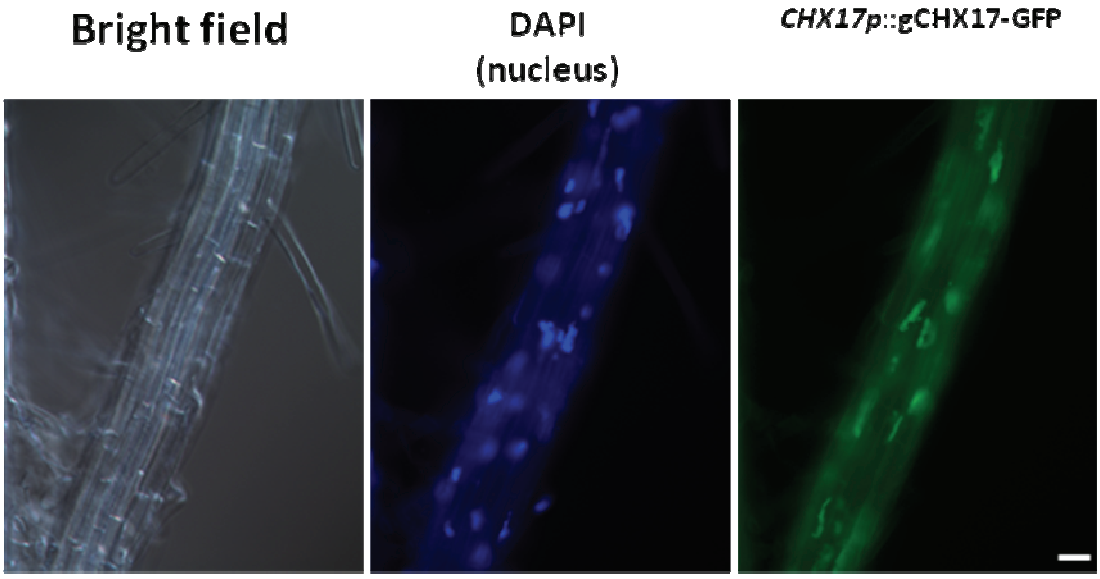

Fig A-V-6. Localization of native CHX17 in intracellular aggregates.

CHX17p::gCHX17-GFP transgenic plants were grown on 0.5X MS solid medium for 14 d. Roots were incubated in 1 μg/ml DAPI (4′,6-diamino-phenylindole) in 0.5X MS for 10 min then washed with 0.5X MS twice. Root GFP and DAPI fluorescent signals from mature region were observed under epifluorescence microscope. Both DAPI (labeled nucleus) and GFP (labeled CHX17-localizing compartments) showed fluorescent signals as aggregates (center and right) without overlapping to each other indicating that the aggregates observed in CHX17-localizing compartments were not associated with nucleus. Bright-field image is shown on the left. Scale bars = 20 μm. Results are from at least 3 independent observation.

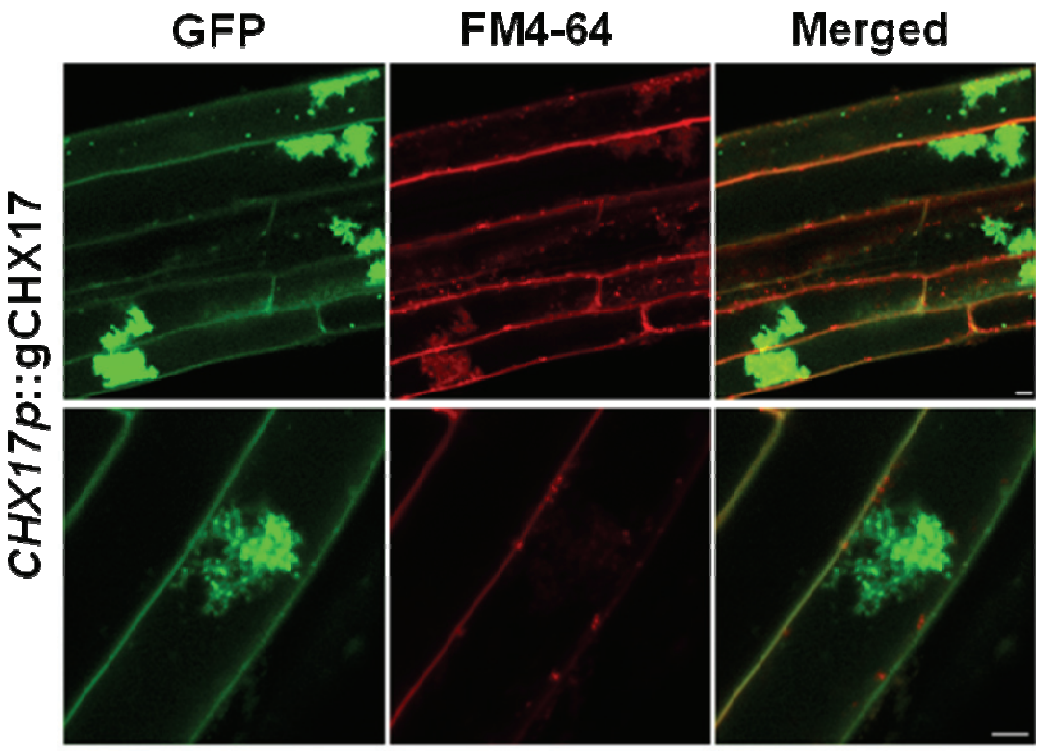

Fig A-V-7. Intracellular aggregates derived from CHX17-GFP driven by its native promoter were not associated with TGN.

Transgenic plant harboring genomic CHX17-GFP fusion under the control of its native promoter were grown in 0.5X MS solid medium for 7 d then transferred to GB with low K^+ for 3 d. Roots were incubated with 10 μM FM4-64 for 10 min then washed and submerged in GB medium with 2 mM K^+. GFP signals (left) and FM4-64 signals (middle) were merged at the right. Images were taken from root epidermis at the mature zone. Results are from 2 independent experiments. Scale bar = 5 μm.

(Top) CHX17-GFP interchangeably localized at the puncta and aggregates that were not co-localized with FM4-64 labeled early endosomes or TGN.

(Bottom) Enlarged view of aggregates of 5-20 μm.

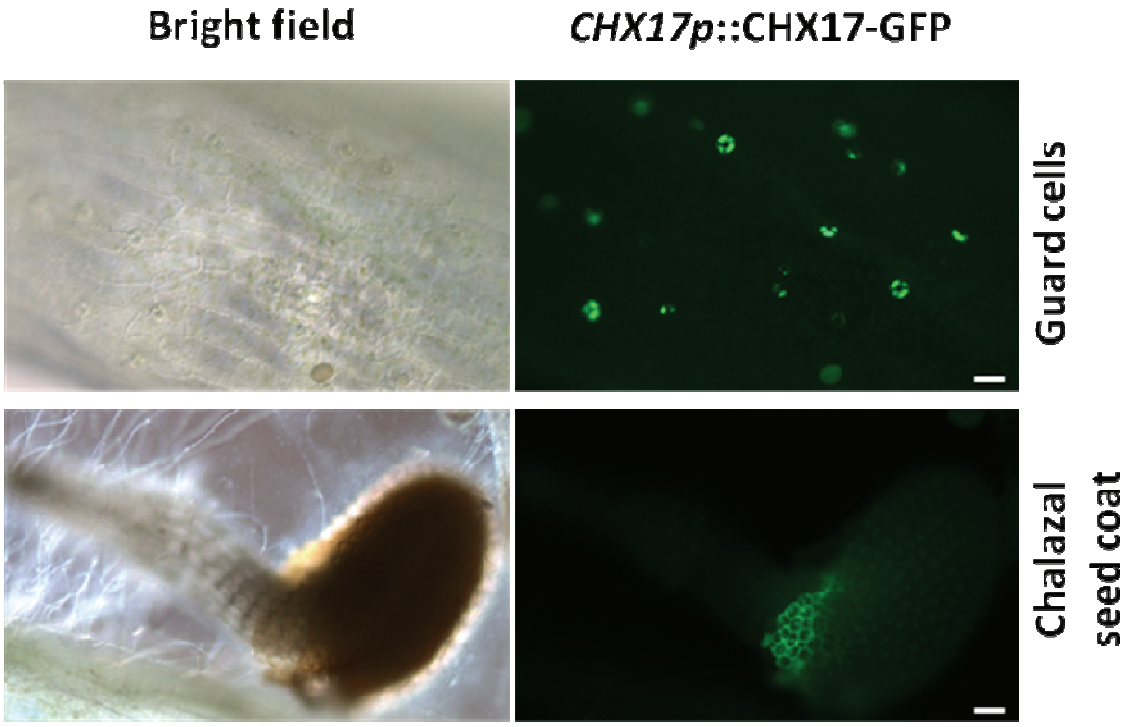

Fig A-V-8. CHX17 was constitutively expressed in the chalazal seed coat yet preferentially expressed in guard cells after incubation in water for 3 d.

Mature siliques from transgenic plant harboring CHX17p::YFP were soaked with water for 3 d. Fluorescent signals were observed in guard cells of siliques (top) and in the chalazal seed coat region (bottom). The latter was also observed during seed development in chalazal/micropylar region. Data are from a single observation. Scale bar = 30 μm.

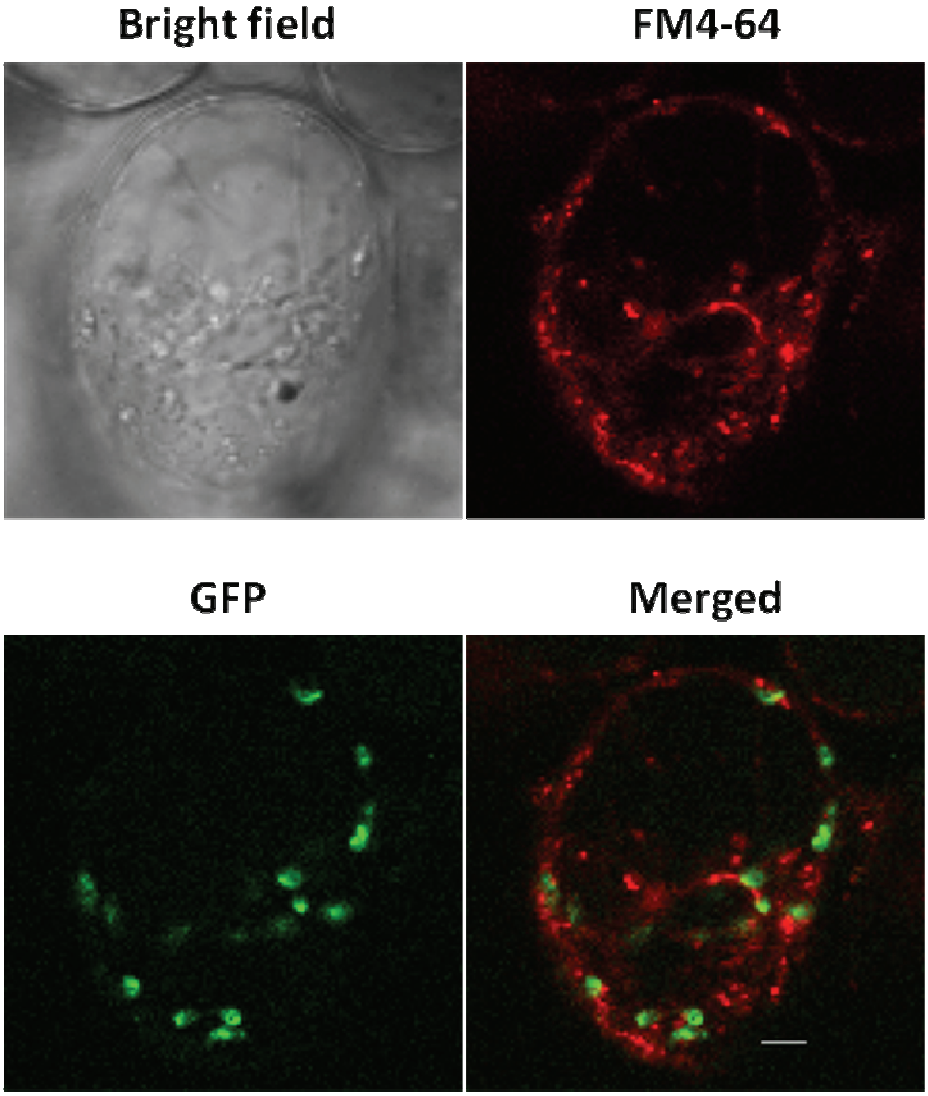

Fig A-V-9. Localization of CHX17-GFP in chalazal seed coat.

Wt seedlings harboring *35S*::*CHX17-GFP* were incubated with 10 μM FM4-64 for 10 min, then washed. CHX17-GFP appeared at the puncta and did not co-localize with FM4-64, labeling early endosomes or TGN, in chalazal seed coat cells where *CHX17* was expressed (Fig. A-V-8). Fluorescent signals were observed using confocal microscopy. Images are representative of two independent observations. Scale bar = 5 μm.

Fig A-V-10. Dark induced stomata closure was retarded in *chx17* mutants at pH_e 7.6.

A-B) *chx17* mutants failed to close stomata at pH 7.6. *Wt* (col-0), *chx17-1* mutant and *chx17-4* mutant were grown in soil for 3 wk. Leaves were detached and vacuum-infiltrated with incubation buffer containing 10 mM MES-KOH pH 6.15 or 10 mM HEPES-KOH pH 7.61. Infiltrated leaves were incubated for 3 h in the dark then incubated in the light or dark for 3 h. (A) There is no significant difference in guard cell movement between *Wt* and *chx17* mutants at pH_e 6.15. (B) *chx17* mutant stomata could not close as much as *Wt* stomata at pH_e 7.61. Results are representative of two independent experiments, 2 lines of *Wt* or mutant plants (*chx17-1* and *chx17-4*) per experiment. At least 6 leaves were sampled from each plant. The total of 68-171 stomata were measured per treatment. Bars = SEM.

C) ABA induced stomata closure in both *Wt* and *chx17* mutants at pH 7.6. *Wt* (col-0), *chx17-1* mutant and *chx17-4* mutant were grown in soil for 3 wk. Leaves were detached and vacuum-infiltrated with incubation buffer containing 10 mM HEPES-KOH pH 7.61. Infiltrated leaves were incubated for 3 h in the light then transferred to 10 μM ABA (abscisic acid) in the same buffer with light for 1 h. Stomata closure was induced by ABA in *Wt*, *chx17-1* and *chx17-4* mutants though *chx17-1* and *chx17-4* mutants demonstrated less closure relative to *Wt*. Results are from a single experiment. At least 3 leaves were sampled from each plant. The total of 30-56 stomata were measured per treatment. Bars = SEM.

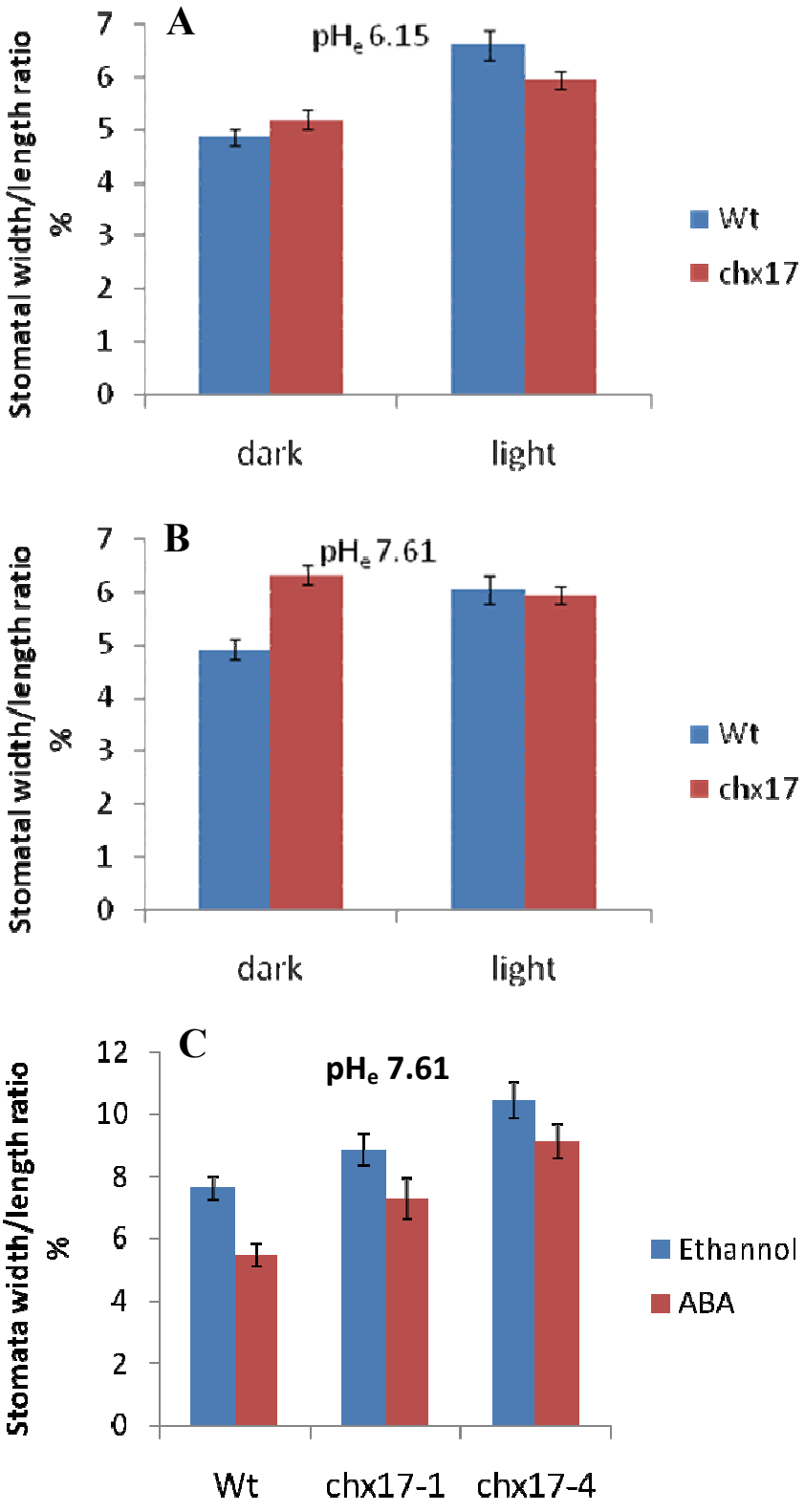
A
pH$_e$ 6.15
Stomatal width/length ratio %
0
1
2
3
4
5
6
7
dark
light
Wt
chx17
B
pH$_e$ 7.61
Stomatal width/length ratio %
0
1
2
3
4
5
6
7
dark
light
Wt
chx17
C
pH$_e$ 7.61
Stomata width/length ratio %
0
2
4
6
8
10
12
Wt
chx17-1
chx17-4
Ethannol
ABA

A

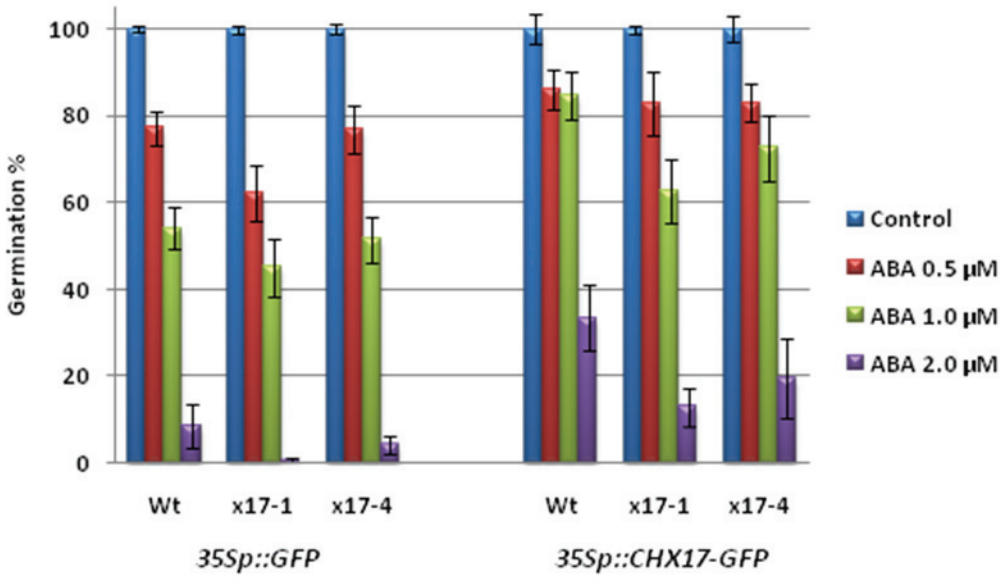

Fig. A-V-11. Overexpression of CHX17 reduced inhibitory effect of ABA in seed germination.

Seeds of transgenic *Wt* (col-0), *chx17-1* mutant and *chx17-4* mutant harboring *35Sp::GFP* or *35Sp::CHX17-GFP* constructs were germinated under light in 0.5X MS-MES medium pH 5.8 supplemented 1% sucrose for 3 d. Seedlings with emerging radicles longer than 1 mm were considered as germinated seeds.

A) Inhibitory effect of ABA in seed germination was less in CHX17 over-expressing plants. There is no significant difference between *Wt* and *chx17* mutants in seed germination inhibition by ABA (bars on the left). Over-expression of CHX17 enhanced seed germination in the presence of ABA (bars on the right). Results are from 5 independent experiments, 2 transgenic lines per experiment and 50-200 seeds per lines. Bars = SEM.

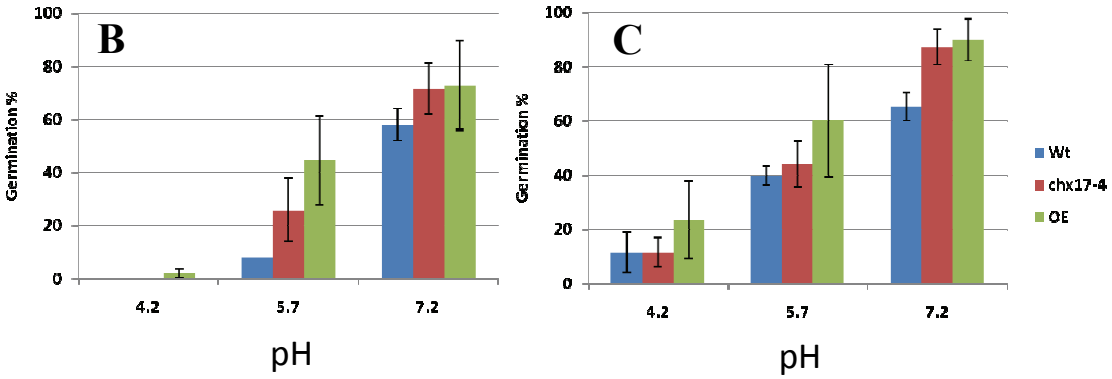

Fig. A-V-11. B-C) Effect of CHX17 over-expression in reduction of ABA inhibitory effect on seed germination was independent of external pH or sucrose. Seeds were germinated on medium without sucrose (A) or with 1% sucrose (B) for 3 d. Seedlings with emerging radicles longer than 0.5 mm were considered as germinated seeds. Seed germination of *Wt* or *chx17-4* mutant over-expressing *CHX17* (OE) was less inhibited by ABA regardless of the external pH or the presence of sucrose. Alkaline pH and sucrose reduced the inhibitory effect of ABA on seed germination in all tested seeds. Results are from a single experiment, 2-3 transgenic lines per experiment and 30 seeds per lines. Bars = SEM.

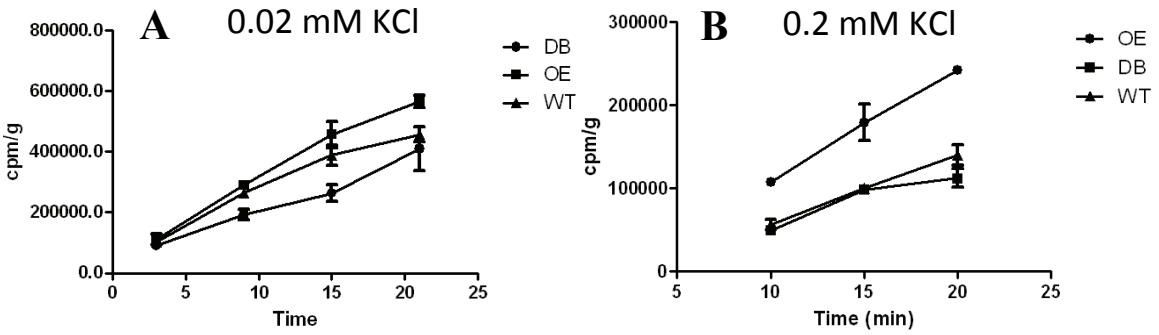

Fig. A-V-12. Over-expression of CHX17 enhanced Rb(K^+) uptake in roots.

Transgenic *Wt₄* (wild-type sibling; WT), *chx17-4, chx18-1* double mutant (DB) and *Wt* over-expressing *CHX17* (OE) were grown in 0.5X MS media for 7 d then starved for K^+ by replacing with the K^+-free 0.5X MS for 3 d. Roots were washed and cut in the same medium then placed into K^+-free 0.5X MS pH 5.7 supplemented with 0.5 µCi ^{86}Rb and 0.02 (A) or 0.2 (B) mM KCl and incubated for the indicated periods of time. ^{86}Rb uptake was terminated by filtering through nitrocellulose paper and incubated for 10 min and washed two times with iced-cold K^+-free 0.5X MS pH 5.7 supplemented with 1.75 mM RbCl. Roots were surface-dried and weighed before adding scintillation cocktails. Radioactivity was measured with a scintillation counter. Over-expression of *CHX17* increased root ^{86}Rb uptake compared to *Wt* or *chx17-4* mutant. ^{86}Rb uptake was significant higher when the external concentration of K^+ is 0.2 mM (B) compared to 0.02 mM (A). Results are from a single experiment, 2 transgenic lines per experiment, and 3 replicates per time point.

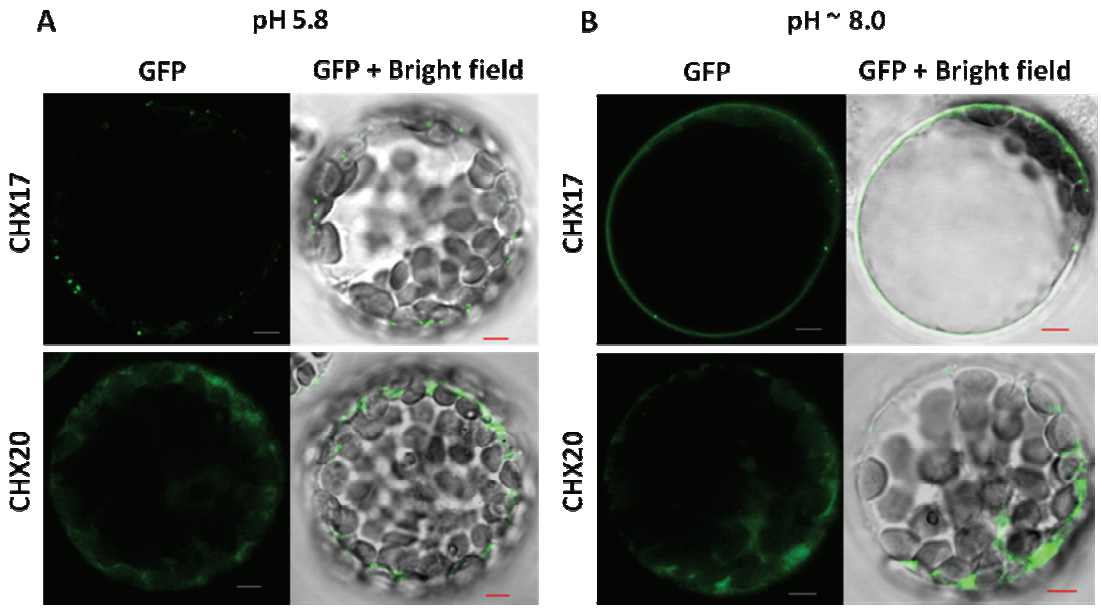

Fig. A-V-13. CHX17-GFP appeared at the cell periphery after treated at ~ pH 8.0.

Arabidopsis leaf protoplasts were transfected with *CHX17-GFP* or *CHX20-GFP* as described in section A.1.g. After 18 to 24 h, transfected protoplasts were treated (diluted) with regular incubation buffer pH 5.8 or ~pH 8.0 (10 mM BTP pH 9.0) and incubated for another 3 h. Fluorescent signals were observed using LSM 510 confocal microscope.

A) CHX17-GFP mainly localized to puncta whereas CHX20-GFP localized to reticulate structures at pH 5.8.

B) At pH ~ 8.0, many protoplasts were burst though several of CHX17-GFP positive protoplasts showed additional localization at the PM (top). No change in pattern of localization was observed in CHX20-GFP expressing protoplasts in reticulate structures (bottom).

Results are representative of 2 independent experiments. At least 8 transfected protoplasts were observed per experiment. Scale bars = 5 µm.

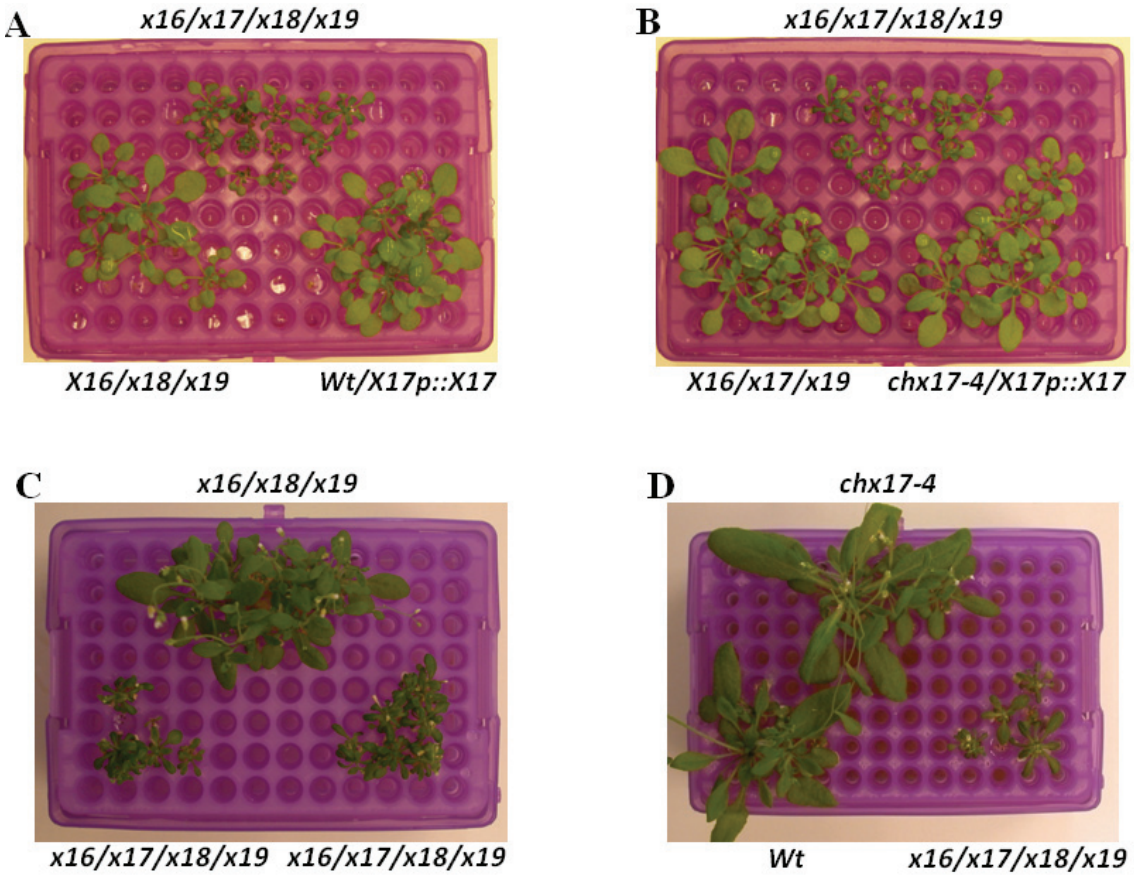

Fig. A-V-14. Growth of *chx16/17/18/19* quadruple mutants decreased after 3 weeks in hydroponic solution.

Wt_4 (wild-type sibling), single *chx17-4* mutant, *Wt* (*col-0*) expressing genomic *CHX17* (*X17p*::*X17*) , single *chx17-4* mutant expressing genomic *CHX17* (*X17p*::*X17*), *chx16/18/19* triple mutants, *chx16/17/19* triple mutants and *chx16/17/18/19* quadruple mutants were grown in hydroponic solution (GB) with 1.75 mM K^+ for 3-5 wk. After the third week of growth (A, B), quadruple mutants started to grow slower than triple mutant siblings, single *chx17-4* mutants or *Wt* plants. Growth difference was prominent after 4 wk (C) or 5 wk (D) in hydroponic system. Results are representative of 4 independent experiments and two independent transgenic lines or mutant siblings.

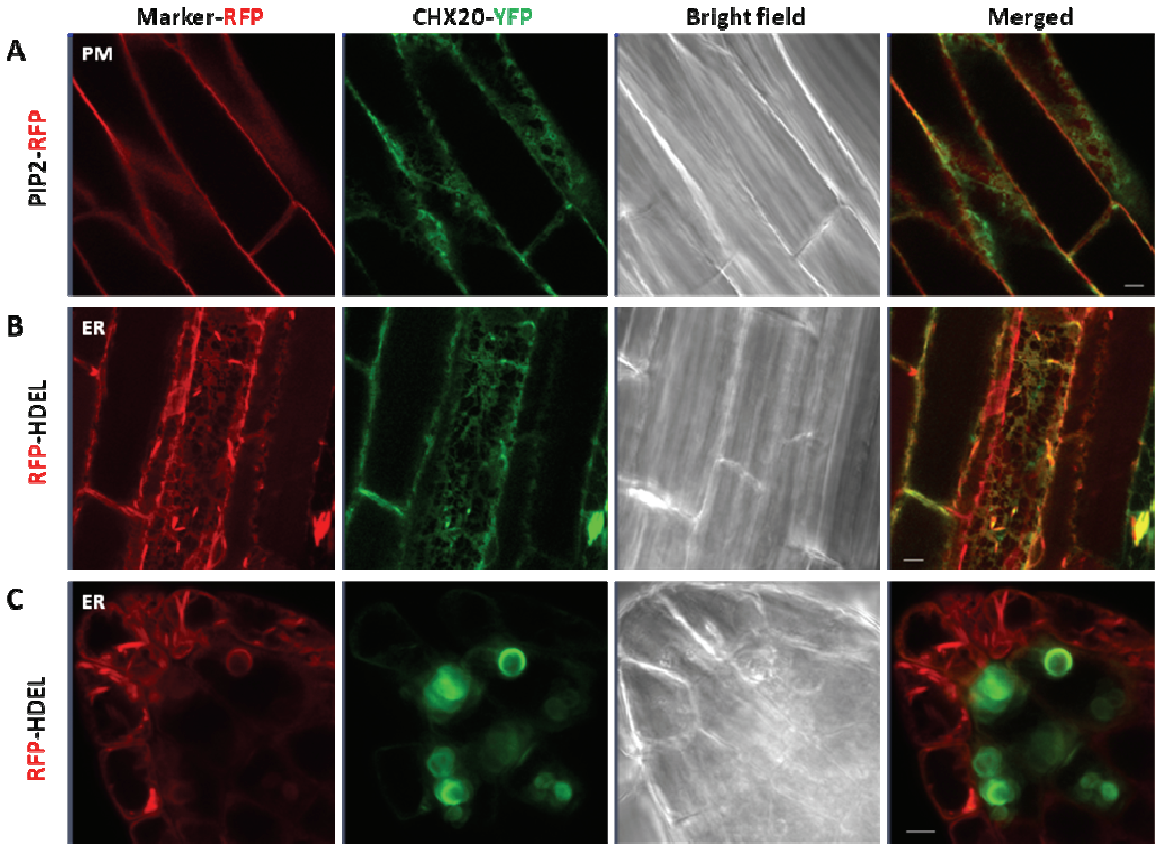

Fig. A-V-15. CHX20-GFP localized to ER and unknown compartments in transgenic plants.

Trangenic lines (*Wt col-1* background) co-expressing *GFP* and *RFP* fusion constructs were obtained from a cross between plants expressing *35Sp*::*CHX20-GFP* and *35Sp*::*AtPIP2-RFP* (A) or *35Sp*::*RFP-HDEL* (B-C). F1 seeds were germinated in 0.5X MS solid medium for 10 d before observation. Fluorescent signals were observed under confocal microscopy. Images are representative of at least two independent transgenic lines. Scale bar = 5 μm.

(A) CHX20-GFP did not co-localize with PIP2-RFP, a PM marker. Images were taken from root epidermis of mature zone.

(B) CHX20-GFP co-localized with RFP-HDEL, an ER marker. Images were taken from root epidermis of mature zone.

(C) CHX20-GFP localized to multiple ring-like structures of about 5 μm in diameter at the root tip.

VI. REFERENCES

Ali R, Brett CL, Mukherjee S, Rao R (2004) Inhibition of sodium/proton exchange by a Rab-GTPase-activating protein regulates endosomal traffic in yeast. J Biol Chem **279:** 4498-4506

Almagro L, Ros LVG, Belchi-Navarro S, Bru R, Barcelo AR, Pedreno MA (2009) Class III peroxidases in plant defence reactions. Journal of Experimental Botany **60:** 377-390

An Q, van Bel AJ, Huckelhoven R (2007) Do plant cells secrete exosomes derived from multivesicular bodies? Plant Signal Behav **2:** 4-7

An QL, Huckelhoven R, Kogel KH, Van Bel AJE (2006) Multivesicular bodies participate in a cell wall-associated defence response in barley leaves attacked by the pathogenic powdery mildew fungus. Cellular Microbiology **8:** 1009-1019

An R, Chen QJ, Chai MF, Lu PL, Su Z, Qin ZX, Chen J, Wang XC (2007) AtNHX8, a member of the monovalent cation: proton antiporter-1 family in Arabidopsis thaliana, encodes a putative Li/H antiporter. Plant J **49:** 718-728

Appel M, Hizlan D, Vinothkumar KR, Ziegler C, Kuhlbrandt W (2009) Conformations of NhaA, the Na+/H+ exchanger from Escherichia coli, in the pH-activated and ion-translocating states. J Mol Biol **388:** 659-672

Apse MP, Aharon GS, Snedden WA, Blumwald E (1999) Salt tolerance conferred by overexpression of a vacuolar Na+/H+ antiport in Arabidopsis. Science **285:** 1256-1258

Apse MP, Sottosanto JB, Blumwald E (2003) Vacuolar cation/H+ exchange, ion homeostasis, and leaf development are altered in a T-DNA insertional mutant of AtNHX1, the Arabidopsis vacuolar Na+/H+ antiporter. Plant Journal **36:** 229-239

Arcaro A, Wymann MP (1993) Wortmannin is a potent phosphatidylinositol 3-kinase inhibitor: the role of phosphatidylinositol 3,4,5-trisphosphate in neutrophil responses. Biochem J **296 (Pt 2):** 297-301

Baluska F, Hlavacka A, Samaj J, Palme K, Robinson DG, Matoh T, McCurdy DW, Menzel D, Volkmann D (2002) F-actin-dependent endocytosis of cell wall pectins in meristematic root cells. Insights from brefeldin A-induced compartments. Plant Physiology **130:** 422-431

Baluska F, Liners F, Hlavacka A, Schlicht M, Van Cutsem P, McCurdy DW, Menzel D (2005) Cell wall pectins and xyloglucans are internalized into dividing root cells and accumulate within cell plates during cytokinesis. Protoplasma **225:** 141-155

Banerjee S, Basu S, Sarkar S (2010) Comparative genomics reveals selective distribution and domain organization of FYVE and PX domain proteins across eukaryotic lineages. Bmc Genomics **11:** -

Banuelos MA, Sychrova H, Bleykasten-Grosshans C, Souciet JL, Potier S (1998) The Nha1 antiporter of Saccharomyces cerevisiae mediates sodium and potassium efflux. Microbiology **144 (Pt 10):** 2749-2758

Banuelos MG, Moreno DE, Olson DK, Nguyen Q, Ricarte F, Aguilera-Sandoval CR, Gharakhanian E (2010) Genomic analysis of severe hypersensitivity to hygromycin B reveals linkage to vacuolar defects and new vacuolar gene functions in Saccharomyces cerevisiae. Curr Genet **56:** 121-137

Bassil E, Ohto MA, Esumi T, Tajima H, Zhu Z, Cagnac O, Belmonte M, Peleg Z, Yamaguchi T, Blumwald E (2011) The Arabidopsis Intracellular Na+/H+ Antiporters NHX5 and NHX6 Are Endosome Associated and Necessary for Plant Growth and Development. Plant Cell **23:** 224-239

Birnbaum K, Shasha DE, Wang JY, Jung JW, Lambert GM, Galbraith DW, Benfey PN (2003) A gene expression map of the Arabidopsis root. Science **302:** 1956-1960

Bock KW, Honys D, Ward JM, Padmanaban S, Nawrocki EP, Hirschi KD, Twell D, Sze H (2006) Integrating membrane transport with male gametophyte development and function through transcriptomics. Plant Physiol **140:** 1151-1168

Bolte S, Talbot C, Boutte Y, Catrice O, Read ND, Satiat-Jeunemaitre B (2004) FM-dyes as experimental probes for dissecting vesicle trafficking in living plant cells. Journal of Microscopy-Oxford **214:** 159-173

Booth IR, Ferguson GP, Miller S, Li C, Gunasekera B, Kinghorn S (2003) Bacterial production of methylglyoxal: a survival strategy or death by misadventure? Biochem Soc Trans **31:** 1406-1408

Bosch M, Hepler PK (2005) Pectin methylesterases and pectin dynamics in pollen tubes. Plant Cell **17:** 3219-3226

Bowers K, Levi BP, Patel FI, Stevens TH (2000) The sodium/proton exchanger Nhx1p is required for endosomal protein trafficking in the yeast Saccharomyces cerevisiae. Molecular Biology of the Cell **11:** 4277-4294

Braun NA, Morgan B, Dick TP, Schwappach B (2010) The yeast CLC protein counteracts vesicular acidification during iron starvation. J Cell Sci **123:** 2342-2350

Brett CL, Donowitz M, Rao R (2005) Evolutionary origins of eukaryotic sodium/proton exchangers. Am J Physiol Cell Physiol **288:** C223-239

Brett CL, Tukaye DN, Mukherjee S, Rao R (2005b) The yeast endosomal Na+K+/H+ exchanger Nhx1 regulates cellular pH to control vesicle trafficking. Mol Biol Cell **16:** 1396-1405

Brodersen DE, Clemons WM, Jr., Carter AP, Morgan-Warren RJ, Wimberly BT, Ramakrishnan V (2000) The structural basis for the action of the antibiotics tetracycline, pactamycin, and hygromycin B on the 30S ribosomal subunit. Cell **103:** 1143-1154

Buurman ET, Kim KT, Epstein W (1995) Genetic evidence for two sequentially occupied K+ binding sites in the Kdp transport ATPase. J Biol Chem **270:** 6678-6685

Campanoni P, Blatt MR (2007) Membrane trafficking and polar growth in root hairs and pollen tubes. J Exp Bot **58:** 65-74

Carcia-Salcedo R, Montiel V, Calero F, Ramos J (2007) Characterization of DhKHA1, a gene coding for a putative Na+ transporter from Debaryomyces hansenii. Fems Yeast Research **7:** 905-911

Casey JR, Grinstein S, Orlowski J (2010) Sensors and regulators of intracellular pH. Nat Rev Mol Cell Biol **11:** 50-61

Cellier F, Conejero G, Ricaud L, Luu DT, Lepetit M, Gosti F, Casse F (2004) Characterization of AtCHX17, a member of the cation/H+ exchangers, CHX family, from Arabidopsis thaliana suggests a role in K+ homeostasis. Plant J **39:** 834-846

Chae K, Lord EM (2011) Pollen tube growth and guidance: roles of small, secreted proteins. Ann Bot

Chatre L, Wattelet-Boyer V, Melser S, Maneta-Peyret L, Brandizzi F, Moreau P (2009) A novel di-acidic motif facilitates ER export of the syntaxin SYP31. J Exp Bot **60:** 3157-3165

Ciamporova M, Mistrik I (1993) The Ultrastructural Response of Root-Cells to Stressful Conditions. Environmental and Experimental Botany **33:** 11-26

Curtis MD, Grossniklaus U (2003) A gateway cloning vector set for high-throughput functional analysis of genes in planta. Plant Physiol **133:** 462-469

Darley CP, van Wuytswinkel OC, van der Woude K, Mager WH, de Boer AH (2000) Arabidopsis thaliana and Saccharomyces cerevisiae NHX1 genes encode amiloride sensitive electroneutral Na+/H+ exchangers. Biochem J **351:** 241-249

Davidson HW (1995) Wortmannin causes mistargeting of procathepsin D. evidence for the involvement of a phosphatidylinositol 3-kinase in vesicular transport to lysosomes. J Cell Biol **130:** 797-805

DeFelice LJ, Goswami T (2007) Transporters as channels. Annu Rev Physiol **69:** 87-112

Dhonukshe P, Tanaka H, Goh T, Ebine K, Mahonen AP, Prasad K, Blilou I, Geldner N, Xu J, Uemura T, Chory J, Ueda T, Nakano A, Scheres B, Friml J (2008) Generation of cell polarity in plants links endocytosis, auxin distribution and cell fate decisions. Nature **456:** 962-966

Domozych DS, Serfis A, Kiemle SN, Gretz MR (2007) The structure and biochemistry of charophycean cell walls: I. Pectins of Penium margaritaceum. Protoplasma **230:** 99-115

Donaldson JG, Finazzi D, Klausner RD (1992) Brefeldin A inhibits Golgi membrane-catalysed exchange of guanine nucleotide onto ARF protein. Nature **360:** 350-352

Donowitz M, Mohan S, Zhu CX, Chen TE, Lin R, Cha B, Zachos NC, Murtazina R, Sarker R, Li X (2009) NHE3 regulatory complexes. J Exp Biol **212:** 1638-1646

Edgar RC (2010) Quality measures for protein alignment benchmarks. Nucleic Acids Res **38:** 2145-2153

Edwards K, Johnstone C, Thompson C (1991) A Simple and Rapid Method for the Preparation of Plant Genomic DNA for Pcr Analysis. Nucleic Acids Research **19:** 1349-1349

Ellson CD, Andrews S, Stephens LR, Hawkins PT (2002) The PX domain: a new phosphoinositide-binding module. J Cell Sci **115:** 1099-1105

Ferguson GP, Battista JR, Lee AT, Booth IR (2000) Protection of the DNA during the exposure of Escherichia coli cells to a toxic metabolite: the role of the KefB and KefC potassium channels. Mol Microbiol **35:** 113-122

Ferguson GP, Munro AW, Douglas RM, McLaggan D, Booth IR (1993) Activation of potassium channels during metabolite detoxification in Escherichia coli. Mol Microbiol **9:** 1297-1303

Ferguson GP, Nikolaev Y, McLaggan D, Maclean M, Booth IR (1997) Survival during exposure to the electrophilic reagent N-ethylmaleimide in Escherichia coli: role of KefB and KefC potassium channels. J Bacteriol **179:** 1007-1012

Fernandez-Borja M, Wubbolts R, Calafat J, Janssen H, Divecha N, Dusseljee S, Neefjes J (1999) Multivesicular body morphogenesis requires phosphatidylinositol 3-kinase activity. Current Biology **9:** 55-58

Finet C, Timme RE, Delwiche CF, Marletaz F (2010) Multigene phylogeny of the green lineage reveals the origin and diversification of land plants. Curr Biol **20:** 2217-2222

Flis K, Hinzpeter A, Edelman A, Kurlandzka A (2005) The functioning of mammalian ClC-2 chloride channel in Saccharomyces cerevisiae cells requires an increased level of Kha1p. Biochem J **390:** 655-664

Fraile-Escanciano A, Kamisugi Y, Cuming AC, Rodriguez-Navarro A, Benito B (2010) The SOS1 transporter of Physcomitrella patens mediates sodium efflux in planta. New Phytologist **188:** 750-761

Franke R, Hofer R, Briesen I, Emsermann M, Efremova N, Yephremov A, Schreiber L (2009) The DAISY gene from Arabidopsis encodes a fatty acid elongase condensing enzyme involved in the biosynthesis of aliphatic suberin in roots and the chalaza-micropyle region of seeds. Plant Journal **57:** 80-95

Friml J (2010) Subcellular trafficking of PIN auxin efflux carriers in auxin transport. Eur J Cell Biol **89:** 231-235

Fujisawa M, Ito M, Krulwich TA (2007) Three two-component transporters with channel-like properties have monovalent cation/proton antiport activity. Proc Natl Acad Sci U S A **104:** 13289-13294

Gaxiola RA, Rao R, Sherman A, Grisafi P, Alper SL, Fink GR (1999) The Arabidopsis thaliana proton transporters, AtNhx1 and Avp1, can function in cation detoxification in yeast.

Proceedings of the National Academy of Sciences of the United States of America **96:** 1480-1485

Geldner N, Anders N, Wolters H, Keicher J, Kornberger W, Muller P, Delbarre A, Ueda T, Nakano A, Jurgens G (2003) The Arabidopsis GNOM ARF-GEF mediates endosomal recycling, auxin transport, and auxin-dependent plant growth. Cell **112:** 219-230

Geldner N, Friml J, Stierhof YD, Jurgens G, Palme K (2001) Auxin transport inhibitors block PIN1 cycling and vesicle trafficking. Nature **413:** 425-428

Geldner N, Hyman DL, Wang X, Schumacher K, Chory J (2007) Endosomal signaling of plant steroid receptor kinase BRI1. Genes Dev **21:** 1598-1602

Geldner N, Robatzek S (2008) Plant receptors go endosomal: a moving view on signal transduction. Plant Physiol **147:** 1565-1574

Gibeaut DM, Hulett J, Cramer GR, Seemann JR (1997) Maximal biomass of Arabidopsis thaliana using a simple, low-maintenance hydroponic method and favorable environmental conditions. Plant Physiol **115:** 317-319

Gietz RD, Schiestl RH (2007) Frozen competent yeast cells that can be transformed with high efficiency using the LiAc/SS carrier DNA/PEG method. Nat Protoc **2:** 1-4

Goswami P, Paulino C, Hizlan D, Vonck J, Yildiz O, Kuhlbrandt W (2011) Structure of the archaeal Na+/H+ antiporter NhaP1 and functional role of transmembrane helix 1. EMBO J **30:** 439-449

Grunewald W, Friml J (2010) The march of the PINs: developmental plasticity by dynamic polar targeting in plant cells. EMBO J **29:** 2700-2714

Haan C, Behrmann I (2007) A cost effective non-commercial ECL-solution for Western blot detections yielding strong signals and low background. J Immunol Methods **318:** 11-19

Han MV, Zmasek CM (2009) phyloXML: XML for evolutionary biology and comparative genomics. BMC Bioinformatics **10:** 356

Hanton SL, Renna L, Bortolotti LE, Chatre L, Stefano G, Brandizzi F (2005) Diacidic motifs influence the export of transmembrane proteins from the endoplasmic reticulum in plant cells. Plant Cell **17:** 3081-3093

Harholt J, Suttangkakul A, Vibe Scheller H (2010) Biosynthesis of pectin. Plant Physiol **153:** 384-395

Hawes C, Saint-Jore C, Martin B, Zheng HQ (2001) ER confirmed as the location of mystery organelles in Arabidopsis plants expressing GFP! Trends Plant Sci **6:** 245-246

Hem S, Rofidal V, Sommerer N, Rossignol M (2007) Novel subsets of the Arabidopsis plasmalemma phosphoproteome identify phosphorylation sites in secondary active transporters. Biochem Biophys Res Commun **363:** 375-380

Hruz T, Laule O, Szabo G, Wessendorp F, Bleuler S, Oertle L, Widmayer P, Gruissem W, Zimmermann P (2008) Genevestigator v3: a reference expression database for the meta-analysis of transcriptomes. Adv Bioinformatics **2008:** 420747

Hudak J, Walles B, Vennigerholz F (1993) The Transmitting Tissue in Brugmansia-Suaveolens L - Ultrastructure of the Stylar Transmitting Tissue. Annals of Botany **71:** 177-186

Inaba M, Sakamoto A, Murata N (2001) Functional expression in Escherichia coli of low-affinity and high-affinity Na(+)(Li(+))/H(+) antiporters of Synechocystis. J Bacteriol **183:** 1376-1384

Inoue N, Yamada S, Nagata Y, Shimmen T (2002) Rhizoid differentiation in Spirogyra: Position sensing by terminal cells. Plant and Cell Physiology **43:** 479-483

Irani NG, Russinova E (2009) Receptor endocytosis and signaling in plants. Curr Opin Plant Biol **12:** 653-659

Jolie RP, Duvetter T, Van Loey AM, Hendrickx ME (2010) Pectin methylesterase and its proteinaceous inhibitor: a review. Carbohydr Res **345:** 2583-2595

Jones L, Milne JL, Ashford D, McQueen-Mason SJ (2003) Cell wall arabinan is essential for guard cell function. Proc Natl Acad Sci U S A **100:** 11783-11788

Jordan EG (1970) Ultrastructural aspects of cell wall synthesis in Spirogyra. Protoplasma **69:** 405-416

Jurgens G (2004) Membrane trafficking in plants. Annu Rev Cell Dev Biol **20:** 481-504

Kane PA (2006) The where, when, and how of organelle acidification by the yeast vacuolar H+-ATPase. Microbiology and Molecular Biology Reviews **70:** 177-191

Kanter U, Hauser A, Michalke B, Draxl S, Schaffner AR (2010) Caesium and strontium accumulation in shoots of Arabidopsis thaliana: genetic and physiological aspects. J Exp Bot **61:** 3995-4009

Karnik SK, Trelease RN (2007) Arabidopsis peroxin 16 trafficks through the ER and an intermediate compartment to pre-existing peroxisomes via overlapping molecular targeting signals. J Exp Bot **58:** 1677-1693

Karol KG, McCourt RM, Cimino MT, Delwiche CF (2001) The closest living relatives of land plants. Science **294:** 2351-2353

Katiyar-Agarwal S, Zhu J, Kim K, Agarwal M, Fu X, Huang A, Zhu JK (2006) The plasma membrane Na+/H+ antiporter SOS1 interacts with RCD1 and functions in oxidative stress tolerance in Arabidopsis. Proc Natl Acad Sci U S A **103:** 18816-18821

Katzmann DJ, Odorizzi G, Emr SD (2002) Receptor downregulation and multivesicular-body sorting. Nat Rev Mol Cell Biol **3:** 893-905

Kinclova-Zimmermannova O, Gaskova D, Sychrova H (2006) The Na+,K+/H+ -antiporter Nha1 influences the plasma membrane potential of Saccharomyces cerevisiae. FEMS Yeast Res **6:** 792-800

Kinclova O, Ramos J, Potier S, Sychrova H (2001) Functional study of the Saccharomyces cerevisiae Nha1p C-terminus. Mol Microbiol **40:** 656-668

Kleine-Vehn J, Dhonukshe P, Sauer M, Brewer PB, Wisniewska J, Paciorek T, Benkova E, Friml J (2008) ARF GEF-dependent transcytosis and polar delivery of PIN auxin carriers in Arabidopsis. Curr Biol **18:** 526-531

Krichevsky A, Kozlovsky SV, Tian GW, Chen MH, Zaltsman A, Citovsky V (2007) How pollen tubes grow. Developmental Biology **303:** 405-420

Lakkaraju A, Rodriguez-Boulan E (2008) Itinerant exosomes: emerging roles in cell and tissue polarity. Trends Cell Biol **18:** 199-209

Lang I, Barton DA, Overall RL (2004) Membrane-wall attachments in plasmolysed plant cells. Protoplasma **224:** 231-243

Larkin MA, Blackshields G, Brown NP, Chenna R, McGettigan PA, McWilliam H, Valentin F, Wallace IM, Wilm A, Lopez R, Thompson JD, Gibson TJ, Higgins DG (2007) Clustal W and Clustal X version 2.0. Bioinformatics **23:** 2947-2948

Le BH, Cheng C, Bui AQ, Wagmaister JA, Henry KF, Pelletier J, Kwong L, Belmonte M, Kirkbride R, Horvath S, Drews GN, Fischer RL, Okamuro JK, Harada JJ, Goldberg RB (2010) Global analysis of gene activity during Arabidopsis seed development and identification of seed-specific transcription factors. Proc Natl Acad Sci U S A **107:** 8063-8070

Lee MH, Min MK, Lee YJ, Jin JB, Shin DH, Kim DH, Lee KH, Hwang I (2002) ADP-ribosylation factor 1 of Arabidopsis plays a critical role in intracellular trafficking and maintenance of endoplasmic reticulum morphology in Arabidopsis. Plant Physiol **129:** 1507-1520

Leidi EO, Barragan V, Rubio L, El-Hamdaoui A, Ruiz MT, Cubero B, Fernandez JA, Bressan RA, Hasegawa PM, Quintero FJ, Pardo JM (2010) The AtNHX1 exchanger mediates potassium compartmentation in vacuoles of transgenic tomato. Plant Journal **61:** 495-506

Li HT, Liu H, Gao XS, Zhang HX (2009) Knock-out of Arabidopsis AtNHX4 gene enhances tolerance to salt stress. Biochemical and Biophysical Research Communications **382:** 637-641

Li J, Wen J, Lease KA, Doke JT, Tax FE, Walker JC (2002) BAK1, an Arabidopsis LRR receptor-like protein kinase, interacts with BRI1 and modulates brassinosteroid signaling. Cell **110:** 213-222

Li XY, Chanroj S, Wu ZY, Romanowsky SM, Harper JF, Sze H (2008) A distinct endosomal Ca2+/Mn2+ pump affects root growth through the secretory process. Plant Physiology **147:** 1675-1689

Lindmo K, Stenmark H (2006) Regulation of membrane traffic by phosphoinositide 3-kinases. Journal of Cell Science **119:** 605-614

Lisenbee CS, Karnik SK, Trelease RN (2003) Overexpression and mislocalization of a tail-anchored GFP redefines the identity of peroxisomal ER. Traffic **4:** 491-501

Liu H, Tang RJ, Zhang Y, Wang CT, Lv QD, Gao XS, Li WB, Zhang HX (2010) AtNHX3 is a vacuolar K+/H+ antiporter required for low-potassium tolerance in Arabidopsis thaliana. Plant Cell and Environment **33:** 1989-1999

Lu Y, Chanroj S, Zulkifli L, Johnson MA, Uozumi N, Cheung A, Sze H (2011) Pollen tubes lacking a pair of k+ transporters fail to target ovules in Arabidopsis. Plant Cell **23:** 81-93

Maeder ML, Thibodeau-Beganny S, Sander JD, Voytas DF, Joung JK (2009) Oligomerized pool engineering (OPEN): an 'open-source' protocol for making customized zinc-finger arrays. Nat Protoc **4:** 1471-1501

Majewska-Sawka A, Munster A, Rodriguez-Garcia MI (2002) Guard cell wall: immunocytochemical detection of polysaccharide components. J Exp Bot **53:** 1067-1079

Maresova L, Sychrova H (2005) Physiological characterization of Saccharomyces cerevisiae kha1 deletion mutants. Mol Microbiol **55:** 588-600

Maresova L, Sychrova H (2006) Arabidopsis thaliana CHX17 gene complements the kha1 deletion phenotypes in Saccharomyces cerevisiae. Yeast **23:** 1167-1171

Maresova L, Sychrova H (2010) Genetic interactions among the Arl1 GTPase and intracellular Na+/H+ antiporters in pH homeostasis and cation detoxification. Fems Yeast Research **10:** 802-811

Maresova L, Urbankova E, Gaskova D, Sychrova H (2006) Measurements of plasma membrane potential changes in Saccharomyces cerevisiae cells reveal the importance of the Tok1 channel in membrane potential maintenance. FEMS Yeast Res **6:** 1039-1046

Marjamaa K, Kukkola EM, Fagerstedt KV (2009) The role of xylem class III peroxidases in lignification. Journal of Experimental Botany **60:** 367-376

McCourt RM (1995) Green algal phylogeny. Trends Ecol Evol **10:** 159-163

McCourt RM, Delwiche CF, Karol KG (2004) Charophyte algae and land plant origins. Trends Ecol Evol **19:** 661-666

Miesenbock G, De Angelis DA, Rothman JE (1998) Visualizing secretion and synaptic transmission with pH-sensitive green fluorescent proteins. Nature **394:** 192-195

Mikosch M, Hurst AC, Hertel B, Homann U (2006) Diacidic motif is required for efficient transport of the K+ channel KAT1 to the plasma membrane. Plant Physiol **142:** 923-930

Mincheva-Nilsson L, Baranov V (2010) The role of placental exosomes in reproduction. Am J Reprod Immunol **63:** 520-533

Moustacas AM, Nari J, Borel M, Noat G, Ricard J (1991) Pectin Methylesterase, Metal-Ions and Plant Cell-Wall Extension - the Role of Metal-Ions in Plant Cell-Wall Extension. Biochemical Journal **279:** 351-354

Mukherjee S, Kallay L, Brett CL, Rao R (2006) Mutational analysis of the intramembranous H10 loop of yeast Nhx1 reveals a critical role in ion homoeostasis and vesicle trafficking. Biochem J **398:** 97-105

Mullen RT, Trelease RN (2000) The sorting signals for peroxisomal membrane-bound ascorbate peroxidase are within its C-terminal tail. J Biol Chem **275:** 16337-16344

Nagano Y, Takao S, Kudo T, Iizasa E, Anai T (2007) Yeast-based recombineering of DNA fragments into plant transformation vectors by one-step transformation. Plant Cell Reports **26:** 2111-2117

Nam KH, Li J (2002) BRI1/BAK1, a receptor kinase pair mediating brassinosteroid signaling. Cell **110:** 203-212

Nelson H, Nelson N (1990) Disruption of genes encoding subunits of yeast vacuolar H(+)-ATPase causes conditional lethality. Proc Natl Acad Sci U S A **87:** 3503-3507

Nicholas KB, Nicholas H.B. Jr., and Deerfield, D.W. II. (1997) GeneDoc: Analysis and Visualization of Genetic Variation. EMBNEW.NEWS **4**

Nishi T, Forgac M (2002) The vacuolar (H+)-ATPases--nature's most versatile proton pumps. Nat Rev Mol Cell Biol **3:** 94-103

Oh DH, Lee SY, Bressan RA, Yun DJ, Bohnert HJ (2010) Intracellular consequences of SOS1 deficiency during salt stress. J Exp Bot **61:** 1205-1213

Ohgaki R, Nakamura N, Mitsui K, Kanazawa H (2005) Characterization of the ion transport activity of the budding yeast Na+/H+ antiporter, Nha1p, using isolated secretory vesicles. Biochim Biophys Acta **1712:** 185-196

Ohnishi M, Fukada-Tanaka S, Hoshino A, Takada J, Inagaki Y, Iida S (2005) Characterization of a novel Na+/H+ antiporter gene InNHX2 and comparison of InNHX2 with InNHX1, which is responsible for blue flower coloration by increasing the vacuolar pH in the Japanese morning glory. Plant Cell Physiol **46:** 259-267

Oldenburg KR, Vo KT, Michaelis S, Paddon C (1997) Recombination-mediated PCR-directed plasmid construction in vivo in yeast. Nucleic Acids Res **25:** 451-452

Olias R, Eljakaoui Z, Li J, De Morales PA, Marin-Manzano MC, Pardo JM, Belver A (2009) The plasma membrane Na+/H+ antiporter SOS1 is essential for salt tolerance in

tomato and affects the partitioning of Na+ between plant organs. Plant Cell and Environment **32:** 904-916

Onate-Sanchez L, Vicente-Carbajosa J (2008) DNA-free RNA isolation protocols for Arabidopsis thaliana, including seeds and siliques. BMC Res Notes **1:** 93

Orlowski J, Grinstein S (2007) Emerging roles of alkali cation/proton exchangers in organellar homeostasis. Curr Opin Cell Biol **19:** 483-492

Otegui MS, Spitzer C (2008) Endosomal functions in plants. Traffic **9:** 1589-1598

Padmanaban S, Chanroj S, Kwak JM, Li X, Ward JM, Sze H (2007) Participation of endomembrane cation/H+ exchanger AtCHX20 in osmoregulation of guard cells. Plant Physiol **144:** 82-93

Panikashvili D, Shi JX, Bocobza S, Franke RB, Schreiber L, Aharoni A (2010) The Arabidopsis DSO/ABCG11 Transporter Affects Cutin Metabolism in Reproductive Organs and Suberin in Roots. Molecular Plant **3:** 563-575

Pardo JM, Cubero B, Leidi EO, Quintero FJ (2006) Alkali cation exchangers: roles in cellular homeostasis and stress tolerance. J Exp Bot **57:** 1181-1199

Passardi F, Cosio C, Penel C, Dunand C (2005) Peroxidases have more functions than a Swiss army knife. Plant Cell Reports **24:** 255-265

Pelchen-Matthews A, Raposo G, Marsh M (2004) Endosomes, exosomes and Trojan viruses. Trends Microbiol **12:** 310-316

Pelloux J, Rusterucci C, Mellerowicz EJ (2007) New insights into pectin methylesterase structure and function. Trends Plant Sci **12:** 267-277

Penel C, Greppin H (1994) Binding of plant isoperoxidases to pectin in the presence of calcium. FEBS Lett **343:** 51-55

Perlin DS, Brown CL, Haber JE (1988) Membrane potential defect in hygromycin B-resistant pma1 mutants of Saccharomyces cerevisiae. J Biol Chem **263:** 18118-18122

Pilzer D, Gasser O, Moskovich O, Schifferli JA, Fishelson Z (2005) Emission of membrane vesicles: roles in complement resistance, immunity and cancer. Springer Semin Immunopathol **27:** 375-387

Plant PJ, Manolson MF, Grinstein S, Demaurex N (1999) Alternative mechanisms of vacuolar acidification in H(+)-ATPase-deficient yeast. J Biol Chem **274:** 37270-37279

Popper ZA, Michel G, Herve C, Domozych DS, Willats WG, Tuohy MG, Kloareg B, Stengel DB (2011) Evolution and diversity of plant cell walls: from algae to flowering plants. Annu Rev Plant Biol **62:** 567-590

Pyo YJ, Gierth M, Schroeder JI, Cho MH (2010) High-affinity K(+) transport in Arabidopsis: AtHAK5 and AKT1 are vital for seedling establishment and postgermination growth under low-potassium conditions. Plant Physiol **153:** 863-875

Qi Z, Spalding EP (2004) Protection of plasma membrane K+ transport by the salt overly sensitive1 Na+-H+ antiporter during salinity stress. Plant Physiol **136:** 2548-2555

Qiu QS, Barkla BJ, Vera-Estrella R, Zhu JK, Schumaker KS (2003) Na+/H+ exchange activity in the plasma membrane of Arabidopsis. Plant Physiol **132:** 1041-1052

Qiu QS, Guo Y, Dietrich MA, Schumaker KS, Zhu JK (2002) Regulation of SOS1, a plasma membrane Na+/H+ exchanger in Arabidopsis thaliana, by SOS2 and SOS3. Proceedings of the National Academy of Sciences of the United States of America **99:** 8436-8441

Qiu QS, Guo Y, Quintero FJ, Pardo JM, Schumaker KS, Zhu JK (2004) Regulation of vacuolar Na+/H+ exchange in Arabidopsis thaliana by the salt-overly-sensitive (SOS) pathway. J Biol Chem **279:** 207-215

Quintero FJ, Blatt MR, Pardo JM (2000) Functional conservation between yeast and plant endosomal Na(+)/H(+) antiporters. FEBS Lett **471:** 224-228

Quintero FJ, Martinez-Atienza J, Villalta I, Jiang X, Kim WY, Ali Z, Fujii H, Mendoza I, Yun DJ, Zhu JK, Pardo JM (2011) Activation of the plasma membrane Na/H antiporter Salt-Overly-Sensitive 1 (SOS1) by phosphorylation of an auto-inhibitory C-terminal domain. Proc Natl Acad Sci U S A **108:** 2611-2616

Quintero FJ, Ohta M, Shi HZ, Zhu JK, Pardo JM (2002) Reconstitution in yeast of the Arabidopsis SOS signaling pathway for Na+ homeostasis. Proceedings of the National Academy of Sciences of the United States of America **99:** 9061-9066

Raikhel N, Hicks G (2007) Signaling from plant endosomes: compartments with something to say! Genes Dev **21:** 1578-1580

Ralet MC, Lerouge P, Quemener B (2009) Mass spectrometry for pectin structure analysis. Carbohydr Res **344:** 1798-1807

Ramirez J, Ramirez O, Saldana C, Coria R, Pena A (1998) A Saccharomyces cerevisiae mutant lacking a K+/H+ exchanger. J Bacteriol **180:** 5860-5865

Reeve RM (1959) A specific hydroxylamine-ferric chloride reaction for histochemical localization of pectin. Stain Technol. **34:** 209-211

Robinson DG, Jiang L, Schumacher K (2008) The endosomal system of plants: charting new and familiar territories. Plant Physiol **147:** 1482-1492

Robinson DG, Langhans M, Saint-Jore-Dupas C, Hawes C (2008b) BFA effects are tissue and not just plant specific. Trends Plant Sci **13:** 405-408

Rodriguez-Rosales MP, Galvez FJ, Huertas R, Aranda MN, Baghour M, Cagnac O, Venema K (2009) Plant NHX cation/proton antiporters. Plant Signal Behav **4:** 265-276

Rodriguez-Rosales MP, Jiang X, Galvez FJ, Aranda MN, Cubero B, Venema K (2008) Overexpression of the tomato K+/H+ antiporter LeNHX2 confers salt tolerance by improving potassium compartmentalization. New Phytol **179:** 366-377

Rubio F, Aleman F, Nieves-Cordones M, Martinez V (2010) Studies on Arabidopsis athak5, atakt1 double mutants disclose the range of concentrations at which AtHAK5, AtAKT1 and unknown systems mediate K uptake. Physiol Plant **139:** 220-228

Rubio F, Nieves-Cordones M, Aleman F, Martinez V (2008) Relative contribution of AtHAK5 and AtAKT1 to K+ uptake in the high-affinity range of concentrations. Physiol Plant **134:** 598-608

Sabba RP, Lulai EC (2002) Histological analysis of the maturation of native and wound periderm in potato (Solanum tuberosum L.) Tuber. Ann Bot **90:** 1-10

Saier MH, Jr. (2000) A functional-phylogenetic classification system for transmembrane solute transporters. Microbiol Mol Biol Rev **64:** 354-411

Samaj J, Baluska F, Voigt B, Schlicht M, Volkmann D, Menzel D (2004) Endocytosis, actin cytoskeleton, and signaling. Plant Physiol **135:** 1150-1161

Sandoval RM, Molitoris BA (2004) Gentamicin traffics retrograde through the secretory pathway and is released in the cytosol via the endoplasmic reticulum. Am J Physiol Renal Physiol **286:** F617-624

Schachtman DP, Schroeder JI, Lucas WJ, Anderson JA, Gaber RF (1992) Expression of an inward-rectifying potassium channel by the Arabidopsis KAT1 cDNA. Science **258:** 1654-1658

Schreiber L (2010) Transport barriers made of cutin, suberin and associated waxes. Trends Plant Sci **15:** 546-553

Schulte A, Lorenzen I, Bottcher M, Plieth C (2006) A novel fluorescent pH probe for expression in plants. Plant Methods **2:** 7

Schumacher K, Krebs M (2010) The V-ATPase: small cargo, large effects. Curr Opin Plant Biol **13:** 724-730

Serrano R, Bernal D, Simon E, Arino J (2004) Copper and iron are the limiting factors for growth of the yeast Saccharomyces cerevisiae in an alkaline environment. J Biol Chem **279:** 19698-19704

Shah K, Penel C, Gagnon J, Dunand C (2004) Purification and identification of a Ca(2+)-pectate binding peroxidase from Arabidopsis leaves. Phytochemistry **65:** 307-312

Shi H, Ishitani M, Kim C, Zhu JK (2000) The Arabidopsis thaliana salt tolerance gene SOS1 encodes a putative Na+/H+ antiporter. Proc Natl Acad Sci U S A **97:** 6896-6901

Shi H, Quintero FJ, Pardo JM, Zhu JK (2002) The putative plasma membrane Na(+)/H(+) antiporter SOS1 controls long-distance Na(+) transport in plants. Plant Cell **14:** 465-477

Sieben C, Mikosch M, Brandizzi F, Homann U (2008) Interaction of the K(+)-channel KAT1 with the coat protein complex II coat component Sec24 depends on a di-acidic endoplasmic reticulum export motif. Plant J **56:** 997-1006

Sorensen I, Domozych D, Willats WG (2010) How have plant cell walls evolved? Plant Physiol **153:** 366-372

Southworth TW, Guffanti AA, Moir A, Krulwich TA (2001) GerN, an endospore germination protein of Bacillus cereus, is an Na(+)/H(+)-K(+) antiporter. J Bacteriol **183:** 5896-5903

Stamatakis A (2006) RAxML-VI-HPC: maximum likelihood-based phylogenetic analyses with thousands of taxa and mixed models. Bioinformatics **22:** 2688-2690

Stefanowska M, Kuras M, Kacperska A (2002) Low temperature-induced modifications in cell ultrastructure and localization of phenolics in winter oilseed rape (Brassica napus L. var. oleifera L.) leaves. Annals of Botany **90:** 637-645

Stenmark H, Aasland R, Driscoll PC (2002) The phosphatidylinositol 3-phosphate-binding FYVE finger. FEBS Lett **513:** 77-84

Sterling C (1970) Crystal structure of rhutenium red and stereochemistry os its pectin stain. Amer. J. Bot. **57:** 172-175

Stumpe S, Bakker EP (1997) Requirement of a large K+-uptake capacity and of extracytoplasmic protease activity for protamine resistance of Escherichia coli. Arch Microbiol **167:** 126-136

Sun LX, van Nocker S (2010) Analysis of promoter activity of members of the PECTATE LYASE-LIKE (PLL) gene family in cell separation in Arabidopsis. Bmc Plant Biology **10:** -

Sutter JU, Campanoni P, Tyrrell M, Blatt MR (2006) Selective mobility and sensitivity to SNAREs is exhibited by the Arabidopsis KAT1 K+ channel at the plasma membrane. Plant Cell **18:** 935-954

Sychrova H, Ramirez J, Pena A (1999) Involvement of Nha1 antiporter in regulation of intracellular pH in Saccharomyces cerevisiae. FEMS Microbiol Lett **171:** 167-172

Sze H (1985) H+-Translocating Atpases - Advances Using Membrane-Vesicles. Annual Review of Plant Physiology and Plant Molecular Biology **36:** 175-208

Sze H, Padmanaban S, Cellier F, Honys D, Cheng NH, Bock KW, Conejero G, Li X, Twell D, Ward JM, Hirschi KD (2004) Expression patterns of a novel AtCHX gene family highlight potential roles in osmotic adjustment and K+ homeostasis in pollen development. Plant Physiol **136:** 2532-2547

Sze H, Ward JM, Lai S (1992) Vacuolar H(+)-translocating ATPases from plants: structure, function, and isoforms. J Bioenerg Biomembr **24:** 371-381

Taglicht D, Padan E, Schuldiner S (1991) Overproduction and purification of a functional Na+/H+ antiporter coded by nhaA (ant) from Escherichia coli. J Biol Chem **266:** 11289-11294

Takano J, Miwa K, Yuan L, von Wiren N, Fujiwara T (2005) Endocytosis and degradation of BOR1, a boron transporter of Arabidopsis thaliana, regulated by boron availability. Proc Natl Acad Sci U S A **102:** 12276-12281

Takano J, Noguchi K, Yasumori M, Kobayashi M, Gajdos Z, Miwa K, Hayashi H, Yoneyama T, Fujiwara T (2002) Arabidopsis boron transporter for xylem loading. Nature **420:** 337-340

Takano J, Tanaka M, Toyoda A, Miwa K, Kasai K, Fuji K, Onouchi H, Naito S, Fujiwara T (2010) Polar localization and degradation of Arabidopsis boron transporters through distinct trafficking pathways. Proc Natl Acad Sci U S A **107:** 5220-5225

Thackray PD, Behravan J, Southworth TW, Moir A (2001) GerN, an antiporter homologue important in germination of Bacillus cereus endospores. J Bacteriol **183:** 476-482

Tian GW, Chen MH, Zaltsman A, Citovsky V (2006) Pollen-specific pectin methylesterase involved in pollen tube growth. Developmental Biology **294:** 83-91

Timme RE, Delwiche CF (2010) Uncovering the evolutionary origin of plant molecular processes: comparison of Coleochaete (Coleochaetales) and Spirogyra (Zygnematales) transcriptomes. BMC Plant Biol **10:** 96

Tsunekawa K, Shijuku T, Hayashimoto M, Kojima Y, Onai K, Morishita M, Ishiura M, Kuroda T, Nakamura T, Kobayashi H, Sato M, Toyooka K, Matsuoka K, Omata T, Uozumi N (2009) Identification and characterization of the Na+/H+ antiporter Nhas3 from the thylakoid membrane of Synechocystis sp. PCC 6803. J Biol Chem **284:** 16513-16521

Ueda T, Yamaguchi M, Uchimiya H, Nakano A (2001) Ara6, a plant-unique novel type Rab GTPase, functions in the endocytic pathway of Arabidopsis thaliana. EMBO J **20:** 4730-4741

Uemura T, Ueda T, Ohniwa RL, Nakano A, Takeyasu K, Sato MH (2004) Systematic analysis of SNARE molecules in Arabidopsis: dissection of the post-Golgi network in plant cells. Cell Struct Funct **29:** 49-65

Uozumi N (2001) Escherichia coli as an expression system for K(+) transport systems from plants. Am J Physiol Cell Physiol **281:** C733-739

Uozumi N, Gassmann W, Cao Y, Schroeder JI (1995) Identification of strong modifications in cation selectivity in an Arabidopsis inward rectifying potassium channel by mutant selection in yeast. J Biol Chem **270:** 24276-24281

Uozumi N, Nakamura T, Schroeder JI, Muto S (1998) Determination of transmembrane topology of an inward-rectifying potassium channel from Arabidopsis thaliana based on functional expression in Escherichia coli. Proc Natl Acad Sci U S A **95:** 9773-9778

Venema K, Belver A, Marin-Manzano MC, Rodriguez-Rosales MP, Donaire JP (2003) A novel intracellular K+/H+ antiporter related to Na+/H+ antiporters is important for K+ ion homeostasis in plants. J Biol Chem **278:** 22453-22459

Venema K, Quintero FJ, Pardo JM, Donaire JP (2002) The arabidopsis Na+/H+ exchanger AtNHX1 catalyzes low affinity Na+ and K+ transport in reconstituted liposomes. J Biol Chem **277:** 2413-2418

Vert G, Chory J (2006) Downstream nuclear events in brassinosteroid signalling. Nature **441:** 96-100

Vinothkumar KR, Smits SH, Kuhlbrandt W (2005) pH-induced structural change in a sodium/proton antiporter from Methanococcus jannaschii. EMBO J **24:** 2720-2729

Viotti C, Bubeck J, Stierhof YD, Krebs M, Langhans M, van den Berg W, van Dongen W, Richter S, Geldner N, Takano J, Jurgens G, de Vries SC, Robinson DG, Schumacher K (2010) Endocytic and secretory traffic in Arabidopsis merge in the trans-Golgi network/early endosome, an independent and highly dynamic organelle. Plant Cell **22:** 1344-1357

Wagner MC, Molnar EE, Molitoris BA, Goebl MG (2006) Loss of the homotypic fusion and vacuole protein sorting or golgi-associated retrograde protein vesicle tethering complexes results in gentamicin sensitivity in the yeast Saccharomyces cerevisiae. Antimicrob Agents Chemother **50:** 587-595

Walker DJ, Leigh RA, Miller AJ (1996) Potassium homeostasis in vacuolate plant cells. Proc Natl Acad Sci U S A **93:** 10510-10514

Wang X, Chory J (2006) Brassinosteroids regulate dissociation of BKI1, a negative regulator of BRI1 signaling, from the plasma membrane. Science **313:** 1118-1122

Weeden NF (1981) Genetic and biochemical implications of the endosymbiotic origin of the chloroplast. J Mol Evol **17:** 133-139

Wegner LH, De Boer AH, Raschke K (1994) Properties of the K+ inward rectifier in the plasma membrane of xylem parenchyma cells from barley roots: effects of TEA+, Ca2+, Ba2+ and La3+. J Membr Biol **142:** 363-379

Wodniok S, Brinkmann H, Glockner G, Heidel AJ, Philippe H, Melkonian M, Becker B (2011) Origin of land plants: Do conjugating green algae hold the key? Bmc Evolutionary Biology **11:** -

Wright K, Northcote DH (1974) The relationship of root-cap slimes to pectins. Biochem J **139:** 525-534

Wu SJ, Ding L, Zhu JK (1996) SOS1, a Genetic Locus Essential for Salt Tolerance and Potassium Acquisition. Plant Cell **8:** 617-627

Wywial E, Singh SM (2010) Identification and structural characterization of FYVE domain-containing proteins of Arabidopsis thaliana. Bmc Plant Biology **10:** -

Xiang M, Feng M, Muend S, Rao R (2007) A human Na+/H+ antiporter sharing evolutionary origins with bacterial NhaA may be a candidate gene for essential hypertension. Proc Natl Acad Sci U S A **104:** 18677-18681

Yamaguchi T, Aharon GS, Sottosanto JB, Blumwald E (2005) Vacuolar Na+/H+ antiporter cation selectivity is regulated by calmodulin from within the vacuole in a Ca2+- and pH-dependent manner. Proceedings of the National Academy of Sciences of the United States of America **102:** 16107-16112

Yamaguchi T, Apse MP, Shi HZ, Blumwald E (2003) Topological analysis of a plant vacuolar Na+/H+ antiporter reveals a luminal C terminus that regulates antiporter cation selectivity. Proceedings of the National Academy of Sciences of the United States of America **100:** 12510-12515

Yenush L, Mulet JM, Arino J, Serrano R (2002) The Ppz protein phosphatases are key regulators of K+ and pH homeostasis: implications for salt tolerance, cell wall integrity and cell cycle progression. EMBO J **21:** 920-929

Yin Y, Vafeados D, Tao Y, Yoshida S, Asami T, Chory J (2005) A new class of transcription factors mediates brassinosteroid-regulated gene expression in Arabidopsis. Cell **120:** 249-259

Yokoi S, Quintero FJ, Cubero B, Ruiz MT, Bressan RA, Hasegawa PM, Pardo JM (2002) Differential expression and function of Arabidopsis thaliana NHX Na+/H+ antiporters in the salt stress response. Plant J **30:** 529-539

Yoo SD, Cho YH, Sheen J (2007) Arabidopsis mesophyll protoplasts: a versatile cell system for transient gene expression analysis. Nat Protoc **2:** 1565-1572

Yoo SH, Fishman ML, Savary BJ, Hotchkiss AT, Jr. (2003) Monovalent salt-induced gelation of enzymatically deesterified pectin. J Agric Food Chem **51:** 7410-7417

Yoshida K, Miki N, Momonoi K, Kawachi M, Katou K, Okazaki Y, Uozumi N, Maeshima M, Kondo T (2009) Synchrony between flower opening and petal-color change from red to blue in morning glory, Ipomoea tricolor cv. Heavenly Blue. Proceedings of the Japan Academy Series a-Mathematical Sciences **85:** 187-197

Yu Q, Hlavacka A, Matoh T, Volkmann D, Menzel D, Goldbach HE, Baluska F (2002) Short-term boron deprivation inhibits endocytosis of cell wall pectins in meristematic cells of maize and wheat root apices. Plant Physiology **130:** 415-421

Zhang X, Henriques R, Lin SS, Niu QW, Chua NH (2006) Agrobacterium-mediated transformation of Arabidopsis thaliana using the floral dip method. Nat Protoc **1:** 641-646

Zhao J, Cheng NH, Motes CM, Blancaflor EB, Moore M, Gonzales N, Padmanaban S, Sze H, Ward JM, Hirschi KD (2008) AtCHX13 is a plasma membrane K+ transporter. Plant Physiol **148:** 796-807

Zhou GA, Jiang Y, Yang Q, Wang JF, Huang J, Zhang HS (2006) Isolation and characterization of a new Na+/H+ antiporter gene OsNHA1 from rice (Oryza sativa L.). DNA Sequence **17:** 24-30